Design and validation of Fully-Uncoupled Multi-Directional lay-ups to evaluate interlaminar fracture toughness

Torquato Garulli

▶ **To cite this version:**

HAL Id: tel-02968779

https://theses.hal.science/tel-02968779v2

Submitted on 22 Oct 2020

Cosupervised Thesis
submitted to

UNIVERSITY OF BORDEAUX
Sciences Physiques et de l'Ingénieur

UNIVERSITY OF PISA
Industrial Engineering

by
Torquato GARULLI
in partial fulfilment of the requirements
for the degrees of

Docteur
en Mécanique

Doctor of Philosophy
in Aerospace Engineering

Design and validation of Fully-Uncoupled Multi-Directional lay-ups to evaluate interlaminar fracture toughness

Realised under the supervision of:

Mr. Eric MARTIN, Full Professor, Bordeaux INP   - Director
Mr. Daniele FANTERIA, Associate Professor, UNIPI Pisa   - Co-Director
Mrs. Anita CATAPANO, Associate Professor, Bordeaux INP   - Supervisor

Presented on the 10th of July 2020, in front of the Commission:

Mr. Cristophe BOUVET, Full Professor, ISAE-SUPAERO Toulouse   - President
Mr. Nicolas CARRERE, Associate Professor, HDR, ENSTA Bretagne   - Reviewer
Mr. Pedro CAMANHO, Full Professor, University of Porto   - Reviewer
Mr. Josep COSTA, Full Professor, University of Girona   - Examiner
Mr. Fabrizio RICCI, Associate Professor, University of Naples   - Examiner
Mr. Julien JUMEL, Associate Professor, HDR, ENSTA Bretagne   - Invited

Aut viam inveniam aut faciam.

Funding

Acknowledgements

It seems like yesterday that I was packing my stuff and getting ready for a long car ride... from Pisa to Bordeaux. It's by looking back and remembering all that's happened that I can get a feeling of the fact that more than three years have passed. Three years full of amazing people and experiences. Now that this Ph.D. adventure has come to an end, it is the moment to look back again and to thank all those that have made it a wonderful journey. And you are so many...

To begin with, I would like to thank all my supervisors.

Anita Catapano and Daniele Fanteria, for giving me the possibility to pursue this Ph.D. program. Thanks for the time and energy you invested to make this possible and for the support throughout these years. Thanks for pushing and allowing me to make my journey through conferences and other events; for the useful discussions and for your guidance.

Julien Jumel, former director of my thesis. Thanks for giving me the possibility and the tools to perform many of the activities that were fundamental in my research.

Eric Martin, who promptly took over the direction of the thesis when Julien had to move. Thanks for the trust you offered when doing so, it has been deeply appreciated. And thanks for the constructive and supportive feedbacks that you always provided.

Thanks also to Marco Montemurro, for the precious help.

Thanks to all those that have made my time in France one of the most beautiful experiences of my life...

Thanks Florent, for hosting a complete stranger at your place in a random February night. Your kindness has been astonishing. I hope you could always be with people like yourself in your life!

Thanks to all the people I met at the A4! My office mates: Aurore, Enrico, Mahfoudh, Timothée; all interns, Ph.D. students, researchers, profs and employees. Merci du temps ensemble, merci pour chaque fois que vous m'avez appris un nouveau mot, pour chaque fois qu'on s'est bien amusés. C'était un plaisir d'être avec vous. Merci aussi à tous les autres membres du labo qui n'étaient pas à l'A4, mais avec qui on a partagé des moments ensemble. Merci Marie et Olivier, pour m'avoir donné la possibilité d'encadrer des TP. Cela a été une expérience formidable. Aussi, votre aide a été essentiel afin de la rendre faisable et agréable. Merci Wenyi pour le support avec ton activité de stage et pour le travail fait ensemble.

Merci à Véronique Teichmann, pour l'enthousiasme que tu as apporté à chaque minute de leçon. Grâce à cela, apprendre le Français a été un plaisir.

Merci aux nageurs du BEC, qui m'ont accueilli et m'ont permis de m'entraîner et de concourir avec eux. J'ai vraiment apprécié votre disponibilité et votre compagnie.

Thanks Pilar, too, for the talks and for the fun time at the pool together. I hope to see you soon again!

Thanks also to the Italians that made Bordeaux feel like home. Grazie Pietro e Lorenzo. Grazie Michele, specie per l'ospitalità quando ne ho avuto bisogno. Grazie Giulio, per le chiacchierate insieme e, indimenticabilmente, per la voglia di venire in piscina con me persino in quelle gelide domeniche mattina invernali :D!

Grazie Giulia. Ci siamo trovati sulla stessa barca, a condividere una situazione nuova e difficile. Ma è stata l'occasione per capirsi e volersi bene da subito. Grazie per la tua

trasparenza, per la tua sincerità. Grazie perchè sai ascoltare. Grazie per la disponibilità ed il supporto. Vorrei che tu sapessi che sei molto più forte di quello che pensi. Grazie per i bellissimi momenti passati insieme e per essere vera e gentile come sei.

Grazie Luca. Visto che oramai mi conosci, sono sicuro che saprai che, prima che tu arrivassi in casa, da soli si stava bene... Ma sono altrettanto sicuro che saprai che, quando poi sei arrivato, si stava ancora meglio! Grazie per tutte le risate, il tempo insieme e per aver condiviso tutte le meravigliose assurdità che abbiamo visto. Grazie per le cene, per le uscite coi nostri mezzi preferiti (specie nelle mie precarie fasi iniziali)! Grazie per tutto.

Thanks also to those that have made my comeback to Pisa pleasurable...

Thanks to Joanne Spataro, and to all the Badgers. Spending time with you has been a fun and somewhat exotic parenthesis in the well known Pisan land. I really enjoyed our time together, and I learned a lot. I wish you all the best for your future.

Thanks to all those with whom I have shared time, talks and fun at the Aerospace department and outside. Grazie Luca, Giuseppe, Karim, Marco, Alessandro, Riccardo, Gabriele. Grazie Federico, per tutto il tempo passato insieme in ufficio, per il supporto e i consigli. Grazie per aver cercato un compromesso con i miei bisogni termici :D! Merci Clément, pour ton temps avec nous. Grazie a tutti quelli che mi hanno aiutato, in un modo o nell'altro; i tecnici di laboratorio, il personale del dipartimento, il prof. Lazzeri.

Grazie Federico, per aver sempre mantenuto i contatti, per esserti sempre genuinamente interessato, per il supporto e le visite. Sono davvero contento che tu stia facendo un percorso che ti soddisfa. Continua così!

Grazie ai miei compagni di squadra, ed al nostro allenatore. In questi anni siete stati un punto di riferimento importante. In molti momenti, quando le preoccupazioni in testa erano tante e i pensieri non proprio positivi, siete stati, forse senza nemmeno saperlo, un supporto fondamentale. La sicurezza di venire in piscina, trovarvi e stare con voi mi ha aiutato tantissimo. Mi sono gustato ogni allenamento, ogni vasca, ogni risata, ogni gara, ogni chiacchierata sincera, ogni momento con voi; sicuramente più di quanto sia trasparito. Vi voglio bene. Grazie.

Thanks to those that, in the short time of a ride together, were eager to open up, share their stories and establish a connection. As Tyler Durden would have said, you have been the most interesting single-serving friends I've ever met.

Thanks to all those people with whom, despite the very short time together, I have been able to establish a close relationship. Grazie Mascia. Merci Marwa. Thanks to all the wonderful guys met in Vicenza, especially thanks Donato, America, Daniele, Dario, Davide, Goran, Nada and Nitesh! I hope to see you soon, hopefully with some Limoncello :D. I wish you the best, for your research and for everything else!

Thanks to all those that made conferences some of the most enjoyable moments of this journey!

Eventually, a big thanks to those that have always been there...

Grazie ai miei amici moglianesi. Nonostante in questi anni io sia stato decisamente assente, stare con voi è sempre stato bello e mi avete sempre fatto sentire a casa. Grazie per i ritrovi, per le chiacchierate, le mangiate, le nuotate e tutti i momenti insieme.

Grazie Francesco, anche tu sei oramai una costante :D! Sono contento che in tutti questi anni il nostro rapporto, in tutta semplicità, non sia invecchiato di un singolo giorno! E

che alla fine, in un modo o nell'altro, ci si vede sempre!

Un grazie enorme alla mia famiglia. Ai cugini e agli zii che sono sempre rimasti vicini nonostante le distanze. Ai miei genitori, a Chiara, a Luca e ai piccoli Arianna e Jacopo. Nonostante questa avventura mi abbia tenuto spesso (forse troppo) lontano, siete sempre nella mia testa e nel mio cuore. Pensarvi e sentirvi mi ha sempre fatto star bene, nei momenti felici e nei momenti difficili. Tutte le difficoltà, i fallimenti, i successi... tutto il loro peso si ridimensiona ogni volta che penso alla fortuna che ho ad avere voi. Grazie ai nonni. Nonostante non siate più con noi, questo traguardo è in gran parte merito vostro. Grazie per tutto quello che mi avete insegnato.

Un grazie infinito a Giulia. So che questa pezzo della mia vita è stato difficile anche per te. So che alcune mie scelte sono state difficili da capire ed accettare. Allora il primo grazie è per aver fatto tutto quello che hai fatto, nonostante tutto. Grazie poi per l'impegno che hai messo nel cercare di capire quegli aspetti di me che ti sembravano così strani. Grazie per avere ascoltato. Grazie per aver continuato a condividere tutto con me, per essere ancora qui. Grazie per i momenti *incredibbili*! Grazie per avermi aiutato, specie nella fase finale di questo percorso, in cui le complicazioni non sono mancate.

Abstract

The object of this study is the development of a novel class of stacking sequences for the design of multidirectional polymer matrix laminated composite specimens for interlaminar fracture toughness (or delamination) tests. These sequences allow to obtain multidirectional specimens that, in the framework of Classic Laminated Plate Theory, have a thermo-elastic behaviour that closely matches that of unidirectional specimens: they are completely free from elastic couplings and they do not develop laminate-level thermally-induced deformations due to the curing process. Furthermore, they allow to test delamination interfaces between plies of any desired orientation. Because of their properties, they were labelled *Fully-Uncoupled Multi-Directional* (FUMD).

In order to design these layups, Quasi-Trivial (QT) solutions were exploited. Firstly, an algorithm for the creation of a database of such solutions was conceived and implemented. Thanks to it, more and longer QT solutions were found than in previous studies. Then, analytical rules were established allowing to obtain new QT solutions from the superposition of known ones. These criteria allow to obtain QT sequences of any desired length, thus overcoming existing computational limitations arising when searching for QT solutions using the algorithm. Combining QT solutions with a few basic laminate design principles and the superposition criteria, FUMD stacking sequences are designed.

In order to assess the properties of delamination specimens obtained with FUMD layups, a Finite Element model of a Double Cantilever Beam specimen was developed and used to compare the behaviour of a FUMD layup with that of other sequences proposed in relevant literature on the topic of delamination in multidirectional laminates. By means of the standard and of a revised Virtual Crack Closure Technique formulations, Energy Release Rate distributions and modal partitions of the specimens were evaluated. It emerged that the FUMD layup resulted in an optimal behaviour of the specimen.

Eventually, a mode I interlaminar fracture toughness experimental campaign was performed. FUMD Double Cantilever Beam specimens were fabricated, along with with unidirectional ones. A *UD-fabric* material was used to reduce the likelihood of delamination migration. Rotations of the specimens arms and the shape of the delamination fronts were studied in order to assess the capability of the specimens to yield the correct mechanical behaviour for mode I delamination testing. For both aspects, FUMD specimens yielded results similar to those obtained with unidirectional specimens. With respect to interlaminar fracture toughness, specimens with identical delamination interface yielded similar values, even if their global stiffness was different. On the other hand, different interfaces led to different interlaminar fracture toughness, related to different fracture behaviours.

While this work represents a preliminary study and further research is clearly required, FUMD delamination specimens have shown a good potential, and they may stand out as a viable solution for interlaminar fracture toughness tests. Possibly, they could be considered for an extension of the scopes of existing standard test methods to multidirectional laminates and interfaces.

Résumé

Le sujet de cette étude est le développement de séquences d'empilement pour la conception d'éprouvettes multidirectionnelles en matériaux composite à matrice polymère destinées à des essais de délaminage. Ces séquences permettent d'obtenir des éprouvettes multidirectionnelles qui, dans le cadre de la théorie classique des stratifiés, montrent un comportement thermoélastique qui reproduit celui des composites unidirectionnels : elles sont complètement libres de tout type de couplage élastique et ils ne développent pas des déformations résiduelles dues au cycle de cuisson. Par ailleurs, ces empilements permettent de tester n'importe quelle interface de délaminage.

La conception de ces empilements est basée sur les solutions Quasi-Triviales (QT). Un algorithme pour la création d'une base de données de ces solutions a été conçu et implémenté. Grace à cela, un nombre plus grand de solutions QT et des solutions QT avec un nombre plus grand de plis que dans des études précédentes ont été trouvées. Ensuite, des critères analytiques permettant d'obtenir de nouvelles solutions à partir de la superposition des solutions connues ont été établis. Ces critères permettent d'obtenir des séquences QT avec n'importe quel nombre de couches. En combinant les solutions QT, les principes usuels de conception des stratifiés et les critères de superposition, les séquences d'empilement Fully-Uncoupled Multi-Directional (FUMD) ont été obtenues.

Pour évaluer les propriétés des éprouvettes de délaminage obtenues avec ces séquences, un modèle Éléments Finis d'une éprouvette Double Cantilever Beam (DCB) a été développé pour comparer le comportement d'une séquence FUMD à celui d'autres séquences proposées dans la littérature pour les essais de délaminage. En utilisant la méthode de refermeture (Virtual Crack Closure) dans ses formulations originale et révisée, les distributions du taux de restitution d'énergie (Energy Release Rate) et ses partitions modales ont été évaluées. La séquence FUMD démontre les meilleurs résultats.

Finalement, une campagne expérimentale de caractérisation du délaminage en mode I a été menée. Des éprouvettes DCB avec des séquences FUMD ont été conçues et fabriquées. Des plis tissés déséquilibrés ont été utilisés pour réduire la probabilité de changement de plan de délaminage. Les rotations des bras des éprouvettes et la forme du front du délaminage ont été étudiés pour évaluer la capacité des éprouvettes à garantir un comportement mécanique optimal lors du test de délaminage en mode I. Les résultats obtenus avec les éprouvettes FUMD sont proches de ceux obtenus avec les éprouvettes unidirectionnelles. En ce qui concerne l'énergie de rupture, les éprouvettes ayant la même interface de délaminage ont montré des valeurs très proches, même si leur rigidité était sensiblement différente. Par ailleurs, la caractérisation d'interfaces différentes a abouti à des énergies de rupture différentes, résultants des modes de ruptures non identiques.

Ce travail ne représente qu'une étude préliminaire et des recherches complémentaires sont nécessaires. Néanmoins les éprouvettes de délaminage FUMD ont démontré un bon potentiel, et sont intéressantes pour les essais de délaminage.

Introduction

Nowadays, fibre reinforced composite materials, and in particular laminates, are widely used for structural applications, in many different sectors. One of the most important reasons is that these materials typically combine good mechanical properties with low density, thus resulting in excellent specific properties. As a matter of fact, composite laminates, when compared with metals, often allow to build more efficient and lightweight structures. This aspect is extremely valuable in the transportation sector, where structural efficiency translates in weight savings, which in turn lead to cheaper operations of the structure, and hence in a more competitive product. This is especially true for the aerospace industry, where weight reduction is one of the most important design drivers.

Furthermore, with the increasing sensitivity of the public opinion to climate change issues, a renewed and special attention is currently devoted to reduce pollutant emissions caused by transports. In this context, an improvement in structural efficiency represents a real chance, since emissions are significantly affected by weight.

Nonetheless, in many applications, and most of all in the aerospace sector, safety represents another critical issue: reliability of composite structures used for safety-critical applications must be guaranteed. In order to design structures that can meet the required safety standards, the damage and failure mechanism of the structure itself and of the material must be known in extreme depth. Any element of ignorance in this regards is reflected in a safety coefficient to be applied, that in turn leads to additional structural weight and its consequences: inefficiency, pollution and costs.

Among the different damage mechanisms typical of composite laminates, interlaminar fracture, or delamination, is one of the most critical. It consists in the separation of the layers that make up the laminate and, since it may appear and grow inside a component without being noticeable from the outside, it is very dangerous. Moreover, it drastically reduces the mechanical properties of the structure, especially in compression, which usually is already a weak point for composite laminates.

Consequently, both academia and industry have committed great resources to the study of delamination phenomena. Nowadays, concepts derived from Fracture Mechanics are used to quantify the interlaminar fracture toughness of polymer matrix composites. In particular, the critical value of strain Energy Release Rate (i.e. the energy required for unit area propagation of delamination) is commonly used. To date, consolidated standard test procedures for the characterisation of interlaminar fracture toughness of composites have been published by the American Society for Testing and Materials (ASTM), the Japanese Industrial Standards organisation (JIS) and the International Organization for Standardization (ISO). However, these standard methods recommend, in all cases, to use laminates with unidirectional layups and in which delamination is propagated parallel to the fibres direction. Thus, the delamination resistance of the material may be evaluated exclusively in a specific interface (between two equally oriented layers) and in a very

specific condition (propagation along the fibre direction). This restriction was historically introduced because early pre-standardisation studies identified delamination migration as a factor preventing from obtaining meaningful toughness measurements, and subsequent experimental studies leading to the development of standards were mainly performed using unidirectional specimens.

Nonetheless, the interest in characterising interlaminar fracture toughness of interfaces other than the standard one never faded out. Indeed, real components and structures are most often built using multidirectional laminates, in which delamination may appear in any interface and may propagate in any direction with respect to the fibre orientation. Therefore, research on the subject never stopped since the 80's and is still highly active. Standard methods for unidirectional laminates have been widely used to test multidirectional specimens as well. The results obtained, though, were often inconsistent or even contradictory. Still, this research effort allowed to identify the most important problems arising in the attempt to evaluate interlaminar fracture toughness of multidirectional laminates.

Besides delamination migration, which remains a major issue in actual experimental testing, elastic couplings and thermal effects, typical of multidirectional laminates, have been shown to be critical issues. Elastic couplings complicate the kinematics of specimens and may cause unwanted rotations and deformations. This may affect the test by introducing undesired energy release rate modal contributions, so that the actual loading mode is not easily predictable, even in standard test configurations. Additionally, they introduce three-dimensional effects that may invalidate the hypothesis assumed by data reduction techniques. The presence of thermal residual stresses or strains, on the other hand, was demonstrated to influence interlaminar fracture toughness evaluation and was correlated to an increased risk of delamination migration.

Within the research context just sketched, the main purpose of this study is to design multidirectional layups for delamination specimens that could enable to test any type of interface while also eliminating elastic couplings and undesired thermal effects typical of multidirectional laminates.

This would represent an important improvement in delamination testing capabilities and it could possibly help moving toward an inclusion of multidirectional laminates in the scopes of existing standard procedures. If this happens, an effective and consistent characterisation of interlaminar fracture toughness would be possible for any delamination interface. This could stretch the potential of structural design beyond its actual limits, leading to safer and more efficient structures.

The manuscript is divided into three parts. Part I aims to present in a complete and consistent way the scientific problem to be faced and the tools to be used throughout the entire study.

Chapter 1 introduces the research problem. After a brief introduction on composite materials and on the reasons behind their widespread adoption, especially in the aerospace sector, the discussion is focused on laminates, which are most often used for lightweight high-performance structures. The main types of damage mechanisms encountered in such composites are presented, and delamination is identified as one of the most dangerous. Our actual limitations in characterising delamination resistance of multidirectional laminates are acknowledged, and the reasons for these limitations are hinted at. A discussion on the importance of overcoming such limitations, and hence of the present study, closes the

chapter.

In Chapter 2, starting from general anisotropic elasticity, the thermoelastic behaviour of a lamina is described and the framework of Classical Laminated Plate Theory is introduced. Within this framework, elastic couplings and thermal effects, typical of multidirectional laminates, are formalised. The concepts presented in this chapter will allow a deeper understanding of the problems arising in delamination testing of multidirectional laminates and will be used to derive the most important results of this work.

Chapter 3 focuses in a much more detailed way on the phenomenon of delamination in composite laminates. The first part of the chapter reports an historical perspective and describes the established knowledge and the standard practices for the characterisation of interlaminar fracture toughness. Then, the second part of the chapter is devoted to a thorough bibliographic review of literature concerning the problem of delamination testing of multidirectional laminates.

Part II of the manuscript is dedicated to the design of Fully-Uncoupled Multi-Directional delamination specimens. In more detail, Chapters 4 and 5 present the development of important tools that are later used in Chapter 6 to eventually obtain Fully-Uncoupled Multi-Directional delamination specimens.

Chapter 4 covers the attainment of Quasi-Trivial solutions. The interest for this class of stacking sequences is briefly explained, followed by a description of their fundamentals and of related complexities. Finally, the strategies adopted to conceive and implement an efficient algorithm to generate a database Quasi-Trivial solutions are presented, along with some results in terms of number of solutions.

Chapter 5 presents the derivation of analytical superposition rules for Quasi-Trivial solutions. Initially, the formalism and the notation used in the analytical developments are described. Then, the actual derivation of the superposition rules is presented for the cases of uncoupling, membrane-bending homogeneity and quasi-homogeneity of the sequence obtained by the superposition. In particular, for all cases, the superposition of uncoupled, membrane-bending homogeneous and quasi homogeneous QT solutions is treated. Finally, the application of the superposition rules to the particular case of the superposition of only two solutions is presented, along with some examples.

Chapter 6 presents in detail the process by which Fully-Uncoupled Multi-Directional specimens are obtained. Firstly, it details which features an ideal delamination specimen should possess and why unidirectional delamination specimens are so suited for standard tests. Then, it shows how it is possible to use Quasi-Trivial solutions, obtained in Chapter 4, and their superposition rules, derived in Chapter 5, to design Fully-Uncoupled Multi-Directional delamination specimens that reproduce accurately the desirable thermoelastic behaviour of unidirectional ones.

In Part III of the manuscript, two preliminary studies to validate the concept of Fully-Uncoupled Multi-Directional delamination specimens are presented.

In Chapter 7, one example of Fully-Uncoupled Multi-Directional layup is designed and compared to a selection of other multidirectional layups. These latter are obtained from relevant literature on the topic of delamination in multidirectional laminates. Firstly, a comparison in terms of thermoelastic properties of the delamination specimens that may be obtained using these layups is performed. Then, Finite Element models of Double Cantilever Beam specimens using these layups are developed. The Virtual Crack Closure Technique, in its original formulation and in a revised one, is used to obtain a qualitative

assessment of the behaviour of the specimens.

Chapter 8 presents a mode I interlaminar fracture testing campaign performed using Fully-Uncoupled Multi-Directional Double Cantilever Beam specimens. Firstly, the material system and the layups selected are introduced, along with the motivations for their choices. Then, the fabrication process, the experimental setup and the testing procedure are carefully described. Test results in terms of force-displacement behaviour, initiation and propagation values of interlaminar fracture toughness and fracture behaviour at the delamination interface are presented and discussed. Eventually, the specimens arms rotations during the tests and the shapes of delamination fronts at the end of the test are studied in order to assess the mechanical behaviour of Fully-Uncoupled Multi-Directional specimens compared to that of unidirectional ones.

General conclusions and perspectives for future developments end the manuscript.

Résumé long

Les matériaux composites à renfort de fibres longues, et en particulier les stratifiés, sont très répandus pour les applications structurales, dans de nombreux secteurs industriels. Ces matériaux conjuguent des bonnes propriétés mécaniques avec des densités réduites, ce qui amène à des propriétés spécifiques excellentes. Les stratifiés composites permettent ainsi de construire des structures qui sont plus efficientes et plus légères que celles obtenues avec un matériau métallique. Cet aspect est appréciable dans le domaine des transports, où l'efficience structurale se traduit en gain de poids, qui à son tour amène à une utilisation plus économique de la structure, et donc à un produit plus compétitif. Cela est autant plus vrai pour l'industrie aérospatiale, dans laquelle la réduction du poids est un des critères de conception les plus importants.

Dans ce secteur, la sécurité est un autre aspect critique : la fiabilité des structures en composites qui sont utilisées pour applications critiques doit être garantie. Pour concevoir des structures qui peuvent satisfaire les standards de sécurité demandés les mécanismes d'endommagement et de rupture de la structure et du matériau doivent être connus de manière approfondie. Tout élément d'ignorance à ce sujet se traduit par un coefficient de sécurité à appliquer, qui à son tour entraine à une augmentation de poids avec ses conséquences négatives : pollution et couts.

Parmi les différents mécanismes d'endommagement typiques des stratifiés composites, la rupture interlaminaire, ou délaminage, est un des plus critiques. Elle consiste dans la séparation des couches qui forment le stratifié et, comme elle peut apparaitre et se propager intérieurement à une pièce sans être visible à l'extérieur, elle est très dangereuse. De plus, elle réduit fortement les propriétés mécaniques de la structure, particulièrement en compression, qui est souvent déjà un point faible des stratifiés composites.

En conséquence, le mécanisme de délaminage a été largement étudié par les acteurs académiques et industriels. Aujourd'hui, des concepts issus de la mécanique de la rupture sont utilisés pour quantifier la résistance au délaminage des composites à matrice polymére. Plus précisément, la valeur critique du taux de restitution d'énergie (i.e. l'énergie nécessaire pour la propagation d'une aire unitaire du délaminage) est utilisée. A ce jour, des procédures de test standardisées pour cette caractérisation ont été établies par l'American Society for Testing and Materials (ASTM), le Japanese Industrial Standards Organisation (JIS) and the International Organization for Standardization (ISO). Néanmoins, le champ d'application de ces normes est limité, dans tous les cas, aux stratifiés avec une séquence d'empilement unidirectionnel et dans lesquels le délaminage se propage dans la direction parallèle aux fibres. Donc, la résistance au délaminage ne peut être évaluée que pour une interface spécifique (entre deux couches à orientation identique) et dans une condition spécifique (propagation dans la direction des fibres). Cette limitation a été introduite historiquement parce que des études avant la normalisation avaient identifié le changement du plan de délaminage comme un facteur empêchant la

bonne évaluation de la résistance à la rupture interlaminaire. Par conséquent les études expérimentales utilisées pour le développement des normes ont été réalisées avec des éprouvettes unidirectionnelles.

Néanmoins, l'intérêt pour la caractérisation de la résistance à la rupture des interfaces non standard n'a jamais disparu. En effet, les structures réelles sont, dans la plupart des cas, réalisées avec des stratifiées multidirectionnels, dans lesquels le délaminage peut apparaitre dans n'importe quelle interface et se propager dans n'importe quelle direction par rapport à celle des fibres. En conséquence, la recherche sur ce sujet ne s'est jamais arrêtée et elle est toujours très active. Les méthodes normalisées pour les éprouvettes unidirectionnelles ont été largement utilisées pour tester aussi les éprouvettes multidirectionnelles. Les résultats obtenus, toutefois, étaient souvent incompatibles ou aussi contradictoires. Cependant, cet effort de recherche a permis d'identifier les problèmes les plus importants qui apparaissent pour évaluer la résistance au délaminage des stratifiés multidirectionnels.

A côté du changement du plan de délaminage, qui reste un problème majeur, les couplages élastiques et les effets thermiques, qui sont typiques des stratifiés multidirectionnels, sont des questions critiques. Les couplages élastiques compliquent la cinématique de l'éprouvette et peuvent introduire des rotations et des déformations indésirables. Cela peut compromettre le test en introduisant des contributions modales non souhaitées, si bien que la condition de chargement réelle n'est pas facilement prévisible, même dans des configurations de test standards. De plus, ces couplages introduisent des effets tridimensionnels qui peuvent invalider les hypothèses des techniques d'exploitation des données. La présence des contraintes résiduelles thermiques influence aussi l'évaluation de la résistance au délaminage et elle a été aussi corrélée à un risque majeur de changement de plan de délaminage.

L'objectif principale de cette étude est de concevoir des séquences d'empilement multidirectionnelles pour des éprouvettes de délaminage qui puissent permettre de tester n'importe quel type d'interface tout en éliminant les couplages élastiques et les effets thermiques indésirables qui sont typiques des stratifiés multidirectionnels.

Cela représenterait un progrès important pour les essais de délaminage et permettrait d'inclure les stratifiés multidirectionnels dans le champ d'application des procédures de test standard. Il serait alors possible de caractériser de façon efficace et systématique la résistance à la rupture interlaminaire de tout type d'interface. Cela pourra étendre le potentiel de la conception structurale au-delà de ses limites actuelles, et donc aboutir à des structures plus efficientes et plus sures.

Le manuscrit est divisé en trois parties. La Partie I présente le problème qui est l'objet de cette étude et les outils qui seront utilisés. Le Chapitre 1 introduit la problématique. Après une courte introduction sur les matériaux composites et les raisons derrière leur adoption, surtout dans le secteur aérospatial, la discussion se focalise sur les stratifiés, qui sont souvent utilisés pour les structures légères à haute performance. Les principaux mécanismes d'endommagement de ces composites sont présentés, et le délaminage est identifié comme l'un des plus dangereux. Les limitations actuelles dans la caractérisation de la résistance au délaminage des stratifiés composites sont reconnues et les raisons de ces limitations sont mentionnées. Une discussion sur l'importance de dépasser ces limitations, et donc de cette étude, conclut le chapitre.

Le Chapitre 2 décrit, à partir de l'élasticité anisotrope, le comportement thermoélastique d'un pli composite afin d'introduire le cadre de la théorie classique des stratifiés. Les cou-

plages élastiques et les effets thermiques, typiques des stratifiés multidirectionnel sont formalisés. Les concepts présentés dans ce chapitre permettent une compréhension plus profonde des problèmes qui apparaissent lors des tests de délaminage des éprouvettes multidirectionnelles et seront utilisés afin d'obtenir les résultats les plus important de cette étude.

Le Chapitre 3 se focalise de façon plus détaillée sur le phénomène du délaminage dans le stratifiés composites. La première partie du chapitre est une perspective historique et décrit la connaissance actuelle et les procédures standardisées qui existent pour la caractérisation de la résistance au délaminage. Puis, la deuxième partie du chapitre est dédiée à une étude bibliographique détaillée sur le sujet du délaminage dans les stratifiés composites.

La Partie II du manuscrit est dédiée à la conception des nouvelles éprouvettes de délaminage Fully-Uncoupled Multi-Directional (FUMD). Plus en détail, les Chapitres 4 et 5 présentent le développement des outils qui sont utilisés dans le Chapitre 6 pour obtenir finalement les éprouvettes FUMD.

Le Chapitre 4 est consacré à la recherche des solutions Quasi-Triviales (QT). L'intérêt pour cette classe de séquence d'empilement est brièvement expliqué, suivi d'une description de leurs concepts de base. Finalement, les stratégies adoptées pour concevoir et implémenter un algorithme efficient afin de générer une base de données des solutions QT sont présentées, accompagnées des résultats en termes de nombre de solutions trouvées.

Le Chapitre 5 établit les critères analytiques pour la superpositions des solutions QT. Le formalisme et la notation utilisées dans les développements analytiques sont décrits. La démarche analytique est présentée pour les différents cas de quasi-trivialité de la séquence obtenue par la superposition. En particulier, pour tous les cas, la superposition des solutions QT découplées, membrane flexion homogènes et quasi-homogènes sont traités. Enfin, l'application des critères de superposition au cas particulier de la superposition de deux solutions est présentée, à l'aide de quelques exemples.

Le Chapitre 6 présente en détail la procédure pour obtenir des séquences FUMD. Premièrement, les caractéristiques d'une éprouvette de délaminage idéale sont décrites. Puis, on montre comment il est possible d'utiliser les solutions QT, obtenues dans le Chapitre 4, et les critères de superposition, dérivés du Chapitre 5, pour concevoir des éprouvettes FUMD qui reproduisent le comportement thermoélastique des éprouvettes unidirectionnelles.

Dans la Partie III du manuscrit, deux études préliminaires pour valider le concept des séquences FUMD sont présentés.

Dans le Chapitre 7, un exemple de séquence FUMD est conçu et comparé avec une sélection d'autres séquences multidirectionnelles issues de la littérature. D'abord, une comparaison en termes de propriétés thermoélastiques de ces séquences a été effectuée. Puis, des modèles Eléments Finis de éprouvettes Double Cantilever Beam ont été développés. La méthode de refermeture, dans sa formulation originale et dans une formulation révisée, a été utilisée pour valider le comportement de l'éprouvette.

Le Chapitre 8 présente une campagne expérimentale de délaminage en mode I à l'aide d'éprouvettes Double Cantilever Beam. Premièrement le matériau utilisé et les séquences sélectionnées sont introduits, accompagnés des raisons pour leur choix. Puis, la procédure de fabrication, le dispositif expérimental et la procédure de test sont décrits en détail. Les résultats en termes de comportement force-déplacement, des valeurs d'énergie de

rupture à l'amorçage et pendant la propagation sont abordés. Finalement, les rotations des bras des éprouvettes et les formes des fronts de délaminage à la fin des tests sont étudiés pour évaluer le comportement des éprouvettes FUMD par rapport aux éprouvettes unidirectionnelles.

Des conclusions générales et de perspectives pour les développements futurs concluent le manuscrit.

Acronyms and Abbreviations

2D Two-dimensional

3D Three-dimensional

UD Unidirectional

MD Multidirectional

AFP Automated Fibre Placement

VAT Variable Angle Tow

LEFM Linear Elastic Fracture Mechanics

ERR Energy Release Rate

CLPT Classic Laminated Plate Theory

CTE Coefficient of Thermal Expansion

QT Quasi-Trivial

ASTM American Society for Testing and Materials

ESIS European Structural Integrity Society

JIS Japanese Industrial Standards organisation

DCB Double Cantilever Beam

NL Non-Linear

VIS Visual

5/MAX 5 percent compliance offset or Maximum load

MBT Modified Beam Theory

CC Compliance Calibration

MCC Modified Compliance Calibration

ENF End Notched Flexure

ELS End Loaded Split

NPC Non Pre-Cracked

PC Pre-Cracked

MMB Mixed Mode Bending

FE Finite Element

CZM Cohesive Zone Model

VCCT Virtual Crack Closure Technique

FUMD Fully-Uncoupled Multi-Directional

Contents

Part I

Basic concepts

Chapter 1

Composite materials, laminates and delamination

1.1 Introduction

The aim of this chapter is to introduce the reader to the context, the motivation and the purpose of this study. A logic line is drawn from the broad generic background of composite materials to the very specific issue to be faced. To this aim, Section 1.2 starts by introducing the concept of *composite materials*, and telling why the aerospace industry has major interests in such materials. Section 1.3 restricts the discussion to a particular type of composites: *laminates*. It also explains why they are ideal candidates to build efficient structures. Nonetheless, laminates may suffer from different damage mechanisms that may lead them to failure; these are described in Section 1.4. Section 1.5 focuses on the mechanism of delamination and gives a general perspective about it. Section 1.6 brings to the reader's attention the major limitations affecting our current knowledge on delamination. Addressing some of these limitations is the purpose of this study, as explained in Section 1.7.

1.2 Composites and the aerospace industry

The term *composites* is used to refer to those materials composed by two or more constituents, which are present in separate phases [1]. While many composite materials already exist in nature, man-made composites are created by combining different constituents in order to obtain a new material that better suits the designer's needs. Thanks to the broad range of possible combinations, composites are used in many different fields. This whole study is concerned with composite materials typically employed for structural applications, and in particular with long fibre reinforced composites. These materials are used in a variety of structural applications in different sectors [2, 3, 4], the reason being their extremely interesting mechanical properties.

When it comes to structural composites, the aerospace industry is one of the most relevant stakeholders in the field [5, 6]. As a matter of fact, these materials, when compared to metals, often allow to build more efficient and lightweight structures, a major driver in the sector [7]. In order to achieve these structural performances, low density materials exhibiting excellent strength-to-weight and stiffness-to-weight ratios are required. Continuous fibre reinforced composites are, at present, the ones that best respond to these

needs, and consequently the most used. Such composites are made of two phases: a relatively weak binder, or matrix, and much stiffer and stronger fibres, acting as a reinforcement, see Fig. 1.1. The matrix is a continuous phase that holds together the fibres.
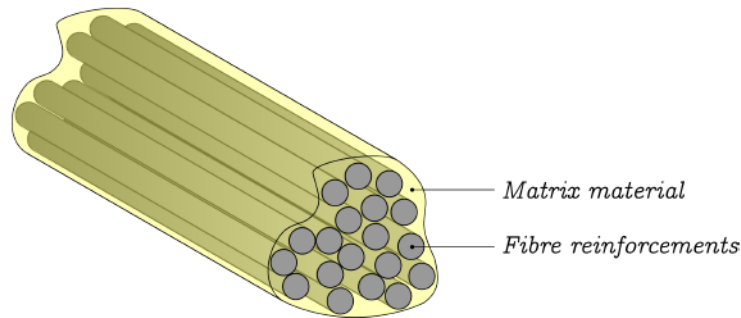
Figure 1.1: Schematic representation of a continuous fibre reinforced composite, with reference to its main constituents.

It transfers loads to the fibres, and carries some loads itself. It protects and insulates the fibres from the environment, thus preventing deterioration and/or corrosion. Most often, polymers are used as matrix materials, because they allow to obtain cost effective composites. Metals and ceramics are much more expensive and are used only for limited specific applications. Fibre reinforcements are the element giving strength and stiffness to the composite. Their mechanical properties are even better than those of the corresponding bulk material [8]. This is because of the reduced number of defects that they contain and, in some cases, to the preferential orientation of molecules along the fibre direction. The most common fibres used for structural composites are carbon fibre, glass fibres, aramid fibres and boron fibres.

1.3   From composites to laminates

As explained in Section 1.2, high-performance structural composites may be obtained by combining stiff and strong fibre reinforcements with weaker matrix materials that holds them together. However, the stiffening and strengthening effects given by fibres are significant only in the fibre direction, while mechanical properties in other directions are matrix dominated, and so poor. To overcome this problem, fibres should be distributed along multiple directions. In order to achieve this goal, layered structures, or *laminates*, are used. In a laminate many different layers, or *laminae* (also called plies), are stacked together. Most often, pre-impregnated (or *prepreg*) laminae are used, even if this is not the only solution. Prepreg laminae consist in thin layers of composite material in which the fibres have already been impregnated by the resin, which is not cured yet. Each lamina may be placed with the desired orientation.

In addition, a lamina can be *unidirectional* (UD), if it contains fibres that are straight and all oriented along the same direction, or it can contain *fabrics*, in which fibres are oriented along two or more directions. Due to the fact that out-of-plane fibre waviness in fabrics weakens mechanical properties, laminates obtained by stacking UD laminae are preferred when such properties are important. For this reason, UD laminae are usually preferred for important structural applications. According to the orientations of its laminae, a laminate can be itself unidirectional (UD), if all laminae are oriented in the same direction, or *multidirectional* (MD), if laminae assume different orientations. In almost

25

all practical applications, MD laminates are used, in order to ensure good mechanical properties along several directions. Nowadays, composite laminates are adopted in many primary structures.

Variable Angle Tow (VAT) laminates

Recently, developments of new manufacturing processes, such as Automated Fibre Placement (AFP), have led to the appearance of a novel type of laminates, called *Variable Angle Tow* (VAT) composites [9, 10]. In these materials, fibres are placed along curvilinear patterns, differently from classical straight-fibres laminates. As a consequence, the material properties (stiffness, strength, etc.) change point-wise in the laminate. This offers designers the possibility to tailor structural components, in order to obtain more efficient lightweight structures [11, 12, 13]. Of course, design using VAT laminate is much more complex than using classic laminates, but research is actively ongoing [14, 15, 16].

1.4 Damage mechanisms of laminates

With the adoption of composite laminates for many safety critical structures, it is of paramount importance to guarantee their reliability [8, 17]. To do that, it is necessary to thoroughly study and understand the possible damage and failure mechanisms of this relatively new class of materials.

Composite laminates may exhibit different damage mechanisms, taking place at different length scales [18, 19, 20, 21]:

- **fibre-matrix debonding**: it is the separation at the interface between matrix and fibres [22, 23], Fig. 1.2 [24]. This type of damage is difficult to observe due to its microscopic scale. It may also be the precursor to other damage mechanisms, such as matrix cracking;

50 µm
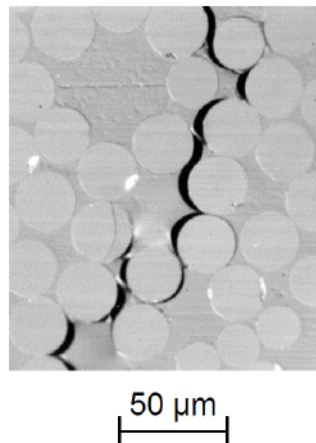
Figure 1.2: Micrograph of fibre-matrix debonds coalescing [24].

- **matrix cracking**: it is a common and dangerous damage mechanism in laminates [25], Fig. 1.3 [26]. It reduces the mechanical properties of the structure and it may facilitate the appearance of other types of damage;

26
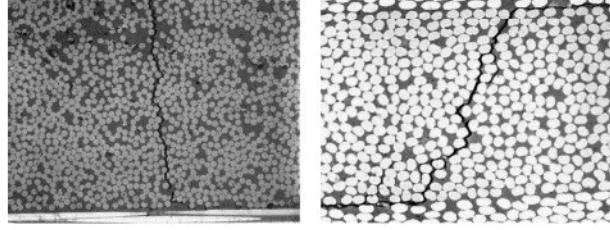
Figure 1.3: Examples of matrix cracks in different laminates [26].

- **fibre fracture**: fibres may fail in region of stress concentration (e.g. caused by matrix cracking or voids). Isolate fibres may fail (due to the statistical distribution of strength) and lead to subsequent failure of other fibres in the same region, originating clusters of failed fibres, Fig. 1.4 [27];
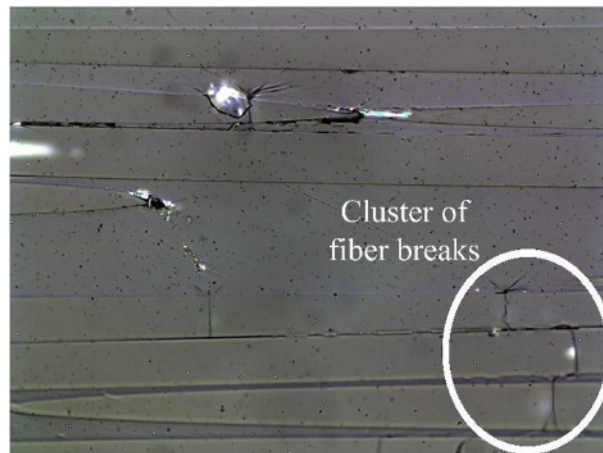
Figure 1.4: Experimentally observed fibre breaks during uniaxial tension–tension fatigue tests of a glass/epoxy composite [27].

- **delamination**: it is the separation at the interface between layers of a laminate, Fig. 1.5 [28]. Usually this is a resin rich region, which makes it particularly weak and prone to fail.
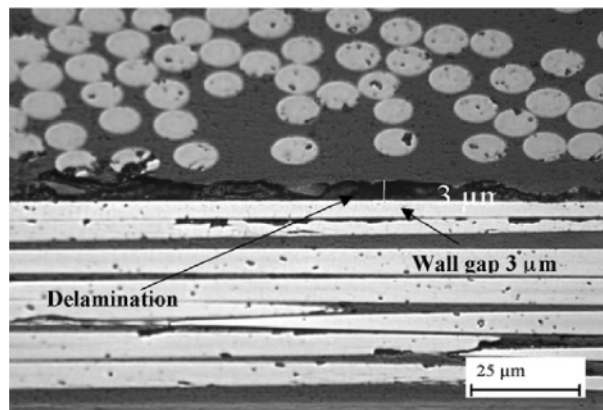
Figure 1.5: Delamination between two differently oriented composite laminae [28].

27

All these different damage mechanisms may interact with each other and give rise to extremely complex damage scenarios.

To prevent primary structures from failing, they often have to be designed using a *damage tolerant* [29, 30, 31, 32] approach: the structure is conceived and realised such that an hypothetical damage cannot reach a critical (i.e.: leading to failure) size in a time shorter than that between two consecutive inspections. Of course, to adopt such an approach, the damage mechanisms of the structure must be known in extreme depth. Any lack of knowledge in this regard must be compensated by a coefficient of safety, that in turn leads to additional structural weight and its nefarious consequences: inefficiency, costs and pollution.

1.5 The problem of delamination

It is then evident that a better knowledge of how damage appears and evolves in composite laminates could lead to better structural design.

Among the different damage mechanisms of composite laminates, delamination is one of the most critical [33, 34, 35, 36, 37, 38, 39]. It consists in a separation between laminae. It may appear and grow inside a component without being noticeable from the outside, which makes it extremely dangerous. Moreover, it drastically reduces the mechanical properties of structures [40], especially in compression [41], which is already a weak point for long fibres composites.

For this reason, both the academy and the industry have invested a lot to study delamination. Nowadays, concepts derived from Linear Elastic Fracture Mechanics (LEFM) are used to describe the delamination behaviour of composite materials [42, 43, 44, 45]. In particular, to evaluate the delamination (or *interlaminar*) fracture toughness of the material, the concept of critical strain Energy Release Rate (ERR), i.e. the energy required for unit area propagation of delamination, introduced by Irwin [46, 47], is commonly used. Test procedures to evaluate the critical ERR, under different loading conditions (or *modes*), have been proposed, studied, improved, and eventually standardised [43, 48, 49, 50, 51]. These interlaminar fracture toughness tests are a fundamental part of the characterisation (and certification) of composite materials. The information they provide are critical to an efficient and safe design of composite structures.

1.6 Delamination and multidirectional laminates

Despite the extensive research effort, all existing standard procedures for interlaminar fracture toughness characterisation have been originally conceived for UD reinforced materials and for UD stacking sequences, having an initial delamination front perpendicular to the fibre direction. Thus, when evaluating interlaminar fracture toughness of a composite according to standards, only one very specific delamination interface (i.e. the one between two equally oriented layers, also referred to as *UD interface* hereafter), under one very specific propagation condition (i.e. propagation in a direction parallel to the fibre orientation), is considered. On the other hand, virtually all real structures are built using MD laminates, in which delamination may appear in any interface (also those between differently oriented layers, referred to as *MD interfaces* hereafter) and may propagate in any direction with respect to the fibre orientation. In this situation, the interlaminar fracture toughness of the material may be different from that obtained in standard tests on

UD interfaces [52, 53]. Consequently, since the '80s, many studies have been carried out to try and characterise fracture toughness in MD interfaces. However, more than twenty years later, a comprehensive review [54] on several experimental studies conducted up to then outlined the fact that no general trend could be found to describe in a rigorous way all results, which in some cases appeared to be even contrasting. Even later, another in-depth review on delamination resistance testing of composites [48], with an emphasis on standardisation of test methods, reached the following conclusion:

"Developing suitable testing and analysis procedures for the determination of the delamination resistance of multidirectional laminates under quasi-static and fatigue loading in the different modes remains a challenge."

As of today, the challenge is still open: no general consensus has been reached by the scientific community and therefore standard procedures for determination of delamination resistance of MD laminates do not exist yet.

1.7 Motivation for this study

Despite no definitive solution has been found to evaluate interlaminar fracture toughness in MD interfaces, the contribution by researchers in the literature is considerable. Nowadays, thanks to this important effort, the main issues have been identified and are currently under investigation.

One first important issue, arising during experiments, is the appearance of additional damage mechanisms other than delamination [55, 56]. Of course, this should be avoided, if possible, in order to obtain a sound characterisation of interlaminar properties of the material.

Another big obstacle is a distinctive feature of MD laminates (and so MD delamination specimens) themselves: their intrinsically coupled behaviour [57, 58, 59, 60]. Indeed, thermal effects and elastic couplings existing in MD laminates are the cause of a series of problems that complicate experimental practices, lead to inaccuracies and may even invalidate experimental results and data reduction theories. If standard procedures for interlaminar fracture toughness testing of MD laminates are to be developed, a way to avoid these problems must be found. **Therefore, the purpose of this study is to design MD stacking sequences for delamination specimens that could solve, for the very first time, all problems related to laminate-level thermal effects and elastic couplings, and concurrently allow to test any type of MD delamination interface.**

Reaching such a goal could lead to many positive consequences. Firstly, it would likely be an important step toward the standardisation of interlaminar fracture toughness testing of MD laminates. This, in turn, would be beneficial for the qualification new materials, for screening during materials selection and to develop new interface-dependent delamination failure criteria. Secondly, the chance to have MD delamination specimens free of thermal effects and elastic couplings would allow the scientific community to study other problems (such as delamination migration) without undesired interference. Eventually, it would make possible to study in detail the effect of the local orientation of fibres on the delamination process, a subject of fundamental importance in the design of VAT laminates.

1.8 Concluding remarks

In this chapter, the context, the motivation and the purpose of the present study were presented. Starting from the general concept of composite materials and their interest in the aerospace sector, the focus has been then narrowed to the phenomenon of delamination in structural composite laminates. Specifically, delamination in MD laminates has been shown to be an active topic of research, with some major issues yet to be solved. Among these issues, elastic couplings and thermal effects represent big obstacles to interlaminar fracture toughness characterisation of MD laminates. While this chapter was designed to provide a short and simple, yet complete, introduction, Chapter 2 and Chapter 3 will provide more in-depth contents. In more detail, Chapter 2 will present some analytical tools that will be useful for different scopes: first, they will be used in the following of the manuscript to obtain some of the most important results of this study; second, they will allow a deeper understanding of the problems to be solved, and of the detailed literature review on delamination in MD laminates presented in Chapter 3.

Chapter 2

Mechanics of composite laminates

2.1 Introduction

In Chapter 1, it was stated that the purpose of this study is to design MD layups for delamination specimens that could solve all problems related to elastic couplings and undesired thermal effects.

The first step toward this goal is to understand what elastic couplings and thermal effects in a laminate are, and to define a theoretical framework in which they can be analysed. Hence, the mechanical behaviour of a laminate need to be formalised by means of an appropriate mathematical representation. This is what is done in this chapter.

In Section 2.2, the behaviour of a general anisotropic material as described by the generalised Hooke's constitutive law is introduced. Two reduced notations, proposed by Voigt and Kelvin, that allow to express Hooke's law in matrix form, are then presented. Contrarily to what happens in the great majority of books on the subject, the choice made here was to use Kelvin's notation, rather than Voigt's one. The reasons for this choice will be made clear in this chapter. Afterwards, the effects of a frame rotation on Hooke's law are explained. This allows to introduce the different elastic symmetries and the technical constants of elasticity.

Section 2.3 opens with a brief introduction on the behaviour of a composite lamina. Then, the behaviour of a laminate is formalised in terms of the Classical Laminated Plate Theory (CLPT). The results of this theory are then specialised to the case of laminates made with identical plies. Moreover, an overview of the most common laminate types employed in industrial applications is presented. In particular, they are classified first in terms of elastic properties, and then in terms of characteristics (e.g. symmetry) of their stacking sequence. To end the chapter, the most important results of CLPT are extended to include thermoelastic effects.

2.2 General anisotropic elasticity

2.2.1 Generalised Hooke's law

Anisotropic elasticity gives the constitutive laws describing the elastic relationship between strains and stresses in anisotropic materials. In order to derive such constitutive equations, some assumptions are made:

1. material coefficients in constitutive laws do not change with respect to time. Phenomena such as creep and stress relaxation are not taken into account;

2. the material behaviour is assumed to be linear and elastic;

3. strains are assumed to be infinitesimal.

Under these assumptions, the material strain in a body is defined by the infinitesimal strain tensor ϵ [61], while the stress state is described by Cauchy's stress tensor $\boldsymbol{\sigma}$; both are symmetric second order tensors, thus having six independent components. If we define $\boldsymbol{\sigma}^0$ as a general initial stress state, the most general constitutive law to describe the material behaviour is [61, 62]:

$$\boldsymbol{\sigma} = \mathbb{E}\boldsymbol{\epsilon} + \boldsymbol{\sigma}^0\,,$$
$$\sigma_{ij} = E_{ijkl}\epsilon_{kl} + \sigma_{ij}^0\,. \tag{2.1}$$

Here, $\mathbb{E}$ is a fourth order tensor called the *stiffness elasticity tensor* (or simply *elasticity tensor*) of the material. Its 81 components represent the proportionality constants among components of the stress and strain tensors. Equation (2.1) is best known as *generalised Hooke's law*. Due to the symmetry of tensor $\boldsymbol{\sigma}$, it is:

$$\sigma_{ij} = \sigma_{ji} \;\Rightarrow\; E_{ijkl}\epsilon_{kl} = E_{jikl}\epsilon_{kl} \;\Rightarrow\; E_{ijkl} = E_{jikl}\,, \tag{2.2}$$

while the symmetry of tensor $\boldsymbol{\epsilon}$ implies:

$$\epsilon_{ij} = \epsilon_{ji} \;\Rightarrow\; E_{ijkl}\epsilon_{kl} = E_{ijlk}\epsilon_{lk} = E_{ijkl}\epsilon_{lk} \;\Rightarrow\; E_{ijkl} = E_{ijlk}\,. \tag{2.3}$$

Eqs. (2.2) and (2.3) are the so-called *minor symmetries*, and reduce the number of independent component of tensor $\mathbb{E}$ from 81 to 36. For a linear elastic anisotropic material under infinitesimal deformation it is possible to define the *strain energy density* (or *elastic potential*) V, such that:

$$\sigma_{ij} = \frac{\partial V}{\partial \epsilon_{ij}} = E_{ijkl}\epsilon_{kl} + \sigma_{ij}^0\,, \tag{2.4}$$

and thus:

$$\frac{\partial^2 V}{\partial \epsilon_{ij}\partial \epsilon_{kl}} = E_{ijkl}\,. \tag{2.5}$$

In Eq. (2.5), the order of differentiation is arbitrary, so that:

$$E_{ijkl} = \frac{\partial^2 V}{\partial \epsilon_{ij}\partial \epsilon_{kl}} = \frac{\partial^2 V}{\partial \epsilon_{kl}\partial \epsilon_{ij}} = E_{klij} \;\Rightarrow\; E_{ijkl} = E_{klij}\,. \tag{2.6}$$

Eq. (2.6) is the *major symmetry* of tensor $\mathbb{E}$, and further reduces its independent components down to 21. Hence, 21 is the highest number of independent moduli that an elastic material can have. Such a material is referred to as *completely anisotropic* or *triclinic*.

The generalised Hooke's law, Eq. (2.1), may also be inverted as follows:

$$\boldsymbol{\epsilon} = \mathbb{Z}\boldsymbol{\sigma} + \boldsymbol{\epsilon}^0\,, \tag{2.7}$$
$$\boldsymbol{\epsilon}^0 = \mathbb{E}^{-1}\boldsymbol{\sigma}^0\,, \tag{2.8}$$
$$\mathbb{Z} = \mathbb{E}^{-1}\,, \tag{2.9}$$

where tensor $\mathbb{Z}$ is the *compliance elasticity tensor* (or simply *compliance tensor*).

2.2.2 Reduced notations

As seen in Eq. (2.1), the tensor representation of Hooke's law requires the use of four indexes, which may be impractical for engineering purposes. However, it was observed in Subsection 2.2.1 that both tensors ϵ and σ, being symmetric, have only six independent components. They are related by tensor $\mathbb{E}$, that has 21 independent components in the most general case. This allows to adopt some particular notations that transform tensors ϵ, σ and $\mathbb{E}$ in order to obtain a matrix representation of Eq. (2.1).

Here, two notations are introduced. The first one is Voigt's notation [63]. It is the most widely known, but it brings some disadvantages. The second is Kelvin's notation, which is less known and used, but has arguably interesting advantages [64].

Voigt's notation

According to Voigt's approach, tensors ϵ and σ may be rewritten as 6-components vectors:

$$\{\sigma\} = \begin{Bmatrix} \sigma_1 = \sigma_{11} \\ \sigma_2 = \sigma_{22} \\ \sigma_3 = \sigma_{33} \\ \sigma_4 = \sigma_{23} \\ \sigma_5 = \sigma_{31} \\ \sigma_6 = \sigma_{12} \end{Bmatrix} , \quad \{\epsilon\} = \begin{Bmatrix} \epsilon_1 = \epsilon_{11} \\ \epsilon_2 = \epsilon_{22} \\ \epsilon_3 = \epsilon_{33} \\ \epsilon_4 = 2\epsilon_{23} \\ \epsilon_5 = 2\epsilon_{31} \\ \epsilon_6 = 2\epsilon_{12} \end{Bmatrix} . \tag{2.10}$$

In the following, as in Eq. (2.10), braces are used to remember that a matrix representation, and not a tensor one, is being used. The multiplying coefficient 2 appearing in terms ϵ_4, ϵ_5 and ϵ_6 is a consequence of the symmetries of tensors ϵ and σ in Hooke's law. Eq. (2.10) shows the indexes transformation rule adopted in Voigt's notation (the transformation is reported also for the case of reference frames using x, y, z indexes):

$$11 \to 1, \quad 22 \to 2, \quad 33 \to 3, \quad 23 \to 4, \quad 31 \to 5, \quad 12 \to 6,$$
$$xx \to x, \quad yy \to y, \quad zz \to z, \quad yz \to q, \quad zx \to r, \quad xy \to s. \tag{2.11}$$

A useful trick to correctly associate indexes 4, 5 and 6 of Voigt's notation to the corresponding tensor components is to remember that the former are obtained as $9 - (i + j)$, where i and j are the indexes of the latter. Correspondingly, tensor $\mathbb{E}$ is transformed in a 6x6 symmetric matrix, its symmetry being a consequence of the major symmetry of $\mathbb{E}$, Eq. (2.6). Such matrix is referred to as $[C]$ (brackets are used to remark that $[C]$ is expressed in matrix notation), to avoid confusions with tensor $\mathbb{E}$. With this notation, Eq. (2.1) is reduced to (for an initially unstressed condition, $\sigma^0 = 0$):

$$\{\sigma\} = [C]\{\epsilon\} \to \begin{Bmatrix} \sigma_1 \\ \sigma_2 \\ \sigma_3 \\ \sigma_4 \\ \sigma_5 \\ \sigma_6 \end{Bmatrix} = \begin{bmatrix} C_{11} & C_{12} & C_{13} & C_{14} & C_{15} & C_{16} \\ C_{12} & C_{22} & C_{23} & C_{24} & C_{25} & C_{26} \\ C_{13} & C_{23} & C_{33} & C_{34} & C_{35} & C_{36} \\ C_{14} & C_{24} & C_{34} & C_{44} & C_{45} & C_{46} \\ C_{15} & C_{25} & C_{35} & C_{45} & C_{55} & C_{56} \\ C_{16} & C_{26} & C_{36} & C_{46} & C_{56} & C_{66} \end{bmatrix} \begin{Bmatrix} \epsilon_1 \\ \epsilon_2 \\ \epsilon_3 \\ \epsilon_4 \\ \epsilon_5 \\ \epsilon_6 \end{Bmatrix} . \tag{2.12}$$

Thanks to the introduction of coefficient 2 in ϵ_4, ϵ_5 and ϵ_6, the elements of matrix $[C]$ have a direct correspondence (by applying the indexes relationship Eq. (2.11)) to those of tensor $\mathbb{E}$:

$$[C_{ij}] = \begin{bmatrix} [E_{ppqq}] & [E_{pprs}] \\ [E_{pprs}] & [E_{pqrs}] \end{bmatrix} ; \quad i, j = 1, ..., 6; \quad p, q, r, s = 1, 2, 3. \tag{2.13}$$

Eq. (2.12) may be inverted to obtain:

$$
\{\epsilon\} = [S]\{\sigma\} \rightarrow
\begin{Bmatrix}
\epsilon_1 \\ \epsilon_2 \\ \epsilon_3 \\ \epsilon_4 \\ \epsilon_5 \\ \epsilon_6
\end{Bmatrix}
=
\begin{bmatrix}
S_{11} & S_{12} & S_{13} & S_{14} & S_{15} & S_{16} \\
S_{12} & S_{22} & S_{23} & S_{24} & S_{25} & S_{26} \\
S_{13} & S_{23} & S_{33} & S_{34} & S_{35} & S_{36} \\
S_{14} & S_{24} & S_{34} & S_{44} & S_{45} & S_{46} \\
S_{15} & S_{25} & S_{35} & S_{45} & S_{55} & S_{56} \\
S_{16} & S_{26} & S_{36} & S_{46} & S_{56} & S_{66}
\end{bmatrix}
\begin{Bmatrix}
\sigma_1 \\ \sigma_2 \\ \sigma_3 \\ \sigma_4 \\ \sigma_5 \\ \sigma_6
\end{Bmatrix}.
\tag{2.14}
$$

In the case of Eq. (2.14), the consequence of the factor 2 in ϵ_4, ϵ_5 and ϵ_6 is that the components of matrix [S] are not equal to the corresponding components of tensor $\mathbb{Z}$. In more detail:

$$
[S_{ij}] =
\begin{bmatrix}
[Z_{ppqq}] & 2[Z_{pprs}] \\
2[Z_{pprs}] & 4[Z_{pqrs}]
\end{bmatrix}
; \quad i,j = 1,...,6; \quad p,q,r,s = 1,2,3.
\tag{2.15}
$$

To conclude, using Voigt's notation allows for a simplified matrix representation of Hooke's law. However, the difference in the definition of vectors $\{\sigma\}$ and $\{\epsilon\}$ (namely, the factor 2 appearing in $\{\epsilon\}$), bring some disadvantages. First, when rotating the reference frame, care must be paid, as vectors $\{\sigma\}$ and $\{\epsilon\}$ will transform in different ways. The same is true for matrices [C] and [S]. Additionally, it was already observed that a direct correspondence exists between the elements of $\mathbb{E}$ and [C], but not between those of $\mathbb{Z}$ and [S].

Kelvin's notation

Kelvin's notation, while being less known than Voigt's one, presents some advantages. The stress and strain tensors are transformed as follows:

$$
\{\sigma\} =
\begin{Bmatrix}
\sigma_1 = \sigma_{11} \\
\sigma_2 = \sigma_{22} \\
\sigma_3 = \sigma_{33} \\
\sigma_4 = \sqrt{2}\sigma_{23} \\
\sigma_5 = \sqrt{2}\sigma_{31} \\
\sigma_6 = \sqrt{2}\sigma_{12}
\end{Bmatrix}
, \quad
\{\epsilon\} =
\begin{Bmatrix}
\epsilon_1 = \epsilon_{11} \\
\epsilon_2 = \epsilon_{22} \\
\epsilon_3 = \epsilon_{33} \\
\epsilon_4 = \sqrt{2}\epsilon_{23} \\
\epsilon_5 = \sqrt{2}\epsilon_{31} \\
\epsilon_6 = \sqrt{2}\epsilon_{12}
\end{Bmatrix}.
\tag{2.16}
$$

In this case, the factor 2 is equally distributed among stresses and strains. This way, there is no difference between stress and strain when transforming from tensor to matrix notation: matrices [C] and [S] are obtained similarly from tensors $\mathbb{E}$ and $\mathbb{Z}$, respectively. Indeed, we have:

$$
[C_{ij}] =
\begin{bmatrix}
[E_{ppqq}] & \sqrt{2}\,[E_{pprs}] \\
\sqrt{2}\,[E_{pprs}] & 2[E_{pqrs}]
\end{bmatrix}
; \quad i,j = 1,...,6; \quad p,q,r,s = 1,2,3.
\tag{2.17}
$$

$$
[S_{ij}] =
\begin{bmatrix}
[Z_{ppqq}] & \sqrt{2}\,[Z_{pprs}] \\
\sqrt{2}\,[Z_{pprs}] & 2[Z_{pqrs}]
\end{bmatrix}
; \quad i,j = 1,...,6; \quad p,q,r,s = 1,2,3.
\tag{2.18}
$$

Eqs. (2.12) and (2.14) still hold:

$$
\{\sigma\} = [C]\{\epsilon\},
\tag{2.19}
$$

$$
\{\epsilon\} = [S]\{\sigma\}.
\tag{2.20}
$$

It was shown in [65] that matrices [C] and [S] obtained using Kelvin's notation may be interpreted as representations of second order tensors in $\mathbb{R}^6$. An interesting consequence is that rotation of these matrices is made using the same transformation matrix, while this is not the case using Voigt's notation. In general, the adoption of Kelvin's notation allows to obtain a great simplification in analytical expressions. For this reason, Kelvin's notation will be used in the following of this manuscript.

2.2.3 Change of reference frame

In order to derive the constitutive laws even in the case of a change in the reference frame, the concepts of orthogonal tensors and of tensor conjugation product are here introduced. In the following, the ordinary 3D space of Euclidean geometry, indicated by $\mathcal{E}$, is considered. Each element of this space is a point, identified by its three geometrical coordinates. The vector space of translations associated with $\mathcal{E}$ is indicated by $\mathcal{V}$. Linear applications in $\mathcal{V}$ are represented by second-order tensors; the space of such application is Lin. Finally, $\mathbb{L}in$ is the space of linear applications in Lin, that is of fourth-order tensors.

Orthogonal tensors

A second order tensor is defined orthogonal when it preserves the inner product in the vector space $\mathcal{V}$:

$$\mathbf{U}\mathbf{v_1} \cdot \mathbf{U}\mathbf{v_2} = \mathbf{v_1} \cdot \mathbf{v_2} \quad \forall \mathbf{v_1}, \mathbf{v_2} \in \mathcal{V}. \tag{2.21}$$

In particular, angles between vectors and vector lengths are preserved. For these reasons, any rigid transformation of the vector space can be expressed by an orthogonal tensor. For orthogonal tensors the following relationships hold:

$$\mathbf{U}\mathbf{U}^T = \mathbf{U}^T\mathbf{U} = \mathbf{I}, \tag{2.22}$$

$$\mathbf{U}^{-1} = \mathbf{U}^T, \tag{2.23}$$

$$det(\mathbf{U}) = \pm 1. \tag{2.24}$$

An orthogonal tensor $\mathbf{U}$ with a positive determinant may represent a transformation that maintains the orientation of the vector space (e.g. rotation about an axis); one with a negative determinant may represent a transformation that changes the orientation of the vector space (e.g. symmetry with respect to a plane).

Tensor conjugation product

Given two second order tensors $\mathbf{A}$ and $\mathbf{B}$, it is possible to define their conjugation product $\mathbf{A} \boxtimes \mathbf{B}$ as:

$$(\mathbf{A} \boxtimes \mathbf{B})\mathbf{C} := \mathbf{A}\mathbf{C}\mathbf{B}^T \quad \forall \mathbf{C} \in Lin. \tag{2.25}$$

The conjugation product is a fourth order tensor. It can be shown that:

$$(\mathbf{A} \boxtimes \mathbf{B})_{ijkl} = A_{ik}B_{jl}, \tag{2.26}$$

$$(\mathbf{A} \boxtimes \mathbf{B})^T = \mathbf{A}^T \boxtimes \mathbf{B}^T. \tag{2.27}$$

For an orthogonal second order tensor $\mathbf{U}$ it is possible to define its orthogonal conjugator $\mathbb{U}$:

$$\mathbb{U} := \mathbf{U} \boxtimes \mathbf{U}\,,$$
$$\mathbb{U}_{ijkl} = U_{ik}U_{jl}\,. \tag{2.28}$$

Tensor $\mathbb{U}$ is an orthogonal tensor in the space of fourth order tensors; in other words it preserves the inner product of second order tensors:

$$\mathbb{U}\mathbf{A} \cdot \mathbb{U}\mathbf{B} = \mathbf{A} \cdot \mathbf{B} \quad \forall \mathbf{A}, \mathbf{B} \in Lin\,, \tag{2.29}$$

and verifies the following relationship:

$$\mathbb{U}\mathbb{U}^T = \mathbb{U}^T\mathbb{U} = \mathbb{I}\,, \tag{2.30}$$

where $\mathbb{I}$ is the fourth order identity tensor.

Change of reference frame: tensorial notation

In $\mathcal{V}$, we can define two different reference frames:

$$\mathcal{R} = \{o, \mathcal{B}\} \qquad \textit{with base} \quad \mathcal{B} = \{\mathbf{e}_1, \mathbf{e}_2, \mathbf{e}_3\}\,, \quad o \in \mathcal{E}\,, \tag{2.31}$$
$$\mathcal{R}' = \{o', \mathcal{B}'\} \qquad \textit{with base} \quad \mathcal{B}' = \{\mathbf{e}'_1, \mathbf{e}'_2, \mathbf{e}'_3\}\,, \quad o' \in \mathcal{E}\,. \tag{2.32}$$

The prime symbol indicates that a vector component is expressed with respect to base $\mathcal{B}'$; it will be used also for vectors and tensors whose components are meant to be expressed with respect to base $\mathcal{B}'$.

A reference frame transformation from $\mathcal{R}$ to $\mathcal{R}'$ is a rigid transformation of the vector space $\mathcal{V}$, that can be represented by an orthogonal second order tensor, $\mathbf{U}$. In particular, tensor $\mathbf{U}$ is defined by:

$$\mathbf{e}_i = \mathbf{U}\mathbf{e}'_i \ \Rightarrow \ \mathbf{e}'_i = \mathbf{U}^T \mathbf{e}_i\,. \tag{2.33}$$

Using tensor $\mathbf{U}$ and its orthogonal conjugator $\mathbb{U}$, Eq. (2.28), it is possible to express how vectors, second order tensors and fourth order tensors transform from one reference frame to the other. Respectively:

$$\mathbf{w}'_i = \mathbf{U}\mathbf{w}_i \ \Rightarrow \ w'_i = U_{ij}w_j\,. \tag{2.34}$$

$$\mathbf{L}' = \mathbf{U}\mathbf{L}\mathbf{U}^T = (\mathbf{U} \boxtimes \mathbf{U})\mathbf{L} = \mathbb{U}\mathbf{L} \ \Rightarrow \ L'_{ij} = U_{im}U_{jn}L_{mn}\,, \tag{2.35}$$

$$\mathbb{E}' = (\mathbf{U} \boxtimes \mathbf{U})\mathbb{E}(\mathbf{U} \boxtimes \mathbf{U})^T = \mathbb{U}\mathbb{E}\mathbb{U}^T \ \Rightarrow \ E'_{ijkl} = U_{im}U_{jn}U_{kp}U_{lq}E_{mnpq}\,. \tag{2.36}$$

Change of reference frame: Kelvin's notation

Eqs. (2.35) and (2.36) may be expressed in matrix form, if the matrix representation of tensor $\mathbb{U}$, $[R]$, is introduced:

$$[L'] = [R][L]\,, \tag{2.37}$$
$$[E'] = [R][E][R]^T\,. \tag{2.38}$$

If U_{ij} are the components of the orthogonal tensor **U** representing the transformation, matrix [R] is expressed by [65]:

$$[R] = \begin{bmatrix} U_{11}^2 & U_{12}^2 & U_{13}^2 & \sqrt{2}U_{12}U_{13} & \sqrt{2}U_{13}U_{11} & \sqrt{2}U_{11}U_{12} \\ U_{21}^2 & U_{22}^2 & U_{23}^2 & \sqrt{2}U_{22}U_{23} & \sqrt{2}U_{23}U_{21} & \sqrt{2}U_{21}U_{22} \\ U_{31}^2 & U_{32}^2 & U_{33}^2 & \sqrt{2}U_{32}U_{33} & \sqrt{2}U_{33}U_{31} & \sqrt{2}U_{31}U_{32} \\ \sqrt{2}U_{21}U_{31} & \sqrt{2}U_{22}U_{32} & \sqrt{2}U_{23}U_{33} & U_{23}U_{32}+U_{22}U_{33} & U_{33}U_{21}+U_{31}U_{23} & U_{31}U_{22}+U_{32}U_{21} \\ \sqrt{2}U_{31}U_{11} & \sqrt{2}U_{32}U_{12} & \sqrt{2}U_{33}U_{13} & U_{32}U_{13}+U_{33}U_{12} & U_{31}U_{13}+U_{33}U_{11} & U_{31}U_{12}+U_{32}U_{11} \\ \sqrt{2}U_{11}U_{21} & \sqrt{2}U_{12}U_{22} & \sqrt{2}U_{13}U_{23} & U_{11}U_{23}+U_{13}U_{22} & U_{11}U_{23}+U_{13}U_{21} & U_{11}U_{22}+U_{12}U_{21} \end{bmatrix} .$$

$$(2.39)$$

Matrix [R] is an orthogonal matrix of $\mathbb{R}^6$. Hence it may be thought as the representation of a second order tensor of the vector space $\mathbb{R}^6$. It is extremely important to remember that, using this notation, the stress tensor $\boldsymbol{\sigma}$ and the strain tensor $\boldsymbol{\epsilon}$ are represented in the same way. This translates into the fact that Eq. (2.37) applies to both tensors with the same matrix [R]. In other words:

$$\{\sigma'\} = [R]\{\sigma\}, \tag{2.40}$$

$$\{\epsilon'\} = [R]\{\epsilon\}. \tag{2.41}$$

Concerning matrix [C], in the two reference frames:

$$\{\sigma\} = [C]\{\epsilon\} \qquad in\ frame\ \mathcal{R}, \tag{2.42}$$

$$\{\sigma'\} = [C']\{\epsilon'\} \qquad in\ frame\ \mathcal{R}'. \tag{2.43}$$

Substituting Eqs. (2.40) and (2.41) in Eq. (2.43), one obtains:

$$[R]\{\sigma\} = [C'][R]\{\epsilon\} \quad \Rightarrow \quad \{\sigma\} = [R]^T[C'][R]\{\epsilon\}. \tag{2.44}$$

Using Eq. (2.42), the transformation equation for matrix [C] is obtained:

$$[C] = [R]^T[C'][R] \quad \Rightarrow \quad [C'] = [R][C][R]^T. \tag{2.45}$$

Similarly, for matrix [S]:

$$\{\epsilon\} = [S]\{\sigma\} \qquad in\ frame\ \mathcal{R}, \tag{2.46}$$

$$\{\epsilon'\} = [S']\{\sigma'\} \qquad in\ frame\ \mathcal{R}'. \tag{2.47}$$

Substituting Eqs. (2.40) and (2.41) in Eq. (2.47), the transformation equation for matrix [S] is obtained:

$$[R]\{\epsilon\} = [S'][R]\{\sigma\} \quad \Rightarrow \quad \{\epsilon\} = [R]^T[S'][R]\{\sigma\}, \tag{2.48}$$

$$[S] = [R]^T[S'][R] \quad \Rightarrow \quad [S'] = [R][S][R]^T. \tag{2.49}$$

Two general and extremely useful examples of reference frame transformation are the rotation about an axis and the symmetry with respect to a plane. Results for these cases are presented below.

Rotation about an axis

The particular case of the rotation of the reference frame about an axis is here detailed. If we assume a positive rotation of an angle δ about the axis x_3, tensor $\mathbf{U}$ has the following form:

$$\mathbf{U} = \begin{bmatrix} c & s & 0 \\ -s & c & 0 \\ 0 & 0 & 1 \end{bmatrix}, \quad c = cos(\delta), \quad s = sin(\delta). \tag{2.50}$$

Matrix $[R]$ is obtained from Eq. (2.39):

$$[R] = \begin{bmatrix} c^2 & s^2 & 0 & 0 & 0 & \sqrt{2}cs \\ s^2 & c^2 & 0 & 0 & 0 & -\sqrt{2}cs \\ 0 & 0 & 1 & 0 & 0 & 0 \\ 0 & 0 & 0 & c & -s & 0 \\ 0 & 0 & 0 & s & c & 0 \\ -\sqrt{2}cs & \sqrt{2}cs & 0 & 0 & 0 & c^2 - s^2 \end{bmatrix}. \tag{2.51}$$

Symmetry with respect to a plane

For the case of symmetry about a plane, assuming such plane to be $x_3 = 0$, tensor $\mathbf{U}$ and matrix $[R]$ become:

$$\mathbf{U} = \begin{bmatrix} 1 & 0 & 0 \\ 0 & 1 & 0 \\ 0 & 0 & -1 \end{bmatrix}, \quad [R] = \begin{bmatrix} 1 & 0 & 0 & 0 & 0 & 0 \\ 0 & 1 & 0 & 0 & 0 & 0 \\ 0 & 0 & 1 & 0 & 0 & 0 \\ 0 & 0 & 0 & -1 & 0 & 0 \\ 0 & 0 & 0 & 0 & -1 & 0 \\ 0 & 0 & 0 & 0 & 0 & 1 \end{bmatrix}. \tag{2.52}$$

2.2.4 Elastic symmetries

In Subsection 2.2.1, the behaviour of a general anisotropic material was formalised. Interestingly, not all materials have such a general behaviour. In fact, many materials possess one or more elastic symmetries. This means that the elastic behaviour do not change along specific directions, called *equivalent directions*. In other words, material properties are undistinguishable in an initial reference frame and in a transformed one obtained by exchanging some equivalent directions and leaving unchanged all the others. This translates into the fact that some relationships exist among the components of matrix $[C]$ (and therefore of tensor $\mathbb{E}$), thus reducing the number of independent material moduli. If $\mathcal{R}$ is the initial reference frame, and $\mathcal{R}'$ is the transformed one, according to the material symmetry considered, this means:

$$\{\sigma\} = [C]\{\epsilon\} \qquad in\ frame\ \mathcal{R}, \tag{2.53}$$

$$\{\sigma'\} = [C]\{\epsilon'\} \qquad in\ frame\ \mathcal{R}'. \tag{2.54}$$

Using Eqs. (2.40) and (2.41) in Eq. (2.54) one obtains:

$$[R]\{\sigma\} = [C][R]\{\epsilon\} \quad \Rightarrow \quad \{\sigma\} = [R]^T[C][R]\{\epsilon\}, \tag{2.55}$$

and equating to Eq. (2.53) it follows:

$$[C] = [R]^T[C][R]. \tag{2.56}$$

Eq. (2.56) gives the relationships among components of matrix [C] (and, correspondingly, of tensor $\mathbb{E}$) established by the elastic symmetry of the material. In the following, for the sake of brevity, only the most common material symmetries will be briefly recalled.

Monoclinic material

A material is defined *monoclinic* if it possesses one plane of symmetry. If we assume such plane to be $x_3 = 0$, using Eqs. (2.52) and (2.56), we obtain:

$$[C] = \begin{bmatrix} C_{11} & C_{12} & C_{13} & 0 & 0 & C_{16} \\ & C_{22} & C_{23} & 0 & 0 & C_{26} \\ & & C_{33} & 0 & 0 & C_{36} \\ & & & C_{44} & C_{45} & 0 \\ & sym & & & C_{55} & 0 \\ & & & & & C_{66} \end{bmatrix}. \tag{2.57}$$

Hence, 13 elastic constants are required to define the material behaviour.

Orthotropic material

A material is defined orthotropic when it has three orthogonal planes of symmetry. It is possible to demonstrate that symmetry with respect to two orthogonal planes implies also symmetry with respect to a third plane, orthogonal to the previous two. Here the symmetry planes, for the sake of simplicity, are assumed to coincide with the coordinate planes. Hence, matrix [C] is obtaining applying twice Eq. (2.56), each time with a matrix [R] corresponding to symmetry with respect to one coordinate plane. It follows:

$$[C] = \begin{bmatrix} C_{11} & C_{12} & C_{13} & 0 & 0 & 0 \\ & C_{22} & C_{23} & 0 & 0 & 0 \\ & & C_{33} & 0 & 0 & 0 \\ & & & C_{44} & 0 & 0 \\ & sym & & & C_{55} & 0 \\ & & & & & C_{66} \end{bmatrix}. \tag{2.58}$$

For such a material 9 constants are sufficient to describe the elastic behaviour. It is also easy to verify that for an orthotropic material matrix [S] has the same shape as matrix [C]:

$$[S] = \begin{bmatrix} S_{11} & S_{12} & S_{13} & 0 & 0 & 0 \\ & S_{22} & S_{23} & 0 & 0 & 0 \\ & & S_{33} & 0 & 0 & 0 \\ & & & S_{44} & 0 & 0 \\ & sym & & & S_{55} & 0 \\ & & & & & S_{66} \end{bmatrix}. \tag{2.59}$$

Transversely isotropic material

A material is defined as *transversely isotropic* when it possesses an axis of cylindrical symmetry. Hence the properties of the material do not change when expressed in two reference frames which differ by a rotation around this axis. For such a material the

elastic matrix is completely defined by 5 distinct elastic constant. If we assume the axis of symmetry to be x_3, using Eqs. (2.51) and (2.56), we obtain:

$$[C] = \begin{bmatrix} C_{11} & C_{12} & C_{13} & 0 & 0 & 0 \\ & C_{11} & C_{13} & 0 & 0 & 0 \\ & & C_{33} & 0 & 0 & 0 \\ & & & C_{44} & 0 & 0 \\ & sym & & & C_{44} & 0 \\ & & & & & C_{11} - C_{12} \end{bmatrix} . \qquad (2.60)$$

Isotropic material

Finally, an isotropic material is a material for which all directions are equivalent. Thus, its properties do not change with respect to the reference frame adopted. The elastic matrix of an isotropic material looks as follows:

$$[C] = \begin{bmatrix} C_{11} & C_{12} & C_{12} & 0 & 0 & 0 \\ & C_{11} & C_{12} & 0 & 0 & 0 \\ & & C_{11} & 0 & 0 & 0 \\ & & & C_{11} - C_{12} & 0 & 0 \\ & sym & & & C_{11} - C_{12} & 0 \\ & & & & & C_{11} - C_{12} \end{bmatrix} . \qquad (2.61)$$

In this case only two elastic constants are sufficient to describe the material behaviour.

2.2.5 The technical constants of elasticity

In engineering practice, the use of the so called *technical* or *engineering* constants is usually preferred to the use of the components C_{ij} of the elastic stiffness matrix. The technical constants are useful as they are usually measurable from simple laboratory tests and have a direct and obvious physical meaning. Since they must completely define the behaviour of the material, their number is, in the most general case, 21. However, similarly to what observed above, the number is reduced when the material considered possesses some elastic symmetries. For a complete treatise on the subject, the reader is addressed to [62]. Here, since orthotropic materials will be the most general case treated, only those engineering constants of interests are presented. Namely, they are:

1. Young's moduli: they measure the extension stiffness along the three reference axes:

$$E_i = \frac{\sigma_i}{\epsilon_i} ; \quad i = 1, 2, 3 ; \quad \sigma_i \neq 0 ; \quad \sigma_j = 0 \ \forall j \neq i ; \quad j = 1, ..., 6 ; \qquad (2.62)$$

2. Shear moduli: they measure the stiffness of the material with respect to shear:

$$G_{ij} = \frac{\sigma_k}{2\epsilon_k} ; \quad i, j = 1, 2, 3 ; \quad i \neq j ; \quad k = 4, 5, 6 ; \quad \sigma_k \neq 0 ;$$

$$\sigma_h = 0 \ \forall h \neq k ; \quad h = 1, ..., 6 ; \qquad (2.63)$$

3. Poisson's coefficients: they measure the deformation in a direction transversal to that of a normal stress applied:

$$\nu_{ij} = \frac{\epsilon_j}{\epsilon_i} ; \quad i, j = 1, 2, 3 ; \quad \sigma_i \neq 0 ; \quad \sigma_h = 0 \ \forall h \neq i ; \quad h = 1, ..., 6 . \qquad (2.64)$$

2.2.6 Thermoelasticity

In the previous subsections, the constitutive equations that describe the elastic behaviour of a material were derived for the isothermal case, that is, no effects of temperature were taken into account. However, they can be generalised in order to include thermal effects. Here, we assume that thermal variations happen at a slow rate, so that the temperature within the body may be considered uniform at all times (i.e. no thermal gradients within the body exist).

In general thermoelasticity, the total strain tensor of the material is given by the sum of a mechanical part and of a thermal part:

$$\epsilon = \epsilon_m + \epsilon_t. \tag{2.65}$$

The mechanical strain is obtained as in Eq. (2.7) (considering an initially unstrained condition):

$$\epsilon_m = \mathbb{Z}\boldsymbol{\sigma}, \tag{2.66}$$

while the thermal strain is assumed to be a linear function of the temperature change T:

$$\epsilon_t = T\boldsymbol{\alpha}. \tag{2.67}$$

The temperature change T is defined as the difference between actual temperature with respect to that of an unstrained condition ($T = T_{act}$ - T_0). From Eq. (2.67), $\boldsymbol{\alpha}$ is a second order symmetric tensor, which contains the Coefficients of Thermal Expansion (CTEs) of the material. Also this tensor may be represented by a 6-component vector using Kelvin's reduced notation. Eq. (2.65) may be rewritten to obtain:

$$\epsilon = \mathbb{Z}\boldsymbol{\sigma} + T\boldsymbol{\alpha}, \tag{2.68}$$

in tensor notation, and:

$$\{\epsilon\} = [S]\{\sigma\} + T\{\alpha\}, \tag{2.69}$$

in matrix notations. Eq. (2.68) is the *Duhamel-Neumann law* for anisotropic bodies. It may also be inverted to obtain:

$$\boldsymbol{\sigma} = \mathbb{E}(\epsilon - T\boldsymbol{\alpha}), \tag{2.70}$$

or, in matrix notation:

$$\{\sigma\} = [C](\{\epsilon\} - T\{\alpha\}). \tag{2.71}$$

2.3 Mechanics of composite laminates

2.3.1 Mechanics of a lamina

In order to model the behaviour of a laminate, that of a single lamina must be described first. To do so, the following assumptions are adopted:

1. the lamina acts as a continuum. In other words, the macro-mechanical behaviour of the lamina is considered;

2. the lamina material behaves in a linear elastic way; hence, the generalised Hooke's law may be used.

3D constitutive behaviour

Let us consider a lamina and its material frame $\mathcal{R} \equiv (x_1, x_2, x_3)$, Fig. 2.1. Under the assumptions made, the results of Section 2.2 may be used. In particular, a composite lamina may be modelled in different ways. If it is a unidirectional (UD) lamina, its
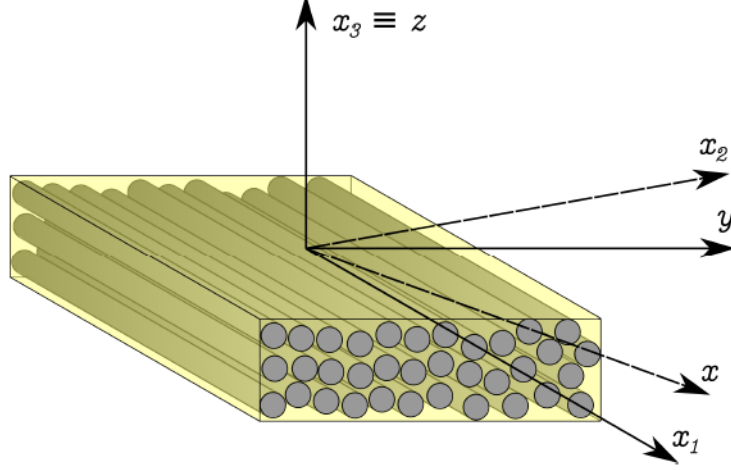
Figure 2.1: Lamina material frame and global reference frame.

behaviour is often assumed to be as transversely isotropic, with the fibres direction being the axis of cylindrical symmetry. If it is a fabric lamina with fibres in two perpendicular directions, then it may be modelled as an orthotropic material, whose orthotropy axes are the fibres directions and the axis normal to the lamina plane. Hence, in the most general case, an orthotropic behaviour may be assumed. The orthotropic behaviour of the lamina in its material frame is described by matrices [C] and [S], so that:

$$
\begin{Bmatrix} \sigma_1 \\ \sigma_2 \\ \sigma_3 \\ \sigma_4 \\ \sigma_5 \\ \sigma_6 \end{Bmatrix} = \begin{bmatrix} C_{11} & C_{12} & C_{13} & 0 & 0 & 0 \\ & C_{22} & C_{23} & 0 & 0 & 0 \\ & & C_{33} & 0 & 0 & 0 \\ & & & C_{44} & 0 & 0 \\ & sym & & & C_{55} & 0 \\ & & & & & C_{66} \end{bmatrix} \begin{Bmatrix} \epsilon_1 \\ \epsilon_2 \\ \epsilon_3 \\ \epsilon_4 \\ \epsilon_5 \\ \epsilon_6 \end{Bmatrix} \rightarrow \{\sigma\} = [C]\{\epsilon\}, \qquad (2.72)
$$

$$
\begin{Bmatrix} \epsilon_1 \\ \epsilon_2 \\ \epsilon_3 \\ \epsilon_4 \\ \epsilon_5 \\ \epsilon_6 \end{Bmatrix} = \begin{bmatrix} S_{11} & S_{12} & S_{13} & 0 & 0 & 0 \\ & S_{22} & S_{23} & 0 & 0 & 0 \\ & & S_{33} & 0 & 0 & 0 \\ & & & S_{44} & 0 & 0 \\ & sym & & & S_{55} & 0 \\ & & & & & S_{66} \end{bmatrix} \begin{Bmatrix} \sigma_1 \\ \sigma_2 \\ \sigma_3 \\ \sigma_4 \\ \sigma_5 \\ \sigma_6 \end{Bmatrix} \rightarrow \{\epsilon\} = [S]\{\sigma\}. \qquad (2.73)
$$

When forming a laminate, multiple laminae are superposed, and each lamina may be oriented differently from the others. The constitutive description of the laminate, however, has to be done with respect to one global reference frame $\mathcal{R}' \equiv (x, y, z)$, also called *laminate reference frame* hereafter, Fig. 2.1. Hence, material properties of each lamina have to be evaluated with respect to this latter frame. Matrices [C'] and [S'] describing the behaviour of the lamina in the laminate reference frame can be found using Eqs. (2.45) and (2.49). It can be observed that, due to the fact that laminae are stacked to build the laminate, axis z of the laminate reference frame will always coincide with

the material x_3 axis. Hence, the transformation going from one reference to the other is a simple rotation δ (positive counter-clockwise) around such axis. For this particular case, the transformation matrix $[R]$ has already been presented in Eq. (2.51). As a consequence, using such matrix and applying Eqs. (2.45) and (2.49) to (2.58) and (2.59), respectively, one obtains:

$$\begin{Bmatrix} \sigma_x \\ \sigma_y \\ \sigma_z \\ \sigma_q \\ \sigma_r \\ \sigma_s \end{Bmatrix} = \begin{bmatrix} C_{xx} & C_{xy} & C_{xz} & 0 & 0 & C_{xs} \\ & C_{yy} & C_{yz} & 0 & 0 & C_{ys} \\ & & C_{zz} & 0 & 0 & C_{zs} \\ & & & C_{qq} & C_{qr} & 0 \\ & sym & & & C_{rr} & 0 \\ & & & & & C_{ss} \end{bmatrix} \begin{Bmatrix} \epsilon_x \\ \epsilon_y \\ \epsilon_z \\ \epsilon_q \\ \epsilon_r \\ \epsilon_s \end{Bmatrix} \rightarrow \{\sigma'\} = [C']\{\epsilon'\}, \qquad (2.74)$$

$$\begin{Bmatrix} \epsilon_x \\ \epsilon_y \\ \epsilon_z \\ \epsilon_q \\ \epsilon_r \\ \epsilon_s \end{Bmatrix} = \begin{bmatrix} S_{xx} & S_{xy} & S_{xz} & 0 & 0 & S_{xs} \\ & S_{yy} & S_{yz} & 0 & 0 & S_{ys} \\ & & S_{zz} & 0 & 0 & S_{zs} \\ & & & S_{qq} & S_{qr} & 0 \\ & sym & & & S_{rr} & 0 \\ & & & & & S_{ss} \end{bmatrix} \begin{Bmatrix} \sigma_x \\ \sigma_y \\ \sigma_z \\ \sigma_q \\ \sigma_r \\ \sigma_s \end{Bmatrix} \rightarrow \{\epsilon'\} = [S']\{\sigma'\}. \qquad (2.75)$$

Reduced constitutive behaviour

An hypothesis adopted when developing equivalent single layer theories (such as CLPT), is that the normal stress component be negligible, $\sigma_3 = \sigma_z = 0$. Under such hypothesis of plane elasticity, using Eq. (2.20) and considering an orthotropic behaviour, one may obtain, in the lamina material reference frame:

$$\begin{Bmatrix} \epsilon_1 \\ \epsilon_2 \\ \epsilon_6 \end{Bmatrix} = \begin{bmatrix} S_{11} & S_{12} & 0 \\ S_{12} & S_{22} & 0 \\ 0 & 0 & S_{66} \end{bmatrix} \begin{Bmatrix} \sigma_1 \\ \sigma_2 \\ \sigma_6 \end{Bmatrix}, \qquad (2.76)$$

$$\begin{Bmatrix} \epsilon_4 \\ \epsilon_5 \end{Bmatrix} = \begin{bmatrix} S_{44} & 0 \\ 0 & S_{55} \end{bmatrix} \begin{Bmatrix} \sigma_4 \\ \sigma_5 \end{Bmatrix}, \qquad (2.77)$$

$$\epsilon_3 = S_{13}\sigma_1 + S_{23}\sigma_2. \qquad (2.78)$$

The components S_{ij} appearing in Eqs. (2.76)-(2.77) are exactly the same as those of the original 3D compliance matrix, Eq. (2.59). Eqs. (2.76) and (2.77) may be inverted to obtain:

$$\begin{Bmatrix} \sigma_1 \\ \sigma_2 \\ \sigma_6 \end{Bmatrix} = \begin{bmatrix} Q_{11} & Q_{12} & 0 \\ Q_{12} & Q_{22} & 0 \\ 0 & 0 & Q_{66} \end{bmatrix} \begin{Bmatrix} \epsilon_1 \\ \epsilon_2 \\ \epsilon_6 \end{Bmatrix}, \qquad (2.79)$$

$$\begin{Bmatrix} \sigma_4 \\ \sigma_5 \end{Bmatrix} = \begin{bmatrix} Q_{44} & 0 \\ 0 & Q_{55} \end{bmatrix} \begin{Bmatrix} \epsilon_4 \\ \epsilon_5 \end{Bmatrix}. \qquad (2.80)$$

In Eqs. (2.79) and (2.80), terms Q_{ij} are different from the corresponding terms of the complete matrix $[C]$, as they are obtained by inversion of Eqs. (2.76) and (2.77). For this reason they are called *reduced stiffnesses* and indicated by a different letter. When Eqs.

(2.76) and (2.77) are expressed in the laminate reference frame, they become:

$$
\begin{Bmatrix} \epsilon_x \\ \epsilon_y \\ \epsilon_s \end{Bmatrix} = \begin{bmatrix} S_{xx} & S_{xy} & S_{xs} \\ S_{xy} & S_{yy} & S_{ys} \\ S_{xs} & S_{ys} & S_{ss} \end{bmatrix} \begin{Bmatrix} \sigma_x \\ \sigma_y \\ \sigma_s \end{Bmatrix} , \tag{2.81}
$$

$$
\begin{Bmatrix} \epsilon_q \\ \epsilon_r \end{Bmatrix} = \begin{bmatrix} S_{qq} & S_{qr} \\ S_{qr} & S_{rr} \end{bmatrix} \begin{Bmatrix} \sigma_q \\ \sigma_r \end{Bmatrix} , \tag{2.82}
$$

and thus, in terms of reduced stiffnesses:

$$
\begin{Bmatrix} \sigma_x \\ \sigma_y \\ \sigma_s \end{Bmatrix} = \begin{bmatrix} Q_{xx} & Q_{xy} & Q_{xs} \\ Q_{xy} & Q_{yy} & Q_{ys} \\ Q_{xs} & Q_{ys} & Q_{ss} \end{bmatrix} \begin{Bmatrix} \epsilon_x \\ \epsilon_y \\ \epsilon_s \end{Bmatrix} , \tag{2.83}
$$

$$
\begin{Bmatrix} \sigma_q \\ \sigma_r \end{Bmatrix} = \begin{bmatrix} Q_{qq} & Q_{qr} \\ Q_{qr} & Q_{rr} \end{bmatrix} \begin{Bmatrix} \epsilon_q \\ \epsilon_r \end{Bmatrix} . \tag{2.84}
$$

2.3.2 Thermoelastic behaviour of a lamina

From a thermoelastic point of view, the behaviour of the lamina is described by the vector of CTEs, $\{\alpha\}$. It may be assumed that, in the material reference frame of the lamina, the only non-null components of such vector be α_1, α_2 and α_3; this means that a change in temperature causes only contraction or expansion in the three principal material directions. The 3D thermoelastic constitutive behaviour in the material reference frame of the lamina is thus obtained from Eqs. (2.69) and (2.71):

$$
\{\epsilon\} = [S]\{\sigma\} + T\{\alpha\} , \tag{2.85}
$$

$$
\{\sigma\} = [C](\{\epsilon\} - T\{\alpha\}) , \tag{2.86}
$$

in which matrices [S] and [C] possess the form already seen in Eqs. (2.73) and (2.72) respectively.

If the 3D thermoelastic constitutive behaviour is described with respect to the laminate reference frame, also vector $\{\alpha\}$ transforms due to the change in reference frame. In particular, it transforms in the same way strains do, according to Eq. (2.41). Eqs. (2.85) and (2.86) then become:

$$
\{\epsilon'\} = [S']\{\sigma'\} + T\{\alpha'\} , \tag{2.87}
$$

$$
\{\sigma'\} = [C'](\{\epsilon'\} - T\{\alpha'\}) , \tag{2.88}
$$

in which matrices [S] and [C] are the same as in Eqs. (2.75) and (2.74) respectively.

The reduced constitutive behaviour of the lamina in its material frame, expressed by Eqs. (2.76), (2.79), now becomes:

$$
\begin{Bmatrix} \epsilon_1 \\ \epsilon_2 \\ \epsilon_6 \end{Bmatrix} = \begin{bmatrix} S_{11} & S_{12} & 0 \\ S_{12} & S_{22} & 0 \\ 0 & 0 & S_{66} \end{bmatrix} \begin{Bmatrix} \sigma_1 \\ \sigma_2 \\ \sigma_6 \end{Bmatrix} + T \begin{Bmatrix} \alpha_1 \\ \alpha_2 \\ 0 \end{Bmatrix} \quad \rightarrow \{\epsilon\} = [S]\{\sigma\} + T\{\alpha\} , \tag{2.89}
$$

$$
\begin{Bmatrix} \sigma_1 \\ \sigma_2 \\ \sigma_6 \end{Bmatrix} = \begin{bmatrix} Q_{11} & Q_{12} & 0 \\ Q_{12} & Q_{22} & 0 \\ 0 & 0 & Q_{66} \end{bmatrix} \begin{Bmatrix} \epsilon_1 - T\alpha_1 \\ \epsilon_2 - T\alpha_2 \\ \epsilon_6 \end{Bmatrix} \quad \rightarrow \{\sigma\} = [Q](\{\epsilon\} - T\{\alpha\}) , \tag{2.90}
$$

while Eqs. (2.81) and (2.83) for a general laminate reference frame become:

$$\begin{Bmatrix} \epsilon_x \\ \epsilon_y \\ \epsilon_s \end{Bmatrix} = \begin{bmatrix} S_{xx} & S_{xy} & S_{xs} \\ S_{xy} & S_{yy} & S_{ys} \\ S_{xs} & S_{ys} & S_{ss} \end{bmatrix} \begin{Bmatrix} \sigma_x \\ \sigma_y \\ \sigma_s \end{Bmatrix} + T \begin{Bmatrix} \alpha_x \\ \alpha_y \\ \alpha_s \end{Bmatrix} \quad \rightarrow \{\epsilon'\} = [S']\{\sigma'\} + T\{\alpha'\}, \qquad (2.91)$$

$$\begin{Bmatrix} \sigma_x \\ \sigma_y \\ \sigma_s \end{Bmatrix} = \begin{bmatrix} Q_{xx} & Q_{xy} & Q_{xs} \\ Q_{xy} & Q_{yy} & Q_{ys} \\ Q_{xs} & Q_{ys} & Q_{ss} \end{bmatrix} \begin{Bmatrix} \epsilon_x - T\alpha_x \\ \epsilon_y - T\alpha_y \\ \epsilon_s - T\alpha_s \end{Bmatrix} \quad \rightarrow \{\sigma'\} = [Q'](\{\epsilon'\} - T\{\alpha'\}). \quad (2.92)$$

It should be remarked that in a general reference frame, also the component α_s of the vector of CTEs may be different from zero.

2.3.3 Classical Laminated Plate Theory

Hypotheses

Let us now consider a laminate, as shown in Fig. 2.2. Laminates are characterised by having planar dimensions significantly larger than their thickness. For this reason they are treated as plate elements. CLPT may be classified as an equivalent single layer theory
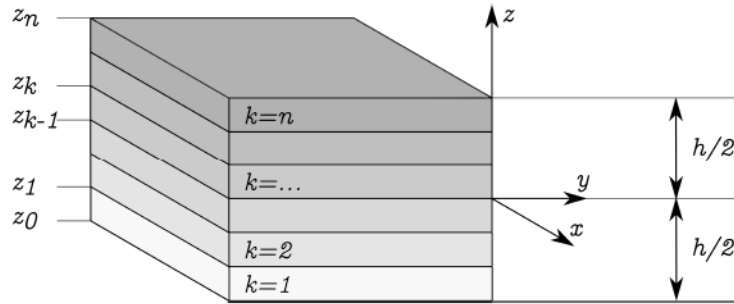
Figure 2.2: Laminate with definition of relevant quantities.

[61]: thanks to suitable assumptions on the kinematics of deformation and on the stress state through the thickness, the 3-D elastic problem is reduced to a 2-D one. Within the framework of CLPT, the behaviour of a composite laminate is described by three tensors (extension, coupling and bending). It is noteworthy that such tensors are not altered by using higher order theories [62].

In order to develop the CLPT, the following assumptions are made:

1. the material of each layer has a linear elastic, orthotropic behavior;

2. each layer is of uniform thickness;

3. layers are perfectly bonded;

4. the thickness of the resulting laminate is small if compared with its in-plane dimensions;

5. displacements, rotations and strains of the laminate remain small;

6. transverse shear stresses on the top and bottom surfaces of the laminate are zero;

7. the Kirchhoff kinematic model is assumed, i.e. straight material segments perpendicular to the midplane of the laminate:

(a) remain straight after deformation;

(b) rotate such that they remain perpendicular to the midplane;

(c) are inextensible.

As a consequence of these assumptions the transverse displacement is independent of the transverse coordinate, and transverse strains are null.

Displacement field
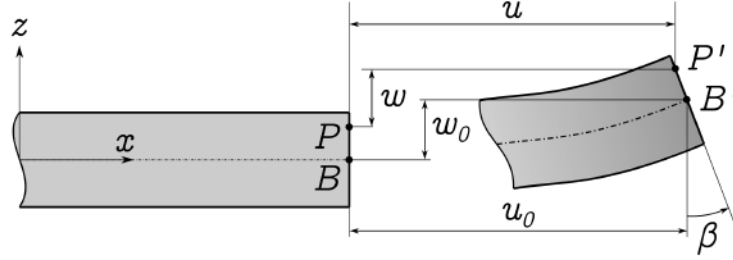
Figure 2.3: Representation of a laminate undeformed and deformed configurations.

A generic change in configuration of the laminate, which respects Kirchhoff hypotheses, is represented in Fig. 2.3. As a consequence of the Kirchhoff kinematics and of the hypothesis of small displacements and rotations, for angle β, as defined in Fig. 2.3, it holds:

$$\beta \simeq sin\beta, \quad cos\beta \simeq 1.$$

(2.93)

Consequently, the position change of a generic material point $P \equiv (x, y, z)$ of the laminate is expressed by the following displacement field:

$$u(x, y, z) = u_0(x, y) - z\frac{\partial w_0}{\partial x},$$

$$v(x, y, z) = v_0(x, y) - z\frac{\partial w_0}{\partial y},$$

(2.94)

$$w(x, y, z) = w_0(x, y),$$

where (u_0, v_0, w_0) are the displacements of point B, i.e. the material point projection of P on the midplane of the laminate. Once the midplane displacements (u_0, v_0, w_0) are known, displacements of any point in the laminate are found by means of Eq. (2.94). Furthermore, under these hypotheses, in-plane displacements are linear with respect to z.

Strain tensor

The strains associated with the displacement field of Eq. (2.94) are:

$$
\begin{aligned}
\epsilon_{xx} &= \frac{\partial u}{\partial x} = \frac{\partial u_0}{\partial x} - z\frac{\partial^2 w_0}{\partial x^2}\,, \\[4pt]
\epsilon_{yy} &= \frac{\partial v}{\partial y} = \frac{\partial v_0}{\partial y} - z\frac{\partial^2 w_0}{\partial y^2}\,, \\[4pt]
\epsilon_{zz} &= \frac{\partial w_0}{\partial z} = 0\,, \\[4pt]
\epsilon_{xz} &= \frac{1}{2}\left[\frac{\partial u}{\partial z} + \frac{\partial w}{\partial x}\right] = \frac{1}{2}\left[-\frac{\partial w_0}{\partial x} + \frac{\partial w_0}{\partial x}\right] = 0\,, \\[4pt]
\epsilon_{yz} &= \frac{1}{2}\left[\frac{\partial v}{\partial z} + \frac{\partial w}{\partial y}\right] = \frac{1}{2}\left[-\frac{\partial w_0}{\partial y} + \frac{\partial w_0}{\partial y}\right] = 0\,, \\[4pt]
\epsilon_{xy} &= \frac{1}{2}\left[\frac{\partial u}{\partial y} + \frac{\partial v}{\partial x}\right] = \frac{1}{2}\left[\frac{\partial u_0}{\partial y} + \frac{\partial v_0}{\partial x}\right] - z\frac{\partial^2 w_0}{\partial x \partial y}\,.
\end{aligned}
\tag{2.95}
$$

It can be observed that three out of the six components of tensor ϵ are null. Moreover, tensor ϵ can be decomposed into the sum of two tensors:

$$
\epsilon = \epsilon^0 + z\chi\,.
\tag{2.96}
$$

Here, ϵ^0 is the *midplane extension strain tensor* of the laminate, while χ is the *curvature tensor* of the laminate. Using Kelvin's notation:

$$
\{\epsilon\}^0 = \left\{\begin{array}{c} \epsilon_x^0 \\ \epsilon_y^0 \\ \epsilon_s^0 \end{array}\right\} = \left\{\begin{array}{c} \frac{\partial u_0}{\partial x} \\[4pt] \frac{\partial v_0}{\partial y} \\[4pt] \frac{1}{\sqrt{2}}\left[\frac{\partial u_0}{\partial y} + \frac{\partial v_0}{\partial x}\right] \end{array}\right\}\,,
\tag{2.97}
$$

$$
\{\chi\} = \left\{\begin{array}{c} \chi_x \\ \chi_y \\ \chi_s \end{array}\right\} = \left\{\begin{array}{c} \frac{\partial^2 w_0}{\partial x^2} \\[4pt] \frac{\partial^2 w_0}{\partial y^2} \\[4pt] \sqrt{2}\left[\frac{\partial^2 w_0}{\partial x \partial y}\right] \end{array}\right\}\,.
\tag{2.98}
$$

Due to the form of the strain field and to the fact that the behaviour of each lamina may be considered orthotropic, it can easily be shown, using Eqs. (2.12) and (2.74), that:

$$
\sigma_{xz} = \sigma_{yz} = 0\,.
\tag{2.99}
$$

As already hinted at, a further hypothesis that is adopted, on a heuristic base, in order to develop CLPT, is that the normal stress component be negligible, $\sigma_{zz} = 0$. Hence, the strains and the stresses in the laminate are fully described by their in-plane components.

Generalised forces acting on the laminate

In order to describe the constitutive behaviour of the laminate, the internal actions acting on it must be found and related to its strains. Such actions, as represented in Fig. 2.4,
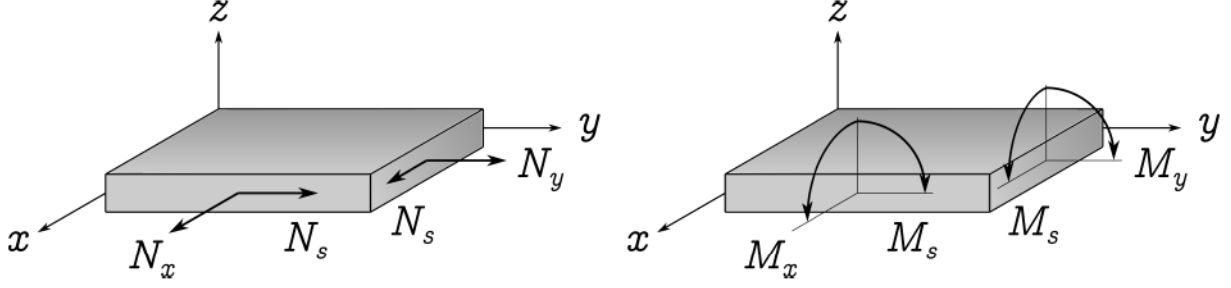
Figure 2.4: Internal actions acting on a laminate.

consist in *in-plane forces*, tensor $\mathbf{N}$, and *bending moments*, tensor $\mathbf{M}$, respectively defined as:

$$\mathbf{N} = \int_{-\frac{h}{2}}^{\frac{h}{2}} \boldsymbol{\sigma}\, dz \quad \rightarrow \quad \begin{Bmatrix} N_x \\ N_y \\ N_s \end{Bmatrix} = \begin{Bmatrix} \int_{-\frac{h}{2}}^{\frac{h}{2}} \sigma_x dz \\ \int_{-\frac{h}{2}}^{\frac{h}{2}} \sigma_y dz \\ \int_{-\frac{h}{2}}^{\frac{h}{2}} \sigma_s dz \end{Bmatrix}, \quad (2.100)$$

$$\mathbf{M} = \int_{-\frac{h}{2}}^{\frac{h}{2}} z\boldsymbol{\sigma}\, dz \quad \rightarrow \quad \begin{Bmatrix} M_x \\ M_y \\ M_s \end{Bmatrix} = \begin{Bmatrix} \int_{-\frac{h}{2}}^{\frac{h}{2}} \sigma_x z\, dz \\ \int_{-\frac{h}{2}}^{\frac{h}{2}} \sigma_y z\, dz \\ \int_{-\frac{h}{2}}^{\frac{h}{2}} \sigma_s z\, dz \end{Bmatrix}. \quad (2.101)$$

In Eqs. (2.100) and (2.101), the stress tensor $\boldsymbol{\sigma}$ has to be integrated over the thickness h of the laminate. However, such tensor is not continuous through the plies that build up the laminate. The integral must be therefore split into the different contributes from each ply, see Fig. 2.2, as follows:

$$\mathbf{N} = \sum_{k=1}^{n} \int_{z_{k-1}}^{z_k} \boldsymbol{\sigma}_k dz, \quad (2.102)$$

$$\mathbf{M} = \sum_{k=1}^{n} \int_{z_{k-1}}^{z_k} \boldsymbol{\sigma}_k z\, dz. \quad (2.103)$$

In Eqs. (2.102) and (2.103), as the integrals are now separated, tensor $\boldsymbol{\sigma}$ may be replaced using the constitutive law of each ply. Under the hypothesis adopted, the behaviour of a ply is described by Eq. (2.79), in its material frame. With respect to the laminate frame, instead, such behaviour is described by Eq. (2.83). If we define δ_k the angle by which the k-th ply is rotated with respect to the laminate frame, Eq. (2.83) may be written as:

$$\boldsymbol{\sigma}_k = \mathbf{Q}_k(\delta_k)\boldsymbol{\epsilon}, \quad (2.104)$$

48

where the reduced stiffness matrix of the ply has been indicated by the symbol $\mathbf{Q}_k(\delta_k)$. Hence, from Eqs. (2.102) and (2.103), we get:

$$
\begin{aligned}
\mathbf{N} &= \sum_{k=1}^{n} \int_{z_{k-1}}^{z_k} \mathbf{Q}_k(\delta_k)[\epsilon^0 + z\chi]dz = \\
&= \left[\sum_{k=1}^{n} \int_{z_{k-1}}^{z_k} \mathbf{Q}_k(\delta_k)dz\right]\epsilon^0 + \left[\sum_{k=1}^{n} \int_{z_{k-1}}^{z_k} \mathbf{Q}_k(\delta_k)zdz\right]\chi\,,
\end{aligned}
\tag{2.105}
$$

$$
\begin{aligned}
\mathbf{M} &= \sum_{k=1}^{n} \int_{z_{k-1}}^{z_k} \mathbf{Q}_k(\delta_k)z[\epsilon^0 + z\chi]dz = \\
&= \left[\sum_{k=1}^{n} \int_{z_{k-1}}^{z_k} \mathbf{Q}_k(\delta_k)zdz\right]\epsilon^0 + \left[\sum_{k=1}^{n} \int_{z_{k-1}}^{z_k} \mathbf{Q}_k(\delta_k)z^2dz\right]\chi\,.
\end{aligned}
\tag{2.106}
$$

Observing the previous equations, it appears convenient to define:

- the tensor of the *extension (or membrane) behaviour*, $\mathbf{A}$:

$$
\mathbf{A} = \frac{1}{h}\sum_{k=1}^{n} \int_{z_{k-1}}^{z_k} \mathbf{Q}_k(\delta_k)dz = \frac{1}{h}\sum_{k=1}^{n}(z_k - z_{k-1})\mathbf{Q}_k(\delta_k)\,,
\tag{2.107}
$$

- the tensor of the *extension-bending coupling behaviour*, $\mathbf{B}$:

$$
\mathbf{B} = \frac{2}{h^2}\sum_{k=1}^{n} \int_{z_{k-1}}^{z_k} \mathbf{Q}_k(\delta_k)zdz = \frac{1}{h^2}\sum_{k=1}^{n}(z_k^2 - z_{k-1}^2)\mathbf{Q}_k(\delta_k)\,,
\tag{2.108}
$$

- the tensor of the *bending behaviour*, $\mathbf{D}$:

$$
\mathbf{D} = \frac{12}{h^3}\sum_{k=1}^{n} \int_{z_{k-1}}^{z_k} \mathbf{Q}_k(\delta_k)z^2dz = \frac{4}{h^3}\sum_{k=1}^{n}(z_k^3 - z_{k-1}^3)\mathbf{Q}_k(\delta_k)\,.
\tag{2.109}
$$

With these definitions Eqs. (2.105) and (2.106) may be rewritten as:

$$
\begin{Bmatrix} \mathbf{N} \\ \mathbf{M} \end{Bmatrix} = \begin{bmatrix} h\mathbf{A} & \frac{h^2}{2}\mathbf{B} \\ \frac{h^2}{2}\mathbf{B} & \frac{h^3}{12}\mathbf{D} \end{bmatrix} \begin{Bmatrix} \epsilon^0 \\ \chi \end{Bmatrix}.
\tag{2.110}
$$

Eq. (2.110) is called the *fundamental law*, and describes the constitutive behaviour of the laminate, relating the internal actions to the deformation state. Tensors $\mathbf{A}$, $\mathbf{B}$ and $\mathbf{D}$ are normalised tensors, sharing the same units (in particular, force over square length). Also, the homogeneity tensor may be defined as follows:

$$
\mathbf{C} = \mathbf{A} - \mathbf{D}\,.
\tag{2.111}
$$

In general $\mathbf{C} \neq \mathbf{0}$; this means that a composite laminate, contrarily to homogeneous plates, behaves in different ways in membrane and bending, as if it was made of two different materials. Eqs. (2.107)-(2.109), show that the laminate stiffnesses depends on:

1. the material stiffness of the basic layers;

49

2. the thickness of the layers;

3. the stacking sequence.

Eq. (2.110) allows to eventually clarify the concept of elastic couplings that has been mentioned so far. To begin with, all terms of tensor **B** relate in-plane forces to curvatures and moments to midplane strains. Therefore, these terms represent *in-plane/out-of-plane* (or, equivalently, *membrane/bending*) couplings. Then, also the terms A_{xs} and A_{ys} of tensor **A** represent elastic couplings, since they relate the extension and shearing behaviours of the laminate; hence, they will be referred to as *extension/shear* couplings. Similarly terms D_{xs} and D_{ys} of tensor **D** represent couplings between bending and twisting behaviour of the laminate, and will be referred to as *bending/twisting* couplings.

Inversion of the fundamental law of laminates

The fundamental law of laminates, Eq. (2.110) may be inverted, to obtain:

$$\left\{ \begin{matrix} \epsilon^0 \\ \chi \end{matrix} \right\} = \begin{bmatrix} \frac{1}{h}\mathcal{A} & \frac{2}{h^2}\mathcal{B} \\ \frac{2}{h^2}\mathcal{B}^T & \frac{12}{h^3}\mathcal{D} \end{bmatrix} \left\{ \begin{matrix} \mathbf{N} \\ \mathbf{M} \end{matrix} \right\}. \tag{2.112}$$

In Eq. (2.112), $\mathcal{A}$ and $\mathcal{D}$ are the compliance membrane and bending tensors, respectively, while tensor $\mathcal{B}$ represents membrane-bending coupling. These tensors are obtained as follows [62]:

$$\mathcal{A} = (\mathbf{A} - 3\mathbf{B}\mathbf{D}^{-1}\mathbf{B})^{-1}, \tag{2.113}$$

$$\mathcal{B} = -3\mathcal{A}\mathbf{B}\mathbf{D}^{-1}, \tag{2.114}$$

$$\mathcal{D} = (\mathbf{D} - 3\mathbf{B}\mathbf{A}^{-1}\mathbf{B})^{-1}. \tag{2.115}$$

2.3.4 Laminates with identical layers

When designing composite laminates, very often identical layers are used for the whole layup. In this case, the results presented above may be simplified. As a first observation, the reduced stiffness matrix in the lamina material frame is identical for all plies in the layup. Hence, Eq. (2.104) becomes:

$$\sigma_k = \mathbf{Q}(\delta_k)\epsilon. \tag{2.116}$$

Moreover, as all layers have the same thickness, it is easy to determine the positions of their upper face:

$$z_k = \frac{2k - n}{2n}h. \tag{2.117}$$
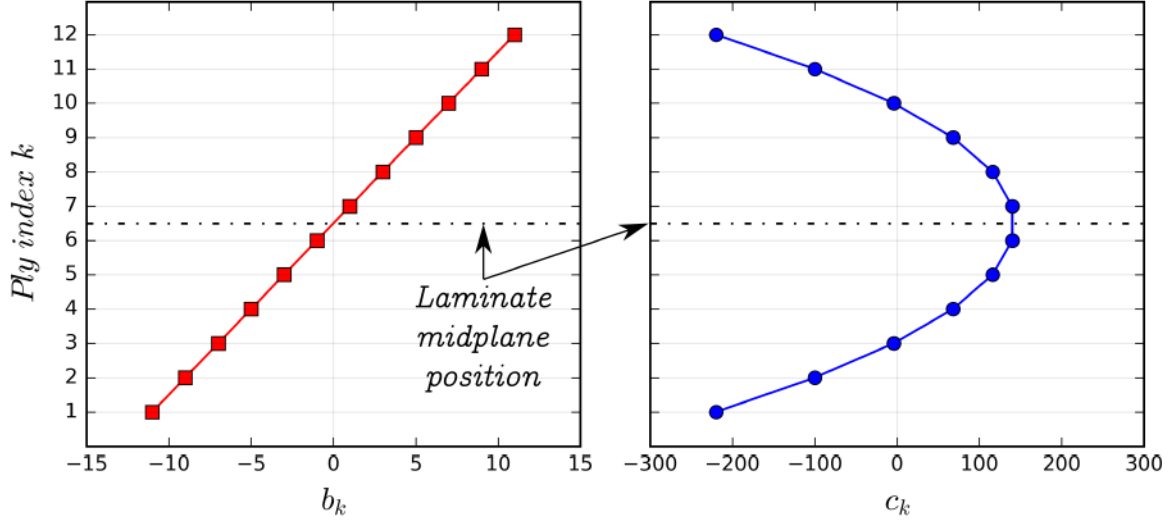
Figure 2.5: Trend of coefficient b_k and c_k, with respect to the ply position index k.

As a consequence tensors $\mathbf{A}$, $\mathbf{B}$, $\mathbf{C}$ and $\mathbf{D}$ may be rewritten as:

$$\mathbf{A} = \frac{1}{n}\sum_{k=1}^{n} a_k \mathbf{Q}(\delta_k)\,, \quad a_k = 1\,, \tag{2.118}$$

$$\mathbf{B} = \frac{1}{n^2}\sum_{k=1}^{n} b_k \mathbf{Q}(\delta_k)\,, \quad b_k = 2k - n - 1\,, \tag{2.119}$$

$$\mathbf{C} = \frac{1}{n^3}\sum_{k=1}^{n} c_k \mathbf{Q}(\delta_k)\,, \quad c_k = -12k(k - n - 1) - 2n^2 - 6n - 4\,, \tag{2.120}$$

$$\mathbf{D} = \frac{1}{n^3}\sum_{k=1}^{n} d_k \mathbf{Q}(\delta_k)\,, \quad d_k = 12k(k - n - 1) + 4 + 3n(n + 2)\,. \tag{2.121}$$

It is interesting to observe some properties of coefficients b_k, c_k and d_k that will be useful in the following. First, the sum of both coefficient b_k and c_k is always null over the ply index interval $[1, n]$. Second, it is observed that coefficient b_k varies linearly with ply index k, whilst c_k and d_k are symmetric with a parabolic variation with respect to k. This is shown in Fig. 2.5 for the case of a laminate with $n = 12$. It is also interesting to observe that the following relationships hold:

$$d_k = 3b_k^2 + 1\,, \tag{2.122}$$

$$c_k = n^2 - d_k = n^2 - 1 - 3b_k^2\,. \tag{2.123}$$

2.3.5   Frequently used laminate types

Using results from CLPT, laminates may be categorised into different types. Often such categorisation is done according to the macroscopic elastic properties of the laminates and to the way these properties may be obtained in terms of stacking sequence, without

a clear distinction between the two aspects, which might be misleading. Here, for this reason, categories of laminates are presented first based on their properties, and then based on their stacking sequence. Also, the list proposed here goes a little bit further than those commonly presented in composite materials textbooks, as this will be useful in the following of the manuscript. Still, such list is not meant to be exhaustive; for reference, the interested reader may found a deeper discussion in [62] and in the literature.

Classification based on elastic properties

Uncoupled laminates

A laminate is defined *uncoupled* if all components of its tensor $\mathbf{B}$ are null:

$$\mathbf{B} = \mathbf{0} \, . \tag{2.124}$$

In such laminates no membrane-bending couplings exist, but extension-shearing coupling (terms A_{xs} and A_{ys}) and bending-twisting coupling (terms D_{xs} and D_{ys}) may exist.

Membrane-bending homogeneous laminates

This definition is not commonly used, but it will be extremely useful in the context of this thesis. A laminate is membrane-bending homogeneous if its homogeneity tensor is identically null:

$$\mathbf{C} = \mathbf{0} \, . \tag{2.125}$$

This means that the normalised tensors $\mathbf{A}$ and $\mathbf{D}$ of the laminate are equal, and therefore that the laminate has the same membrane and bending behaviour, as if it was made of homogeneous material. However it still may have membrane-bending couplings (if $\mathbf{B} \neq \mathbf{0}$).

Quasi-homogeneous laminates

A laminate is defined as quasi-homogeneous if it is both uncoupled and membrane-bending homogeneous:

$$\mathbf{B} = \mathbf{0} \, ,$$
$$\mathbf{C} = \mathbf{0} \, . \tag{2.126}$$

These laminates are obviously extremely interesting for design purposes, thanks to their properties.

Membrane-orthotropic laminates

These laminates have an orthotropic membrane tensor $\mathbf{A}$, i.e.:

$$\mathbf{A} = \begin{bmatrix} A_{xx} & A_{xy} & 0 \\ A_{xy} & A_{yy} & 0 \\ 0 & 0 & A_{ss} \end{bmatrix} \, . \tag{2.127}$$

In other words, there is no extension-shearing coupling. In general, membrane-bending couplings (tensor $\mathbf{B}$) and bending-twisting coupling (D_{xs} and D_{ys}) may still exist.

Fully-orthotropic laminates

These laminates have orthotropic tensors $\mathbf{A}$ and $\mathbf{D}$, with respect to the same orthotropy axes:

$$\mathbf{A} = \begin{bmatrix} A_{xx} & A_{xy} & 0 \\ A_{xy} & A_{yy} & 0 \\ 0 & 0 & A_{ss} \end{bmatrix}, \quad \mathbf{D} = \begin{bmatrix} D_{xx} & D_{xy} & 0 \\ D_{xy} & D_{yy} & 0 \\ 0 & 0 & D_{ss} \end{bmatrix}. \quad (2.128)$$

Therefore, both extension-shearing and bending-twisting couplings are eliminated. Membrane-bending couplings may still exist and it is important to remember that, in general the membrane and bending behaviour may be different (i.e. the laminate may be not membrane-bending homogeneous).

Quasi-isotropic laminates

A quasi-isotropic laminate has an isotropic membrane behaviour:

$$\mathbf{A} = \begin{bmatrix} A_{xx} & A_{xy} & 0 \\ A_{xy} & A_{xx} & 0 \\ 0 & 0 & A_{ss} \end{bmatrix}, \quad A_{ss} = \frac{A_{xx} - A_{xy}}{2}, \quad (2.129)$$

but in general $D_{xx} \neq D_{yy}$, $D_{xs} \neq 0$, $D_{ys} \neq 0$ and $D_{ss} \neq (D_{xx} - D_{xy})/2$, differently from what happens in isotropic plates. In other words, isotropy is limited to the membrane behaviour. Also, these laminates may have $\mathbf{B} \neq \mathbf{0}$. We anticipate here that laminates of this type may be obtained using the Werren and Norris rule [66], which will be mentioned later. However, such rule gives only a sufficient condition, and quasi-isotropic laminates may be obtained also in other ways.

Fully-isotropic laminates

Fully-isotropic laminates are uncoupled and have both tensors $\mathbf{A}$ and $\mathbf{D}$ isotropic:

$$\mathbf{A} = \begin{bmatrix} A_{xx} & A_{xy} & 0 \\ A_{xy} & A_{xx} & 0 \\ 0 & 0 & A_{ss} \end{bmatrix}, \quad A_{ss} = \frac{A_{xx} - A_{xy}}{2},$$

$$\mathbf{D} = \begin{bmatrix} D_{xx} & D_{xy} & 0 \\ D_{xy} & D_{xx} & 0 \\ 0 & 0 & D_{ss} \end{bmatrix}, \quad D_{ss} = \frac{D_{xx} - D_{xy}}{2}, \quad (2.130)$$

$$\mathbf{B} = \mathbf{0}.$$

In addition it should be remarked that fully-isotropic laminates are necessarily quasi-homogeneous, [62]. Hence, they behave like homogeneous isotropic plates.

Classification based on stacking sequence

Besides allowing the previous categorisation of laminates based on their properties, the results of CLPT allow to easily find particular class of stacking sequences that lead to those properties. Hence a categorisation of laminates is possible also in terms of stacking sequence.

Symmetric laminates

Symmetry with respect to the laminate midplane is likely the most simple and widely used technique to obtain an uncoupled laminate ($\mathbf{B} = \mathbf{0}$). Indeed, it is easy to observe that symmetric plies with the same orientation give opposite contributes to the terms of tensor $\mathbf{B}$, due to the trend of b_k coefficients, see Fig. 2.5. However, it is important to remember that symmetry of the laminate is a sufficient but not necessary condition, and it is possible to obtain non-symmetric stacking sequences which are uncoupled; this was first shown in [67].

Balanced laminates

Balanced laminates are those in which, for each ply oriented at θ, another one oriented at $-\theta$ is present. Plies with opposite orientations give opposite contributes to A_{xs} and A_{ys} . Thus, using balanced layups, membrane-orthotropic laminates are obtained. Balanced laminates may also be made to be symmetric; in this case they are also uncoupled. Symmetric and balanced laminates are often used in practical application.

Angle-ply laminates

Angle-ply laminates are balanced laminates in which only one orientation and its opposite appear. Their properties are therefore those of balanced laminates.

Cross-ply laminates

Cross-ply laminates are those in which only plies oriented at 0° or 90° appear. Since each ply has an orthotropic behaviour, the resulting laminate is completely orthotropic, meaning tensors $\mathbf{A}$, $\mathbf{B}$ and $\mathbf{D}$ are all orthotropic. If, in addition, the laminate is symmetric, then it will be also uncoupled.

Anti-symmetric laminates

An anti-symmetric laminate has opposite plies, with respect to the laminate midplane, which have opposite orientations. As a consequence, it is a particular type of balanced laminate. Due to the shape of coefficient d_k, in addition to $A_{xs} = A_{ys} = 0$, it follows that $D_{xs} = D_{ys} = 0$. Therefore, antisymmetric laminates are fully-orthotropic.

Werren and Norris (quasi-isotropic) laminates

Werren and Norris [66] were the first to give a general rule to obtain stacking sequences that result in quasi-isotropic laminates (i.e. with isotropic tensor $\mathbf{A}$). In particular they found that if the n plies of a laminate are divided into a number $m \geq 3$ of groups, each one having the same number of plies (thus n/m), and the groups have orientations that differ by an angle $2\pi/m$, then the laminate is isotropic in extension.

Quasi-trivial laminates

Quasi-trivial (QT) laminates are obtained using QT stacking sequences, which are obtained as a particular class of solutions to the equations of uncoupling, Eq. (2.124), membrane-bending homogeneity, Eq. (2.125), or both, introduced by Vannucci and

Verchery, [68]. As a consequence, uncoupled, membrane-bending homogeneous and quasi-homogeneous laminates are directly obtained using QT stacking sequences. Furthermore, using QT solutions in conjunction with some of the stacking technique shown before, even more interesting properties may be obtained. For example, fully-orthotropic laminates in [69] and fully-isotropic ones in [70] were found. These sequences are extremely interesting for design purposes, and have been a cornerstone in the development of the present thesis. For this reason, they will be comprehensively described in Part II of the manuscript, and in particular in Chapter 4.

2.3.6 CLPT in thermo-elasticity

When a non-isothermal situation is considered, the results of CLPT may be extended as follows. A linear thermal field in the laminate, with temperatures t_{top} and t_{bottom} at the upper and lower surfaces of the laminate, respectively, may be thought as the sum of:

- a constant field:

$$T = \frac{t_{top} + t_{bottom}}{2} \, ; \tag{2.131}$$

- an anti-symmetric field characterised by the constant gradient:

$$\nabla T = \frac{t_{top} - t_{bottom}}{h} \, . \tag{2.132}$$

In these and in the following expressions, all temperatures are evaluated with respect to the temperature T_0 of an unstrained condition for the laminate. As an example T_0 may assumed to be the curing temperature. Taking into account the thermoelastic constitutive behaviour of each lamina, in particular Eq. (2.92), the fundamental law of laminates, Eq. (2.110), becomes:

$$\left\{ \begin{array}{c} \mathbf{N} \\ \mathbf{M} \end{array} \right\} = \left[\begin{array}{cc} h\mathbf{A} & \frac{h^2}{2}\mathbf{B} \\ \frac{h^2}{2}\mathbf{B} & \frac{h^3}{12}\mathbf{D} \end{array} \right] \left\{ \begin{array}{c} \epsilon^0 \\ \chi \end{array} \right\} - T \left\{ \begin{array}{c} h\mathbf{U} \\ \frac{h^2}{2}\mathbf{V} \end{array} \right\} - \nabla T \left\{ \begin{array}{c} \frac{h^2}{2}\mathbf{V} \\ \frac{h^3}{12}\mathbf{W} \end{array} \right\} , \tag{2.133}$$

where we identify $\mathbf{U}$, tensor of in-plane actions per unit temperature variation T; $\mathbf{V}$, tensor of bending moments per unit temperature variation; $\mathbf{W}$, tensor of bending moments per unit of thermal gradient ∇T; they are respectively defined as:

$$\mathbf{U} = \frac{1}{h} \sum_{k=1}^{n} \int_{z_{k-1}}^{z_k} \mathbf{Q}_k(\delta_k)\boldsymbol{\alpha}_k(\delta_k)dz = \frac{1}{h} \sum_{k=1}^{n} (z_k - z_{k-1})\mathbf{Q}_k(\delta_k)\boldsymbol{\alpha}_k(\delta_k) , \tag{2.134}$$

$$\mathbf{V} = \frac{2}{h^2} \sum_{k=1}^{n} \int_{z_{k-1}}^{z_k} \mathbf{Q}_k(\delta_k)\boldsymbol{\alpha}_k(\delta_k)zdz = \frac{1}{h^2} \sum_{k=1}^{n} (z_k^2 - z_{k-1}^2)\mathbf{Q}_k(\delta_k)\boldsymbol{\alpha}_k(\delta_k) , \tag{2.135}$$

$$\mathbf{W} = \frac{12}{h^3} \sum_{k=1}^{n} \int_{z_{k-1}}^{z_k} \mathbf{Q}_k(\delta_k)\boldsymbol{\alpha}_k(\delta_k)z^2dz = \frac{4}{h^3} \sum_{k=1}^{n} (z_k^3 - z_{k-1}^3)\mathbf{Q}_k(\delta_k)\boldsymbol{\alpha}_k(\delta_k) . \tag{2.136}$$

If laminates made of identical layers are considered, then the expressions of tensors $\mathbf{U}$, $\mathbf{V}$ and $\mathbf{W}$ are simplified:

$$\mathbf{U} = \frac{1}{n}\sum_{k=1}^{n} a_k \mathbf{Q}(\delta_k)\boldsymbol{\alpha}(\delta_k)\,, \quad a_k = 1\,, \tag{2.137}$$

$$\mathbf{V} = \frac{1}{n^2}\sum_{k=1}^{n} b_k \mathbf{Q}(\delta_k)\boldsymbol{\alpha}(\delta_k)\,, \quad b_k = 2k - n - 1\,, \tag{2.138}$$

$$\mathbf{W} = \frac{1}{n^3}\sum_{k=1}^{n} d_k \mathbf{Q}(\delta_k)\boldsymbol{\alpha}(\delta_k)\,, \quad d_k = 12k(k - n - 1) + 4 + 3n(n + 2)\,. \tag{2.139}$$

It is noteworthy that coefficients a_k and b_k in Eqs. (2.137) and (2.138) are the same of Eqs. (2.118) and (2.119).

Eq. (2.133) introduces for the first time the thermal effects mentioned so far. It shows how they may affect the constitutive behaviour and thus the stress/deformation state of a laminate.

2.4   Concluding remarks

In this chapter, a detailed formal description of the mechanical behaviour of composite laminates was presented. In particular, the thermoelastic equations of CLPT were illustrated. These will be used in the following of the manuscript to obtain some of the most important result of this study. It is worth to remember that more refined (higher-order) theories do exist to model laminates behaviour, but they add no required features for the purposes of this study, and so need not be used.

Thanks to the representation introduced in this chapter, it has been possible to highlight what elastic couplings and thermal effects in a laminate are and where they come from. The next step to be taken is, of course, to understand why and how they could affect delamination testing of MD laminates. Chapter 3 will deal with this issue.

Chapter 3

Delamination in advanced composite materials

3.1 Introduction

In Chapter 1, it was shown how, according to literature, elastic couplings and thermal effects still represent big obstacles to interlaminar fracture toughness characterisation of MD laminates. In Chapter 2, the description of the mechanics of laminates by means of CLPT allowed to formally define elastic couplings and thermal effects. The objective of this chapter, then, is to explain how these effects play a role in delamination testing.

In order to do so, Section 3.2 explains why it is extremely important to have standardised tests and the basic ideas behind the exploitation of Linear Elastic Fracture Mechanics for interlaminar fracture toughness testing. Then, the tests configurations that, to date, have been standardised are presented in Sections 3.3-3.5. A particular attention is dedicated to mode I delamination testing, for which also historical details of the process to standardisation are discussed. This analysis will be relevant for the work and discussions presented in following chapters. Eventually, Section 3.6 presents a thorough bibliography of interlaminar fracture testing in MD laminates: the main problems emerging from almost four decades of intense research activity are reviewed. This will give the opportunity to deeply understand the main challenges that need to be faced.

3.2 Interlaminar fracture toughness testing

3.2.1 The need for standard test methods

Standardisation represents a critical point when it comes to fracture toughness: as reported by relevant experts, evaluation of this property is much more complex than others (e.g.: stiffness or strength) [43, 71]. Hence, the existence of widely accepted standards is essential. Besides, from a practical point of view, several reasons exists for developing standard interlaminar fracture test methods.

To begin with, the layered structure of composite laminates allows to tailor their thickness and lay-up to suit the needs of each specific application. However, resin rich interlaminar regions often represent weak spots. For this reason, an important effort is constantly devoted to the development of new materials with enhanced properties. In this context, standard test procedures are fundamental to qualify new materials and to

screen and select them [43, 72]. Moreover, due to the fact that these materials are traded worldwide, internationally recognised standards are highly desirable [43].

Another important aspect motivating the development of effective standard test methods concerns the attainment of interlaminar fracture toughness properties to be used for structural calculations. As reviewed in Chapter 1, interlaminar fracture is one of the most critical damage mode in composite laminates. Consequently, the availability of failure envelopes and/or failure criteria is of major interests in structural design [43, 72]. This is especially true for applications where safety and efficiency are primary concerns.

Eventually, standard test procedures may prove useful for quality control in manufacturing and failure analysis of composites parts and structures [48].

The activities to create standards for interlaminar fracture toughness tests have been carried out mainly by three organisations: the American Society for Testing and Materials (ASTM), the European Structural Integrity Society (ESIS) and the Japanese Industrial Standards organisation (JIS).

3.2.2 Fracture mechanics in interlaminar fracture testing

A delamination propagating in the interlaminar regions of a laminate, differently from other damage mechanisms observed in polymer matrix composites, shows significant similarities with the concept of *crack*, commonly adopted in Fracture Mechanics [45]. As a consequence, LEFM has been widely and successfully used to study delamination [42, 43, 44]. According to Irwin's work [46, 47], the material parameter governing crack, or delamination, propagation is the critical value of ERR. ERR, often indicated by G, is the rate of change of elastic potential energy with respect to crack extension. It is a function of the geometry, of the material properties and of the loading conditions. Within the framework of LEFM, propagation is assumed to occur when ERR attains its critical value, G_c. Therefore, under the conditions for which LEFM is considered applicable, the interlaminar fracture toughness of the material is assumed to coincide with the value of ERR at propagation, G_c. Consequently, in order to characterise the interlaminar fracture toughness of a composite material, appropriate tests to determine the critical value of ERR have to be performed.

Ideally, three pure loading modes exist for a crack, as shown in Fig. 3.1:

1. Mode I, or opening;

2. Mode II, or sliding;

3. Mode III, or tearing.

In a body made of homogeneous isotropic material, subjected to static loads, a crack propagates following a path such that a pure opening mode at its tip is maintained [73]. On the other hand, delamination is usually confined to propagate in an interlaminar layer, thus allowing the possibility to be loaded in all three different modes [44, 73, 74]. In addition, it was shown that the interlaminar fracture toughness is a function of the mode mix under which delamination propagates [74, 75]. As a consequence, characterisation of such property should be performed under the three pure modes loading conditions and under mixed mode, too [43, 44].

Nowadays, thanks to important research efforts [43, 48, 72, 76, 77, 78, 79, 80, 81], delamination tests have been proposed, improved and eventually standardised for pure mode I [49], mode II [50] and mixed mode I-II [51]. Concerning mode III propagation, no
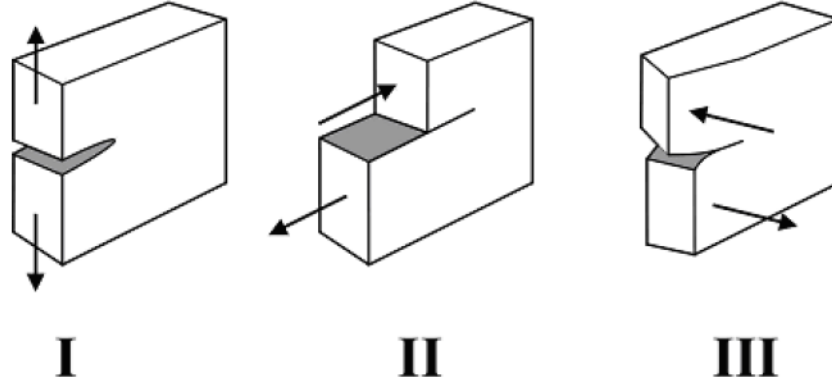
Figure 3.1: Loading modes of a crack.

standard exists yet, mainly due to difficulties in finding appropriate test configurations. Probably the most known approach proposed up to now is the Edge Crack Torsion test [82]. However, research is still ongoing [83] and mode III toughness values obtained with this test configuration may not be accurate and reliable [84].

3.3 Mode I interlaminar fracture toughness testing

The mode I interlaminar fracture toughness of polymer matrix composites, G_{Ic} is commonly evaluated using the Double Cantilever Beam (DCB) test. To date, the DCB test method for interlaminar fracture toughness testing of polymer matrix composites is standardised and well established [49].

DCB standard test method

Specimen description

The DCB specimen is a uniform thickness and uniform width UD laminate with a rectangular in-plane shape, Fig. 3.2. Is should contain an even number of plies, so that during
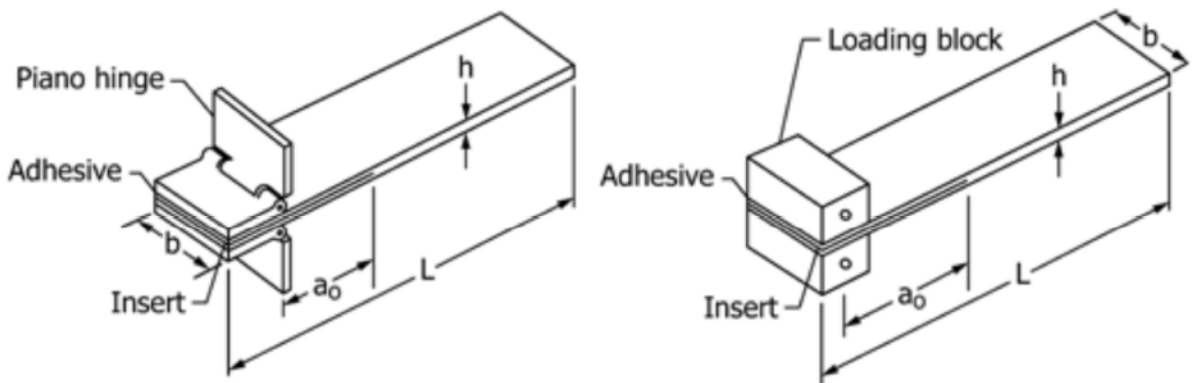
Figure 3.2: Representation of the DCB specimen with piano hinges or loading blocks [49].

manufacturing a non-adhesive and thin insert film is placed at the midplane at one end

of the specimen. The objective of the insert film is to act as a delamination initiator. The specimens should be at least 125 mm long and 25 mm wide, with an insert length of about 63 mm. This, taking into account the length required for hinges or blocks bonding, should result in an initial delamination length a_0 of 50 mm (distance from the load line to the tip of the insert, see Fig. 3.2). Further recommendations may be found in [49].

Test procedure

An opening load is applied through the piano hinges or loading blocks bonded to the two arms of the specimen in the insert region, Fig. 3.2. The displacement is controlled during the test, while the load and the delamination length are recorded. The ASTM standard suggests to perform a first loading phase at a constant crosshead speed between 1 and 5 mm/min. This loading phase should be stopped, and the specimen unloaded, when a delamination propagation of 3 to 5 mm from the insert tip is obtained. The specimen should then be loaded again at the same constant crosshead speed used in the first loading phase to make delamination propagate for a sufficient length. Finally, the specimen should be unloaded, and the unloading part of the load displacement curve should be recorded as well.

Interlaminar fracture toughness definition

Interlaminar fracture toughness may be evaluated both at the very beginning of delamination advancement (initiation) and during propagation. The ASTM standard states that both initiation and propagation values of the mode I interlaminar fracture toughness, G_{Ic}, should be obtained and reported. Three different definitions of initiation points are suggested in [49]:

1. point of deviation from linearity (NL): it is the point at which the load displacement plot of the test deviates from linearity. It is usually the initiation point yielding the lowest values of G_{Ic} [76] and it has been associated with the beginning of delamination propagation inside the specimen, in the central part of the insert tip [85];

2. point of visual observation of delamination onset (VIS): it is the point on the load displacement plot corresponding to the instant at which delamination propagation is firstly observed visually on the specimen side. The point obtained could be rather operator-dependent [72]. To reduce this dependency, visual observation should be performed with a travelling microscope or another magnifying device;

3. point of 5% increase in compliance or of maximum load (5%/MAX): it is the point at which the compliance of the specimen has increased by 5%. If such point is reached after the point of maximum load registered, then the point corresponding to maximum load should be used instead.

In order to obtain propagation values of G_{Ic}, the specimen should be painted and marked at regular interval on its sides. In this way, delamination propagation can be monitored during the test: when it reaches given crack lengths, the corresponding load and displacement are recorded. From these data G_{Ic} may be computed and plotted as a function of the delamination propagation length, $a - a_0$, to obtain the so called resistance curve (or R-curve).

Data reduction techniques

The computation of interlaminar fracture toughness may be performed by means of three different data reduction schemes, namely:

1. Modified Beam Theory (MBT) [49, 86].
   The Modified Beam Theory exploits results from simple beam theory, but takes into account the fact that the specimen arms are not perfectly clamped at their root section: an effective delamination length $a + \Delta$ is assumed, such that perfect clamp conditions are realised at the corresponding sections of the specimen arms. A least squares plot of the the cube root of compliance, $C^{1/3}$ (where $C = \delta/p$ is the compliance), as a function of delamination length is generated; Δ is found as the absolute value of the abscissa for which null $C^{1/3}$ is obtained on the plot. ERR can then be calculated as:

$$G_I = \frac{3P\delta}{2b(a + \Delta)} \, , \qquad (3.1)$$

   where P is the applied load, δ is the opening displacement, b is the specimen width and a is the delamination length. This approach also allows calculation of the flexural modulus of elasticity in the longitudinal specimen direction $E_{1,f}$, as follows:

$$E_{1,f} = \frac{64(a + |\Delta|)^3 P}{\delta b h^3} \, , \qquad (3.2)$$

   where h is the specimen thickness. The values of $E_{1,f}$ obtained should be independent of delamination length.

2. Compliance calibration (CC) [49, 87].
   According to Compliance Calibration, ERR is computed as follows:

$$G_I = \frac{nP\delta}{2ba} \, , \qquad (3.3)$$

   In other words, it is assumed that the slope coefficient of the relationship between applied load and opening displacement depends on the n-th power of the delamination length. This is a generalisation of the simple beam theory result, for which $n = 3$. By using experimental data, a least square plot of $log(C)$ versus $log(a)$ is generated and the slope n of the line fitting the data may be obtained.

3. Modified Compliance Calibration (MCC) [49, 79].
   If the Modified Compliance Calibration is used, then:

$$G_I = \frac{3P^2 C^{2/3}}{2A_1 bh} \, , \qquad (3.4)$$

   where h is the specimen thickness and A_1 is the slope of the least square line of the plot of a/h as a function of $C^{1/3}$.

Usually, results obtained with the three techniques are within few percent points of difference [49]. The MBT is recommended, since during round robin testing it was the technique yielding the most conservative values of interlaminar fracture toughness, for most of the tests performed [76].

Historical perspective

The DCB test configuration emerged as the preferred one for mode I interlaminar fracture toughness evaluation from early studies, due to its simplicity and effectiveness [42, 43, 88]. Nonetheless, a long time and an important effort were required to achieve the creation of a standard.

Early studies [89] identified problems with delamination branching in specimens with off-axis plies (plies not aligned to the longitudinal axis of the specimen) embedding the initial delamination plane. For this reason, further studies mainly focused on UD specimens.

It was soon discovered, however, that UD specimens could be affected by fibre bridging [90, 91]. In UD composites, indeed, nesting of fibres between adjacent layers may occur during fabrication. Consequently, nested fibres at the midplane of a DCB specimen may bridge the delamination during propagation. This results in an apparent increase in G_{Ic} with increasing delamination length, thus giving an increasing R-curve for UD specimens. Since fibre bridging was considered to be an artefact of the UD DCB specimen, not occurring in structural composite laminates, where delamination usually develops between differently oriented plies, the attention was focused on evaluation of G_{Ic} from the insert tip [43, 80].

In this context, extensive investigations were conducted on the effect of the thickness and the material of the insert film [72, 76, 79]. It was found that aluminium inserts were problematic due to crimping, tears and folds at their edges, likely caused during cut. This led to the formation of undesired resin pockets at the tip of the insert (even for the thinnest insert, 7 μm thick) that in turn resulted in initiation G_{Ic} values higher than propagation ones and unstable initial propagation [76, 80]. Significant resin pockets, invalidating evaluation of G_{Ic} from the insert tip, were observed also for thicker polymer insert films [79]. It was found that reliable initiation values of G_{Ic} could be obtained with polymer inserts with thickness equal or smaller than 13 μm [72, 76]. This led ASTM to publish a DCB standard recommending the use of polymer insert films with thickness of 13 μm [76] or less. It also recommended that the entire R-curve of the test, with delamination propagating past the insert, be reported, in order to provide useful information and confirm the validity of the initiation value of G_{Ic} obtained from the insert. Concurrently, however, in JIS round robin tests it was found that precracking the DCB specimen could represent a simple way to avoid all problems related to thickness and material of the insert film [79]. Consequently, JIS published a DCB standard that recommended wedge precracking of the DCB specimens before testing. This was also justified by the fact that some new toughened matrix materials appeared on the market and created problems with the validity of delamination G_{Ic} measurements from the insert [43]. For this reason, the ESIS and the ASTM created a new DCB test protocol suggesting to evaluate G_{Ic} from the insert, then unloading and reloading the specimen and evaluating G_{Ic} from the natural mode I precrack created during the first loading phase [43, 72].

Most of the recommendations found in actual standards derive from the historical aspects reviewed here. Still today, their scope is restricted to UD laminates, due to the fact that most of the experience gained in round robin tests was limited to this case. The ASTM standard acknowledge how specimens with different layups may experience delamination migration, which would invalidate the tests. It also mentions the fact that nonuniform delamination growth in MD laminates would affect G_{Ic}, especially at initiation.

3.4　Mode II interlaminar fracture toughness testing

The creation of standard test procedures for mode II interlaminar fracture toughness followed a more cumbersome path than that of mode I [43]. One first issue was the existence of a number of different test configurations, without one of them being clearly superior to the others. In particular, the End Notched Flexure (ENF) and the End Loaded Split (ELS) beam tests were the main competitors. Moreover, each organisation seemed to prefer a different test method, which resulted in difficulties toward the creation of an international standard [43]. Despite the fact that JIS published a standard in 1993, based on a stabilized (i.e. allowing a stable delamination propagation) version of the ENF configuration [78], mode II interlaminar fracture toughness characterisation remained controversial for quite some time [48, 72]. Practical issues (such as unstable propagation in the ENF configuration, friction effects and choice of precracking, if any) as well as theoretical arguments on the validity of mode II fracture toughness data [43, 92] contributed to this situation.

Eventually, in 2014, a mode II interlaminar fracture toughness standard using the ENF test configuration was published also by ASTM [50]. A very detailed review of the research and the rationale supporting the creation of this standard may be found in [93].

ENF standard test method

Presumably, the ENF test configuration is the most widely adopted for mode II interlaminar fracture toughness evaluation. A sketch of the ENF specimen and the test set-up is shown in Fig. 3.3. The ENF specimen looks very similar to the DCB one. Also in
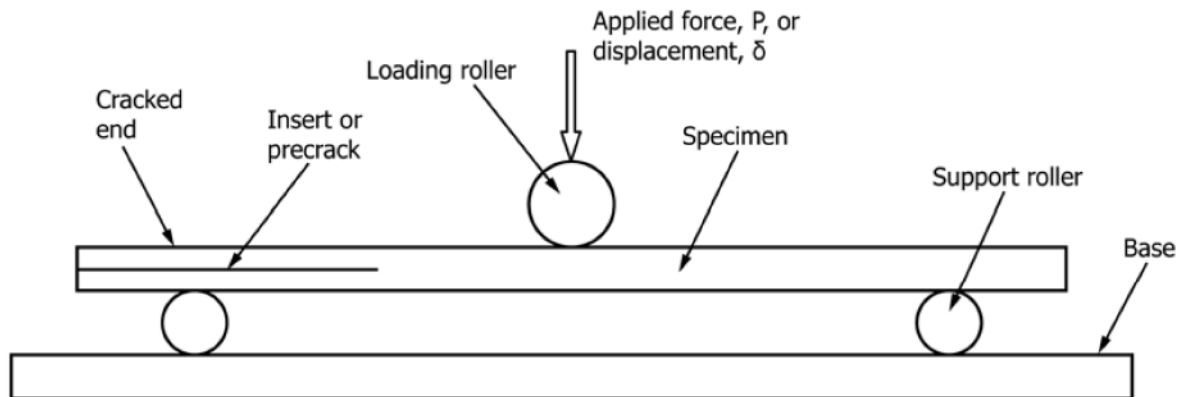
Figure 3.3: Representation of the ENF specimen and its test set-up [50].

this case, the scope of the standard is limited to UD materials. A non-adhesive polymer insert film is placed at the midplane during manufacturing in order to act as a delamination starter. The specimen is loaded in three point bending by means of two lateral support rollers and a central loading roller. The test is performed in displacement control. The recent ASTM standard procedure [50] envisages determination of the interlaminar fracture toughness in both the Non-Pre-Cracked (NPC) condition and the Pre-Cracked (PC) condition, with a second loading phase. It is recommended that the precrack be

obtained by static mode II propagation, which also allows to perform both NPC and PC evaluations using the same specimen. If other precracking techniques are used, a report of the delamination front shape before PC evaluation should be obtained. The unique data reduction technique proposed in [50] is a compliance calibraction method. Hence, before both NPC and PC fracture tests, compliance calibration tests have to be performed. Mode II interlaminar fracture toughness should be evaluated from the maximum force point (P_{Max}) obtained during the test.

3.5 Mixed mode I/II interlaminar fracture toughness testing

As discussed before, a complete intelaminar fracture toughness characterisation does require testing not only in pure modes, but also in mixed mode conditions. To date, the only condition that has been widely investigated is the mixed mode I/II condition. The ASTM published a mixed mode I/II standard test method in 2001, well before publishing the mode II standard [51]. This was likely due to some issues with pure mode II testing and to the greater interest in evaluation of interlaminar fracture toughness in mixed mode conditions rather than in pure mode II [92]. While other configurations have been proposed in the literature, the Mixed Mode Bending (MMB) set-up emerged as the best option, and was used in the ASTM standard. The reasons for this are: the same specimen geometry as for the DCB and ENF tests is used; it allows to vary the mixed mode ratio over the whole range from pure mode I to pure mode II in a rather simple way [72], it maintains a fairly constant mixed mode ratio as the delamination grows [43].

MMB standard test method

The MMB set-up is shown in Fig 3.4. The base of the set-up holds the specimen, while the lever is used to introduce the load. At the insert end, tabs are bonded to both arms of the specimen. The specimen rests on the base: at the undelaminated end it bears on a
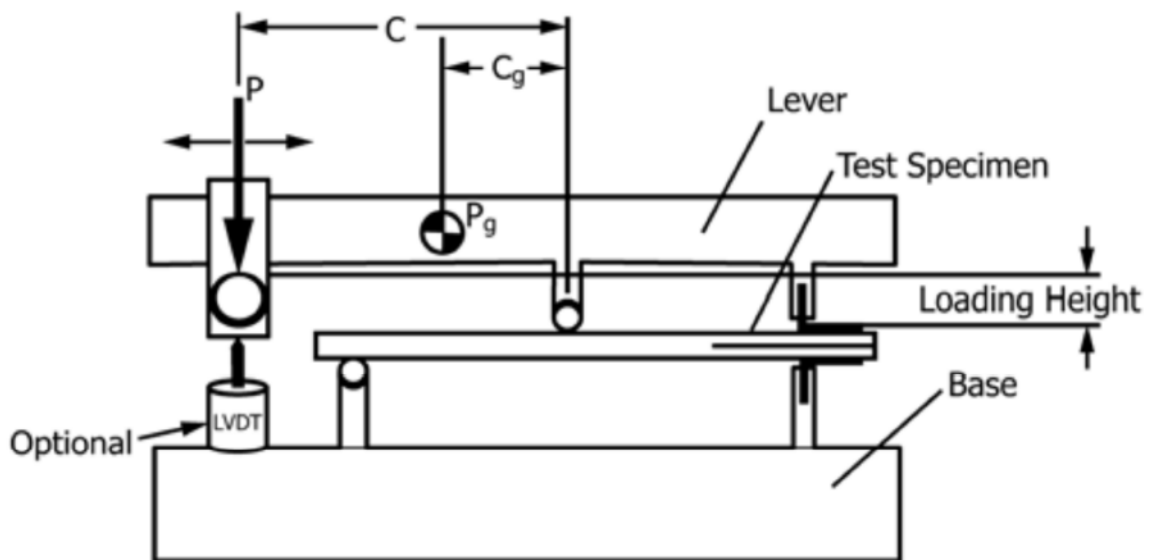
Figure 3.4: Representation of the MMB specimen and its test set-up [51].

support roller, while at the insert end the tab of the lower arm is fixed to the base. The upper tab is connected to the lever, which also bears down on the specimen by means of a roller placed halfway between the the base roller and the tabs. A load is applied to the lever as shown in Fig. 3.4. The lever roller pushes down the specimen in its central region and acts as a fulcrum, thus causing the lever to open the specimen at the tabs location. The mode mix of the test may be adjusted by changing the lever arm (C in Fig. 3.4). The ASTM standard [51] proposes the same definitions of initiation toughness seen for the DCB standard: NL, VIS and 5%/MAX. Delamination propagation in the MMB test may be stable or not, depending on the mode mix. If it is stable, then propagation values of the fracture toughness may be obtained. Similarly to what happens in mode I, and depending on the actual mode mix of the tests, these values may be affected by fibre bridging. The ASTM standard also gives the equation for the computation of the mode mix and of the total fracture toughness.

3.6 Interlaminar fracture testing of multidirectional laminates

Despite the fact that standardisation of interlaminar fracture toughness tests was pursued only using UD laminates, the interest in characterizing interlaminar fracture toughness of MD interfaces never faded out, for obvious reasons: real applications demand, in most cases, MD laminates, where delamination may appear and grow at any interface. Research on the subject never stopped since the 80's and is still highly active. Standard test configurations for UD laminates have been widely used to study delamination in MD laminates. The results obtained, though, were often inconsistent or even contradictory [54]. For this reason, to the present day, no consensus on standard practices has been reached yet. Nonetheless, all the research performed in the past decades allowed to shed some light on the most important problems arising in the attempt to test interlaminar fracture toughness of MD laminates. Besides delamination migration, which remains a major issue in actual experimental testing, other important questions have been risen. In this section, all these issues are reviewed.

3.6.1 Additional energy dissipation mechanisms

Interlaminar fracture, or delamination, may be regarded as a meso-scale (ply level) damage mechanism. At a lower scale (constituents level), it consists mainly in matrix cleavage or cohesive fracture in the resin rich interlaminar region and fibre-matrix interface (also called *interphase*) debonding [71], in proportions that mostly depend on the properties of the constituent materials and of the interphase. As long as no other micro or meso-scale damage mechanism is involved, the interlaminar toughness may be effectively characterised using concepts from LEFM [42, 43, 44, 45], thus according to the standard test procedures reviewed in the previous sections.

However, when MD laminates are involved, one major problem appears: off-axis plies are weak with respect to bending induced normal stresses arising during interlaminar fracture toughness tests. This may lead to the appearance of additional dissipation mechanisms that contribute to the absorption of energy. In this case, LEFM methods may prove inadequate [94].

One first dissipation mechanism is plastic yielding of the matrix, resulting in permanent deformation after the tests. It has been observed both for glass fibre composites [95, 96, 97, 98] and carbon fibre ones [99], especially when specimens had few or no 0° oriented plies. Such yielding does absorb energy during the delamination test, and if it is not properly accounted for or avoided, it may lead to wrong estimations of the interlaminar fracture toughness [95].

Another important mechanism that contributes to energy dissipation is intralaminar damage, mostly in the form of matrix cracking. In order to obtain correct values of interlaminar fracture toughness, such damage must be taken into account or avoided [100]. In fact, intralaminar damage has proved to be one of the main issues in interlaminar fracture testing of MD laminate [54]. Matrix cracks in the off-axis plies embedding the initial delamination plane usually interacts with delamination itself, leading to different undesired and complex propagation modes. In DCB tests on specimens with 0°//90° and 90°//90° interfaces, phenomena of delamination wandering inside 90° plies, creating a saw-tooth appearance [101], were often observed [100, 102, 103, 104, 105, 106]. Similar observations were reported also for mixed-mode tests [107]. Concerning mode II, some authors reported intralaminar fracture of the 90° ply and delamination migration directly from the tip of the insert film, before any propagation [108, 109]. During mode I tests of interfaces with off-axis angles smaller than 90°, delamination bifurcation and migration (or *jump*) phenomena have been observed in a consitent number of studies [102, 104, 106, 110, 111, 112, 113, 114, 115]. Similar phenomena were observed for mode II propagation [109, 113, 116, 117, 118, 119]. In some studies delamination migration was reported to happen only in those specimens having higher angles off-axis plies, both regarding mode I [108, 112] and mode II [120]. It is important to mention that mode I fractures in MD interfaces are usually accompanied by extensive fibre-bridging, often occurring in bundles. In this case, however, bridging is not caused by fibre nesting in adjacent layers as in UD specimens, but rather by the crack propagating inside off-axis plies and separating bundles of fibres from it. It is extremely interesting to observe that Ozdil et al. reported that no jump occurred in their studies [96, 97, 98] and attributed that to the use of a UD-fabric material [97] (i.e. a fabric material in which most of the fibres are aligned in the principal direction and only a small amount of fibres is placed along the transverse direction).

Approaches to avoid matrix cracking and delamination jump were proposed in [112, 121, 122]. In [112], the authors studied the phenomen using the quadratic failure criterion of Tsai-Wu [123], to obtain an estimate of the likelihood of off-axis plies to fail by matrix cracking. A good agreement with experimental results was found. It was suggested that a minimum specimen thickness is required to avoid both geometric (large deformations) and material (matrix damage) non-linearities, and an analytical relationship to calculate such thickness was derived [121]. Finite element (FE) models of DCB specimens with different stacking sequences were developed in [122]. The models included a Cohesive Zone Model (CZM) approach to simulate delamination and an implementation of the LaRC04 in-plane tensile matrix failure criterion [124] to evaluate the tendency of off-axis plies to fail. In this way, the most promising stacking sequences were identified and used for experimental tests in a subsequent study [125]. Strategies to model the phenomenon of delamination migration through matrix cracking phenomenon are currently being investigated [126, 127, 128].

3.6.2 Residual stresses

In MD laminates, due to the different orientation of the layers, ply-level thermal residual stresses may develop [129, 130, 131]. In 1996, Robinson et al. [132] performed mode I delamination tests on carbon/epoxy DCB MD specimens having a standard 0°//0° delamination interface. They found that thermal residual stresses in the specimens greatly affected the apparent interlaminar fracture toughness, despite the standard delamination interface. Similar results were found in [133]: MD laminates of the type $[\pm\theta_2/0]_s$ (thus having 0°//0° delamination interface) with $\theta = 30°, 45°, 60°, 90°$ were tested. Increasing θ led to increased thermal residual stresses, which in turn led to higher fracture toughness.

Nairn developed a theory to account for effects of such stresses in the fracture mechanics analysis of cracks in composite materials [134]. He analysed the standard UD DCB specimen and confirmed that residual stresses do not affect delamination in this particular case. In a later study, he analysed the case of composite DCB specimens with MD layups [135]. He demonstrated that major inaccuracies in the evaluation of the interlaminar fracture toughness may result from the presence of residual stresses. Such inaccuracies depend on the specimen stacking sequence. It was suggested that delamination specimens in which both arms are symmetric laminates be used. The same analysis was extended to other test configurations in [136] and it was specialised for DCB, ENF and MMB test configurations by Yokozeki et al. [137]. Subsequent extensions of this analysis dealt with the problem of the bimaterial interface (which will be introduced later) [138], non-uniform thermal gradients [139] and presence of bending-extension couplings [140]. An expression to obtain energy release rate for symmetric and antisymmetric angle ply laminates including residual stresses was derived in [60].

De Morais et al. performed FE analyses and observed that, with appropriate stacking sequences, effects of thermal residual stresses on the average ERR values obtained by the analyses were negligible [141]. The models, however, did not account for possible intralaminar damage. On the other hand, in [122] an extremely important result was found: the presence of thermal residual stresses, while being hardly noticeable in the force displacement behaviour of delamination specimens, may promote the phenomenon of delamination migration. In other words, not only residual stresses complicate, or even preclude, evaluation of fracture toughness, but they may also trigger other undesirable effects.

3.6.3 Problems related to elastic couplings

Generally, as seen in Chapter 2, MD laminates may present different types of elastic couplings. These couplings have a series of negative consequences that complicates interlaminar fracture toughness evaluation.

Modal contribution and modal partition

In the first place, couplings may affect the mode mix of the tests. When pure mode tests are performed, contributions from other modes should not exist. On the other hand, when performing mixed-mode tests, knowledge of the exact mode-mix is required, in order to meaningfully reduce and exploit experimental data. While standard test configurations [49, 50, 51] address these issues for UD specimens, it is not guaranteed that the same results are achieved when using MD specimens, due to the presence of the couplings that may modify the kinematics of the specimen and may induce unwanted rotations and

parasite modes contributions [112]. This was proven to affect the measured interlaminar fracture toughness [132]. For this reason, Shi et al. [120] urged other researchers publishing results in terms of fracture toughness to ascertain with precision the mode of propagation relevant to the results presented.

However, determination of the modal partition for MD laminates is a challenging task. A procedure that has been widely used is the adoption of the Virtual Crack Closure Technique (VCCT) [142], to calculate ERR modal partition (in most cases, this is done assuming a straight delamination front of the specimen, which is an approximation). The VCCT is a numerical implementation of Irwin's crack closure integral [143]. It was firstly presented in [144] for 2-D problems and then extended in [145] for 3-D cases. Since then, it has been widely used in fracture mechanics analysis.

Though, it should be remarked that when using VCCT to obtain ERR modal partitioning for a crack propagating between two materials with different elastic properties (the so called *bimaterial* interface), such as two differently oriented plies, some problems arise. In 1959 Williams [146] derived the crack-tip stress field for bimaterial interfaces and observed that the singularity at the tip of the crack has an oscillatory behaviour. Subsequently, Raju et al. [147] showed that, for bimaterial interfaces, while the total ERR assumes a well-defined value, ERR modal components do depend on the virtual crack increment Δa, and have an oscillatory behaviour, too. As a consequence, if modal partition is performed using VCCT, a dependence on the mesh size is expected. This problem is treated in some detail in [44, 148]. Additionally, reference [148] reviews available techniques to deal with modal partition for bimaterial interfaces. When dealing with delamination in composite laminate one widely used technique consists in finding an appropriate mesh size to be used at the crack front (Δa), in order to obtain a valid ERR modal partition. Value of Δa such that $1/20 \leq \Delta a/t_{ply} \leq 1$ (where t_{ply} is the basic ply thickness) have generally been found to give good results.

ERR distribution and delamination front shape

Another problematic aspect of mechanical couplings, which is strictly related to those explained in the previous paragraph, is that they affect ERR distribution along the delamination front and, consequently, how such front develops. Indeed, in order to process data obtained from delamination tests, reduction techniques based on 2D theories [49] are usually adopted: a straight front and a uniform ERR distribution are assumed, even though this has long been proven to be an idealisation [85]. Nowadays, tools to predict delamination growth direction are actively being developed, following geometrical considerations [149], or within the framework of CZM [150].

When it comes to MD laminates, moreover, 3D effects may become relevant, and may affect interlaminar fracture toughness evaluation. Historically, two laminate parameters have been used to evaluate these effects. The first is D_c, Eq. (3.5), and the second is B_t, Eq. (3.6):

$$D_c = \frac{D_{xy}^2}{D_{xx}D_{yy}}, \tag{3.5}$$

$$B_t = \left| \frac{D_{xs}}{D_{xx}} \right|, \tag{3.6}$$

where terms D_{ij} are the components of the laminate stiffness matrix, obtained by CLPT; D_c was derived in [151] as a measure of the relative difference in the deflection of the specimen arms between plane strain and plane stress conditions, thus quantifying 3D effects.

From a physical point of view it expresses the importance of the anticlastic (bending-bending) coupling of the laminate. Hence, specimens with higher D_c, are expected to develop more curved ERR distributions and, consequently, delamination fronts. B_t was introduced in [152, 153], in order to quantify another important coupling effect: the bending-twisting one. It was shown that B_t could correlate quite well with the asymmetry of the ERR distribution along a straight delamination front. Subsequent studies analysed the effects of these two parameters in different tests configuration and for different specimen layups [154, 155, 156, 157]. The general conclusion was that both D_c and B_t should be as low as possible. Prombut et al. [52] recommended to verify values of these parameters for all regions of a delamination specimen: both cracked arms considered separately and the entire undelaminated laminate. They also recommended to eliminate the in-plane extension/shear coupling ($A_{xs} = A_{ys} = 0$) and the in-plane/out-of-plane coupling ($\mathbf{B = 0}$). Recently, further numerical investigations were performed by Samborski on both standard DCB [57] and ENF [58] test configuration for MD laminates with mechanical couplings. His results confirmed that stacking sequence has a major effect on critical ERR distribution along delamination front. Experimental evidences of the effects of couplings on the shape of delamination fronts were given in [96, 97, 98].

3.6.4 Approaches to MD specimens design

While some alternative test configurations were tested in the literature [111, 113], their use never gained ground, probably due to their complexity, hardly justifiable in view of standardisation purposes. Therefore, much effort was devoted to the search of optimal MD layups to be used in the standard delamination test methods described in Sections 3.3-3.5 and that could solve, or at least minimise, the problems mentioned in Subsections 3.6.1-3.6.3.

Early design strategies involved the use of sequences containing many 0°-oriented plies, in order to reduce the effects of the presence of off-axis plies at the delamination interface. Examples of this approach may be found in [108, 109, 117, 152, 155]. In no case, however, it was possible to obtain specimens that could completely eliminate elastic couplings and/or thermal effects.

In recent years, some authors adopted QT solutions to design layups for MD delamination specimens. In [53], two QT quasi-homogeneous layups were used to build the arms of symmetric and antisymmetric delamination specimens. Thus, three types of multidirectional specimens free of elastic couplings and having delamination interfaces of the types $\theta//\theta$ and $\theta//-\theta$ (θ being a generic angle) were obtained. While the uncoupling properties of the symmetric specimens presented are easily deduced, it was not explained why also antisymmetric specimens yielded those same properties. In [158, 159] QT quasi-homogeneous sequences with 24 plies were chosen to obtain fully-isotropic laminates, with slightly different lay-ups, but identical elastic properties, according to CLPT. Each sequence was then used as one arm in symmetric delamination specimens. This allowed to obtain specimens having $\theta//\theta$ delamination interfaces with varying θ, but identical elastic properties. One of the sequences proposed in [53] was used also in [160] with a fabric material to obtain quasi-isotropic quasi-homogeneous laminates and thus specimens with 0°//0°, 0°//45° and 45°//45° delamination interfaces. Eventually, in [161] a 18 plies QT sequence was used to build two specimens with 0°//45° delamination interface. While these studies highlight the potential of QT solutions for the problem at hand, they still present limitations with respect to the layups suggested and thus to the type of delami-

nation interfaces that may be obtained.

3.7 Concluding remarks

When it comes to obtaining important material properties, standardisation of test methods is fundamental. This is especially true for toughness, which is often considered one of the most difficult properties to be evaluated.

For interlaminar fracture toughness of polymer matrix composites, standard test methods, reviewed in this chapter, exist, but their scope is limited to UD laminates. This is due partly to historical reasons and partly to the existence of problems that still need a solution, namely appereance of additional dissipation mechanism, presence of thermal residual stresses and of elastic couplings. The extensive research activity in this regard, which is still in progress, has contributed to the understanding of these issues and of their consequences.

Over the years, researchers have proposed different approaches to the design of multidirectional layups in order to try and eliminate elastic couplings and thermal effects. To date, however, no general consensus has been reached and optimal layups are yet to be found.

Consequently, as already mentioned in Chapter 1, the purpose of this study is to develop multidirectional layups free of elastic couplings and of thermal effects. Since in recent studies delamination specimens with very interesting properties were obtained exploiting QT solutions [53, 158, 159, 160, 161], such sequences are adopted in this study as well. Part II of the manuscript will detail the complete approach developed for the layups design. In particular, Chapters 4 and 5 present some developments required for the actual design process, presented in Chapter 6.

Part II

Analytical design of Fully-Uncoupled Multi-Directional stacking sequences for delamination tests

Chapter 4

Search for Quasi-Trivial solutions

4.1 Introduction

As explained in Chapter 3, QT solutions were used in different studies to design MD delamination specimens [53, 158, 159, 160, 161], and showed very interesting features. Indeed, these sequences allow to design laminates with very interesting properties and, as will be shown in this chapter, yield wider design spaces than those typically obtained with classical design strategies (symmetric layups etc.).

As a matter of fact, a number of studies has confirmed the potential of these layups in laminate design problems. In [70], they were used together with the Werren and Norris rule [66] to obtain fully-isotropic laminates. In [69], anti-symmetrical QT uncoupled stacking sequences were used to obtain fully-orthotropic laminates. In [162], it was shown that fully-orthotropic laminates may be obtained using QT quasi-homogeneous solutions with angle-ply orientations; these layups were then used to find optimal solutions with respect to flexural properties of laminates. QT quasi-homogeneous solutions with angle-ply orientations were used in [163] too, within an optimisation procedure for thin laminated shells. Recently, QT sequences were successfully applied in the framework of a multi-scale two-level optimisation strategy for many different engineering problems [14, 15, 16, 164, 165, 166].

Despite their potential, however, QT solutions are not widely used yet. One cause is probably the fact that only a limited number of QT solutions is available in the literature and that they are not easily obtained. Because of this reason, in order to exploit QT solutions for the purpose of this study, the development of an algorithm able to find such solutions and to create a rich database was required. In this Chapter, the details about the conception and the implementation of such algorithm are detailed. Section 4.2 shows how QT solutions are derived in the context of CLPT. Section 4.3 explains the principles and difficulties behind the search for QT solutions and details the design and implementation of the algorithm developed. Eventually, Section 4.4 briefly reports details on the results of the search and some comments. Concluding remarks end the chapter.

4.2 Quasi-Trivial solutions: fundamentals

The existence of QT solutions was demonstrated by Vannucci and Verchery in [68]. They used the polar formalism, first introduced by Verchery [167], in order to represent tensors $\mathbf{A}$, $\mathbf{B}$ and $\mathbf{D}$. This allowed separating the contributions deriving from the mechanical

properties of the basic ply material and from geometrical configuration of the layup (position and orientation of plies). This way, Eq. (2.124) for uncoupling of the laminate and Eq. (2.125) for membrane-bending homogeneity could be rewritten, using the same notation of Chapter 2, respectively as follows:

$$\sum_{k=1}^{n} b_k e^{4i\delta_k} = 0 , \quad \sum_{k=1}^{n} b_k e^{2i\delta_k} = 0 , \qquad (4.1)$$

$$\sum_{k=1}^{n} c_k e^{4i\delta_k} = 0 , \quad \sum_{k=1}^{n} c_k e^{2i\delta_k} = 0 . \qquad (4.2)$$

Coefficients b_k and c_k have been defined in Chapter 2, and are here recalled for the sake of convenience:

$$b_k = 2k - n - 1 , \qquad (4.3)$$

$$c_k = -12k(k - n - 1) - 2n^2 - 6n - 4 . \qquad (4.4)$$

QT sequences are a particular class of solutions to Eq. (4.1), Eq. (4.2), or both. The concurrent fulfilment of both Eqs. (4.1) and (4.2) gives quasi-homogeneity of the laminate. The concept behind these solutions can be explained as follows. Consider a laminate composed of n plies with m different orientation angles θ_j ($j = 1, ..., m$); in Fig. 4.1 an example is given, to visually clarify the concepts explained here. Let G_j be the set of indexes of those plies that share the same orientation angle θ_j, i.e.:

$$G_j = \{k : \delta_k = \theta_j\} ; \quad j = 1, .., m . \qquad (4.5)$$

The union of all the m G_j sets gives the complete set of ply indexes of the laminate, $k = 1, ..., n$. Eqs. (4.1) and (4.2) can be split as sums over the different sets G_j ($j = 1, ..., m$):

$$\sum_{k=1}^{n} b_k e^{4i\delta_k} = \sum_{j=1}^{m} e^{4i\theta_j} \sum_{k\in G_j} b_k , \quad \sum_{k=1}^{n} b_k e^{2i\delta_k} = \sum_{j=1}^{m} e^{2i\theta_j} \sum_{k\in G_j} b_k , \qquad (4.6)$$

$$\sum_{k=1}^{n} c_k e^{4i\delta_k} = \sum_{j=1}^{m} e^{4i\theta_j} \sum_{k\in G_j} c_k , \quad \sum_{k=1}^{n} c_k e^{2i\delta_k} = \sum_{j=1}^{m} e^{2i\theta_j} \sum_{k\in G_j} c_k . \qquad (4.7)$$

A group of plies all oriented at the same angle θ_j is defined as *saturated group* with respect to b_k, c_k or both, if the sums of the relevant coefficients for its plies are null:

$$\sum_{k\in G_j} b_k = 0 , \qquad (4.8)$$

$$\sum_{k\in G_j} c_k = 0 . \qquad (4.9)$$

Accordingly, the associated set G_j of ply indexes is called *saturated set*. If all the orientation groups appearing in a stacking sequence are saturated, then Eqs. (4.1) and (4.2) are satisfied, regardless of the value assumed by the orientations θ_j. In other words, only the way orientations are distributed within the stack are relevant to fulfil these requirements. A sequence entirely composed by saturated groups is a QT solution [68]. Then, the following three types of QT solutions may be recognised:
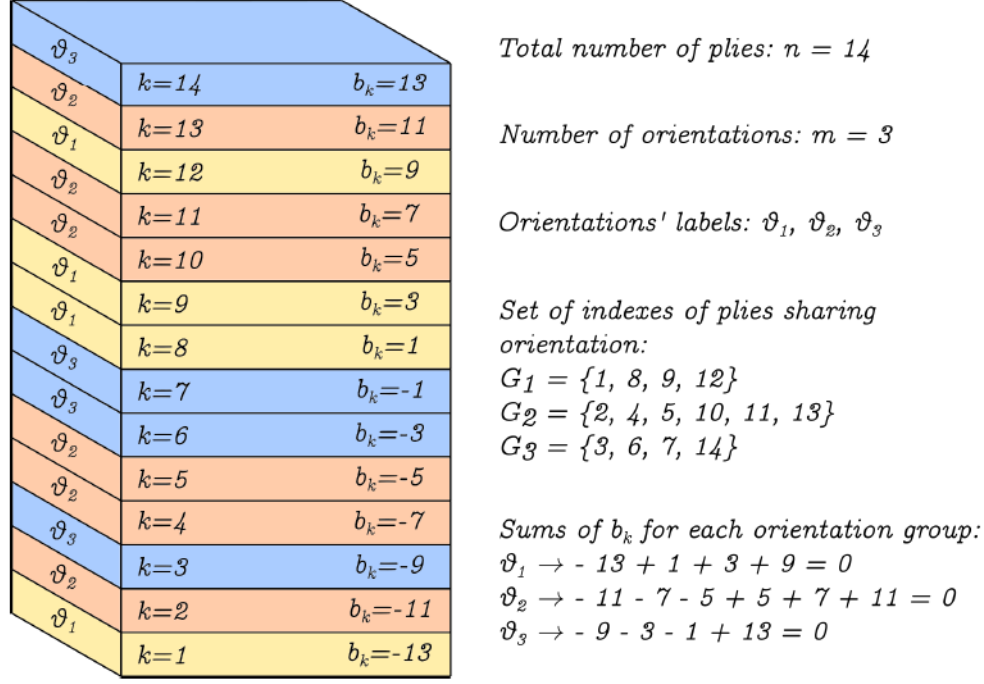
Figure 4.1: Graphic explanation of the concept of QT solution.

1. *uncoupled*: all orientation groups are saturated with respect to coefficient b_k;

2. *membrane-bending homogeneous*: all orientation groups are saturated with respect to coefficient c_k;

3. *quasi-homogeneous*: all orientation groups are saturated with respect to both coefficients b_k and c_k.

The following sequence, with $n = 14$ and $m = 3$, used in Fig. 4.1, is an example of QT quasi-homogeneous solution:

$$[\,\theta_1\,/\,\theta_2\,/\,\theta_3\,/\,\theta_2\,/\,\theta_2\,/\,\theta_3\,/\,\theta_3\,/\,\theta_1\,/\,\theta_1\,/\,\theta_2\,/\,\theta_2\,/\,\theta_1\,/\,\theta_2\,/\,\theta_3\,]\,.$$

By arbitrarily choosing the values of θ_j angles, an infinite number of lamination sequences can be obtained. A remarkable consequence is that, using QT solutions, the orientation angles of the plies can be chosen to tailor the mechanical properties of the laminate according to some given requirement (strength, stiffness, dynamic response etc.), while the properties of uncoupling and membrane-bending homogeneity are automatically satisfied. This makes this class of sequences extremely effective for the design and optimization of composite laminates.

4.3 Search for QT solutions

Despite their potential, QT solutions are not often used, the main reason being that the literature offers only a limited number of examples. On the other hand, finding QT solutions requires the implementation of a dedicated algorithm, for which a clear description and implementation guidelines are lacking.

4.3.1 The problem of QT search

The only information available on the strategy to find QT solutions was given in [68]. In particular, it was stated that they may be found exploiting their basic properties, and in particular identifying saturated groups, with respect to coefficient b_k, c_k or both. Hence, the search for QT solutions reduces to the resolution of a combinatorial problem whose main goal is the identification of null sums of integers. In general, the process may be thought as described in Algorithm 1: first, all possible sequences should be generated; second, a quasi-triviality check should establish which sequences are entirely composed by saturated groups; finally, only QT solutions, and only independent ones (this concept will be better explained later), have to be stored.

Algorithm 1 Simple QT solutions finder algorithm

1. Set inputs: n and m;
2. Generate all possible sequences with n, m;
3. For each sequence generated at step 2, check for quasi-triviality:
   3.1 Perform the desired check (on b_k, c_k, or both);
   3.2 Store QT solutions;
4. Eliminate *non-independent* QT solutions.

Despite its conceptual simplicity, Algorithm 1 soon encounters efficiency problems. It is easy to observe, indeed, that if all possible sequences are generated, their number increases extremely fast with the total numbers of plies n. Consequently, the stacks generation process becomes extremely heavy, and so does the quasi-triviality check: the computational resources required to run the algorithm become prohibitive even for low total numbers of plies n. To put this into perspective, Fig. 4.2 reports the total number of independent QT solutions (in logarithmic scale), for the three different types of quasi-triviality, as a function of the number of plies n. It can be recognised that also the number of QT solutions (which may be thought as a characteristic dimension of the problem) increases extremely fast with n. Moreover, QT solutions only represent a (relatively) small subset of all possible sequences to be generated and checked. This clearly shows how an increment of even one ply in the total length of QT solutions to be found may be a difficult result to obtain. As a consequence of the above, the lowest possible number of sequences should be generated, without however excluding any actual solution. In this way, the operations to be performed in both the generation phase and the quasi-triviality check would be significantly reduced, and longer solutions may be found.

4.3.2 Exploitation of QT solutions properties

In order to reduce the number of sequences to be generated and checked, the properties of QT solutions have to be investigated in depth, so that it becomes possible to recognise, a priori, classes of sequences that cannot be QT solutions, and avoid generating them. The objective of this section is to show some relevant properties of QT solutions, and to explain how they could be exploited in the conception of the QT search algorithm.

Properties of coefficients b_k and c_k

As anticipated in Chapter 2, coefficients b_k and c_k have some interesting properties. Firstly, they always take integer values. Moreover, the sum of both coefficients over
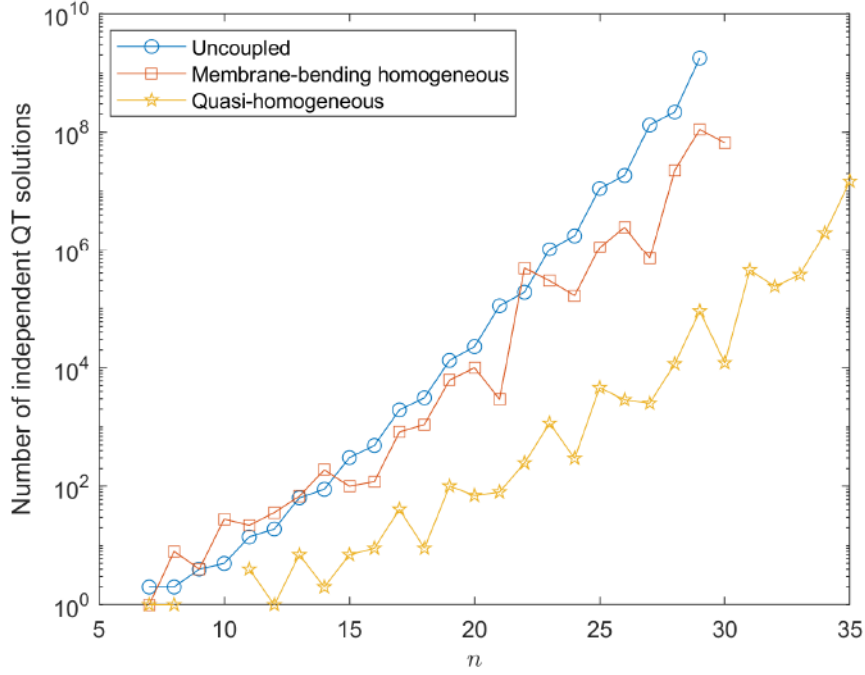
Figure 4.2: Total number of independent QT solutions as a function of the number of plies n.

the entire ply index interval $[1, n]$ is always zero, whichever the number n of plies of the sequence:

$$\sum_{k=1}^{n} b_k = 0 \,, \tag{4.10}$$

$$\sum_{k=1}^{n} c_k = 0 \,. \tag{4.11}$$

It was also observed, see Fig. 2.5, that coefficient b_k varies linearly with ply index k and shows antisymmetric values with respect to the middle plane of the sequence. As a consequence, coefficient b_k assumes the value 0 in sequences having an odd number of plies and only in correspondence of the central ply of the sequence. Coefficient c_k, on the other hand, has a parabolic variation with respect to k and gets symmetric values with respect to the middle plane. Hence, it assumes value 0 only for specific values of n (e.g. $n = 7$ and $n = 26$), and in such cases there are always two symmetric plies, with respect to the middle plane of the sequence, that show $c_k = 0$. It is particularly relevant to know if some plies get $b_k = 0$ or $c_k = 0$, as this means that such plies could stand alone as a saturated group.

Taking into account the previous considerations, it is notably useful to observe that each sequence can be divided in two different set of plies, or *half-stacks*, based on the sign, positive or negative, assumed by the considered coefficient (note that in the case of c_k the number of plies of the two half-stacks may be different). If a sequence has an orientation group appearing only in one of the two half-stacks, then it cannot be a QT solution, as that group simply cannot be saturated. This condition may be used to reduce the number of sequences generated and checked by the algorithm.

Mathematical distinction

Consider the following two QT uncoupled solutions:

$$[\,\theta_1\,/\,\theta_2\,/\,\theta_2\,/\,\theta_2\,/\,\theta_2\,/\,\theta_1\,]\,, \tag{4.12}$$

$$[\,\theta_1\,/\,\theta_2\,/\,\theta_3\,/\,\theta_3\,/\,\theta_2\,/\,\theta_1\,]\,. \tag{4.13}$$

In [68] these solutions were defined as *not mathematically distinct*. This is because the first one can be obtained from the second one by assuming that orientations θ_2 and θ_3 are identical, which is always possible because orientations can be chosen arbitrarily, as explained in Section 4.2. In other words, the second solution is more general, and include the first one as a particular case. Hence, only the second solution should be considered. More in depth, the first solution has a saturated group ($j = 2$) that is composed by two saturated sub-groups: $\{k = 2, 5\}$ and $\{k = 3, 4\}$. In the second solution the sub-group $\{k = 3, 4\}$ is labelled with a different generic orientation (θ_3): all the new groups obtained are still saturated. A solution, then, will be called mathematically distinct if no other QT solutions with a greater number of orientation groups may be obtained from it (in other words, the saturated groups of the sequence do not contain saturated sub-groups). This shows that, in general, a solution with a given number m of orientation groups can be obtained from a mathematically not distinct solution with $m - 1$ orientation groups. Generalising, it is easy to conclude that, for a given n, all QT solutions with $m > 2$ may be found from the set of QT solutions with $m = 2$ including mathematically not distinct solutions.

From a practical point of view, this conclusion may be exploited when devising a search algorithm, in order to drastically reduce the number of sequences generated and checked for quasi-triviality. Indeed, as a consequence, the algorithm may be structured to initially generate and check for quasi-triviality only sequences with $m = 2$. Avoiding generation of sequences with $m > 2$ drastically reduces the amount and the complexity of operations to be performed. Then, the search for QT solutions with $m > 2$ may be performed in the *raw* (i.e. containing mathematically non distinct solutions) set of solutions with $m = 2$, which is, of course, much smaller than the set of all possible sequences with $m > 2$.

Mechanical distinction

Consider now the following two QT uncoupled solutions:

$$[\,\theta_1\,/\,\theta_2\,/\,\theta_3\,/\,\theta_3\,/\,\theta_2\,/\,\theta_1\,]\,, \tag{4.14}$$

$$[\,\theta_3\,/\,\theta_2\,/\,\theta_1\,/\,\theta_1\,/\,\theta_2\,/\,\theta_3\,]\,. \tag{4.15}$$

In [68], these solutions are referred to as *not mechanically distinct*: since θ_j are only labels and the orientations may be chosen arbitrarily, the two sequences are mechanically equivalent. Indeed, the second one may be obtained from the first one by switching the orientation labels θ_1 and θ_3. As a consequence, only one of the two sequences should be considered and stored. In order to effectively eliminate not mechanically distinct solutions, it is suggested in [68] that saturated groups in all solutions be ordered in an ascending way. Thus, not mechanically distinct solutions are easily identified and eliminated.

This same idea may be exploited in the search algorithm to further reduce the number of operations to be performed. Indeed, knowing a priori not mechanically distinct solutions, it is convenient to try and avoid generating them in the first place. If this is accomplished, the sequences generations phase is faster and less sequences are checked for quasi-triviality, thus greatly improving the efficiency of the algorithm. From a practical point of

view, this is possible by restraining the algorithm to generate sequences with orientation groups appearing in an ascending order, so that for example sequence $[\theta_1 / \theta_2 / \theta_2 / \theta_2]$ will be generated and checked for quasi-triviality, but sequence $[\theta_2 / \theta_1 / \theta_1 / \theta_1]$, which is not mechanically distinct from the previous one, will not be generated at all.

When a solution is both mechanically and mathematically distinct from all others, it is called *independent*.

4.3.3 QT solutions search algorithm

Exploiting the ideas explained above, a new algorithm for the search of QT solutions was implemented in Matlab. The flow chart of the algorithm is shown in Fig. 4.3.

As explained before, the algorithm initially finds all QT solutions with $m = 2$, and the only input required is the total number of plies n of the solutions. For this case ($m = 2$), application of the properties explained in subsection 4.3.2 simply translates in generating sequences in which the first ply appearing has orientation θ_1 and in which both half-stacks contain both orientations θ_1 and θ_2. In the algorithm proposed, sequences are not generated as a whole, but rather in half-stacks. It is worth mentioning that the generation phase is slightly different for the different type of QT solutions searched (uncoupling, membrane-bending homogeneity or quasi-homogeneity). For one of the two half-stacks, all possible instances are generated in one single shot, and a variable stores them. Then the algorithm enters a cycle wherein:

1. a certain amount of instances for the second half-stack are generated;

2. complete sequences are assembled;

3. the complete sequences are checked for quasi-triviality;

4. QT solutions are passed as output, other sequences are discarded.

This approach was chosen since it was considered as a good compromise between computational time and memory requirements. At the end of this stage, a set of raw QT solutions (in which mathematically not distinct solutions have not been eliminated) for the case $n, m = 2$ is obtained.

Then, the algorithm enters a second cycle, wherein QT solutions with $m > 2$ are found. The raw set of QT solutions with $m = 2$ enters the cycle as an input for the first loop. To begin with, the raw solutions are analysed by a function that classifies them in three different types:

1. solutions that contain saturated subgroups in the group of orientation θ_{m-1}. Since mathematically not distinct solutions have not been eliminated, also solutions in which the same saturated subgroups assume orientation θ_m will exist. Therefore, solutions of this first type are discarded;

2. solutions that contain saturated subgroups in the group of orientation θ_m. These solutions are not mathematically distinct from solutions obtained by giving a different orientation to a saturated subgroup. For this reason, they are not useful in their actual form, but may be transformed to obtain solutions with higher number of saturated groups. In other words, the existence of solutions of this type is a proof that independent solutions with higher number of saturated groups exist;
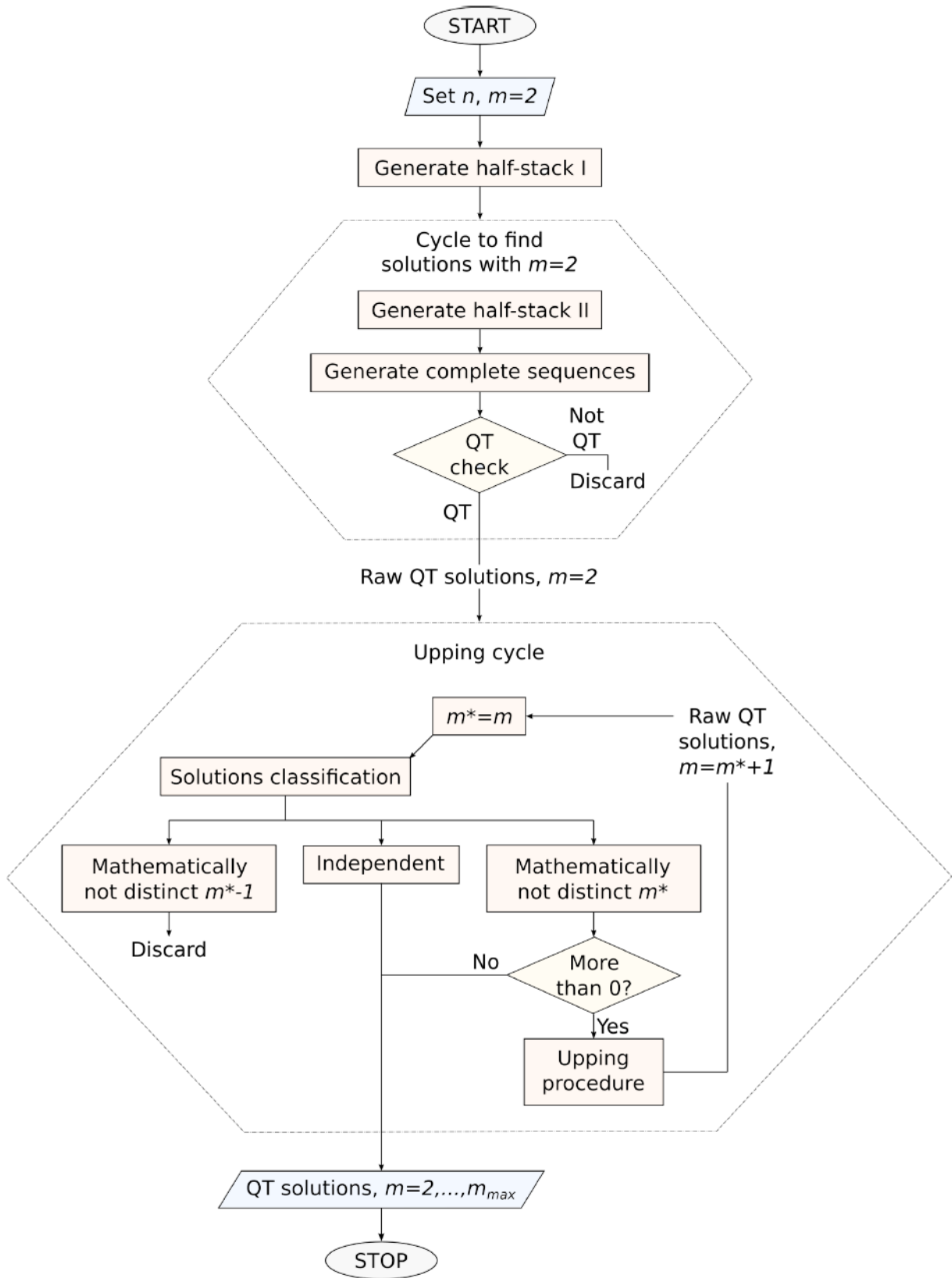
Figure 4.3: Flow chart of the algorithm developed for the search of QT solutions.

3. independent solutions. For the case at hand (n, m), these are the solutions that need to be stored.

After classification, solutions of the first type are discarded, while solutions of the third type are stored, ready to be passed as outputs. The existence of solutions of the second type is the criterion for the algorithm to keep cycling: if no such solution exists, then all independent solutions have already been found and the cycle can be terminated. Otherwise, the algorithm will continue cycling. Firstly, all saturated subgroups in such sequences are found. Then, a dedicated function generates new QT solutions by *upping* (i.e. transforming the orientation from θ_m to θ_{m+1}) these subgroups, one at a time. During this procedure, many new solutions with $m + 1$ saturated groups may be obtained from each solution. Moreover, mechanically not distinct solutions may be obtained, so a dedicated function acts as a filter. The result of this upping procedure is a new set of raw solutions, with higher m, that becomes the input for the next loop of the cycle. The cycle goes on until all independent QT solutions have been found.

4.4   Quasi-Trivial solutions search: results

The results in terms of number of QT solutions found with the algorithm detailed in the previous section are reported in Tables 4.1, 4.2 and 4.3 for the case of uncoupling, membrane-bending homogeneity and quasi-homogeneity, respectively.

Concerning these results, two main aspects should be remarked. To begin with, for a given total number of plies n, the number of QT solutions found in this work exceeds, in some cases, the number reported in previous studies [62, 68, 168]. To confirm this result, these cases were cross-checked by using differently coded algorithms for QT solutions search. It appears, then, that the number of existing QT solutions is higher than what it was believed to be to this date, which is arguably a positive finding. Secondly, it can be observed that, thanks to the proposed algorithm (and to the more powerful hardware available nowadays), QT solutions with higher total number of plies have been found. These solutions may be extremely useful for applications in which laminates made of several plies have to be used. Moreover, as already mentioned, the number of solutions rapidly increases with n, thus allowing very wide design spaces.

In Table 4.1 it can be observed that, for each given number of plies n, there is always one independent QT uncoupled solution with $n/2$ orientation groups, if n is even, or $(n+1)/2$ if n is odd. This particular solution is the only independent symmetric solution existing for the given n. Indeed, all symmetric solutions, whichever the number of different orientations they contain, can be obtained from this one. This shows how much wider the class of QT uncoupled solutions is with respect to that of symmetric solutions.

						N. of groups m									
n	2	3	4	5	6	7	8	9	10	11	12	13	14	15	Total
7	0	1	1	0	0	0	0	0	0	0	0	0	0	0	2
8	1	0	1	0	0	0	0	0	0	0	0	0	0	0	2
9	0	1	2	1	0	0	0	0	0	0	0	0	0	0	4
10	0	4	0	1	0	0	0	0	0	0	0	0	0	0	5
11	0	0	9	4	1	0	0	0	0	0	0	0	0	0	14
12	1	8	9	0	1	0	0	0	0	0	0	0	0	0	19
13	0	0	25	32	6	1	0	0	0	0	0	0	0	0	64
14	0	37	34	17	0	1	0	0	0	0	0	0	0	0	89
15	0	0	10	207	78	9	1	0	0	0	0	0	0	0	305
16	0	58	305	96	29	0	1	0	0	0	0	0	0	0	489
17	0	0	2	893	895	144	12	1	0	0	0	0	0	0	1947
18	0	114	1492	1262	208	45	0	1	0	0	0	0	0	0	3122
19	0	0	0	2216	8192	2663	264	16	1	0	0	0	0	0	13352
20	0	0	7391	11240	3683	396	66	0	1	0	0	0	0	0	22777
21	0	0	0	4936	59701	39986	6283	406	20	1	0	0	0	0	111333
22	0	0	29144	101207	49008	8869	694	93	0	1	0	0	0	0	189016
23	0	0	0	6369	346057	519231	141298	13130	626	25	1	0	0	0	1026737
24	0	0	75421	844224	665507	156300	18569	1118	126	0	1	0	0	0	1761266
25	0	0	0	3863	1775560	6116700	2797033	388970	24060	893	30	1	0	0	11107110
26	0	0	96098	6277657	8836070	2900569	410040	35272	1708	166	0	1	0	0	18557581
27	0	0	0	660	6978620	61170759	51236513	10978670	941503	41907	1261	36	1	0	131349930
28	0	0	136700	40159296	112753933	54164504	9788692	940584	62404	2520	214	0	1	0	218008848
29	0	0	0	20	21692599	561464759	868233466	285533218	34157728	1974630	66910	1682	42	1	1773125055

Table 4.1: Number of independent QT uncoupled solutions obtained as a function of the total number of plies, n, and of the number of saturated orientation groups, m.

	N. of groups m									
n	2	3	4	5	6	7	8	9	10	Total
4	2	0	0	0	0	0	0	0	0	2
5	2	0	0	0	0	0	0	0	0	2
6	4	0	0	0	0	0	0	0	0	4
7	0	1	0	0	0	0	0	0	0	1
8	8	0	0	0	0	0	0	0	0	8
9	4	0	0	0	0	0	0	0	0	4
10	20	8	0	0	0	0	0	0	0	28
11	0	22	0	0	0	0	0	0	0	22
12	36	0	0	0	0	0	0	0	0	36
13	16	52	0	0	0	0	0	0	0	68
14	2	12	32	128	16	0	0	0	0	190
15	0	100	0	0	0	0	0	0	0	100
16	0	32	40	16	32	0	0	0	0	120
17	142	652	32	0	0	0	0	0	0	826
18	34	720	336	16	0	0	0	0	0	1106
19	4	1436	4232	512	0	0	0	0	0	6184
20	68	4856	5104	0	0	0	0	0	0	10028
21	26	500	1168	1248	0	0	0	0	0	2942
22	0	36804	302832	139424	4864	0	0	0	0	483924
23	50	164918	129212	2016	0	0	0	0	0	296196
24	152	5864	159632	0	0	0	0	0	0	165648
25	0	314018	665512	123044	4000	0	0	0	0	1106574
26	0	0	0	7726	475651	1350916	602243	33566	330	2470432
27	0	72760	401544	198288	41984	64	0	0	0	714640
28	0	80016	5805360	11873344	4354656	391168	6144	0	0	22510688
29	0	1581798	58153488	48739304	2370944	0	0	0	0	110845534
30	0	230080	11643720	30155840	19142560	4513920	235520	0	0	65921640
31	0	4078346	684639064	615365800	60452912	1296000	0	0	0	1365832122

Table 4.2: Number of independent QT membrane-bending homogeneous solutions obtained as a function of the total number of plies, n, and of the number of saturated orientation groups, m.

	N. of groups m					
n	2	3	4	5	6	Total
7	1(1)	0	0	0	0	1(1)
8	1	0	0	0	0	1
9	0	0	0	0	0	0
10	0	0	0	0	0	0
11	4(2)	0	0	0	0	4(2)
12	1	0	0	0	0	1
13	4	3	0	0	0	7
14	0	2(1)	0	0	0	2(1)
15	4	3	0	0	0	7
16	6	3(1)	0	0	0	9(1)
17	30	11	0	0	0	41
18	0	9	0	0	0	9
19	60	41	0	0	0	101
20	52	17	1	0	0	70
21	62	18(2)	0	0	0	80(2)
22	32(2)	188(1)	26	2	0	248(3)
23	189(1)	970	0	0	0	1159(1)
24	248	47	1	0	0	296
25	326	4184	98	0	0	4608
26	108	2065 (2)	672 (3)	41 (2)	3	2889 (7)
27	171(1)	1804	510	39	1	2525(1)
28	357	9492(1)	1691(2)	61	9	11610(3)
29	122	75281	15068	167	0	90638
30	106	10923	1009(3)	51	0	12089(3)
31	28	290227	156565(1)	1728	1	448549(1)
32	263	161436(5)	70091	4521	100	236411(5)
33	316	260442	112324	937	0	374019
34	716	1389039 (107)	568492 (35)	12589	38	1970874 (142)
35	2	8291650 (8)	6392064 (7)	90433	82	14774231 (15)

Table 4.3: Number of independent QT quasi-homogeneous solutions obtained as a function of the total number of plies, n, and of the number of saturated orientation groups, m; the number of symmetric solutions is reported in parentheses.

With respect to membrane-bending homogeneous solutions, Table 4.2, it is very interesting to observe what happens for the case $n = 26$. In this case, two plies in the sequence show $c_k = 0$. As these plies can stand alone as saturated groups, the consequence is that there is a shift towards higher values in the number of orientation groups for which independent solutions are found, which is evident in Table 4.2.

Eventually, concerning quasi-homogeneous solutions, the most interesting remark to be made is that their number is significantly lower than that of uncoupled and membrane-bending homogeneous solutions, as observed both in Fig. 4.2 and in Table 4.3. This was

to be expected, since quasi-homogeneity combines both requirements of uncoupling and membrane-bending homogeneity. This is also the reason why it is simpler to find solutions for higher values of n: since their number is lower, the problem remains less demanding than in the other cases.

4.5 Concluding remarks

In this chapter, the details about the design and the implementation of the algorithm used in this work to obtain QT solutions have been presented. It is important to point out that the algorithm proposed here is not the only solution possible, of course. In fact, it seems likely that a more formal approach from a mathematical and programming point of view could lead to further improvements. Nonetheless, thanks to the presented algorithm, some important results were obtained. Firstly, it was found that the number of existing QT solutions is higher than what expected from older studies. In addition, it was possible to find QT solutions with significantly higher total number of plies than in the past. This allowed to create an extensive database of QT uncoupled, membrane-bending homogeneous and quasi-homogeneous solutions. In the context of this work, such solutions will be used with the objective of designing multidirectional delamination specimens, but, as explained in Section 4.1, they may be extremely useful whenever laminate design is concerned.

Chapter 5

Superposition rules for Quasi-Trivial solutions

5.1 Introduction

In Chapter 4, a detailed discussion on QT solutions was presented. Beside the explanation of the properties of these sequences, it was mentioned how important and effective they could be in laminate design. Moreover, this is true even when looking for optimal layups for delamination testing of MD interfaces, as confirmed by the relevant references already introduced [53, 158, 159, 160, 161]. In those studies the authors were able to obtain delamination specimens with excellent uncoupling properties. While this could suggest that QT stacking sequences are a good solution to design MD delamination specimens, what is still missing is a general framework to understand how they could be effectively used and combined in a much more general way than those presented in existing studies.

To respond to this need, superposition rules for QT solutions have been developed, and constitute the main topic of this chapter. The issue of superposition of QT solutions was mentioned in [168], where however the authors concluded that, generally speaking, the superposition of two QT stacks does not yield a new QT one. Here, the superposition rules were derived within the framework of CLPT, as analytical closed form solutions. They give the conditions that some initial QT solutions need to respect in order for their superposition to be another QT solution. The rules were derived for an arbitrary number of superposed sequences. From a practical point of view, this allows to design stacking sequences with a complete control over the properties of some sub-sequences to be superposed, but also over the properties of the resulting sequence.

The chapter is organised as follows. Firstly, Section 5.2 introduces the terms and the notation that will be used in the chapter. In more detail, the notation to describe the QT solutions to be superposed and the sequence obtained is laid out, along with the notation useful to describe the superposition process. Then, Sections 5.3 to 5.5 present the derivation of the criteria to obtain uncoupling, membrane-bending homogeneity and quasi-homogeneity, respectively, of the sequence obtained by the superposition. In particular, in each of these sections, the case of superposed uncoupled, membrane-bending homogeneous and quasi homogeneous QT solutions will be treated. Finally, Section 5.6 will present the application of the superposition rules to the particular case of the superposition of only two QT solutions, along with some examples. Indeed, this case may be of great interest for practical applications, and will be useful for the developments in the following chapters of this manuscript.

5.2 Superposition of QT solutions: notation

In this section, the notation adopted in the chapter is outlined.

To begin with, the term *initial* will be used to identify known QT solutions that are going to be superposed. The sequence resulting from such superposition will be called *macro-sequence*.

5.2.1 Initial QT solutions description

The number of initial QT solutions to be superposed will be maintained general, and is indicated by q. Fig.5.1 graphically represents the description of the initial QT solutions. They are identified by the label QT_i, where $i = 1, ..., q$. The total number of plies in each

$$G_1^{(1)} = \{1, 6, 8\} \qquad G_1^{(i)} = \{1, 5, 6\} \qquad G_1^{(q)} = \{1, 4, 6, 7\}$$
$$G_2^{(1)} = \{2, 4, 9\} \qquad G_2^{(i)} = \{2, 3, 7\} \qquad G_2^{(q)} = \{2, 3, 5, 8\}$$
$$G_3^{(1)} = \{3, 7\} \qquad G_3^{(i)} = \{4\}$$
$$G_4^{(1)} = \{5\}$$
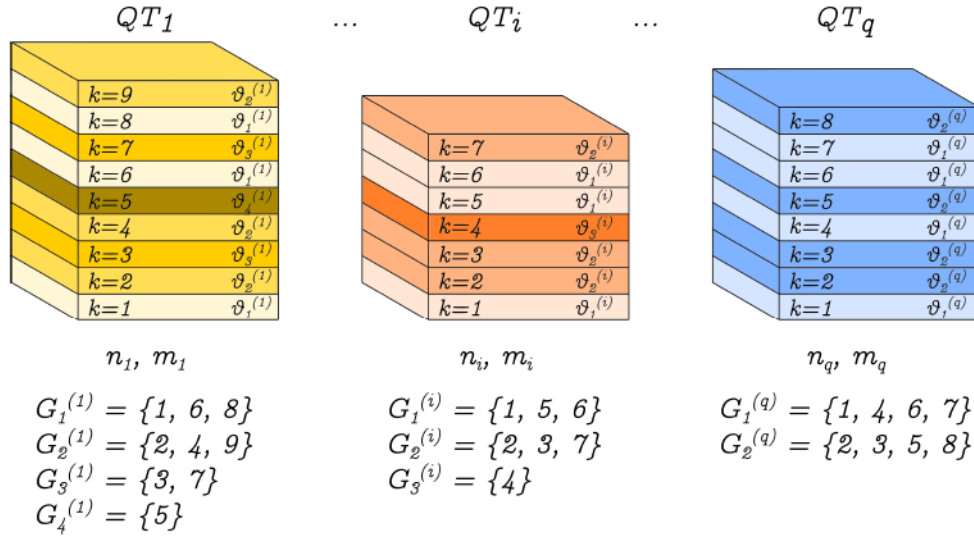
Figure 5.1: Notation associated with initial QT solutions to be superposed.

initial solution is indicated by n_i, while the number of orientation groups existing in the sequence is m_i. Similarly to what was done in Chapter 4, the index j will be used to distinguish such groups. Hence, we will indicate with $\theta_j^{(i)}$ the j-th orientation in sequence QT_i, and with $G_j^{(i)}$ the set of k indexes of plies oriented at $\theta_j^{(i)}$ in sequence QT_i:

$$G_j^{(i)} = \left\{ k : \delta_k = \theta_j^{(i)} \right\}. \tag{5.1}$$

The entire set of k indexes of sequence QT_i is labelled $K^{(i)}$, so that:

$$K^{(i)} = \bigcup_{j=1}^{m_i} G_j^{(i)}. \tag{5.2}$$

Eventually, to completely define the initial solutions, their quasi-triviality type, as explained in Chapter 4, should be specified. Namely, they can be:

1. **Uncoupled QT solutions.** In this case, for each initial sequence QT_i, Eq. (4.8) holds and can be rewritten as:

$$\sum_{k \in G_j^{(i)}} b_k = 0; \qquad \begin{cases} \forall\, i = 1, ..., q\,; \\ \forall\, j = 1, ..., m_i\,. \end{cases} \tag{5.3}$$

Taking into account the general expression of b_k given in Eq. (4.3), Eq. (5.3) becomes:

$$\sum_{k \in G_j^{(i)}} \left(2k - n_i - 1 \right) = 0\,; \qquad \begin{cases} \forall\, i = 1, ..., q\,; \\ \forall\, j = 1, ..., m_i\,. \end{cases} \tag{5.4}$$

2. **Membrane-bending homogeneous QT solutions.** In this case, Eq. (4.9) applies to all initial solutions:

$$\sum_{k \in G_j^{(i)}} c_k = 0\,; \qquad \begin{cases} \forall\, i = 1, ..., q\,; \\ \forall\, j = 1, ..., m_i\,. \end{cases} \tag{5.5}$$

Taking into account the general expression of c_k given in Eq. (4.4), Eq. (5.5) becomes:

$$\sum_{k \in G_j^{(i)}} \left[-12k \left(k - n_i - 1 \right) - 2n_i^2 - 6n_i - 4 \right] = 0\,; \quad \begin{cases} \forall\, i = 1, ..., q\,; \\ \forall\, j = 1, ..., m_i\,. \end{cases} \tag{5.6}$$

3. **Quasi-homogeneous QT solutions.** If the initial QT solutions are quasi-homogeneous, then Eqs. (5.3) to (5.6) all hold.

5.2.2   Macro-sequence description

According to Figure 5.2, the initial solutions are superposed in a bottom-up order: the first one, QT_1, is placed at the bottom of the macro-sequence while the last one, QT_q, is placed at the top. To refer to quantities related to the macro-sequence, the symbol * will
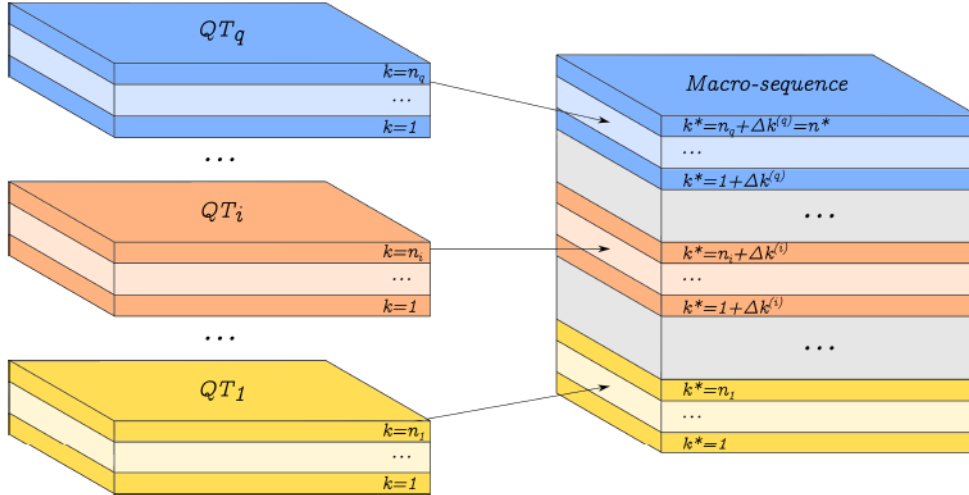
Figure 5.2: Schematic representation of the superposition process to obtain a macro-sequence.

be added as a superscript. For instance, the ply position index in the macro-sequence is denoted by k^*. The total number of plies of the macro-sequence is:

$$n^* = \sum_{i=1}^{q} n_i\,. \tag{5.7}$$

On the other hand, the number of orientation groups that will appear in the macro-sequence depends on how many different orientation groups appear in the initial QT solutions, but it is not necessarily their sum. In particular:

$$m^* \leq \sum_{i=1}^{q} m_i \,. \tag{5.8}$$

Since orientations of saturated groups in the initial solutions can be chosen freely, the case corresponding to the equality in Eq. (5.8) is obtained by choosing all orientations in all initial solutions to be different. Conversely, if some saturated groups are given the same orientation, then the inequality is obtained. Hence, to maintain generality, the subscript l will be used to identify orientations in the macro-sequence. Thus, we can define the set of indexes of plies with a given orientation θ_l:

$$G_l^* = \left\{ k^* : \delta_{k^*} = \theta_l \right\} , \tag{5.9}$$

and the complete set of ply position indexes:

$$K^* = \bigcup_{l=1}^{m^*} G_l^* \,. \tag{5.10}$$

Eventually, coefficients b_k^* and c_k^* are:

$$b_{k^*} = 2k^* - n^* - 1 \,, \tag{5.11}$$

$$c_{k^*} = -12k^* \left(k^* - n^* - 1 \right) - 2n^{*2} - 6n^* - 4 \,. \tag{5.12}$$

5.2.3   Superposition process description

In order to describe the superposition process, relationships that relate the macro-sequence description to that of the initial solutions must be established.

With respect to the ply position index, according to Figure 5.2, the following relationship is obtained:

$$k^* = \begin{cases} k & \text{if } k \in K^{(1)} ; \\ k + \sum\limits_{p=1}^{i-1} n_p & \text{if } k \in K^{(i)} ; \quad i = 2, ..., q \,. \end{cases} \tag{5.13}$$

With the purpose of having a compact and consistent notation, we may introduce the quantity:

$$n_0 = 0 \,, \tag{5.14}$$

so that we can define the shift of the ply index of the initial solutions:

$$\Delta k^{(i)} = \sum_{p=0}^{i-1} n_p ; \quad i = 1, ..., q \,. \tag{5.15}$$

Consequently, Eq. (5.13) can be rewritten as:

$$k^* = k + \Delta k^{(i)} ; \quad k \in K^{(i)} ; \quad i = 1, ..., q \,. \tag{5.16}$$

Eq. (5.16) allows to obtain the position index k^* of a ply in the macro-sequence, once its initial QT solution and its position k in it are known. It is important to mention here that having defined the term n_0 in Eq. (5.14), the total number of plies of the macro-sequence, Eq. (5.7), may be now expressed also as:

$$n^* = \sum_{i=0}^{q} n_i \,.$$

(5.17)

In the macro-sequence, each orientation group will be formed by an aggregate of plies coming from the initial solutions and chosen to belong to that group (this choice, as explained before, is arbitrary). The different sets G_l^* of the macro-sequence may then be expressed as:

$$G_l^* = \bigcup_{i=1}^{q} G_l^{*,(i)} \,,$$

(5.18)

where we have introduced the symbol $G_l^{*,(i)}$ to indicate the set of indexes k^* (which can be obtained from Eq. (5.16)) of those plies of initial solution QT_i that are oriented at the angle $\theta_j^{(i)} = \theta_l$, and therefore belong to set G_l^* in the macro-sequence.

Finally, we want to establish a relationship between coefficients b_k and c_k of the initial solutions and b_{k^*} and c_{k^*} of the macro-sequence. To do that, we substitute Eq. (5.16) in Eqs. (5.11) and (5.12), to obtain respectively:

$$b_{k^*} = 2\left(k + \Delta k^{(i)}\right) - n^* - 1 \,,$$

(5.19)

$$c_{k^*} = -12\left(k + \Delta k^{(i)}\right)\left(\left(k + \Delta k^{(i)}\right) - n^* - 1\right) - 2n^{*2} - 6n^* - 4 \,.$$

(5.20)

These expressions are valid for each ply of the macro-sequence. In particular, i is the index of the initial solution to which the ply considered belongs. Thanks to them, it is possible to compute coefficients b_{k^*} and c_{k^*} for each ply in the macrosequence based on the intial solution of the ply and its position in it. For the sake of simplicity, with a slight abuse of notation, we can define:

$$b_{k+\Delta k^{(i)}} = 2\left(k + \Delta k^{(i)}\right) - n^* - 1 \,,$$

(5.21)

$$c_{k+\Delta k^{(i)}} = -12\left(k + \Delta k^{(i)}\right)\left(\left(k + \Delta k^{(i)}\right) - n^* - 1\right) - 2n^{*2} - 6n^* - 4 \,,$$

(5.22)

so that:

$$b_{k^*} = b_{k+\Delta k^{(i)}} \,,$$

(5.23)

$$c_{k^*} = c_{k+\Delta k^{(i)}} \,.$$

(5.24)

With this notation, it follows:

$$\sum_{k^* \in G_l^{*,(i)}} b_{k^*} = \sum_{k \in G_l^{(i)}} b_{k+\Delta k^{(i)}} \,,$$

(5.25)

$$\sum_{k^* \in G_l^{*,(i)}} c_{k^*} = \sum_{k \in G_l^{(i)}} c_{k+\Delta k^{(i)}} \,.$$

(5.26)

5.3 Uncoupling of superposed QT solutions

In this section, the condition to obtain a QT uncoupled macro-sequence by superposition of initial QT solutions will be derived.

In order for the macro-sequence to be QT uncoupled, it must be formed entirely by saturated groups in terms of coefficient b_{k^*}. In other words, as seen in Eq. (4.8):

$$\sum_{k^* \in G_l^*} b_{k^*} = 0 \, ; \quad l = 1, ..., m^* \, . \tag{5.27}$$

Eq. (5.27) gives the m^* conditions, one for each orientation group, to be satisfied to have a QT uncoupled macro-sequence. In this equation, the set G_l^* may be obtained as shown in Eq. (5.18). As a consequence, the sum over G_l^* can be split in multiple sums over all the sets $G_l^{*,(i)}$:

$$\sum_{k^* \in G_l^*} b_{k^*} = \sum_{i=1}^{q} \sum_{k^* \in G_l^{*,(i)}} b_{k^*} = 0 \, ; \quad l = 1, ..., m^* \, . \tag{5.28}$$

Eq. (5.28) is still written with respect to the macro-sequence indexes. The objective is to translate it in terms of the ply indexes of the initial solutions. So, using Eq. (5.25), Eq. (5.28) becomes:

$$\sum_{i=1}^{q} \sum_{k^* \in G_l^{*,(i)}} b_{k^*} = \sum_{i=1}^{q} \sum_{k \in G_l^{(i)}} b_{k+\Delta k^{(i)}} = 0 \, ; \quad l = 1, ..., m^* \, . \tag{5.29}$$

Then, replacing Eq. (5.21) in Eq. (5.29), one finally obtains:

$$\sum_{i=1}^{q} \sum_{k \in G_l^{(i)}} \left[2\left(k + \Delta k^{(i)}\right) - n^* - 1 \right] = 0 \, ; \quad l = 1, ..., m^* \, . \tag{5.30}$$

Eq. (5.30) represents the general condition to obtain saturated orientation groups with respect to coefficient b_{k^*} in the macro-sequence, and is expressed in terms relative to the initial QT solutions. Hence, it gives the conditions that the initial solutions must respect in order to provide a QT uncoupled macro-sequence. It is important to remark that, up to now, no hypothesis has been formulated with respect to the initial solutions. In the following subsections, Eq. (5.30) will be simplified for the superposition of initial QT solutions of different types.

5.3.1 Uncoupled initial solutions

Here, the case of QT uncoupled initial solutions is considered. Then, for each initial sequence QT_i, Eqs. (5.3) and (5.4) hold. Eq. (5.30) may be further developed, and with some limited manipulation one obtains:

$$\sum_{i=1}^{q} \sum_{k \in G_l^{(i)}} \left[\left(2k - n_i - 1\right) + 2\Delta k^{(i)} - n^* + n_i \right] = 0 \, ; \quad l = 1, ..., m^* \, . \tag{5.31}$$

Eq. (5.31) can be overtly simplified by the condition of uncoupling of the initial solutions superposed, Eq. (5.4). Moreover the remaining terms are not function of k, so that we obtain:

$$\sum_{i=1}^{q} n_{G_l^{(i)}} \left(2\Delta k^{(i)} + n_i - n^* \right) = 0 ; \quad l = 1, ..., m^* . \tag{5.32}$$

In Eq. (5.32), $n_{G_l^{(i)}}$ indicates the number of plies oriented at θ_l in the initial solution QT_i. Using Eqs. (5.15) and (5.17) we can finally obtain the criterion:

$$\sum_{i=1}^{q} n_{G_l^{(i)}} \left[\sum_{p=0}^{i} n_p - \sum_{p=i}^{q} n_p \right] = 0 ; \quad l = 1, ..., m^* . \tag{5.33}$$

Eq. (5.33) represents the analytical condition to be fulfilled by all orientation groups of the macro-sequence in order to be saturated. If the groups satisfy Eq. (5.33) then the macro-sequence is a QT uncoupled solution.

5.3.2 Membrane-bending homogeneous initial solutions

In the case of superposition of QT membrane-bending homogeneous initial solutionse, Eq. (5.6) applies. However, such condition is of no help in simplifying Eq. (5.30). This latter equation, indeed, presents only linear terms in k, and using Eq. (5.6) would introduce quadratic terms in the expression for uncoupling, complicating it even more. For this reason, the present case is not developed further.

5.3.3 Quasi-homogeneous initial solutions

If QT quasi-homogeneous initial solutions are considered, then both Eqs. (5.4) and (5.6) apply. As explained before, Eq. (5.6) is of no help, while, on the other hand, all the simplifications obtained in Subsection 5.3.1 are valid also for this case. Therefore, Eq. (5.33) may be used for this case too.

5.4 Membrane-bending homogeneity of superposed QT solutions

Following the same idea of Section 5.3, the condition to obtain a membrane-bending homogeneous macro-sequence from the superposition of initial QT solutions is derived in this section.

In order for the macro-sequence to be QT membrane-bending homogeneous, it must be formed entirely by saturated groups in terms of coefficient c_{k^*}. In other words, as seen in Eq. (4.9):

$$\sum_{k^* \in G_l^*} c_{k^*} = 0 ; \quad l = 1, ..., m^* . \tag{5.34}$$

Eq. (5.34) gives the m^* conditions to be satisfied to have a QT membrane-bending homogeneous macro-sequence. Once again, the set G_l^* may be obtained as shown in Eq. (5.18), and the sum over G_l^* can be split in multiple sums over all the sets $G_l^{*,(i)}$:

$$\sum_{k^* \in G_l^*} c_{k^*} = \sum_{i=1}^{q} \sum_{k^* \in G_l^{*,(i)}} c_{k^*} = 0 ; \quad l = 1, ..., m^* . \tag{5.35}$$

In this case, in order to express Eq. (5.35) in terms of the ply indexes of the initial solutions, Eq. (5.26) may be used to obtain:

$$\sum_{i=1}^{q} \sum_{k^* \in G_l^{*,(i)}} c_{k^*} = \sum_{i=1}^{q} \sum_{k \in G_l^{(i)}} c_{k+\Delta k^{(i)}} = 0; \quad l = 1, ..., m^*. \tag{5.36}$$

Finally, replacing Eqs. (5.22) and Eq. (5.16) into Eq. (5.36), one obtains:

$$\sum_{i=1}^{q} \sum_{k \in G_l^{(i)}} \left[-12\left(k + \Delta k^{(i)}\right)\left(k + \Delta k^{(i)} - n^* - 1\right) - 2n^{*2} - 6n^* - 4 \right] = 0;$$

$$l = 1, ..., m^*.$$

Eq. (5.37) represents the general condition to obtain saturated orientation groups with respect to coefficient c_{k^*} in the macro-sequence, and is expressed in terms relative to the initial QT solutions. Hence, it gives the conditions that the initial solutions must respect in order to provide a QT membrane-bending homogeneous macro-sequence. In the following subsections, Eq. (5.37) will be simplified for the superposition of initial QT solutions of different types.

5.4.1 Uncoupled initial solutions

As observed before, if the initial solutions are QT uncoupled ones, Eqs. (5.3) and (5.4) hold. To exploit this condition Eq. (5.37) may be developed, and manipulated to obtain:

$$\sum_{i=1}^{q} \sum_{k \in G_l^{(i)}} \left[3\left(2\Delta k^{(i)} - n^* - 1\right)\left(2k - n_i - 1\right) + 6\Delta k^{(i)}\left(\Delta k^{(i)} + n_i - n^*\right) + \right.$$

$$\left. + n^*\left(n^* - 3n_i\right) - 3n_i - 1 + 6k^2 \right] = 0; \quad l = 1, ..., m^*. \tag{5.37}$$

This expression may be simplified using Eq. (5.4). Then, all terms that do not depend on k may be extracted from the internal sum, obtaining:

$$\sum_{i=1}^{q} \left\{ n_{G_l^{(i)}} \left[6\Delta k^{(i)}\left(\Delta k^{(i)} + n_i - n^*\right) + n^*\left(n^* - 3n_1\right) - 3n_i - 1 \right] + 6 \sum_{k \in G_l^{(i)}} k^2 \right\} = 0;$$

$$l = 1, ..., m^*.$$

$$\tag{5.38}$$

At this point, Eqs. (5.15) and (5.17) may be used to obtain the final criterion:

$$\sum_{i=1}^{q} \left\{ n_{G_l^{(i)}} \left[6\sum_{p=0}^{i-1} n_p \left(n_i - \sum_{p=i}^{q} n_p \right) + \sum_{p=0}^{q} n_p \left(\sum_{p=0}^{q} n_p - 3n_i \right) - 3n_i - 1 \right] + 6 \sum_{k \in G_l^{(i)}} k^2 \right\} = 0;$$

$$l = 1, ..., m^*.$$

$$\tag{5.39}$$

Eq. (5.39) gives the m^* conditions (one for each orientation group of the macro-sequence) to obtain a QT membrane-bending homogeneous macro-sequence from the superposition of initial QT uncoupled solutions. This expression is much more complex than that obtained in Eq. (5.33). In particular the k^2 term that does not disappear introduces a dependence on the ply position, which complicates the evaluation of these conditions.

5.4.2 Membrane-bending homogeneous initial solutions

If we assume that the initial solutions are QT membrane-bending homogeneous ones, then Eq. (5.6) holds. Eq. (5.37) can be rearranged in the following form:

$$\sum_{i=1}^{q} \sum_{k \in G_l^{(i)}} \left[-12k\left(k - n_i - 1\right) - 2n_i^2 - 6n_i - 4 + 12k\left(n^* - n_i - 2\Delta k^{(i)}\right) + \right.$$
$$\left. - 12\Delta k^{(i)}\left(\Delta k^{(i)} - n^* - 1\right) + 2\left(n_i^2 - n^{*2}\right) + 6\left(n_i - n^*\right) \right] = 0; \quad l = 1, ..., m^*.$$
$$(5.40)$$

Eq. (5.40) can be simplified using Eq. (5.6). Then, the terms that do not depend on k may be grouped and the following expression is obtained:

$$\sum_{i=1}^{q} \left\{ n_{G_l^{(i)}} \left[6\Delta k^{(i)}\left(n^* - \Delta k^{(i)} + 1\right) + \left(n_i - n^*\right)\left(n_i + n^* + 3\right) \right] + \right.$$
$$\left. + 6\left(n^* - n_i - 2\Delta k^{(i)}\right) \sum_{k \in G_l^{(i)}} k \right\} = 0; \quad l = 1, ..., m^*.$$
$$(5.41)$$

Eventually, Eqs. (5.15) and (5.17) are used to obtain the final form of the criterion:

$$\sum_{i=1}^{q} \left\{ n_{G_l^{(i)}} \left[6\sum_{p=0}^{i-1} n_p \left(\sum_{p=i}^{q} n_p + 1 \right) + \left(n_i - \sum_{p=0}^{q} n_p \right)\left(n_i + \sum_{p=0}^{q} n_p + 3 \right) \right] + \right.$$
$$\left. - 6\left(\sum_{p=0}^{i} n_p - \sum_{p=i}^{q} n_p \right) \sum_{k \in G_l^{(i)}} k \right\} = 0; \quad l = 1, ..., m^*.$$
$$(5.42)$$

Eq. (5.42) gives the m^* conditions to obtain a QT membrane-bending homogeneous macro-sequence from the superposition of initial QT membrane-bending homogeneous solutions. Similarly to the case of Subsection 5.4.1, it is not possible to eliminate the dependence on the ply position, expressed by the linear term in k. These two cases reflect the typical complexities encountered in the design of bending elastic properties of laminates.

5.4.3 Quasi-homogeneous initial solutions

If QT quasi-homogeneous initial solutions are used, Eqs. (5.4) and (5.6) both hold. For this case, Eq. (5.37) may be rewritten as follows:

$$\sum_{i=1}^{q} \sum_{k \in G_l^{(i)}} \left[-12k\left(k - n_i - 1\right) - 2n_i^2 - 6n_i - 4 + 6\left(n^* - 2\Delta k^{(i)} - n_i\right)\left(2k - n_i - 1\right) + \right.$$
$$\left. + 2\left(n_i - n^*\right)\left(n^* - 2n_i\right) + 12\Delta k^{(i)}\left(n^* - \Delta k^{(i)} - n_i\right) \right] = 0; \quad l = 1, ..., m^*.$$
$$(5.43)$$

The previous expression can be clearly simplified using Eqs. (5.4) and (5.6). Moreover, it is easy to see that, in this case, such simplification allows to eliminate all terms depending

on the ply position k. Then, applying as usual Eqs. (5.15) and (5.17), we eventually obtain the criterion desired:

$$\sum_{i=1}^{q} \left\{ n_{G_j^{(i)}} \left[6 \sum_{p=0}^{i-1} n_p \left(\sum_{p=i}^{q} n_p - n_i \right) + \left(n_i - \sum_{p=0}^{q} n_p \right) \left(\sum_{p=0}^{q} n_p - 2n_i \right) \right] \right\} = 0;$$

$$l = 1, ..., m^*.$$

(5.44)

The criterion in Eq. (5.44) is much simpler than both those of Eqs. (5.39) and (5.42), thanks to the fact that the dependence on the ply position k has been eliminated. In other words, it is much simpler to look for QT membrane-bending homogeneous macro-sequences using superposed QT quasi-homogeneous initial solutions rather than using only uncoupled or membrane-bending homogeneous initial solutions.

5.5 Quasi-homogeneity of superposed QT solutions

In order for the macro-sequence obtained by superposition of initial QT solutions to be a QT quasi-homogeneous solution, Eqs. (5.27) and (5.34) must be simultaneously satisfied, namely:

$$\begin{cases} \sum_{k^* \in G_l^*} b_{k^*} = 0; \\ \sum_{k^* \in G_l^*} c_{k^*} = 0; \end{cases} \qquad l = 1, ..., m^*.$$

(5.45)

These two requirements have already been developed to Eqs. (5.30) and (5.37), respectively, so that in this case the following system of requirements is obtained:

$$\begin{cases} \sum_{i=1}^{q} \sum_{k \in G_l^{(i)}} \left[2(k + \Delta k^{(i)}) - n^* - 1 \right] = 0; \\ \sum_{i=1}^{q} \sum_{k \in G_l^{(i)}} \left[-12 \left(k + \Delta k^{(i)} \right) \left(k + \Delta k^{(i)} - n^* - 1 \right) - 2n^{*2} - 6n^* - 4 \right] = 0; \end{cases}$$

(5.46)

$$l = 1, ..., m^*.$$

Eq. (5.46) represents the analytical condition to be fulfilled by all orientation groups of the macro-sequence in order to be saturated with respect to both coefficient b_{k^*} and c_{k^*}. If the groups satisfy Eq. (5.46), then the macro-sequence is a QT quasi-homogeneous solution. The equations forming this system have already been studied in the previous sections. Here, they will be recalled for completeness and ease of reading.

5.5.1 Uncoupled initial solutions

In the case of initial QT uncoupled solutions, both criteria for uncoupling, Eq. (5.33), and membrane-bending homogeneity, Eq. (5.39), have been derived. The system in Eq.

(5.46) then becomes:

$$
\begin{cases}
\sum\limits_{i=1}^{q} n_{G_l^{(i)}} \left(\sum\limits_{p=0}^{i} n_p - \sum\limits_{p=i}^{q} n_p \right) = 0 \,; \\[3mm]
\sum\limits_{i=1}^{q} \left\{ n_{G_l^{(i)}} \left[6 \sum\limits_{p=0}^{i-1} n_p \left(n_i - \sum\limits_{p=i}^{q} n_p \right) + \sum\limits_{p=0}^{q} n_p \left(\sum\limits_{p=0}^{q} n_p - 3n_i \right) - 3n_i - 1 \right] + 6 \sum\limits_{k \in G_l^{(i)}} k^2 \right\} = 0 \,; \\[3mm]
l = 1, ..., m^* \,.
\end{cases}
$$

(5.47)

5.5.2 Membrane-bending homogeneous initial solutions

As explained previously, in the case of membrane-bending homogeneous initial solutions, the condition for uncoupling was not developed further than Eq. (5.30). Instead, the criterion for membrane-bending homogeneity was derived, Eq. (5.42). Therefore, system (5.46) becomes:

$$
\begin{cases}
\sum\limits_{i=1}^{q} \sum\limits_{k \in G_l^{(i)}} \left[2 \left(k + \Delta k^{(i)} \right) - n^* - 1 \right] = 0 \,; \\[3mm]
\sum\limits_{i=1}^{q} \left\{ n_{G_l^{(i)}} \left[6 \sum\limits_{p=0}^{i-1} n_p \left(\sum\limits_{p=i}^{q} n_p + 1 \right) + \left(n_i - \sum\limits_{p=0}^{q} n_p \right) \left(n_i + \sum\limits_{p=0}^{q} n_p + 3 \right) \right] + \right. \\[3mm]
\left. -6 \left(\sum\limits_{p=0}^{i} n_p - \sum\limits_{p=i}^{q} n_p \right) \sum\limits_{k \in G_l^{(i)}} k \right\} = 0 \,; \\[3mm]
l = 1, ..., m^* \,.
\end{cases}
$$

(5.48)

5.5.3 Quasi-homogeneous initial solutions

For the case of initial quasi-homogeneous initial solutions, the condition to be used for uncoupling is Eq. (5.39), while that to be used for membrane-bending homogeneity is Eq. (5.44). Thus, the system obtained is:

$$
\begin{cases}
\sum\limits_{i=1}^{q} n_{G_l^{(i)}} \left(\sum\limits_{p=0}^{i} n_p - \sum\limits_{p=i}^{q} n_p \right) = 0 \,; \\[3mm]
\sum\limits_{i=1}^{q} \left\{ n_{G_j^{(i)}} \left[6 \sum\limits_{p=0}^{i-1} n_p \left(\sum\limits_{p=i}^{q} n_p - n_i \right) + \left(n_i - \sum\limits_{p=0}^{q} n_p \right) \left(\sum\limits_{p=0}^{q} n_p - 2n_i \right) \right] \right\} = 0 \,; \\[3mm]
l = 1, ..., m^* \,.
\end{cases}
$$

(5.49)

5.6 Superposition of two QT solutions

While the results presented up to now are general and may be applied to the superposition of any given number q of initial QT sequences, in this section they are specialised to the case of two initial QT solutions. This particular case is of great practical interest: in engineering scenarios and other practical applications, the superposition of two laminates is likely to appear countless times (e.g.: joints, doubler reinforced plates, repair patches,

etc.). Moreover, this case will be used in following chapters. As it will be shown, the rules reduce to extremely simple expressions for this case, so that they are easily applicable also in early stages of laminates design.

5.6.1 Uncoupling of two superposed uncoupled or quasi- homogeneous solutions

As explained in Section 5.3, Eq. (5.33) represents the condition to obtain an uncoupled QT macro-sequence from the superposition of uncoupled or quasi-homogeneous solution. When imposing $q = 2$ to Eq.(5.33), we obtain:

$$- n_{G_l^{(1)}} n_2 + n_{G_l^{(2)}} n_1 = 0 ; \quad l = 1, ..., m^* ; \tag{5.50}$$

or, in a more convenient form:

$$\frac{n_{G_l^{(1)}}}{n_1} = \frac{n_{G_l^{(2)}}}{n_2} ; \quad l = 1, ..., m^* . \tag{5.51}$$

Eq. (5.51) represents the condition to obtain an uncoupled QT macro-sequence by superposing two initial QT uncoupled or quasi-homogeneous solutions. From this equation, it is possible to draw some conclusions:

1. the initial QT sequences should possess exactly the same orientations. If a certain orientation θ_l exists in only one of the two sequences, Eq. (5.51) is not satisfied and the associated group is not saturated;

2. it must be ensured that, for each l-th orientation, in both sequences QT_1 and QT_2 an equal percentage of plies oriented at θ_l is present, regardless of the position of those plies. In the particular case of $n_1 = n_2$, Eq. (5.51) imposes that the two sequences have the same number of plies for each orientation;

3. no limitations arise on the number of groups that can be involved;

4. the superposition of sequences with $n_1 \neq n_2$ is still possible, allowing for greater design freedom.

To be remarked that the repetition of a single initial QT solution falls under this case study: the macro-sequence obtained is a QT uncoupled solution.

Example 1

Consider the following two QT uncoupled sequences:

$$QT_1 = [1\,2\,2\,1\,3\,3\,2\,1\,1\,2] ,$$
$$QT_2 = [1\,2\,3\,2\,1\,2\,1\,3\,1\,2] .$$

They have the same total number of plies

$$n_1 = n_2 = 10 ,$$

and the same number of plies for each orientation group:

$$n_{G_1^{(1)}} = n_{G_1^{(2)}} = 4\,,$$

$$n_{G_2^{(1)}} = n_{G_2^{(2)}} = 4\,,$$

$$n_{G_3^{(1)}} = n_{G_3^{(2)}} = 2\,.$$

Therefore these sequences satisfy Eq. (5.51) and their superposition yields a new QT uncoupled solution. This can be easily verified with the help of Table 5.1, in which the sequence obtained is described according to the notation used in this chapter:

Group	k^*	b_{k^*}	$\sum_{k^*\in G_1^*} b_{k^*} =$	$\sum_{k^*\in G_2^*} b_{k^*} =$	$\sum_{k^*\in G_3^*} b_{k^*} =$
1	1	-19	-19 +		
2	2	-17		-17 +	
2	3	-15		-15 +	
1	4	-13	-13 +		
3	5	-11			-11 +
3	6	-9			-9 +
2	7	-7		-7 +	
1	8	-5	-5 +		
1	9	-3	-3 +		
2	10	-1		-1 +	
1	11	1	1 +		
2	12	3		3 +	
3	13	5			5 +
2	14	7		7 +	
1	15	9	9 +		
2	16	11		11 +	
1	17	13	13 +		
3	18	15			15 =
1	19	17	17 =		
2	20	19		19 =	
			0	0	0

Table 5.1: Example of QT uncoupled macro-sequence obtained by superposition of two QT solutions with equal number of plies.

It is evident that all orientation groups have null sums of coefficients b_{k^*} and are therefore saturated groups. The sequence is a QT solution with $\mathbf{B} = \mathbf{0}$, as expected according to Eq. (5.51).

Example 2

A more general example is the following. In this case, two QT uncoupled solutions with different total number of plies are superposed:

$$QT_1 = [1\ 2\ 2\ 1\ 3\ 3\ 2\ 1\ 1\ 2]\,,$$

$$n_1 = 10\,, \quad n_{G_1^{(1)}} = 4\,, \quad n_{G_2^{(1)}} = 4\,, \quad n_{G_3^{(1)}} = 2\,,$$

and

$$QT_2 = [1\,2\,1\,2\,3\,3\,2\,1\,2\,1\,2\,1\,3\,1\,2]\,,$$

$$n_2 = 15\,, \quad n_{G_1^{(2)}} = 6\,, \quad n_{G_2^{(2)}} = 6\,, \quad n_{G_3^{(2)}} = 3\,.$$

Even if the total number of plies of the sequences is different, it is easy to conclude that Eq. (5.51) is satisfied. The situation is described in Table 5.2.

Group	k^*	b_{k^*}	$\sum\limits_{k^* \in G_1^*} b_{k^*} =$	$\sum\limits_{k^* \in G_2^*} b_{k^*} =$	$\sum\limits_{k^* \in G_3^*} b_{k^*} =$
1	1	-24	-24 +		
2	2	-22		-22 +	
2	3	-20		-20 +	
1	4	-18	-18 +		
3	5	-16			-16 +
3	6	-14			-14 +
2	7	-12		-12 +	
1	8	-10	-10 +		
1	9	-8	-8 +		
2	10	-6		-6 +	
1	11	-4	-4 +		
2	12	-2		- 2 +	
1	13	0	0 +		
2	14	2		2 +	
3	15	4			4 +
3	16	6			6 +
2	17	8		8 +	
1	18	10	10 +		
2	19	12		12 +	
1	20	14	14 +		
2	21	16		16 +	
1	22	18	18 +		
3	23	20			20 =
1	24	22	22 =		
2	25	24		24 =	
			0	0	0

Table 5.2: Example of QT uncoupled macro-sequence obtained by superposition of two QT solutions with different number of plies.

Once again, it is easy to see that the sequence obtained with the superposition is composed entirely by saturated groups, and therefore it is a QT solution with $\mathbf{B} = \mathbf{0}$.

5.6.2 Membrane-bending homogeneity of two superposed uncoupled solutions

In order to obtain a membrane-bending homogeneous macro-sequence from the superposition of initial uncoupled solutions, Eq. (5.39) must be satisfied. For $q = 2$, such equation

reduces to:

$$n_{G_l^{(1)}}\left[\left(n_1+n_2\right)\left(n_2-2n_1\right)-3n_1-1\right]+6\sum_{k\in G_l^{(1)}}k^2+$$

$$+n_{G_l^{(2)}}\left[\left(n_1+n_2\right)\left(n_1-2n_2\right)-3n_2-1\right]+6\sum_{k\in G_l^{(2)}}k^2=0\,; \tag{5.52}$$

$$l=1,...,m^*.$$

If the superposition of two sequences with equal number of plies is considered, $n_1=n_2=n$, then Eq. (5.52) becomes:

$$\left(n_{G_l^{(1)}}+n_{G_l^{(2)}}\right)\left(n^2+3n+1\right)=6\left(\sum_{k\in G_l^{(1)}}k^2+\sum_{k\in G_l^{(2)}}k^2\right)\,; \quad l=1,...,m^*. \tag{5.53}$$

5.6.3 Membrane-bending homogeneity of two superposed membrane-bending homogeneous solutions

This case is obtained by assuming $q=2$ in Eq. (5.42), that reduces to:

$$n_{G_l^{(1)}}\left[-n_2(2n_1+n_2+3)\right]+6n_2\sum_{k\in G_l^{(1)}}k+n_{G_l^{(2)}}\left[-n_1(n_1-4n_2-3)\right]-6n_1\sum_{k\in G_l^{(2)}}k=0\,;$$

$$l=1,...,m^*.$$

$$\tag{5.54}$$

One useful specific case could be the superposition of two solutions of the same number of plies, $n_1=n_2$. In this particular case, Eq. (5.54) reduces to:

$$\left(n^2+1\right)\left(n_{G_l^{(2)}}-n_{G_l^{(1)}}\right)+2n\left(\sum_{k\in G_l^{(1)}}k-\sum_{k\in G_l^{(2)}}k\right)=0\,; \quad l=1,...,m^*. \tag{5.55}$$

If, in addition, two solutions having the same number of plies per orientation are chosen, $n_{G_l^{(1)}}=n_{G_l^{(2)}}$, then Eq. (5.55) is further simplified to:

$$\sum_{k\in G_l^{(1)}}k-\sum_{k\in G_l^{(2)}}k=0\,; \quad l=1,...,m^*. \tag{5.56}$$

Eq. (5.56) means that, for the particular case considered, in order to obtain a membrane-bending homogeneous QT macro-sequence, the sums of k indexes of each group must be the same for the two initial solutions.

Example

An example of superposition of two QT membrane-bending homogeneous solutions may be obtained considering the following two QT solutions of this type:

$$QT_1=[1\,2\,1\,1\,2\,1\,2\,2\,1\,2]\,,$$

$$QT_2=[1\,1\,2\,2\,1\,2\,1\,1\,2\,2]\,.$$

They have the same number of total plies, and both have the same number of plies per orientation group:

$$n_1 = 10, \quad n_{G_1^{(1)}} = 5, \quad n_{G_2^{(1)}} = 5,$$

$$n_2 = 10, \quad n_{G_1^{(2)}} = 5, \quad n_{G_2^{(2)}} = 5.$$

It is easy to verify that the sums of k indexes of the plies belonging to each orientation group is such that Eq. (5.56) is satisfied. The sequence resulting from their superposition is therefore a QT membrane bending homogeneous solution itself, as proven by Table 5.3.

Group	k^*	c_{k^*}	$\sum_{k^* \in G_1^*} c_{k^*} =$	$\sum_{k^* \in G_2^*} c_{k^*} =$
1	1	-684	-684 +	
2	2	-468		-468+
1	3	-276	-276 +	
1	4	-108	-108 +	
2	5	36		36 +
1	6	156	156 +	
2	7	252		252+
2	8	324		324+
1	9	372	372 +	
2	10	396		396+
1	11	396	396 +	
1	12	372	372 +	
2	13	324		324 +
2	14	252		252 +
1	15	156	156 +	
2	16	36		36 +
1	17	-108	-108 +	
1	18	-276	-276 =	
2	19	-468		-468 +
2	20	-684		-684 =
			0	0

Table 5.3: Example of QT membrane-bending homogeneous macro-sequence obtained by superposition of two QT membrane-bending homogeneous solutions.

5.6.4 Membrane-bending homogeneity of two superposed quasi-homogeneous solutions

This case is obtained from Eq. (5.44), with $q = 2$:

$$\left(n_1 - n_2\right)\left(n_1 n_{G_l^{(2)}} - n_2 n_{G_l^{(1)}}\right) = 0; \quad l = 1, ..., m^*. \tag{5.57}$$

Clearly this condition can be split into:

$$\begin{cases} \left(n_1 - n_2\right) = 0\,; \\ \left(n_1 n_{G_l^{(2)}} - n_2 n_{G_l^{(1)}}\right) = 0\,; \end{cases} \qquad l = 1, ..., m^*\,. \qquad (5.58)$$

It is sufficient that only one of the two conditions in Eq. (5.58) be satisfied to obtain a QT membrane-bending homogeneous macro-sequence. The first condition simply states that both initial solutions have an equal total number of plies, while the second coincide with the condition for uncoupling seen in Eq. (5.51). Therefore, two different situations may arise:

1. the first condition of Eq. (5.58) is satisfied, but not the second one: the resulting macro-sequence is characterised by saturated groups in terms of c_{k^*} coefficients, but not of b_{k^*} ones. Thus, the macro-sequence is membrane-bending homogeneous but not uncoupled;

2. the second condition of Eq. (5.58) is satisfied: in this case the macro-sequence satisfy both Eqs. (5.57) and (5.51) and thus it is a QT quasi-homogeneous solution.

Example

Consider the following two QT quasi-homogeneous solutions with a 13 plies each and 3 orientation groups:

$$QT_1 = [1\ 2\ 3\ 1\ 1\ 3\ 1\ 2\ 1\ 1\ 2\ 3\ 1]\,,$$

$$n_1 = 13\,, \quad n_{G_1^{(1)}} = 7\,, \quad n_{G_2^{(1)}} = 3\,, \quad n_{G_3^{(1)}} = 3\,,$$

and

$$QT_2 = [1\ 2\ 3\ 1\ 3\ 1\ 3\ 2\ 1\ 1\ 2\ 1\ 3]\,,$$

$$n_2 = 13\,, \quad n_{G_1^{(2)}} = 6\,, \quad n_{G_2^{(2)}} = 3\,, \quad n_{G_3^{(2)}} = 4\,.$$

For these sequences the first condition in (5.58) is satisfied, while the second one is not. Therefore, the superposition of these sequences is expected to be membrane-bending homogeneous but not uncoupled. This is confirmed in Table 5.4.

101

Group	k^*	b_{k^*}	c_{k^*}	$\sum\limits_{k^*\in G_1^*} b_{k^*} =$	$\sum\limits_{k^*\in G_2^*} b_{k^*} =$	$\sum\limits_{k^*\in G_3^*} b_{k^*} =$	$\sum\limits_{k^*\in G_1^*} c_{k^*} =$	$\sum\limits_{k^*\in G_2^*} c_{k^*} =$	$\sum\limits_{k^*\in G_3^*} c_{k^*} =$
1	1	-25	-1200	-25 +			-1200+		
2	2	-23	-912		-23 +			-912+	
3	3	-21	-648			-21 +			-648+
1	4	-19	-408	-19 +			-408+		
1	5	-17	-192	-17 +			-192+		
3	6	-15	0			-15 +			0+
1	7	-13	168	-13 +			168+		
2	8	-11	312		-11 +			312+	
1	9	-9	432	-9 +			432+		
1	10	-7	528	-7 +			528+		
2	11	-5	600		-5 +			600+	
3	12	-3	648			- 3 +			648+
1	13	-1	672	-1 +			672+		
1	14	1	672	1 +			672+		
2	15	3	648		3 +			648+	
3	16	5	600			5 +			600+
1	17	7	528	7 +			528+		
3	18	9	432			9 +			432+
1	19	11	312	11 +			312+		
3	20	13	168			13 +			168+
2	21	15	0		15 +			0+	
1	22	17	-192	17 +			-192+		
1	23	19	-408	19 +			-408+		
2	24	21	-648		21 =			-648=	
1	25	23	-912	23 =			-912=		
3	26	25	-1200			25 =			-1200=
				-13	0	13	0	0	0

Table 5.4: Example of QT membrane-bending homogeneous macro-sequence obtained by superposition of two QT quasi-homogeneous solutions.

5.6.5 Quasi-homogeneity of two superposed quasi-homogeneous solutions

The superposition of two QT quasi-homogeneous solutions to obtain a QT quasi-homogeneous macro-sequence is for sure a case of great practical interest. As a matter of fact, the results obtained for this case will be fundamental for the developments in the remaining part of the manuscript. To obtain quasi-homogeneity, both uncoupling and membrane-bending homogeneity have to be ensured. The system to be considered, then, is the one of Eq. (5.49). The two conditions appearing in this system have already been specialised for the case of two superposed solutions, respectively in Eqs. (5.50) and (5.57). Hence, Eq. (5.49) is reduced to:

$$
\begin{cases}
n_1 n_{G_l^{(2)}} - n_2 n_{G_l^{(1)}} = 0\,; \\
\left(n_1 - n_2\right)\left(n_1 n_{G_l^{(2)}} - n_2 n_{G_l^{(1)}}\right) = 0\,;
\end{cases}
\qquad l = 1,...,m^*\,.
\tag{5.59}
$$

It is easy to see that the first condition in Eq. (5.59) implies the second one. This means that, when superposing two QT quasi-homogeneous solutions, uncoupling of the macro-sequence implies also membrane-bending homogeneity, and thus quasi-homogeneity.

Example

Consider the following QT quasi-homogeneous solutions:

$$
QT_1 = [1\ 2\ 1\ 1\ 1\ 2\ 1]\,,
$$

$$
n_1 = 7\,, \quad n_{G_1^{(1)}} = 5\,, \quad n_{G_2^{(1)}} = 2\,,
$$

and

$$
QT_2 = [1\ 2\ 1\ 1\ 1\ 1\ 1\ 2\ 2\ 2\ 1\ 1\ 1\ 1\ 1\ 2\ 1\ 1\ 1\ 1\ 2]\,,
$$

$$
n_2 = 21\,, \quad n_{G_1^{(2)}} = 15\,, \quad n_{G_2^{(2)}} = 6\,.
$$

The first one is the only 7 plies QT quasi-homogeneous independent solution existing, while the second is a 21 plies QT quasi-homogeneous solution not independent. These two sequences satisfy the second condition in Eq. (5.58). As a consequence, their superposition yields a new QT quasi-homogeneous solution, as demonstrated in Tab. 5.5.

Group	k^*	b_{k^*}	c_{k^*}	$\sum\limits_{k^*\in G_1^*} b_{k^*} =$	$\sum\limits_{k^*\in G_2^*} b_{k^*} =$	$\sum\limits_{k^*\in G_1^*} c_{k^*} =$	$\sum\limits_{k^*\in G_2^*} c_{k^*} =$
1	1	-27	-1404	-27 +		-1404 +	
2	2	-25	-1092		-25 +		-1092 +
1	3	-23	-804	-23 +		-804 +	
1	4	-21	-540	-21 +		-540 +	
1	5	-19	-300	-19 +		-300 +	
2	6	-17	-84		-17 +		-84 +
1	7	-15	108	-15 +		108 +	
1	8	-13	276	-13 +		276 +	
2	9	-11	420		-11 +		420 +
1	10	-9	540	-9 +		540 +	
1	11	-7	636	-7 +		636 +	
1	12	-5	708	-5 +		708 +	
1	13	-3	756	-3 +		756 +	
1	14	-1	780	-1 +		780 +	
2	15	1	780		1 +		780 +
2	16	3	756		3+		756 +
2	17	5	708		5 +		708 +
1	18	7	636	7 +		636 +	
1	19	9	540	9 +		540 +	
1	20	11	420	11 +		420 +	
1	21	13	276	13 +		276 +	
1	22	15	108	15 +		108 +	
2	23	17	-84		17 +		-84 +
1	24	19	-300	19 +		-300 +	
1	25	21	-540	21 +		-540 +	
1	26	23	-804	23 +		-804 +	
1	27	25	-1092	25 =		-1092 =	
2	28	27	-1404		27 =		-1404 =
				0	0	0	0

Table 5.5: Example of QT quasi-homogeneous macro-sequence obtained by superposition of two QT quasi-homogeneous solutions.

5.7 Concluding remarks

This chapter presented the derivation of closed form analytical criteria to obtain QT macro-sequences by superposition of known initial QT solutions. Such criteria have been derived to obtain all possible types of quasi-triviality of the macro-sequence (i.e. uncoupling, membrane-bending homogeneity and quasi-homogeneity) and starting from the superposition of all possible types of initial QT solutions (i.e. uncoupled, membrane-bending homogeneous or quasi-homogeneous). Moreover, in the procedure, no simplifying hypothesis were adopted, so that the criteria are completely general. They express the requirements on the initial solutions, in terms of total number of plies and number of plies per orientation groups, in order to obtain quasi-triviality of the macro-sequence.

While the development of these criteria was driven by the specific needs of this study, they might represent powerful tools able to benefit lots of different applications. The potential of QT stacking sequences in laminate design was highlighted in Chapter 4. However, it was also explained how difficult it is to obtain such sequences, especially if high number of plies are desired, due to computational limitations. Thanks to the criteria shown in this chapter, such limitations can be shattered, and QT solutions of any desired number of plies may be obtained. This could be particularly important for application exploiting *thin composite plies*, in which stacking sequences with extremely high number of plies are needed to reach the required thickness.

Additionally, the criteria derived in this chapter could allow for the design of laminates having particular properties, that may be otherwise extremely difficult to be obtained. This is possible thanks to the thorough control over elastic properties that is achieved by using QT stacking sequences and the superposition criteria. The results presented in Chapter 6 will be a striking example of these considerations.

Chapter 6

Design of Fully-Uncoupled Multi-Directional stacking sequences for delamination specimens

6.1 Introduction

In this chapter, the concepts and the results obtained in previous chapters are exploited to design a new class of MD layups for delamination specimens. These layups allow to eliminate elastic couplings and undesired thermal effects (in closed-form solution in the framework of CLPT) in all parts of the specimen. Moreover, any pair of orientations of the plies embedding the delamination plane can be obtained. In virtue of their properties, the specimens obtained have been labelled Fully-Uncoupled Multi-Directional (FUMD).

In Section 6.2, the requirements to design ideal MD delamination specimens are discussed and formalised. Elastic couplings, thermal effects and the possibility to have different delamination interfaces are all discussed. Then, the standard UD specimen is analysed in Section 6.3. This allows to understand the characteristics that make it the ideal specimen for delamination testing and to have a reference when designing MD specimens.

Section 6.4 presents the design procedure to obtain FUMD specimens for delamination testing. Such procedure begins with the selection of appropriate layups for the specimen arms, that could satisfy all the requirements on these two separated regions of the specimen. Then, among the layups identified, those that satisfy all the requirements on the whole specimen must be chosen. To do this, the superposition rules for QT solutions derived in Chapter 5 are used. Some final remarks end the chapter.

6.2 Design requirements for MD delamination specimens

As explained in Chapter 3, delamination testing of MD specimen is a complex task. In order to deal with this issue, a careful design of the MD layups to be used is required. However, nowadays, no universal consensus exists on which may be the best layups for MD delamination specimens; rather, various authors have proposed different solutions, each one showing some advantages and some drawbacks.

In this section the requirements to be satisfied to obtain an optimal MD delamination specimen are discussed and formalised. In detail, this regards:

1. elimination of elastic couplings;

2. elimination of undesired thermal effects;

3. possibility to have multiple types of delamination interfaces.

6.2.1 Elastic couplings

As explained in Chapter 2, in MD laminates different types of elastic couplings exist:

- in-plane/out-of-plane couplings, which are represented by all terms of matrix $\mathbf{B}$;

- extension/shear couplings, represented by the terms A_{xs} and A_{ys};

- bending/twisting couplings, D_{xs} and D_{ys};

- the anticlastic effect, represented by the term D_{xy}.

The term D_{xy}, which is often referred to as a *bending/bending coupling*, is actually a little bit different from the couplings mentioned before. Indeed, while all other couplings may be reduced to zero for some particular layups (e.g. for a UD layup), D_{xy} cannot be zero. This is due to the fact that it is obtained as the sum of strictly positive terms, as can easily be verified from Eqs. (2.121) and (2.122). As already mentioned, this term measures the anticlastic effect of the laminate, which is not entirely disposable.

Hence, in MD laminates, the ideal objective would be to eliminate all the couplings and to reduce the anticlastic effect. A delamination specimen, however, cannot be considered as a single laminate. Instead, three different parts of the specimen may be distinguished: its two arm in the pre-delaminated region, and the entire laminate in the undelaminated region. Couplings should be eliminated from all these parts [52]. It is important to remember that the entire laminate in the undelaminated region results from the superposition of the two arms. Consequently, they cannot be considered independently. Furthermore, the elastic properties of the two arms must be identical in order to avoid undesired rotations.

6.2.2 Thermal effects

Similarly to elastic couplings, undesired thermal effects are typical of MD laminates. A UD lamina, when subjected to a thermal variation and free to expand, will expand/contract along its principal material directions, according to its CTEs. In this case, no thermal stresses will be induced in the lamina (here, we consider ply level stresses only; at a lower scale stresses will be introduced, due to the different thermal properties of fibres and matrix).

On the other hand, when MD layups are used, the thermal expansion properties of the laminate will depend upon the stacking sequence. This may result not only in an expansion along two reference directions, but also in a shearing deformation and in bending and twisting curvatures of the laminate. Furthermore, in this case, plies are restrained by their neighbouring plies, and will therefore develop internal stresses.

Laminates are usually formed through a curing process which consists in a pressure and thermal cycle, whose characteristics depend on the materials used. Generally, a permanence at high temperature is required. The laminate is thus formed at high temperature

and is then cooled to room temperature. Therefore, there exists a thermal difference $T = T_0 - T_{act}$ in temperature between the forming, at temperature T_0, and the operating conditions, at temperature T_{act}. Hence, during cooling from T_0 to T_{act} the laminate may contract, deform and develop internal residual stresses. These effects may be quantified if the laminate CTEs are known. In the following, it is assumed that both heating and cooling phases of curing are performed sufficiently slow, and that the laminate is at a thermal equilibrium without any heat flow acting on it. Hence, no thermal gradient exists within the laminate.

To formally describe this situation, we may recall Eq. (2.133), which defines the thermo-elastic behaviour of a laminate. Due to the absence of thermal gradients, Eq. (2.133) is written as:

$$\left\{ \begin{matrix} \mathbf{N} \\ \mathbf{M} \end{matrix} \right\} = \begin{bmatrix} h\mathbf{A} & \frac{h^2}{2}\mathbf{B} \\ \frac{h^2}{2}\mathbf{B} & \frac{h^3}{12}\mathbf{D} \end{bmatrix} \left\{ \begin{matrix} \epsilon^0 \\ \chi \end{matrix} \right\} - T \left\{ \begin{matrix} h\mathbf{U} \\ \frac{h^2}{2}\mathbf{V} \end{matrix} \right\} . \tag{6.1}$$

By additionally defining:

$$\left\{ \begin{matrix} \mathbf{N}^* \\ \mathbf{M}^* \end{matrix} \right\} = T \left\{ \begin{matrix} h\mathbf{U} \\ \frac{h^2}{2}\mathbf{V} \end{matrix} \right\} , \tag{6.2}$$

we can rewrite Eq. (6.1) as:

$$\left\{ \begin{matrix} \mathbf{N} + \mathbf{N}^* \\ \mathbf{M} + \mathbf{M}^* \end{matrix} \right\} = \begin{bmatrix} h\mathbf{A} & \frac{h^2}{2}\mathbf{B} \\ \frac{h^2}{2}\mathbf{B} & \frac{h^3}{12}\mathbf{D} \end{bmatrix} \left\{ \begin{matrix} \epsilon^0 \\ \chi \end{matrix} \right\} . \tag{6.3}$$

Eq. (6.3) may be inverted to obtain:

$$\left\{ \begin{matrix} \epsilon^0 \\ \chi \end{matrix} \right\} = \begin{bmatrix} \frac{1}{h}\mathcal{A} & \frac{2}{h^2}\mathcal{B} \\ \frac{2}{h^2}\mathcal{B}^T & \frac{12}{h^3}\mathcal{D} \end{bmatrix} \left\{ \begin{matrix} \mathbf{N} + \mathbf{N}^* \\ \mathbf{M} + \mathbf{M}^* \end{matrix} \right\} , \tag{6.4}$$

where, as already seen in chapter 2:

$$\mathcal{A} = (\mathbf{A} - 3\mathbf{B}\mathbf{D}^{-1}\mathbf{B})^{-1} , \tag{6.5}$$

$$\mathcal{B} = -3\mathcal{A}\mathbf{B}\mathbf{D}^{-1} , \tag{6.6}$$

$$\mathcal{D} = (\mathbf{D} - 3\mathbf{B}\mathbf{A}^{-1}\mathbf{B})^{-1} . \tag{6.7}$$

Substituting Eq. (6.2) into Eq. (6.4) gives:

$$\left\{ \begin{matrix} \epsilon^0 \\ \chi \end{matrix} \right\} = \begin{bmatrix} \frac{1}{h}\mathcal{A} & \frac{2}{h^2}\mathcal{B} \\ \frac{2}{h^2}\mathcal{B}^T & \frac{12}{h^3}\mathcal{D} \end{bmatrix} \left\{ \begin{matrix} \mathbf{N} \\ \mathbf{M} \end{matrix} \right\} + T \left\{ \begin{matrix} \alpha_\epsilon \\ \alpha_\chi \end{matrix} \right\} . \tag{6.8}$$

In Eq. (6.8), α_ϵ and α_χ are the vectors of in-plane and out-of-plane effective laminate CTEs, respectively. They quantify the laminate thermally-induced deformation per unit temperature variation and are obtained as:

$$\left\{ \begin{matrix} \alpha_\epsilon \\ \alpha_\chi \end{matrix} \right\} = \begin{bmatrix} \frac{1}{h}\mathcal{A} & \frac{2}{h^2}\mathcal{B} \\ \frac{2}{h^2}\mathcal{B}^T & \frac{12}{h^3}\mathcal{D} \end{bmatrix} \left\{ \begin{matrix} h\mathbf{U} \\ \frac{h^2}{2}\mathbf{V} \end{matrix} \right\} . \tag{6.9}$$

Hence, a laminate free to expand and subjected to a temperature variation T will expand/contract at its midplane with strains which are given by:

$$\epsilon^0 = T\alpha_\epsilon , \tag{6.10}$$

and it will bend/twist with thermal curvatures given by:

$$\chi = T\boldsymbol{\alpha}_\chi. \qquad (6.11)$$

In an ideal situation, shearing deformation and bending and twisting curvatures should be avoided. This translates into having null third component of the vector $\boldsymbol{\alpha}_\epsilon$ and null vector $\boldsymbol{\alpha}_\chi$. When considering delamination specimens, this condition should be satisfied by both arms of the specimen and by the entire laminate in the undelaminated region as well. In addition, these three parts of the specimens should have identical CTEs [169, 170]. If this is not the case, complex stress states would be generated at the junction of the three parts, i.e. at the delamination front.

6.2.3 Interface type

Another important aspect, when designing MD delamination specimens, is the possibility to have the widest possible variety of delamination interfaces. Types of interfaces to be considered are:

- $0°//\theta$;

- $\theta//\theta$;

- $\theta// - \theta$;

- $\theta_1//\theta_2$.

In addition, also the possibility to test the standard $0°//0°$ interface using MD laminates could be interesting, in order to assess the effects, if any, of parameters other than plies orientation on the interlaminar fracture toughness of the interface.

Having the possibility to test different types of interfaces complicates the research of appropriate MD layups. Certain type of interface, for example, exclude the possibility to use standard laminate design principles (e.g. symmetry, anti-symmetry) to obtain some desired elastic properties.

6.2.4 Summary

To sum up, ideal MD layups for delamination specimens should offer the following characteristics:

1. total absence of elastic couplings, in all parts of the specimen;

2. specimen arms with identical elastic properties;

3. absence of thermally-induced shearing deformation and/or bending and twisting curvature due to the curing process, in all parts of the specimen

4. identical CTEs for all parts of the specimen;

5. possibility to have as many different delamination interfaces as possible.

6.3 Portrait of the UD specimen

As explained in Chapter 3, the scope of standard delamination tests is, still today, limited to UD specimens [49, 50, 51]. This reflects the fact that most of the experience gained during round robin testing was on UD specimens [72, 76, 77, 78, 79], which in turn was a consequence of early observations of delamination migration in specimens having off-axis plies embedding the delamination plane [43, 89]. However, the success of the UD delamination specimen is not only due to this, but it depends also on its peculiarly simple thermo-elastic behaviour, as explained in this section.

6.3.1 Elastic couplings

For a UD laminate having its principal material directions aligned with those of the adopted laminate reference frame, from Eqs. (2.118) and (2.121) it is immediately found that:

$$\mathbf{A} = \mathbf{D} = [Q] \,, \tag{6.12}$$

where $[Q]$ is the reduced stiffness matrix of the basic lamina in its material reference frame:

$$[Q] = \begin{bmatrix} Q_{11} & Q_{12} & 0 \\ Q_{12} & Q_{22} & 0 \\ 0 & 0 & Q_{66} \end{bmatrix} \,. \tag{6.13}$$

In other words, the normalised membrane and bending stiffness matrices are identical, and in addition they are equal to the reduced stiffness matrix of the basic ply. Consequently, $A_{xs} = A_{ys} = D_{xs} = D_{ys} = 0$: no shear/extension nor bending/twisting couplings exist. Furthermore, from Eq. (2.119) it follows that for a UD laminate:

$$\mathbf{B} = \mathbf{0} \,, \tag{6.14}$$

meaning that no membrane/bending coupling exist. To sum up, a UD laminate is completely free from elastic couplings.

If a UD delamination specimen is considered, the previous considerations may be applied to all its parts: the specimen is completely uncoupled.

6.3.2 Thermal effects

From a thermo-elastic point of view, from Eq. (2.138), it is easy to see that for a UD laminate:

$$\mathbf{V} = \mathbf{0} \,, \tag{6.15}$$

while from Eq. (2.137) it follows:

$$\mathbf{U} = [Q]\{\alpha\} = \begin{bmatrix} Q_{11} & Q_{12} & 0 \\ Q_{12} & Q_{22} & 0 \\ 0 & 0 & Q_{66} \end{bmatrix} \begin{Bmatrix} \alpha_1 \\ \alpha_2 \\ 0 \end{Bmatrix} = \begin{Bmatrix} Q_{11}\alpha_1 + Q_{12}\alpha_2 \\ Q_{12}\alpha_1 + Q_{22}\alpha_2 \\ 0 \end{Bmatrix} \,. \tag{6.16}$$

Since $\mathbf{B} = \mathbf{0}$, Eqs. (6.5)-(6.7) reduce to:

$$\mathcal{A} = \mathbf{A}^{-1} \,, \tag{6.17}$$

$$\mathcal{B} = \mathbf{0} \,, \tag{6.18}$$

$$\mathcal{D} = \mathbf{D}^{-1} \,. \tag{6.19}$$

The fact that $\mathbf{V} = \mathbf{0}$ together with Eq. (6.18) is already sufficient to conclude from Eq. (6.9) that the out-of-plane CTEs are identically null, $\boldsymbol{\alpha}_\chi = \mathbf{0}$. With respect to the in-plane CTEs, from Eq. (6.9) it follows:

$$\boldsymbol{\alpha}_\epsilon = \left[\tfrac{1}{h} \mathcal{A} \right] h \mathbf{U}. \tag{6.20}$$

From Eqs. (6.17) and (6.19) it follows that matrices $\mathcal{A}$ and $\mathcal{D}$ have the same symmetries as matrices $\mathbf{A}$ and $\mathbf{D}$, respectively: they are orthotropic as well. Since $\mathcal{A}$ is orthotropic and vector $\mathbf{U}$ has identically null third component, then also $\boldsymbol{\alpha}_\epsilon$ has identically null third component. Hence, a UD laminate that undergoes a temperature variation will not show thermally induced shear deformation nor bending and twisting curvatures.

Once again, all the previous considerations may be applied to all the three parts of a UD delamination specimen. Hence, a UD delamination specimen allows to prevent undesired thermal effects.

6.3.3 Interface type

When it comes to the types of interface that may be tested, the UD specimen is obviously limited to the standard 0°//0° one. Testing a UD specimen with fibres with an angle with respect to the longitudinal direction of the specimen would allow to test $\theta//\theta$ delamination interfaces. In that case, however, all the previous considerations would not apply, and the specimen would show a different thermo-elastic behaviour in the adopted laminate reference frame.

6.4 Fully-Uncoupled Multi-Directional specimen design

In this study, in order to obtain MD layups for delamination specimens able to satisfy the requirements summarized in Subsection 6.2.4, QT solutions obtained in Chapter 4 and their superposition rules obtained in Chapter 5 are exploited. The strategy proposed is composed of two consecutive steps:

1. Among QT solutions, sequences able to satisfy all requirements for each one of the two arms of the specimen are searched;

2. Among the sequences found in the first step, those that superposed give a macro-sequence satisfying all the requirements are eventually chosen.

The whole procedure is detailed in the following subsections.

6.4.1 Specimen arms design

The first step of the design process consists in the selection of appropriate stacking sequences for each of the two separate arms of the specimen existing in its predelaminated region.

Elastic couplings

Suppression of in-plane/out-of plane elastic couplings, i.e. $\mathbf{B} = \mathbf{0}$, is easily obtained by restricting the search of an appropriate layup to the set of uncoupled QT solutions. As shown in Chapter 4, the set of uncoupled QT solutions is much wider than that of symmetric layups, which could have represented another possible choice.

Next, extension/shear couplings (terms A_{xs} and A_{ys}) and bending/twisting couplings (terms D_{xs} and D_{ys}) have to be eliminated, meaning orthotropic matrices $\mathbf{A}$ and $\mathbf{D}$ must be obtained. Membrane orthotropy may be obtained using different approaches:

1. balanced layups, i.e. sequences in which for each ply oriented at θ, another one oriented at $-\theta$ exists. Angle-ply and antisymmetric layups are particular cases of balanced ones;

2. cross-ply layups, i.e. sequences containing only $0°$ and $90°$ oriented plies;

3. Werren and Norris layups.

Among these options, that of balanced layups is the most interesting one. Indeed, both cross-ply and Werren and Norris layups are extremely restrictive in terms of design space. Moreover, it is important to remember that a balanced laminate containing also plies with $0°$ and $90°$ orientations will still have orthotropic matrix $\mathbf{A}$. This is because plies with such orientations have their orthotropy axes oriented parallel to the laminate reference axes.

On the other hand, bending orthotropy is much harder to obtain. If standard approaches are considered, anti-symmetric and cross-ply layups could be used. A better approach, resulting in a much wider design space, is to adopt QT quasi-homogeneous solutions. Indeed, for these sequences $\mathbf{A} = \mathbf{D}$, and hence membrane orthotropy ($A_{xs} = A_{ys} = 0$) implies also bending orthotropy ($D_{xs} = D_{ys} = 0$).

To sum up, to eliminate membrane/bending, extension/shear and bending/twisting couplings the research of layups has to be restricted to QT quasi-homogeneous solutions and, among them, to those allowing to obtain a balanced laminate, that may or may not, depending on design choices, include $0°$ and $90°$ oriented plies. Hence, solution with any number of orientation groups may be used. Additionally, if $\bar{m}$ is the number of orientations chosen, solutions with more orientation groups, $m > \bar{m}$, may be used too by enforcing two or more orientation groups to be equal.

Thermal effects

Beside elimination of elastic couplings, thermal properties of the sequences selected must be evaluated. The design choices made up to now have some extremely interesting consequences.

First, since the sequences are QT quasi-homogeneous, it immediately follows from Eq. (2.138) that they have $\mathbf{V} = \mathbf{0}$. On the other hand, the general expression for vector $\mathbf{U}$ was given in Chapter 2, Eq. (2.137):

$$\mathbf{U} = \frac{1}{n} \sum_{k=1}^{n} \mathbf{Q}(\delta_k) \boldsymbol{\alpha}(\delta_k) \,, \tag{6.21}$$

For a ply in its material reference frame (x_1, x_2, x_3) the reduced stiffness matrix, $[Q]$, and the vector of CTEs, $\{\alpha\}$, are given by:

$$[Q] = \begin{bmatrix} Q_{11} & Q_{12} & 0 \\ Q_{12} & Q_{22} & 0 \\ 0 & 0 & Q_{66} \end{bmatrix}, \tag{6.22}$$

$$\{\alpha\} = \begin{Bmatrix} \alpha_1 \\ \alpha_2 \\ 0 \end{Bmatrix}. \tag{6.23}$$

When plies are rotated of an angle δ_k with respect to the laminate reference frame, their reduced stiffness matrix, $\mathbf{Q}(\delta_k)$, and vector of CTEs, $\boldsymbol{\alpha}(\delta_k)$, are found as follows:

$$\mathbf{Q}(\delta_k) = [R(\delta_k)][Q][R(\delta_k)]^T = \begin{bmatrix} Q_{xx} & Q_{xy} & Q_{xs} \\ Q_{xy} & Q_{yy} & Q_{ys} \\ Q_{xs} & Q_{ys} & Q_{ss} \end{bmatrix}, \tag{6.24}$$

$$\boldsymbol{\alpha}(\delta_k) = [R(\delta_k)]\{\alpha\} = \begin{Bmatrix} \alpha_x \\ \alpha_y \\ \alpha_s \end{Bmatrix}, \tag{6.25}$$

where $[R(\delta_k)]$ is a rotation matrix that is obtained from the complete rotation matrix $[R]$ defined in Eq. (2.51) considering only those components relevant to the plane stress case considered here. In particular, by defining:

$$c = cos(\delta_k), \quad s = sin(\delta_k), \tag{6.26}$$

matrix $[R(\delta_k)]$ is expressed, using Kelvin's notation, as follows:

$$[R(\delta_k)] = \begin{bmatrix} c^2 & s^2 & \sqrt{2}cs \\ s^2 & c^2 & -\sqrt{2}cs \\ -\sqrt{2}cs & \sqrt{2}cs & c^2 - s^2 \end{bmatrix}. \tag{6.27}$$

Thus, using Eqs. (6.24) and (6.25), the product term within the sum in Eq. (6.21) is given by:

$$\mathbf{Q}(\delta_k)\boldsymbol{\alpha}(\delta_k) = \begin{bmatrix} Q_{xx} & Q_{xy} & Q_{xs} \\ Q_{xy} & Q_{yy} & Q_{ys} \\ Q_{xs} & Q_{ys} & Q_{ss} \end{bmatrix} \begin{Bmatrix} \alpha_x \\ \alpha_y \\ \alpha_s \end{Bmatrix} = \begin{Bmatrix} Q_{xx}\alpha_x + Q_{xy}\alpha_y + Q_{xs}\alpha_s \\ Q_{xy}\alpha_x + Q_{yy}\alpha_y + Q_{ys}\alpha_s \\ Q_{xs}\alpha_x + Q_{ys}\alpha_y + Q_{ss}\alpha_s \end{Bmatrix} \tag{6.28}$$

For plies with $\delta_k = 0°$ or $\delta_k = 90°$, it holds $Q_{xs} = Q_{ys} = 0$ and $\alpha_s = 0$. Consequently, these plies do not contribute to the third component of the vector $\mathbf{U}$. For plies at an angle δ_k, the components of the reduced stiffness matrix in the laminate reference frame are obtained from Eqs. (6.24) and (6.27) as:

$$Q_{xx} = c^4 Q_{11} + 2 c^2 s^2 (Q_{12} + Q_{66}) + s^4 Q_{22},$$

$$Q_{xs} = -\sqrt{2} c^3 s Q_{11} + \sqrt{2} cs (c^2 - s^2)(Q_{12} + Q_{16}) + \sqrt{2} cs^3 Q_{22},$$

$$Q_{yy} = s^4 Q_{11} + 2 c^2 s^2 (Q_{12} + Q_{66}) + c^4 Q_{22},$$

$$Q_{ys} = -\sqrt{2} cs^3 Q_{11} + \sqrt{2} cs (s^2 - c^2)(Q_{12} + Q_{16}) + \sqrt{2} c^3 s Q_{22}, \tag{6.29}$$

$$Q_{xy} = c^2 s^2 (Q_{11} - 2Q_{66} + Q_{22}) + (s^4 + c^4) Q_{12},$$

$$Q_{ss} = 2 c^2 s^2 (Q_{11} + Q_{22} - 2Q_{12}) + (c^2 - s^2)^2 Q_{66},$$

113

and those of the vector of CTEs are obtained from Eqs. (6.25) and (6.27) as:

$$\alpha_x = c^2\alpha_1 + s^2\alpha_2\,,$$
$$\alpha_y = s^2\alpha_1 + c^2\alpha_2\,,$$
$$\alpha_s = \sqrt{2}cs(\alpha_2 - \alpha_1)\,. \tag{6.30}$$

Hence, using Eqs. (6.29) and (6.30), the following relationships are obtained:

$$
\begin{aligned}
Q_{xx}(-\delta_k) &= Q_{xx}(\delta_k)\,,\\
Q_{xs}(-\delta_k) &= -Q_{xs}(\delta_k)\,,\\
Q_{yy}(-\delta_k) &= Q_{yy}(\delta_k)\,,\\
Q_{ys}(-\delta_k) &= -Q_{ys}(\delta_k)\,,\\
Q_{xy}(-\delta_k) &= Q_{xy}(\delta_k)\,,\\
Q_{ss}(-\delta_k) &= Q_{ss}(\delta_k)\,,
\end{aligned}
\tag{6.31}
$$

$$
\begin{aligned}
\alpha_x(-\delta_k) &= \alpha_x(\delta_k)\,,\\
\alpha_y(-\delta_k) &= \alpha_x(\delta_k)\,,\\
\alpha_s(-\delta_k) &= -\alpha_x(\delta_k)\,.
\end{aligned}
\tag{6.32}
$$

Using Eqs. (6.31) and (6.32) in Eq. (6.28) it is found that plies having opposite orientations, δ_k and $-\delta_k$, give opposite contributes to the third component of vector $\mathbf{U}$. Consequently, for the stacking sequences selected (balanced and possibly containing 0° and 90° oriented plies), the third component of vector $\mathbf{U}$ is identically null.

Since the laminates are uncoupled, similarly to what happens for UD ones, Eqs. (6.5)-(6.7) reduce to:

$$\mathcal{A} = \mathbf{A}^{-1}\,, \tag{6.33}$$
$$\mathcal{B} = \mathbf{0}\,, \tag{6.34}$$
$$\mathcal{D} = \mathbf{D}^{-1}\,. \tag{6.35}$$

Therefore, similar conclusions to those obtained for UD laminates hold for this case: since $\mathbf{V} = \mathbf{0}$ and $\mathcal{B} = \mathbf{0}$, Eq. (6.34), from Eq. (6.9) it follows that the out-of-plane CTEs are identically null, $\alpha_\chi = \mathbf{0}$. Additionally, from Eqs. (6.33) and (6.35) it follows that matrices $\mathcal{A}$ and $\mathcal{D}$ have the same symmetries as matrices $\mathbf{A}$ and $\mathbf{D}$, respectively. Since matrices $\mathbf{A}$ and $\mathbf{D}$ are orthotropic for the sequences designed up to now, matrices $\mathcal{A}$ and $\mathcal{D}$ are orthotropic as well. The in-plane CTEs of the laminate may then be obtained from Eq. (6.9) as:

$$\alpha_\epsilon = \left[\tfrac{1}{h}\mathcal{A}\right] h\mathbf{U}\,. \tag{6.36}$$

Since $\mathcal{A}$ is orthotropic and vector $\mathbf{U}$ has identically null third component, then also α_ϵ has identically null third component.

To sum up, for laminates obtained using the layups selected up to now, the curing process will not cause thermally-induced shearing deformation or bending/twisting curvatures.

Interface type

At this stage, no restrictions have been applied on orientations that may be used. The only condition to be respected is that the layup be balanced. Thanks to this, and to the fact that QT solutions preserve their thermo-elastic properties regardless of the orientation values chosen, the laminates designed up to now allow to use all desired ply orientations.

6.4.2 Complete specimen design

In Subsection 6.4.1, it was shown how it is possible to design optimal layups for the arms of a MD delamination specimen. The laminates obtained at the end of the procedure satisfy all the requirements explained in Section 6.2. Their macro-scale thermo-elastic behaviour is, in closed-form solution in the framework of CLPT, identical to that of a UD laminate, as if they were UD laminates made of a different material.

At this point, however, the same properties are sought for the entire specimen laminate, which of course results from the superposition of those used for its arms. It would be extremely helpful to exploit the same principles adopted for the arm layup design. This, however, requires that the entire specimen layup be a QT solution.

For this reason, superposition rules developed in Chapter 5 are exploited. The arm layups were obtained using QT quasi-homogeneous solutions. In order for the layup of the entire specimen to be a QT quasi-homogeneous solutions, the sequences used for the arm layups have to comply to the superposition rule for two QT quasi-homogeneous solutions, Eq. (5.59). As explained in Chapter 5, Eq. (5.59) is satisfied if:

$$n_1 n_{G_j^{(2)}} - n_2 n_{G_j^{(1)}} = 0 ; \quad j = 1, ..., m^* ; \tag{6.37}$$

where n_i and $n_{G_j^{(i)}}$ $(i = 1, 2)$ are respectively the total number of plies and the number of plies belonging to the j-th orientation group of the i-th sequence.

In this particular case, the objective is to design delamination specimen with a standard geometry, in which the two arms have the same thickness, and thus the same number of plies:

$$n_1 = n_2 . \tag{6.38}$$

Therefore, Eq. (6.37) reduces to:

$$n_{G_j^{(2)}} = n_{G_j^{(1)}} ; \quad j = 1, ..., m^* . \tag{6.39}$$

In other words, it is sufficient that the two superposed sequences have the same number of plies for each orientation group: this is an extremely easy condition to be met, due to the very particular case considered. If condition (6.39) is respected when selecting the arm layup, the following results are obtained.

Equal behaviour of arm laminates

By virtue of Eq. (6.39), the two sequences used for the specimen arms will have identical properties in terms of matrix $\mathbf{A}$; also, thanks to their quasi-homogeneity, they will have identical matrices $\mathbf{B}$ and $\mathbf{D}$. The same is true with respect to vectors $\mathbf{U}$ and $\mathbf{V}$ and consequently also for the CTEs vectors $\boldsymbol{\alpha}_\epsilon$ and $\boldsymbol{\alpha}_\chi$. Thus, by imposing that the entire layup is a QT quasi-homogeneous solutions, the requirement on the specimen arms of having identical elastic and thermal properties is automatically satisfied.

Thermo-elastic behaviour of the complete specimen

The entire layup obtained with the proposed approach is a QT quasi-homogeneous solution. Therefore, it is free from membrane-bending couplings, $\mathbf{B} = \mathbf{0}$, and hence it has $\mathbf{V} = \mathbf{0}$ as well.

Moreover, since the two layups used for the arms are balanced, the complete layup will be balanced too. Consequently, membrane orthotropy is obtained. By virtue of quasi-homogeneity, bending orthotropy is obtained as well. In other words, extension/shearing couplings and bending/twisting couplings have been eliminated from the complete specimen, $A_{xs} = A_{ys} = D_{xs} = D_{ys} = 0$.

Following the same process shown in Subsection 6.4.1, it can be demonstrated that the complete specimen has null third component of the in-plane CTEs vector $\boldsymbol{\alpha}_\epsilon$ and null out-of-plane CTEs vector $\boldsymbol{\alpha}_\chi$.

Furthermore, because of Eq. (6.39), the complete layup will contain the same percentage of plies per each orientation as the arm layups. As a consequence, the complete layup will have normalised elastic matrices $\mathbf{A}$, $\mathbf{B}$ and $\mathbf{D}$ identical to those of its arms, and the same is true for its CTEs vectors $\boldsymbol{\alpha}_\epsilon$ and $\boldsymbol{\alpha}_\chi$.

Interface type

The design procedure of the complete specimen and of its arms has no constraints on the orientations that may be used in the layups. Indeed, not only multiple different QT quasi-homogeneous solutions may be used to design the specimen arms, but also, each layup adopted allow to choose freely plies orientation angles. It is thus possible to obtain interface of any type:

- $0°//\theta$;

- $\theta//\theta$;

- $\theta//-\theta$;

- $\theta_1//\theta_2$;

where θ, θ_1 and θ_2 may assume any desired value.

6.5 Concluding remarks

In this chapter, the problem of the design of MD layups for delamination specimens was tackled. Firstly the design requirements were formalised. Then, thanks to the results obtained in Chapters 4 and 5, QT solutions and their superposition rules have been exploited to try and achieve such design goals. It was shown how, by an appropriate selection of the sequences it is possible to design FUMD layups. These layups allow to obtain delamination specimens which are completely free from elastic couplings in all their parts and allow to avoid undesired thermal effects. In other words, their thermoelastic behaviour closely mimics that of UD specimens. It is important to remark the generality of the result obtained: with this strategy a lot of different FUMD layups may be generated. Moreover, thanks to the fact that QT solutions are used, plies orientations can be chosen freely, thus allowing to test any desired delamination interface.

Hence, FUMD delamination specimens combine an optimal thermoelastic behaviour with a great flexibility. For these reasons they may be potential candidates for a standardisation of interlaminar fracture toughness of MD laminates. For this to happen, however, further research is required. Part III of the manuscript will present the preliminary studies performed in the context of this thesis to obtain a first assessment of FUMD delamination specimens.

Part III

Assessment of Fully-Uncoupled Multi-Directional stacking sequences for delamination tests

Chapter 7

Finite Elements assessment

7.1 Introduction

In this chapter, in order to assess the suitability of FUMD layups for delamination specimens, one example of FUMD sequence is designed and compared with other MD layups. Such layups are selected from relevant literature about delamination in MD laminates and, where necessary, adapted in order to make the comparison as meaningful as possible. They are described, along with the FUMD layup designed, in Section 7.2. Firstly, in Section 7.3, the thermo-elastic properties of all the sequences are analysed in depth. In particular, properties of both the arms and of the entire specimen are evaluated. Then, a comparison in terms of ERR distributions and modal partition, under mode I loading conditions, is detailed in Section 7.4. For such comparison, FE models of DCB MD specimens using the considered layups have been developed. By means of these models, the ERR distributions and modal partitions have been obtained using the standard VCCT. However, due to some inconsistencies appearing, a revised state-of-the-art VCCT formulation has been used to double-check the results.

7.2 Selected layups

In order to assess the effectiveness of the FUMD delamination specimen design, a comparison with other possible designs of MD delamination specimen is sought.

For this reason, the principles established in Chapter 6 were used to design one FUMD layup. QT quasi-homogeneous solutions with a total number of plies of $n = 14$ and with three orientation groups were adopted. This allowed to use the following three orientations: 0°, 45° and -45°. The QT solutions for the specimen arms were chosen so that a 0°//45° delamination interface was obtained. Two reasons dictated this choice: first, such interface is very common in practical applications, and second, existing literature offers some possible layups to be used in this comparison. The complete FUMD layup, with $n = 28$ is reported in Table 7.1, under the label *FUMD*.

In order to set up a meaningful comparison, other layups having the same delamination interface as the *FUMD* one and a a similar number of plies were considered. They are all reported in Table 7.1. Such layups were adapted or taken directly from relevant literature on delamination in MD laminates. In more detail:

1. ***DeM***: this layup was proposed in this exact form in [141]. By means of FE analyses, it was verified that it could be an ideal sequence for DCB delamination specimens;

Label	Stacking sequence	D_{xx}^{down} / D_{xx}^{up} / D_{xx} [GPa]
UD	$[0_{14}//0_{14}]$	113,8 / 113,8 / 113,8
FUMD	$[0/45/-45/-45/0/45/0/0/45/0/-45/-45/45/0//$ $45/0/-45/0/0/-45/-45/45/45/0/0/45/0/-45]$	69,46 / 69,46 / 69,46
DeM	$[(0/\mp 45)_4//(0/\mp 45)_4]$	62,79 / 62,79 / 62,25
QUD	$[0_{14}//45/0_{13}]$	113,8 / 99,41 / 113,8
Sun	$[0_{14}//45/0_{12}/-45]$	113,8 / 85,06 / 106,0
Seb	$[0_{12}//45/-45/0_8/-45/45]$	113,8 / 59,20 / 97,26
LiY	$[0_{14}//45/-45/0_{12}]$	113,8 / 89,13 / 113,7

Table 7.1: Stacking sequences adopted for the comparative study.

2. **QUD**: this label stands for Quasi-UniDirectional. The concept behind this layup, indeed, is an attempt to reproduce as closely as possible the behaviour of a UD specimen by introducing only one off-axis ply, which is the minimum to have the desired MD delamination interface. With a generic orientation for the off-axis ply, this layup would be $[0_n//\theta/0_{n-1}]$. It was used for DCB tests, with $n = 10$ and $\theta = 90°$, in [171]. Later, it was suggested for ENF tests as well [109];

3. **Sun**: this layup was suggested by Sun and Zheng [152]. In particular, after evaluation of several layups, they suggested the sequence $[-\theta_1/0_n/\theta_1//\theta_2/0_n/-\theta_2]$ for testing delamination interfaces of the type $\theta_1//\theta_2$. This generic sequence reduces to the layup in Table 7.1 when choosing $\theta_1 = 0°$ and $\theta_2 = 45°$;

4. **Seb**: this layup was proposed in the general form $[(\theta_1/-\theta_1/0_4)_s//(\theta_2/-\theta_2/0_4)_s]$ in [122], to test interfaces of the type $\theta_1//\theta_2$. The main objective of the authors was to find MD layups that could avoid delamination jump. This particular one, with $\theta_1 = 45°$ and $\theta_2 = -45°$, proved feasible in numerical analyses and was then used in actual DCB tests in [125]. To conform the selected delamination interface, this layup was used setting $\theta_1 = 0°$ and $\theta_2 = 45°$;

5. **LiY**: this layup was proposed in the form $[0_{10}//\pm\theta/0_8]$ in [171], where it was used with $\theta = 30°$ and $60°$ for DCB tests. Here, $\theta = 45°$ and a higher number of $0°$ plies was used.

In order to compare the sequences of Table 7.1, typical material properties of a carbon/epoxy UD lamina have been used; as reported in Table 7.2. Clearly, the elastic

E_{11} [GPa]	E_{22} [GPa]	G_{12} [GPa]	ν_{12}	ν_{23}	α_1 [K^{-1}]	α_2 [K^{-1}]	t_{ply} [mm]
112.7	10.35	3.5	0.32	0.42	$-0.04 \cdot 10^{-6}$	$18.0 \cdot 10^{-6}$	0.125

Table 7.2: Representative elastic properties of a carbon/epoxy UD lamina.

properties of the specimens obtained with the layups of Table 7.1 are different. Consequently, the D_{xx} terms, which are related to the bending stiffness in the longitudinal direction of the specimen, for each specimen and both its arms (D_{xx}^{down} and D_{xx}^{up}) are reported as a reference in Table 7.1.

7.3 Comparison of thermo-elastic properties

Tables 7.3 - 7.5 show a synthesis of the thermo-elastic properties obtained for each specimen. Superscripts *up* and *down* are used to refer to quantities computed for the upper and the lower arm of the specimen, respectively. Parameters D_c and B_t are evaluated according to their definition, Eqs. (3.5) and (3.6) respectively; the stiffness matrices **A**, **B**, **C** and **D** are computed according to CLPT, Eqs. (2.118)-(2.121); the CTEs α_ϵ and α_χ are obtained according to Eq. (6.9).

	UD	*FUMD*	*DeM*	*QUD*	*Sun*	*Seb*	*LiY*
D_c^{down}	0.0094	0.19	0.24	0.0094	0.0094	0.0094	0.0094
B_t^{down}	0	0	0.011	0	0	0	0
$\mathbf{B}^{down} = \mathbf{0}$	✓	✓	X	✓	✓	✓	✓
$\mathbf{C}^{down} = \mathbf{0}$	✓	✓	X	✓	✓	✓	✓
$\alpha_{\epsilon,s}^{down} = \mathbf{0}$	✓	✓	X	✓	✓	✓	✓
$\alpha_\chi^{down} = \mathbf{0}$	✓	✓	X	✓	✓	✓	✓

Table 7.3: Elastic properties of the lower arm sequences.

Table 7.3 is relative to the lower arm of the specimen. It reports parameters D_c^{down} and B_t^{down}, two lines indicating whether the laminate adopted for this arm is uncoupled ($\mathbf{B}^{down} = \mathbf{0}$) and/or whether it is membrane-bending homogeneous ($\mathbf{C}^{down} = \mathbf{0}$), and two more lines indicating whether a null shearing CTE is obtained ($\alpha_{\epsilon,s}^{down} = 0$) and whether null out-of-plane CTEs are obtained ($\alpha_\chi^{down} = 0$). It may be observed that in the cases of sequences *QUD*, *Sun*, *Seb* and *LiY* properties identical to those of the UD one are obtained. This was to be expected, since the lower arm of these sequences is indeed a UD laminate. The lower arm laminate of sequence *FUMD*, while being MD, is able to reproduce correctly the behaviour of a UD one: it shows null B_t^{down}, uncoupled and membrane-bending homogeneous behaviour and null shearing and out-of-plane CTEs. It yields an higher value of D_c^{down}, due to the presence of many off-axis plies.

	UD	*FUMD*	*DeM*	*QUD*	*Sun*	*Seb*	*LiY*
D_c^{up}	0.0094	0.19	0.24	0.044	0.098	0.27	0.081
B_t^{up}	0	0	0.011	0.048	0	0.061	0.015
$\mathbf{B}^{up} = \mathbf{0}$	✓	✓	X	X	X	✓	X
$\mathbf{C}^{up} = \mathbf{0}$	✓	✓	X	X	X	X	X
$\alpha_{\epsilon,s}^{up} = \mathbf{0}$	✓	✓	X	X	✓	✓	X
$\alpha_\chi^{up} = \mathbf{0}$	✓	✓	X	X	X	✓	X

Table 7.4: Elastic properties of the upper arm sequences.

Table 7.4 has the same structure as Table 7.3, but refers to the laminates constituting the upper arm of the specimens. In this case, since all the laminates involved are MD, the situation is quite different. Sequence *Sun* shows null B_t^{up} and $\alpha_{\epsilon,s}^{up}$ and is therefore

able to avoid bending/twisting coupling and thermal shearing deformations in its upper arm. However, it is not uncoupled nor membrane-bending homogeneous, and has non-null out-of-plane CTEs. Sequence Seb is able to eliminate both shearing and out of plane CTEs in its upper arm, which is also uncoupled. However it has non null B_t^{up}, and may thus suffer the effects of bending/twisting couplings. Sequence $FUMD$ is the only one to be able to qualitatively reproduce the behaviour obtained with the UD one: the upper arm laminate has null B_t^{up} and is uncoupled and membrane-bending homogeneous; its shearing and out-of-plane coefficients are identically null. Once again, an higher D_c is observed with respect to the UD specimen, due to the presence of off-axis plies.

Finally, Table 7.5 refers to the complete specimens obtained with the layups of Table 7.1. On top of the same thermoelastic properties shown in Tables 7.3 and 7.4, six additional lines are included. Four assess the equality of the stiffness matrices of laminates of the upper and lower arms; differences in such matrices are associated with a stiffness asymmetry in the specimen, which may lead to parasite modes contributions during delamination tests, and undesired rotations. The remaining two lines assess the equality of CTEs in all regions of the specimen. The results in Table 7.5 show an interesting scenario.

	UD	$FUMD$	DeM	QUD	Sun	Seb	LiY
D_c	0.0094	0.19	0.25	0.0094	0.025	0.051	0.0096
B_t	0	0	0.0029	4.1e-05	0.024	0.0046	0.00025
$\mathbf{B=0}$	✓	✓	X	X	X	X	X
$\mathbf{C=0}$	✓	✓	X	X	X	X	X
$\mathbf{A}^{up}=\mathbf{A}^{down}$	✓	✓	✓	X	X	X	X
$\mathbf{B}^{up}=\mathbf{B}^{down}$	✓	✓	✓	X	X	✓	X
$\mathbf{C}^{up}=\mathbf{C}^{down}$	✓	✓	✓	X	X	X	X
$\mathbf{D}^{up}=\mathbf{D}^{down}$	✓	✓	✓	X	X	X	X
$\alpha_{\epsilon,s}=0$	✓	✓	X	X	X	X	X
$\alpha_\chi=0$	✓	✓	X	X	X	X	X
$\alpha_\epsilon^{down}=\alpha_\epsilon^{up}=\alpha_\epsilon$	✓	✓	X	X	X	X	X
$\alpha_\chi^{down}=\alpha_\chi^{up}=\alpha_\chi$	✓	✓	X	X	X	X	X

Table 7.5: Elastic properties of entire sequences.

Sequences in which the number of 0° oriented plies is dominant (i.e. QUD, Sun, Seb and LiY), while being able to yield the lowest values of D_c, are those that worse reproduce the behaviour of the UD specimen when it comes to couplings, similitude of arms behaviour and thermal properties. Sequence DeM, on the other hand, has an high value of D_c and is not uncoupled, but yields identical stiffness matrices for its arms. Eventually, sequence $FUMD$ is the only one to be able to completely reproduce the behaviour of the UD one, in terms of both elastic couplings and thermal properties.

7.4 Finite Element analyses

In the relevant literature, a standard practice to qualitatively assess the suitability of MD layups for delamination specimens is the use of crack closure techniques, and in particular of VCCT, to evaluate ERR distribution along the width of the specimen [53, 57, 58, 122, 141, 172]. As explained in Chapter 3, flat and symmetric distributions are desired. Moreover it is important to evaluate the ERR partition, in order to qualitatively assess if parasite modal contributions are likely to be present. They should be avoided as much as possible. The use of VCCT allows to obtain both ERR distribution and partition, and hence to observe the effects of the specimen layup on such aspects. Thus, sequences yielding the best results can be screened and used for actual experimental testing.

In order to perform ERR distribution and modal partition computation using the VCCT, a detailed FE model was developed. It was used to assess the qualities of the *FUMD* layup presented and to compare it with the other layups of Table 7.1.

7.4.1 Model description

The commercial FE software Abaqus was used to develop the model of the DCB specimen. In particular, a series of Python coded scripts were developed to automate the generation of the model and make it completely parametric.
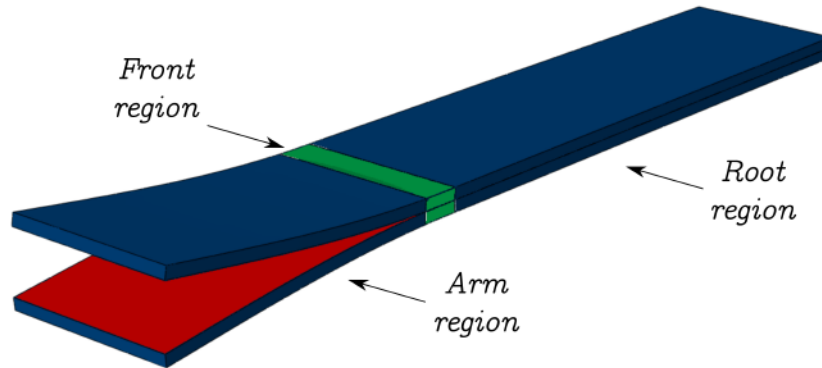

Figure 7.1: Detail of the regions subdivision of the DCB FE model.

The DCB specimen modelled is 150 mm long, 25 mm wide, and has a pre-delaminated region of 50 mm. The model is created defining three regions, as seen in Fig. 7.1:

1. an *arm* region, representing the specimen arms in the pre-delaminated region. It is to remark that this region does not include the arms up to delamination front, but ends before;

2. a *front* region, that is built around the location of the initial delamination front. This region thus includes the remaining portion of the arms in the delaminated region and part of the specimen in its undelaminated region;

3. a *root* region, representing the remaining portion of the undelaminated region of the specimen.

This partition reflects different modelling needs in the different regions. The *front* region is that of greatest interest in the entire model. Here, the adopted mesh has to be extremely fine. This is true both concerning the in-plane dimensions of the elements, which are of fundamental importance in obtaining meaningful results using VCCT, and the number of elements in the thickness direction, which is extremely important to capture the effects of the layup. For these reasons, this region was modelled using fully-integrated eight-node 3D solid elements (C3D8) and a ply-by-ply refinement, i.e. each ply of the laminate is represented with an element through the thickness. Accordingly, each layer of elements was assigned a material orientation corresponding to the orientation of the ply it represented. The elastic properties already presented in Table 7.2 were used, and a transversally isotropic behaviour of the ply was assumed.

The *arm* and *root* regions, on the other hand, are areas of lower interest. Therefore, they have been modelled using eight-node reduced integration continuum shell elements (SC8R). These elements are particularly suited to capture the bending behaviour of laminates while being extremely computationally efficient. Furthermore, with respect to classical shell elements, their three-dimensional geometry allows to use them along with solid elements without the need of shell-to-solid mesh couplings. In these parts, the number of elements in the thickness was automatically adjusted by the Python script generating the parts, based on the total number of plies in the thickness and on the desired number of plies within each element. The material properties in this case are assigned by means of the Abaqus *composite layup* feature. It is worth mentioning that, using this feature, the software assigns the entire layup defined to all layers of elements in the thickness direction of the selected region. So, unless one single elements layer is used in the thickness, separate composite layups (comprehensive only of a part of the entire layup) need to be defined and assigned to each elements layer in the thickness in order to obtain the correct overall stacking sequence. In the present study, this task is automatically managed by the Python generation scripts. The parts constituting the *arm* and *front* regions are joined to that of the front region by means of *Tie* constraints.
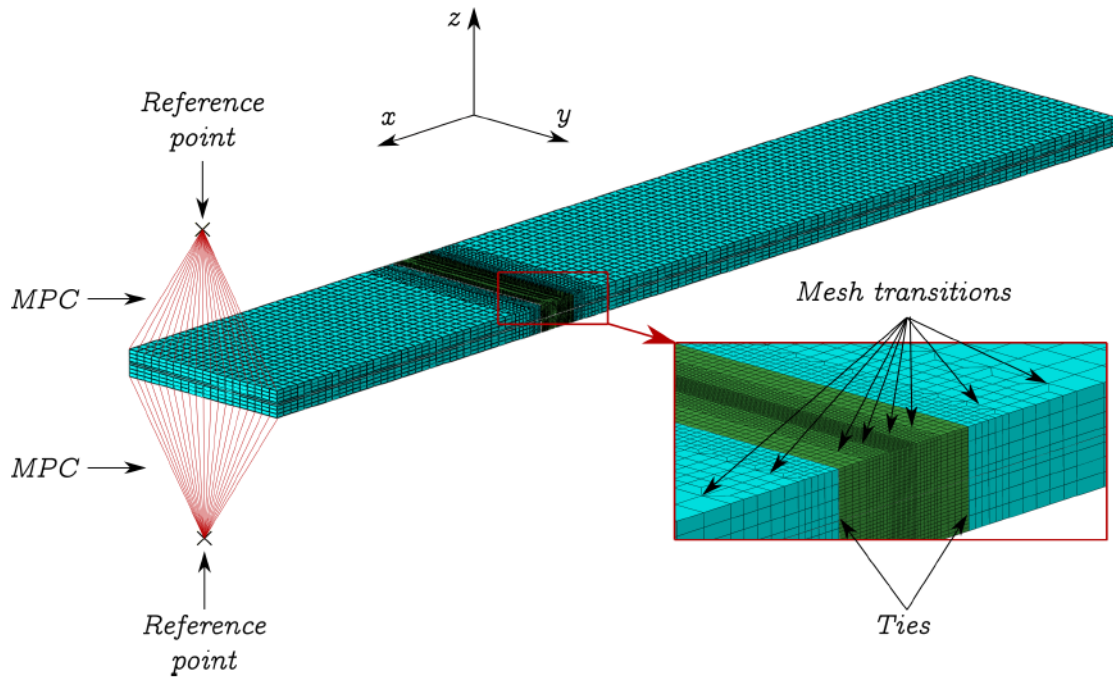

Figure 7.2: Detail of the mesh and of the main features of the DCB FE model.

Several mesh transitions were used in the models to obtain the desired mesh sizes, as can be seen in Fig. 7.2. They are not obtained by joining different parts in the model, but rather geometrically defined within each part. This allows to obtain mesh continuity using no other elements but hexaedral ones. The number and position of the transition may be chosen as inputs to the scripts generating the models, and their creation is completely automated. This allows to obtain an extreme refinement in the vicinity of the front and a coarser mesh in the farther regions, while having the smoothest transition possible. Thus, great accuracy is achieved at crack front, while computational costs remain affordable.

In the *front* region, and in particular in the vicinity of the delamination front, where the arms of the specimen are separated, contact between them is modelled using a *hard contact* pressure-overclosure relationship with *direct enforcement method*, i.e. no interpenetration at all is allowed between the specimen arms. This choice was the result of several analysis trials in which it was observed that, if contact was not modelled or if it was modelled with less restrictive techniques, interpenetration of the specimen arms happened close to the delamination front and to the specimens edges. This was found to profoundly affect ERR distributions in these zones, and should be therefore avoided. Additionally, when using the *hard contact* pressure-overclosure relationship with *direct enforcement method*, it was found that a certain degree of mesh refinement in the *front* region was required in order to avoid contact convergence issues.

To simulate the opening condition observed during a mode I DCB test, a *dynamic* step accounting for geometric non-linearities is performed and the implicit solver of the software is used. The opening displacement is assigned to two *reference points* that are linked to all the nodes of the relevant edges of the specimen by means of *multi-point-constraints* (MPC), see Fig. 7.2.

In these analyses, no thermal steps are performed. This is because it is believed that, in order to obtain meaningful results, a simple thermal step in the analysis of the DCB specimen might not be sufficient. Indeed, in actual practices, specimens are obtained from laminated and cured plates. These plates undergoes the curing process and are therefore subjected to thermal effects. Then, they are cut into specimens: the cutting procedure may lead to a modification of the thermally induced strain and stress state of the material. Hence, in order to accurately capture these states, a simulation involving the entire cycle is probably required. It is noteworthy, however, that sequence *FUMD* is the only one that is expected not to be affected by thermal residual stresses, thanks to the already discussed properties of its CTEs.

7.4.2 Standard VCCT formulation

Crack closure techniques consist in numerical implementations of Irwin's crack closure integral [143]: they lay on the assumption that the energy released when a crack is extended by a small amount Δa, i.e. from a to $a + \Delta a$, is identical to the energy required to close back the crack of the same small amount Δa. In VCCT it is additionally assumed that a crack extension from $a + \Delta a$ to $a + 2\Delta a$ does not significantly affect the state at the crack tip (self-similar propagation) [142]. This allows computation of ERR by means of a single FE analysis, while other techniques require two analyses.

According to VCCT, assuming the crack front is parallel to the y axis direction, in the case of a mesh of 8-node solid elements, the ERR modal components can be calculated
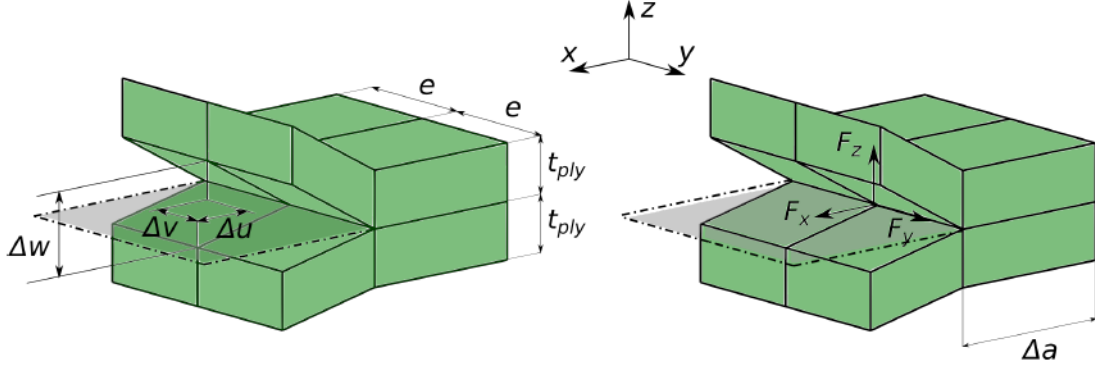
Figure 7.3: Relative displacements and nodal forces used in VCCT.

at each node of the crack tip as:

$$G_I = \frac{1}{2\Delta A} F_z \Delta w \,, \tag{7.1}$$

$$G_{II} = \frac{1}{2\Delta A} F_x \Delta u \,, \tag{7.2}$$

$$G_{III} = \frac{1}{2\Delta A} F_y \Delta v \,, \tag{7.3}$$

In Eqs. (7.1)-(7.3), ΔA is the nodal surface area virtually closed, while Δu, Δv and Δw are the relative displacements along x, y and z axes, respectively, between two corresponding nodes just ahead of the crack tip; F_x, F_y and F_z are the nodal forces acting on the corresponding closed node at the crack-tip, Fig. 7.3. In the case of a rectangular regular mesh with a size Δa in the crack propagation direction and of e in the transversal direction, Fig. 7.3, then $\Delta A = e\Delta a$. The total ERR is obtained as:

$$G_{tot} = G_I + G_{II} + G_{III} \,. \tag{7.4}$$

7.4.3 Bi-material interface problem

As discussed in Chapter 3, the use of VCCT to obtain modal partition in MD delamination interface may be questionable due to the oscillatory behaviour of modal ERR components [44, 148]. However, it was suggested that in most cases good results may be obtained if an appropriate mesh size is used; in particular, values of Δa such that $1/20 \leq \Delta a/t_{ply} \leq 1$ have been suggested [148].

Here, a preliminary study was performed to evaluate the effects of changing the mesh size at the delamination front. Multiple analyses, using the *FUMD* layup, were performed, with mesh sizes Δa yielding $\Delta a/t_{ply}$ ratios falling in the interval [0.3, 1]. The overall modal contributes to the total ERR were evaluated using the VCCT. The results are reported in Fig. 7.4. As observed, all three modal contributes are fairly stable with changing mesh size. A mesh size of 0.078 mm at the delamination front was used, since it represented a good compromise between the desired level of refinement and computational costs. Thus, the final models have 320 elements along the delamination front and a total of 200880 or 237760 elements, for layups with $n = 24$ and for layups with $n = 28$, respectively.

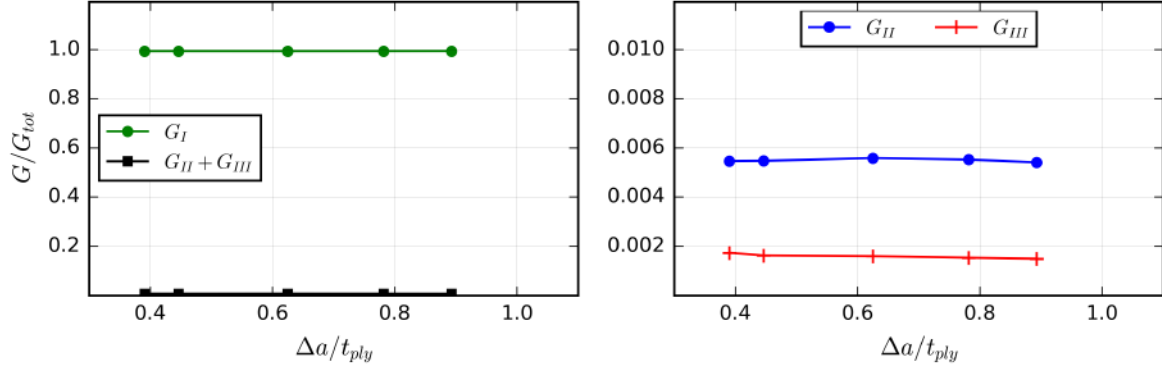Figure 7.4: Effect of mesh size on the overall modal ERR contributes along the specimen width, using *FUMD* layup.

7.4.4 Standard VCCT results

The mode I, II and III ERR distributions along the specimen width have been determined for all the layups listed in Table 7.1.
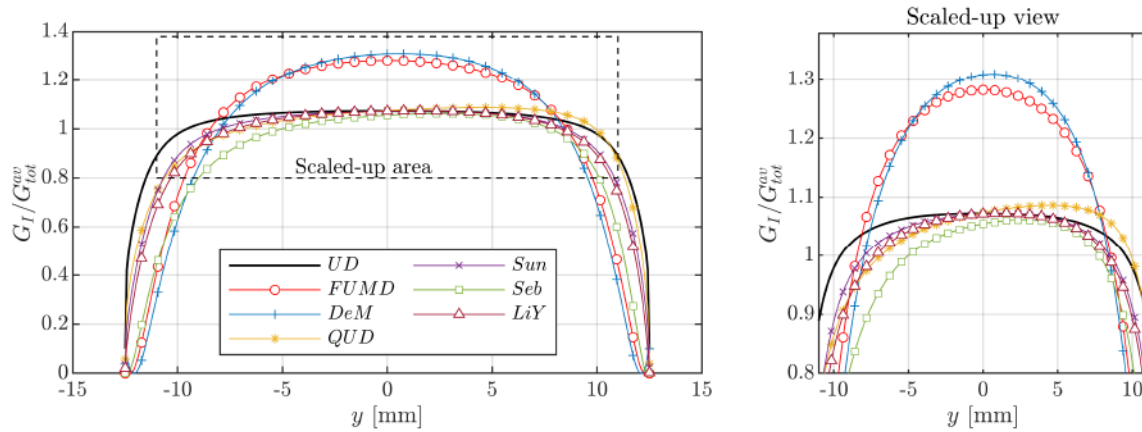

Figure 7.5: Normalised mode I ERR distribution along crack front, found using standard VCCT.

Fig. 7.5 shows the mode I ERR distributions, normalised by the average total ERR. The first remark to be made regards the UD layup: as expected it is the one yielding the most flat and symmetric mode I distribution. Concerning other sequences, two different behaviours may be identified:

1. on one hand, sequences *FUMD* and *DeM* show normalised mode I distributions which are more curved, and reach higher peaks;

2. on the other hand, all other sequences yield normalised mode I distributions which are flatter.

This behaviour is readily explained: sequences *FUMD* and *DeM* have a significantly lower number of $0°$ oriented plies, with respect to the other ones. This translates in a higher D_c value (as already observed in Tables 7.3-7.5) and thus a more pronounced anticlastic effect, which makes mode I ERR distribution more curved. It is noteworthy

127

that this aspect can be improved adopting longer FUMD sequences, which would lead to a reduction of the anticlastic effect and of parameter D_c. When considering symmetry of the distributions, it is evident that $FUMD$ sequence is the only one that gives an almost perfectly symmetric mode I ERR distribution. While some studies have suggested approaches to take into account the curvature of the ERR [53, 172], the same is not true regarding asymmetry.
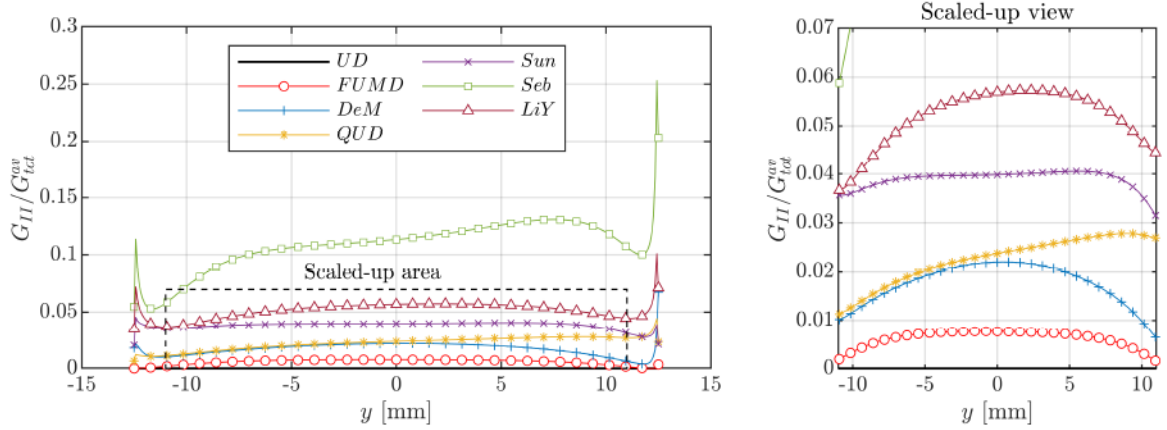

Figure 7.6: Normalised mode II ERR distribution along crack front, found using standard VCCT.

Figs. 7.6 and 7.7 show the normalised mode II and III, respectively, ERR distributions along the specimen width. From these plot some interesting results emerge. The UD layup, due to its symmetry and to the model being geometrically perfect, has identically null distributions for both modes. Remarkably, of all other sequences, the $FUMD$ one is that yielding the lowest distributions of mode II and III ERR, which most closely approach those of the UD one. Also, Fig. 7.6 shows that significant mode II contribution may be present along the whole delamination front (even in the middle of the specimen) in other types of laminates. This may clearly have a major impact on the evaluation of the interlaminar fracture toughness. The mode III distributions reported in Fig. 7.7 are
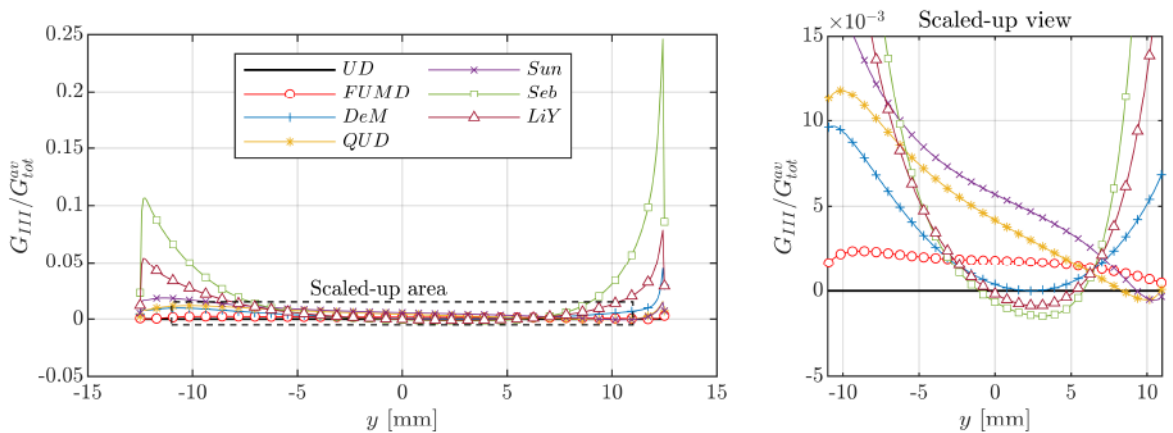

Figure 7.7: Normalised mode III ERR distribution along crack front, found using standard VCCT.

significantly lower than those of mode II. Also in this case, however, the $FUMD$ sequence is the one showing the best behaviour, especially in the lateral regions of the specimen.

These results are confirmed in Fig. 7.8 as well: the bar plot on the left reports the overall mode I ERR contribute versus parasite (mode II plus mode III) overall ERR contributes to the total ERR (along the entire specimen width); the bar plot on the right reports in detail the mode II and mode III overall ERR contributes, as percentages on the total ERR. It can be observed that parasite modal contributes are extremely small for the $FUMD$ layup, while they can become significant with other sequences.
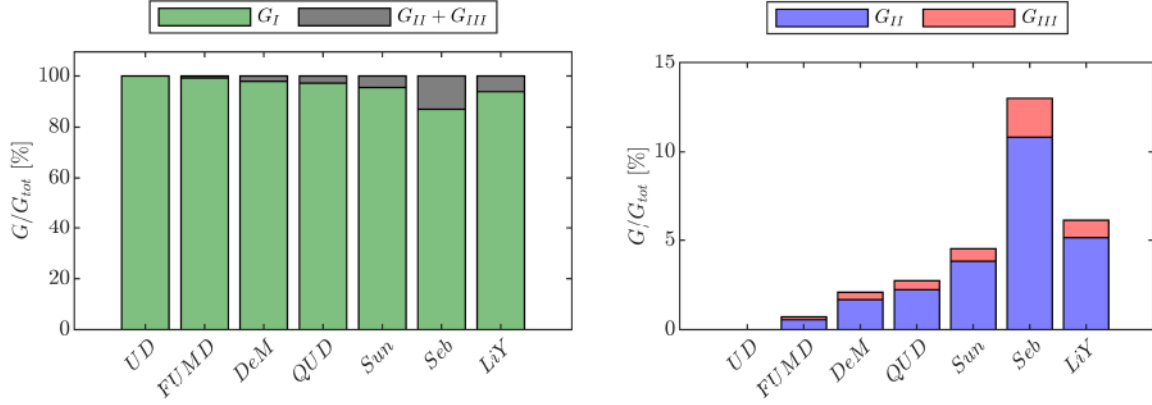

Figure 7.8: Percent overall modes II and II ERR contributes, found using standard VCCT.

It is important here to raise one important issue: in Fig. 7.7 it may be observed that some negative values of ERR along the specimen width are observed. While these values are extremely small in absolute terms, this put into question the validity of the modal partition obtained. Indeed, ERR modal components should be non-negative quantities due to their energetic physical meaning. Negative values show that some inconsistency in the modal partition exists.

7.4.5 Revised VCCT formulation

Inconsistencies of modal partitions similar to those observed in this study had been already observed in the literature [173], and have been explained by Valvo [174]. When performing a virtual crack closure, the energy required to close the crack (which is assumed to be equal to the energy released to open the crack) is obtained by multiplication of the crack-tip forces by the correspondent relative displacement components of the nodes just ahead of the crack tip, as seen in Eqs. (7.1)-(7.3). The three products obtained are considered as the modal components of the ERR, and their sum represents the total ERR. This approach to modal partition, however, is valid only when the problem geometry being analysed reflects the hypotheses under which Irwin's crack closure integral [143] was developed (straight crack embedded in an infinite body, and thus belonging to an axis of symmetry of the problem). Instead, when material or geometrical asymmetries exist in the problem, couplings between the crack-tip forces and the nodal relative displacements in other directions may exist: application of a closure nodal force in one of the three reference direction would cause a displacement not only in the correspondent direction, but also in the other two. A correct modal partition must take this into account. For these reasons, Valvo derived a revised VCCT formulation to solve this issue, for 2D [174] and 3D problems [175].

In order to double check the results obtained in this study with the standard VCCT, the revised VCCT for 3D problems outlined in [175] was used. According to this formu-

lation, for a linear elastic body, the relative displacements may be related to the crack-tip forces by means of a matrix of *flexibility coefficients*:

$$\begin{Bmatrix} \Delta u \\ \Delta v \\ \Delta w \end{Bmatrix} = \begin{bmatrix} f_{xx} & f_{xy} & f_{xz} \\ f_{xy} & f_{yy} & f_{yz} \\ f_{xz} & f_{yz} & f_{zz} \end{bmatrix} \begin{Bmatrix} F_x \\ F_y \\ F_z \end{Bmatrix} \quad \rightarrow \quad \Delta \mathbf{u} = \mathbf{f} \, \mathbf{F}, \qquad (7.5)$$

where the same notation of Subsection 7.4.2 is used. The ij-th flexibility coefficient, f_{ij}, represents the relative displacement in the i-th direction caused by a unit load along the j-th direction. A physically consistent modal partitioning of ERR is obtained by following a three-step closure procedure:

1. during step 1, a force $F_z^{(1)}$ is applied to close the relative displacement in the z-direction, so that the closure displacement is $\Delta w^{(1)} = -\Delta w$. Due to the presence of the coupling terms in the flexibility matrix, displacements in the other directions, $\Delta u^{(1)}$ and $\Delta v^{(1)}$, are caused, too. The amount of work done during this closure step, which is associated to G_I, is $F_z^{(1)}$ times $\Delta w^{(1)}$, as the applied force does not produce work on the other displacement components;

2. in step 2, a force $F_x^{(2)}$ is applied to close the relative displacement in the x direction, hence $\Delta u^{(2)} = -\Delta u - \Delta u^{(1)}$. Concurrently, however, it must be guaranteed that the relative displacement along the z direction, zeroed in the previous step, will not be affected: $\Delta w^{(2)} = 0$. Therefore, an appropriate force $F_z^{(2)}$ should be applied, too. Both these forces causes a displacement in the y direction, $\Delta v^{(2)}$. The amount of work done during this step is $F_x^{(2)}$ times $\Delta u^{(2)}$ and is associated with G_{II};

3. in the final step, the force $F_y^{(3)}$ is applied to completely close the relative displacement in the y direction: $\Delta v^{(3)} = -\Delta v - \Delta v^{(1)} - \Delta v^{(2)}$. Once again, to maintain the relative displacements in the x and z directions null, appropriate forces $F_x^{(3)}$ and $F_z^{(3)}$ are concurrently applied. In this step an amount of work equal to $F_y^{(3)}$ times $\Delta v^{(3)}$ is produced. This work is associated with G_{III}.

While their analytical derivation is not reported here (but can be found in [175]), the expressions obtained for the ERR modal components are:

$$G_I = \frac{1}{2\Delta A_j} f_I r_I^2, \quad G_{II} = \frac{1}{2\Delta A_j} f_{II} r_{II}^2, \quad G_{III} = \frac{1}{2\Delta A_j} f_{III} r_{III}^2, \qquad (7.6)$$

where:

$$f_I = f_{zz} - \frac{f_{zx}^2}{f_{xx}} - \frac{1}{f_{xx}} \frac{(f_{xx} f_{yz} - f_{xy} f_{zx})^2}{f_{xx} f_{yy} - f_{xy}^2}, \quad f_{II} = f_{xx}, \quad f_{III} = f_{yy} - \frac{f_{xy}^2}{f_{xx}}, \qquad (7.7)$$

and:

$$r_I = F_z, \quad r_{II} = F_x + \frac{f_{xy}}{f_{xx}} F_y + \frac{f_{zx}}{f_{xx}} F_z, \quad r_{III} = F_y + \frac{f_{xx} f_{yz} - f_{xy} f_{zx}}{f_{xx} f_{yy} - f_{xy}^2} F_z. \qquad (7.8)$$

It is important to remark that the modal components obtained with this process are positive-defined quantities, thus regaining physical consistency. Their computation requires, similarly to standard VCCT, the crack-tip forces to be obtained by the FE analysis. In addition, however, knowledge of flexibility coefficients is demanded as well.

FE implementation

To obtain the flexibility coefficients, the developed FE model may be used: a unit load in one single reference direction may be applied to the considered crack-tip node, and by reading the displacement components obtained at the end of the analysis, the corresponding flexibility coefficients are obtained. While conceptually simple, this task, for 3D models is quite demanding. In this study, the *load case* feature of the Abaqus software was used. For each model, three load cases for each delamination front node are defined to obtain the flexibility coefficients of that node. A total of 960 load cases is required to obtain all the coefficients. After that, the simulation of the DCB opening, as explained in Subsection 7.4.1 is performed. Modal partition computation according to Eq. (7.6) is implemented as a post-processing procedure.

7.4.6 Revised VCCT results

The results in terms of normalised mode I, II and III ERR distributions along the specimen width obtained using the revised VCCT are shown in Figs. 7.9-7.11.
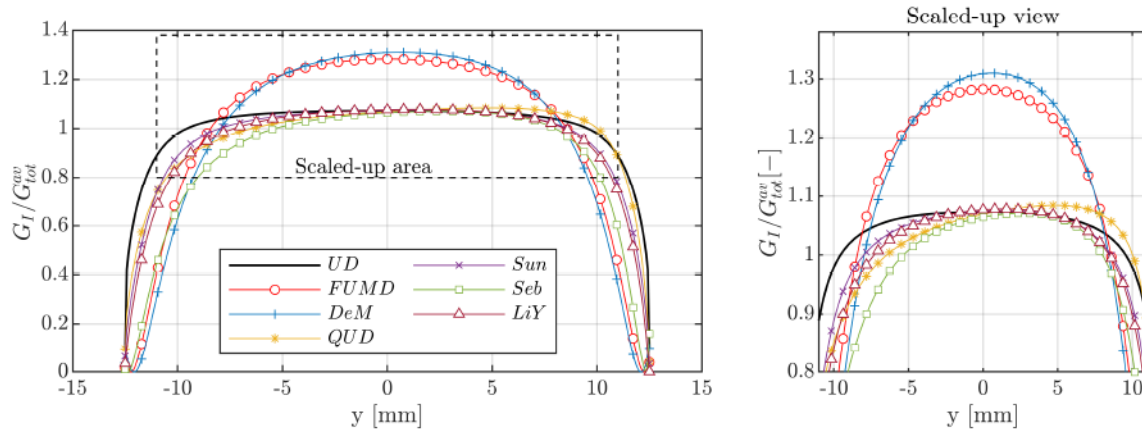

Figure 7.9: Normalised mode I ERR distribution along crack front, found using revised VCCT.

Concerning mode I ERR distributions, Fig. 7.9, no significant differences are observed when comparing revised VCCT results to those obtained using the standard VCCT.

On the other hand, for mode II and III distributions, Figs. 7.10 and 7.11 respectively, some slight differences may be observed. In Fig. 7.10, mode II distributions of sequences QUD and Sun are shifted towards higher values. Important differences are observed near the edges of the specimens. A small increase may be observed also for the distribution obtained with sequence $FUMD$.

On the other hand, mode III distributions in Fig. 7.11 are generally shifted toward lower values than those obtained with the standard VCCT, Fig. 7.7. As already seen for mode II distributions, near the edges of the specimens the differences between results of the two VCCT formulations become more relevant. Most importantly, in this case, the mode III ERR distributions do not show negative values, as expected.

Fig. 7.12, similarly to Fig. 7.8, reports the overall mode I ERR contribute versus parasite contributes, on the left bar plot, and the detail of the mode II and mode III overall ERR contributes, as percentages on the total ERR, on the right bar plot, but with results obtained using the revised VCCT formulations. The only difference that may be
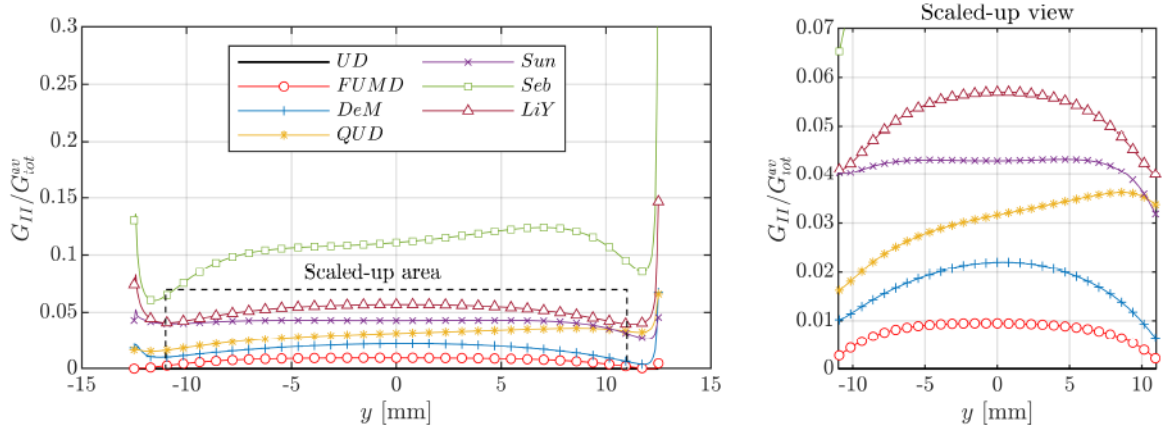
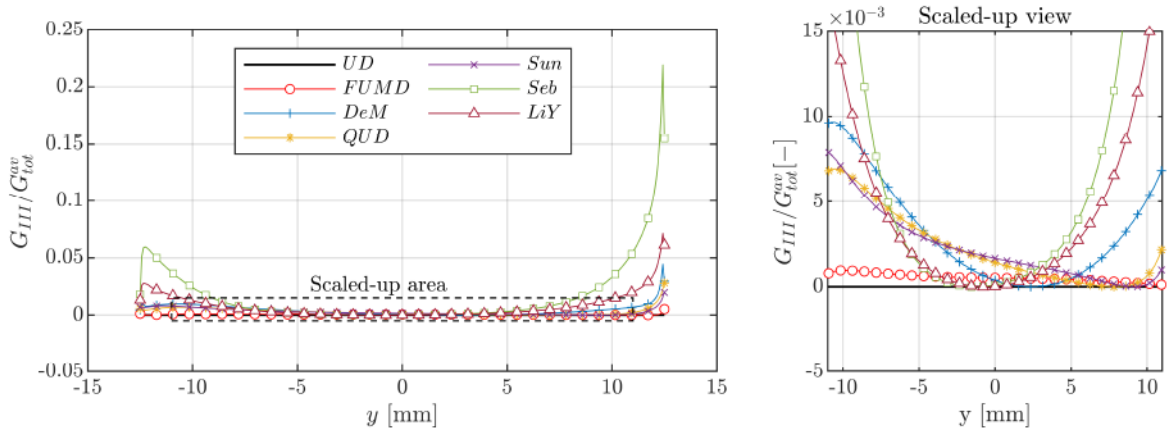Figure 7.10: Normalised mode II ERR distribution along crack front, found using revised VCCT.

Figure 7.11: Normalised mode III ERR distribution along crack front, found using revised VCCT.

observed is a slight increase in mode II overall contributes at the expense of mode III contributes. On the other hand, the qualitative trend already observed in Fig. 7.8 is confirmed.

Hence, while the general conclusions about the performance of the $FUMD$ sequence based on standard VCCT results are confirmed by the results obtained with the revised VCCT, some differences may arise in the evaluation ERR distributions, especially concerning modes II and III and, in particular, toward the edges of the specimen. This may suggest that, in presence of coupling effects and localized mixed mode conditions, the modal partition obtained using the standard VCCT may not be adequate and might yield misleading results. In such situations, caution is advised when interpreting results obtained by means of classic VCCT analyses. For these cases, adoption of the revised VCCT would seem more appropriate. On the other hand, the revised VCCT requires a slightly more sophisticated implementation and a longer computational time, that may be not always required.

While Figs. 7.5-7.7 and 7.9-7.11 report modal ERR distributions normalized by the average value of the total ERR, G_{tot}^{av}, Figs. 7.13-7.15 show the modal ERR distributions normalized by the local value of total ERR[1]. Therefore, these figures show, at any point

---

[1]The value at each point is obtained dividing $G_i(y)$ $(i = I, II, III)$ by the value of $G_{tot}(y)$.
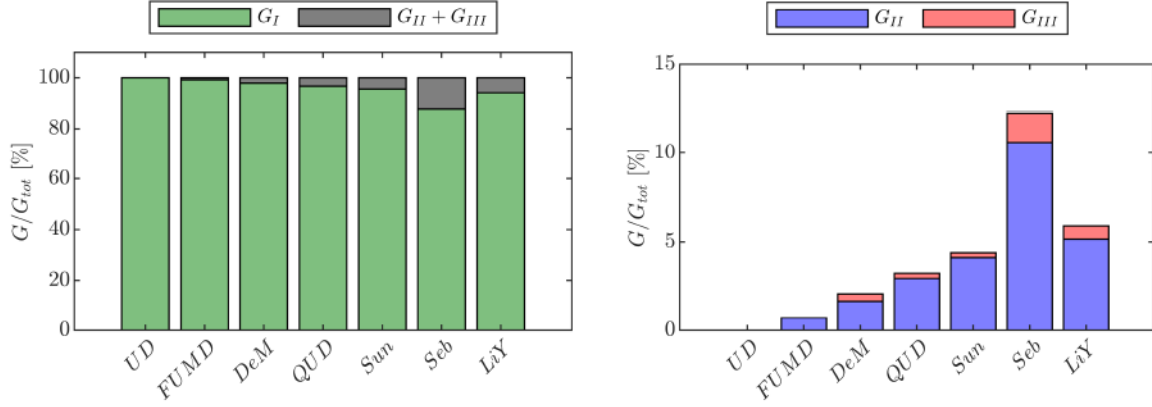
Figure 7.12: Percent overall modes II and III ERR contributes, found using revised VCCT.
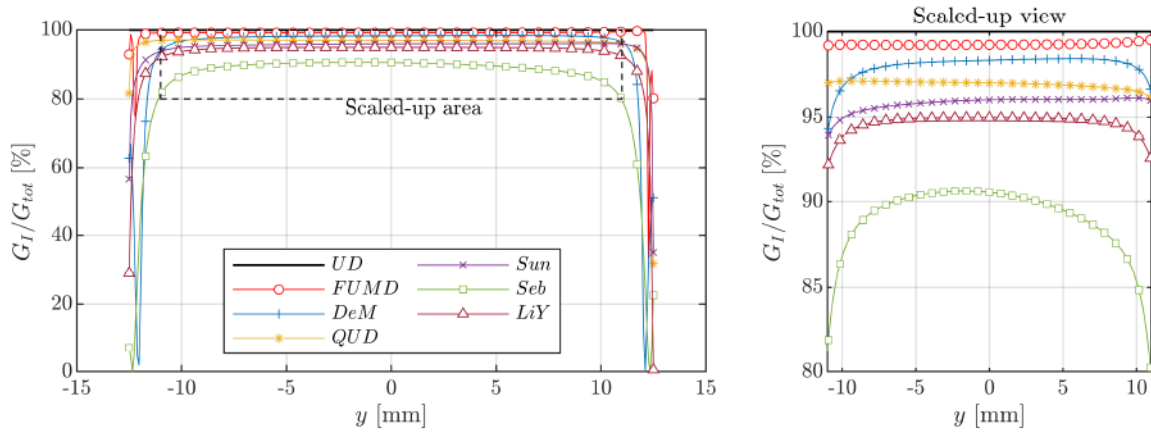

Figure 7.13: Local percent contribution of mode I ERR along crack front.

along the specimen width, the percent contribute of each mode to the total local ERR; thus they give an information on the mode mix at each node. In Fig. 7.13, the UD sequence achieve pure mode I conditions over the entire width of the specimen. Sequence $FUMD$ is the one that gets the closest: a mode I percent contribute close to 100% is maintained over almost the entire width of the specimens. On the other hand, other sequences show lower mode I dominance in the central region of the specimen and a steep decrease when approaching the edges. There, for these sequences, modes II and III become dominant, as confirmed by Figs. 7.14 and 7.15. Sequence $FUMD$ is once again the one that shows the best results, with mode II and III local contributes close to zero. These results confirm the fact that the $FUMD$ sequence does really have a behaviour that closely mimics that of the UD one and is able, as much as it seems possible, to avoid undesired modal contributions.

In order to quantify the effects of the different layups on the ERR distributions and modal contributes, Table 7.6 reports the following quantities:

1. the overall modes II and III ERR percent contributes (G_{II} % and G_{III} %, respectively). Low values of such parameters should be obtained since, for a sound characterisation of pure modes delamination fracture toughness, all contributes from undesired modes should be eliminated. Data show that sequence $FUMD$ is able to keep these parameters much lower than the other sequences;
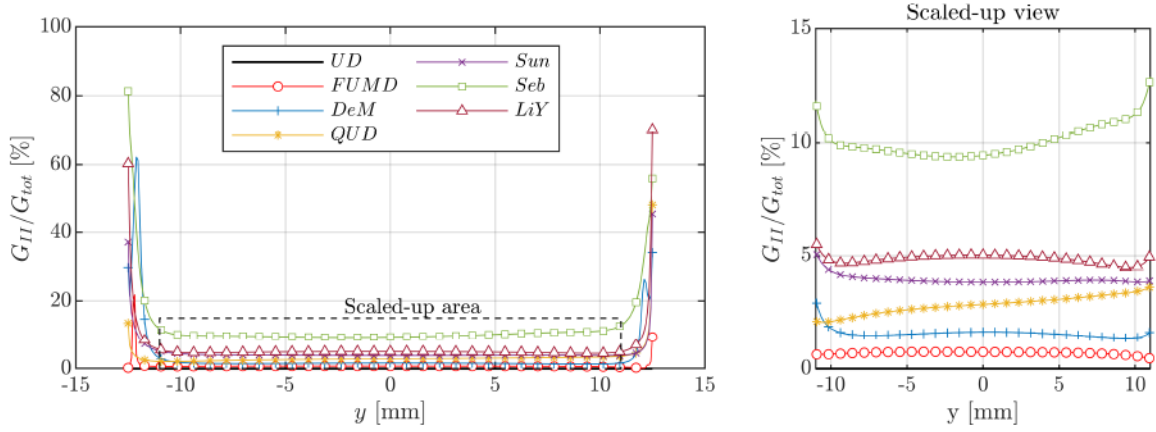
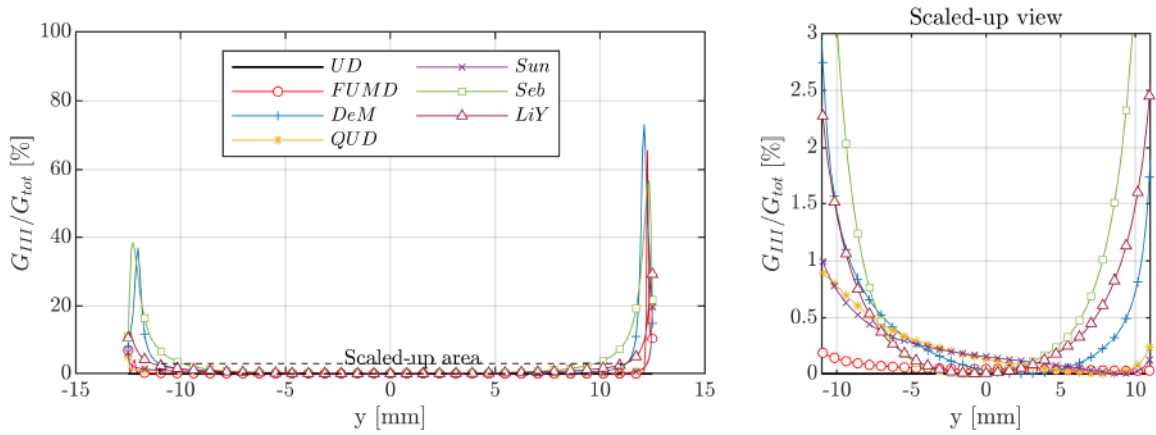Figure 7.14: Local percent contribution of mode II ERR along crack front.

Figure 7.15: Local percent contribution of mode III ERR along crack front.

2. a parameter quantifying curvature of mode I ERR distribution (β) defined as:

$$\beta = \frac{G_I^{max} - G_I^{av}}{G_I^{av}} , \qquad (7.9)$$

and already used in previous studies on the topic [53, 172]. It can be seen that sequences $FUMD$ and DeM show slightly higher values of this parameter compared to other ones, in accordance with their higher values of D_c;

3. a parameter (γ) that quantifies the asymmetry of the distribution of mode I ERR. It evaluates the difference of G_I normalised value between each couple of nodes on the delamination front that are positioned symmetrically with respect to the specimen longitudinal geometrical symmetry plane:

$$\gamma = \sqrt{\frac{\sum\limits_{n^{(+)}} \left(\frac{G_I(y) - G_I(-y)}{G_I^{av}}\right)^2}{n_{nodes}/2}} , \qquad (7.10)$$

where n_{nodes} is the number of nodes along the delamination front and $n^{(+)}$ is the subset of such nodes that have a positive y coordinate. The asymmetry of the ERR distribution may invalidate data reduction procedures. For the UD sequence there is no asymmetry. On the other hand, among the MD layups analysed, sequence $FUMD$ is the one showing the lowest value, as reported in Table 7.6.

	UD	FUMD	DeM	QUD	Sun	Seb	LiY
G_{II} %	0	0.7	1.68	2.96	4.12	10.61	5.15
G_{III} %	0	0.05	0.41	0.28	0.28	1.64	0.74
β	0.0727	0.2925	0.3383	0.1208	0.1248	0.2217	0.1459
γ	0	0.0147	0.0406	0.092	0.0215	0.1006	0.037

Table 7.6: Representative parameters of ERR distributions.

To sum up, the values of the parameters in Table 7.6 should be as low as possible in order to obtain optimal test conditions. Indeed, this is confirmed by observation of the results obtained for the UD sequence, which is the ideal case. Sequence $FUMD$ shows very promising results.

7.5   Concluding remarks

In this Chapter, a preliminary study to assess the performances of FUMD layups for delamination specimens was conducted. A delamination specimen having a 0°/45° delamination interface has been designed using a FUMD sequence and was compared to other solutions proposed in the relevant literature on delamination in MD laminates.

It has been shown that, in terms of thermo-elastic properties, the behaviour of the proposed specimen is the one that better reproduces that of a UD one. Then, FE analyses of a mode I loading condition have been performed and ERR distributions and modal partitions have been evaluated using the standard VCCT and a revised formulation. The numerical results show that the FUMD specimen is the one, after the UD one, that reduces parasite modes contribution the most. Hence, the results obtained with this first assessment seem very promising.

Chapter 8

Mode I delamination experimental assessment

8.1 Introduction

In Chapter 6 and 7 the concept of FUMD specimens was introduced and numerically assessed by means of FE analyses. In this chapter, a mode I interlaminar fracture toughness testing campaign using FUMD DCB specimens is presented. The main objective is to experimentally assess the suitability of FUMD specimens for delamination testing.

A glass/epoxy composite material was used in this study; in Section 8.2 such material system is presented, and the reasons behind its choice are explained. Five different FUMD sacking sequences were conceived for the fabrication of DCB specimens. The details of their design process and the main features of the specimens obtained are detailed in Section 8.3. Section 8.4 reports about the actual fabrication procedure of the specimens. The DCB specimens were tested in mode I opening conditions according to standard methods. The details about the experimental setup and the procedures adopted are given in Section 8.5. Section 8.6 explains how the data collected were elaborated. Eventually, Section 8.7 presents all the results of this study, along with the relevant discussions. Firstly, the force displacement behaviour observed during all tests is revised and commented. Then, results in terms of G_{Ic} are presented, both for the initiation and the propagation (R-curves) phases of delamination. Such results are then correlated to the fracture morphology observed on the specimens. Eventually, an attempt to quantitatively compare the behaviour of FUMD specimens to that of UD ones is done by evaluating the specimens arms rotations during the tests and the shapes of delamination fronts at the end of the test.

8.2 Material system

The material system used for the experimental activity presented in this chapter is a glass/epoxy composite. Its commercial reference is: HexPly © M34N/32%/ 430PUD/G-136x5 and it was available in the form of a pre-impregnated (*prepreg*) roll. The resin material is an epoxy system specifically developed for low temperature curing and suitable for fabrication of thick laminates [176]. The reinforcement is a *UD fabric* material: it consists of a plain weave fabric in which 90% of fibre weight is constituted by the warp yarns (E-glass EC9 136) and the remaining 10% fibre weight is constituted by the

transverse weft yarns (E-glass EC9 68).

The choice of this material is due to one important reason. As explained in Chapter 3, delamination tests of MD specimens may be affected by delamination jump. FUMD specimens are designed to avoid all problems related to thermal residual stresses and mechanical couplings, but they do not address directly the issue of delamination jump. To deal with this issue, Ozdil and Carlsson [96, 97, 98] used a UD-fabric glass/epoxy composite to perform delamination tests on MD specimens. They reported that, with this type of material, no delamination migration was observed, in contrast to studies using UD reinforced composites. Recently, UD-fabric materials were used to study delamination in MD specimens by Gong et al. [53]. For this reason, in order to try and mitigate the problem of delamination jump during actual experimental testing, the material system presented above was selected.

It should be remarked, however, that delamination in woven composites presents some distinctive features, with respect to UD materials [177]. One first difference concerns fibre bridging, which is very common in UD ply materials, but less so in woven composites. Indeed, studies confirmed the absence of fibre bridging in four-harness satin woven glass/vinylester composites [178] and in five-harness satin weave carbon/epoxy composites [179]. Others reported evidence of fibre bridging occurring only for some of the different weave pattern tested [180, 181]. Other differences lay in the fracture process, which in woven composites may be quite complex and is influenced by the weave pattern [178, 179, 180, 181, 182] and the orientation of layers embedding the delamination [53, 97, 179, 180]. Indeed, weave pattern, plies orientation and even plies relative position all influence the micro-structure at the interface level. In particular, they have an effect on the thickness of the interply resin region [178] and on the undulation of the fracture surfaces [178, 183]. This in turn influences the fracture toughness of the interface. In some cases the weave pattern has been found to affect fracture toughness more than fibre type [182].

Elastic properties of the material were obtained by means of a dedicated experimental characterisation campaign based on ASTM standard specimens and tests [184, 185, 186]. All the details about this experimental activity are reported in depth in Appendix B, while Table 8.1 gives the elastic properties obtained along with their coefficient of variation.

	$E_{1,t}$ [GPa]	$E_{1,f}$ [GPa]	$E_{2,t}$ [GPa]	$E_{2,f}$ [GPa]	G_{12} [GPa]	ν_{12} [-]
Average	40.5	39.0	17.4	15.8	6.16	0.248
Std. Dev.	0.745	1.03	0.281	0.475	0.132	$4.33 \cdot 10^{-3}$
C. Var. %	1.84	2.63	1.61	2.95	2.15	1.74

Table 8.1: Elastic properties of the basic ply of the adopted material.

8.3 FUMD specimens design

For this study, five types of FUMD specimens for mode I delamination were designed and fabricated. To do so, two QT quasi-homogeneous solutions were selected, namely:

$$QT_1 = [\theta_1 / \alpha_1 / \beta_1 / \beta_1 / \theta_1 / \alpha_1 / \theta_1 / \theta_1 / \alpha_1 / \theta_1 / \beta_1 / \beta_1 / \alpha_1 / \theta_1],$$

$$QT_2 = [\alpha_2 / \theta_2 / \beta_2 / \theta_2 / \theta_2 / \beta_2 / \beta_2 / \alpha_2 / \alpha_2 / \theta_2 / \theta_2 / \alpha_2 / \theta_2 / \beta_2].$$

As explained in Chapter 4 values for orientations α_1, β_1, θ_1 and α_2, β_2 and θ_2 may be chosen freely. From a practical point of view, these sequences have been chosen for the following reasons:

1. they both have three orientation groups, allocated in the same manner: one appearing in six plies (θ_1 and θ_2) and the other two appearing in four plies each (α_1, β_1 and α_2, β_2). Therefore, these sequences may comply to the superposition rules for QT solutions used for FUMD layups design in Chapter 6, Eq. (6.39), by choosing:

$$\theta_1 = \theta_2 = \theta,$$
$$\alpha_1 = \alpha_2 = \alpha,$$
$$\beta_1 = \beta_2 = \beta;$$

2. they both allow to obtain a balanced laminate, if the θ orientation is aligned to one reference in-plane direction (0° or 90°) and the other two orientations are taken as opposites. So choosing:

$$\theta = 0°,$$
$$\beta = -\alpha,$$

   allows to eliminate the shear-extension and the bending-torsion couplings; thermally-induced shear is eliminated as well;

3. with the previous assumptions, the sequences have different orientations for their outermost plies, allowing to be combined in different ways and thus obtain different delamination interfaces.

Following these choices, the two sequences are transformed to:

$$QT_1 = [0 / \alpha / -\alpha / -\alpha / 0 / \alpha / 0 / 0 / \alpha / 0 / -\alpha / -\alpha / \alpha / 0],$$
$$QT_2 = [\alpha / 0 / -\alpha / 0 / 0 / -\alpha / -\alpha / \alpha / \alpha / 0 / 0 / \alpha / 0 / -\alpha].$$

Table 8.2 reports all the FUMD sequences designed for this study, each with an identifying label highlighting the delamination interface. The standard UD delamination specimen is included as well. In more detail:

1. sequences FUMD 0//15, FUMD 0//30 and FUMD 0//45 are obtained superposing sequence QT_2 to QT_1, and then choosing $\alpha = 15°$, 30° and 45° respectively;

2. sequence FUMD 0//0 is obtained repeating sequence QT_1 two times and choosing $\alpha = 45°$;

3. sequence FUMD -45//45 is obtained repeating sequence QT_2 two times and choosing $\alpha = 45°$.

Label	Stacking sequence	D_c
UD	$[0_{14}//0_{14}]$	0.025
FUMD 0//15	[0 / 15 / -15 / -15 / 0 /15 / 0 / 0 / 15 / 0 / -15 / -15 / 15 / 0 // 15/0 / -15 / 0 / 0 / -15 / -15 / 15 / 15 / 0 / 0 / 15 / 0 / -15]	0.041
FUMD 0//30	[0 / 30 / -30 / -30 / 0 / 30 / 0 / 0 / 30 / 0 / -30 / -30 / 30 / 0 // 30 / 0 / -30 / 0 / 0 / -30 / -30 / 30 / 30 / 0 / 0 / 30 / 0 / -30]	0.085
FUMD 0//45	[0 / 45 / -45 / -45 / 0 / 45 / 0 / 0 / 45 / 0 / -45 / -45 / 45 / 0 // 45 / 0 / -45 / 0 / 0 / -45 / -45 / 45 / 45 / 0 / 0 / 45 / 0 / -45]	0.110
FUMD 0//0	[0 / 45 / -45 / -45 / 0 / 45 / 0 / 0 / 45 / 0 / -45 / -45 / 45 / 0 // 0 / 45 / -45 / -45 / 0 / 45 / 0 / 0 / 45 / 0 / -45 / -45 / 45 / 0]	0.110
FUMD -45//45	[45 / 0 / -45 / 0 / 0 / -45 / -45 / 45 / 45 / 0 / 0 / 45 / 0 / -45 // 45 / 0 / -45 / 0 / 0 / -45 / -45 / 45 / 45 / 0 / 0 / 45 / 0 / -45]	0.110

Table 8.2: FUMD stacking sequences generated and associated labels. The double slash indicates midplane (delamination) interface.

Table 8.2 reports also the values of the parameter D_c, Eq. (3.5) for all sequences, while B_t, Eq. (3.6), is null for all of them.

The FUMD sequences in Table 8.2 were designed in order to allow to investigate different issues:

1. FUMD 0//0 specimens have the same delamination interface as the standard UD ones, but significantly different global stiffness. As reported by some authors [159], this might influence fracture toughness. Hence, results obtained from these two types of specimens may be compared to observe the effects, if any, of stiffness on critical ERR;

2. on the other hand, specimens with sequences FUMD 0//0, FUMD 0//45 and FUMD -45//45 have exactly the same global stiffness, but different interfaces. Therefore, if differences are observed in the fracture toughness obtained with these three types of specimens, they may result from local effects, like the orientations of plies embedding the delamination interface, and of adjacent plies at most;

3. sequences FUMD 0//15, FUMD 0//30 and FUMD 0//45 are used to evaluate effects of the misorientation on fracture toughness of the interface. It is worth mentioning that these sequences have, of course, different global stiffness matrices, as obtained according to CLPT.

8.4 Fabrication procedure

The prepreg material was cut in rectangular patches with a numerically-controlled automated cutting machine, at any desired orientation (0°, 15°, 30°, 45°, 90°) with respect to the longitudinal 0° direction of warp yarns. Plates with the desired stacking sequences were obtained by a manual lay-up process. Whenever eight new plies had been laid up, a compaction phase was performed by means of vacuum bagging. This procedure facilitates the expulsion of the gas that might be trapped during layup, leading to a better quality

of the laminates after curing. During the lay-up, a 25 μm thick Fluorinated Ethylene Propylene (FEP) insert film (Aerovac A5000) was used in order to create the initial pre-delaminated region of the DCB specimens. The rectangular plates thus obtained were cured in an autoclave at a temperature of 75° C and a pressure of 3 bars for 8 hours, according to the producer's indications. No post-cure was performed. From each plate, and thus for each specimen type in table 8.2, seven DCB specimens 25 mm wide and 200 mm long were obtained, by means of water-jet cutting. The cut was tailored in order to obtain the desired insert length of 64 mm.

8.5 Experimental testing procedure

Before testing, all specimens were labelled and measured. The insert tip was accurately marked with the aid of an optical microscope and its length was measured on both specimens sides. Compliance with all dimensional requirements suggested in [49] was verified. All seven UD specimens and five FUMD specimens of each type (those with labels 2, 3, 5, 6, 7) had one side white painted and marked at regular intervals, to keep track of delamination propagation during the test. End blocks were installed on both arms of the specimen. Specimens were not conditioned prior to testing.

Mode I delamination tests were performed at room temperature (23.0 $\pm$ 0.6°C) using a double actuator system, with the specimen in vertical position. This configuration presents some interesting advantages. Firstly, thanks to the vertical position of the specimen, gravity will not introduce asymmetries in the loading conditions. Additionally, the two actuators are controlled with an identical displacement signal, so that they move symmetrically to open the specimen. Thus it is ensured that the loading conditions are as symmetrical as possible. The setup is shown in Fig. 8.1. According to [49], each
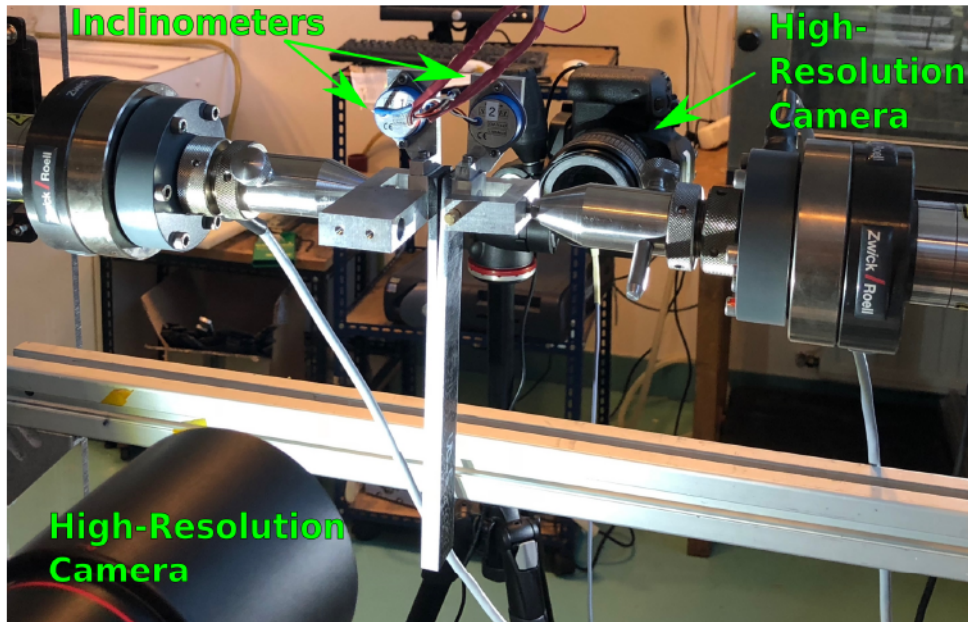

Figure 8.1: View of the experimental set-up used for mode I delamination tests

specimen was firstly loaded up to the beginning of delamination propagation, and until delamination, as visually observed, propagated about 4-7 mm; then the specimen was unloaded. Afterwards, the specimen was loaded again, until delamination propagated up

to about 50 mm from the initial insert tip position. A constant opening displacement rate of 1 mm/min was used during both loading phases.

Along with force and displacements, the load points rotations were recorded by means of inclinometers fixed at the tip of each specimen arm, Fig. 8.1. Two cameras (Canon EOS 800D and Canon EOS 750D) regularly took pictures (at a resolution of 6000 × 4000 pixels) of the specimen from both sides during the test. On one side, a global view of
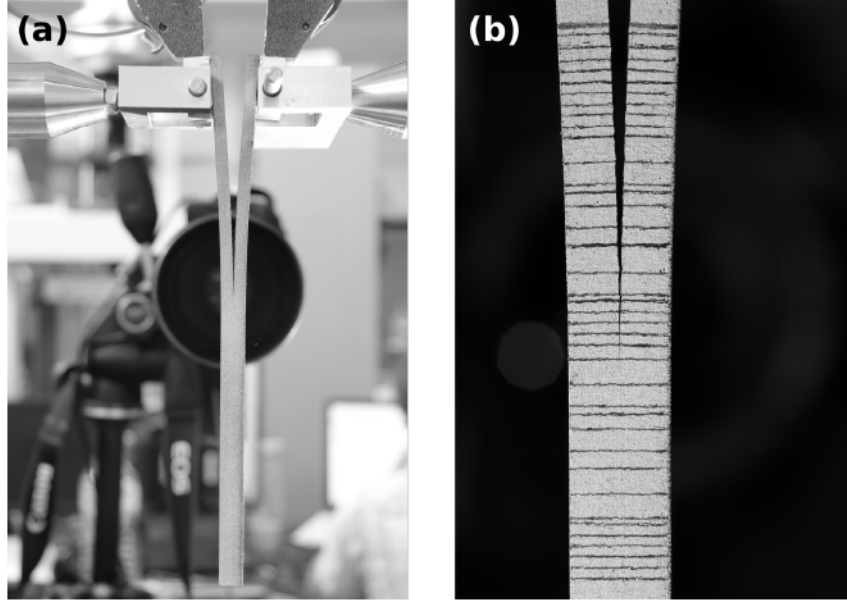

Figure 8.2: Example pictures taken during mode I delamination tests: global view of the specimen (a) and zoom on the propagation region (b).

the specimen was caught, while on the other one a close zoom in the propagation region was set, Fig. 8.2. Loads, displacements and load points rotations corresponding to each pictures were recorded automatically by the acquisition system.

After the tests, the specimens were observed by means of ultrasonic C-scans, performed with an Olympus OmniScan SX device [187, 188, 189]. Eventually, specimens were opened to observe the fracture surfaces and to establish if any delamination jump had occurred.

8.6 Data reduction

8.6.1 Choice of the data reduction technique

Since FUMD specimens have a macroscopic mechanical behaviour that is identical to that of a UD specimen, standard data reduction techniques [49], described in Chapter 3, may be used. Such techniques are: the Modified Beam Theory (MBT), the Compliance calibration (CC) and the Modified Compliance calibration (MCC). All three techniques were used to elaborate the experimental data obtained. However, it was found that the results obtained with different techniques are almost undistinguishable; hence, for the sake of simplicity and without loss of information, only results obtained with MBT are presented.

Recalling from Chapter 3, according to MBT, ERR may be computed as follows:

$$G_I = \frac{3P\delta}{2b(a + \Delta)},$$

(8.1)

where P is the applied load, δ is the load point displacement (opening), b is the specimen width and a is the delamination length. The length correction Δ is determined experimentally according to [49].

8.6.2 Initiation values of G_{Ic}: insert tip *vs* mode I precrack

Initiation values of critical ERR, G_{Ic}, were obtained both for the initial loading phase, with delamination advancing from the insert film tip, and the second loading phase, with delamination advancing from the mode I precrack produced in the first loading phase, as suggested in [49].

The evaluation from the insert film tip presents some advantages. The position of the insert tip is known with great accuracy and it is very consistent for specimens of the same type. In other words the delamination length to be used in Eq. (8.1), a_0, is almost identical for all specimens. This reduces the sources of experimental scatter. In addition, the edge of the insert film is known to be straight. Conversely, during the second loading phase, the initial delamination length, a_0^{pc}, is the sum of the insert length a_0 and the amount of propagation obtained during the first loading phase, which may be different for different specimens. Consequently, specimens of the same family may have lengths a_0^{pc} differing by as much as 2-3 mm. This might introduce some scatter in the results. Also, delamination inside the specimens is likely to have developed a curved front.

On the other hand, reliability of G_{Ic} values obtained from the insert tip is questionable. The thickness, the material and the shape of the insert may affect the evaluation of G_{Ic} [190, 191]. At the tip of the insert a resin pocket usually exists, which may behave very differently from a real, thinner, interlayer region of the composite [79]. Evaluation of G_{Ic} during the second loading phase, instead, avoids all problems related to the presence of the resin pocket at the insert tip. In this case, indeed, delamination is propagating from a mode I precrack, which is a natural delamination. This makes this situation much more representative of what could happen in real applications.

8.6.3 Initiation values of G_{Ic}: initiation points

All initiation points defined in [49] were used to obtain critical ERR initiation values.

The Non-Linear (NL) point was obtained by analysis of the load displacement curves: the second derivative of the curves was obtained and a threshold (identical for all specimens) was established to identify deviation from linearity.

The visual onset (VIS) point was obtained by visual analysis of the high-definition pictures of the propagation region taken during the tests. As shown in Fig. 8.3, the image corresponding to the first observable propagation was identified; then the load and displacement corresponding to such picture were retrieved.

Eventually, the 5% compliance offset or maximum load (5%/MAX) point was obtained according to its definition [49].

All the initiation points mentioned are marked in the force displacement plots of the tests in Fig. 8.4, for both loading phases.

8.6.4 Propagation values of G_{Ic}

Critical ERR was evaluated also during propagation, at different lengths, in order to obtain resistance curves (R-curves) for the different types of interfaces. In this case
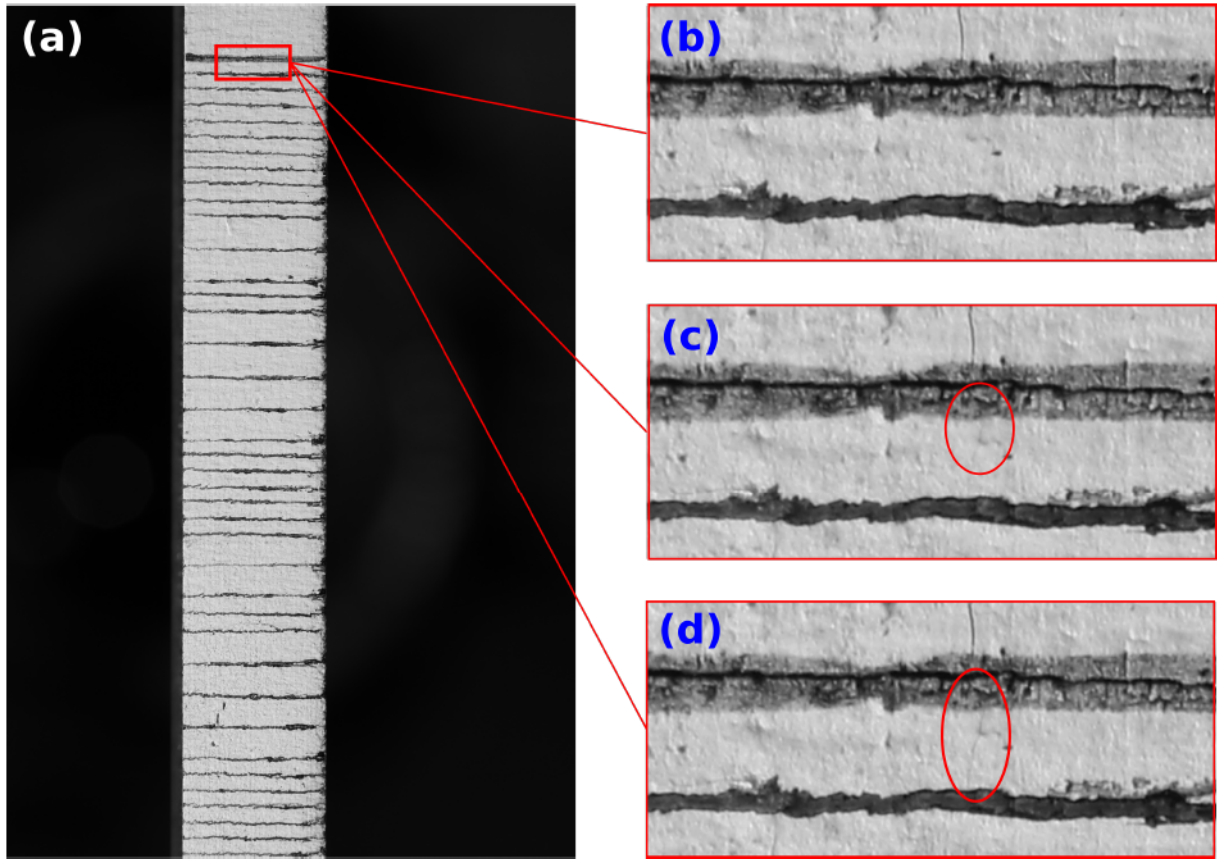
Figure 8.3: Identification of VIS initiation point: (a) general picture of the specimen before loading, (b) zoom of the insert tip region right before visual onset, (c) at visual onset and (d) after visual onset.

too, pictures taken during the tests were analysed to find those corresponding to the delamination reaching given lengths (marked on the side of the specimens). In particular, pictures from both loading phases were used in order to obtain continuous R-curves. The first point of each curve corresponds to the VIS initiation point of the first loading phase. Each subsequent point corresponds to a given propagation length counted from the insert tip. The force applied and opening displacement of the specimens corresponding to each propagation length were thus retrieved and G_{Ic} values were computed using Eq. (8.1).

8.7   Results and discussion

8.7.1   Force-displacement behaviour

The complete force-displacement curves of all DCB specimens tested are shown in Fig. 8.4. They include both the first and the second loading phases, with the respective unloading curves and the initiation points defined in Subsection 8.6.3.

In general, the curves show a very good consistency. During the first loading phase, in particular, specimens of the same family produced almost identical force-displacement responses. This confirms that scatter induced by the material variability and the testing procedures was reasonably low. On the other hand, the little scatter observed during the first unloading and the second loading phases is mainly caused by the different delamination length, for different specimens, obtained at the end of the first loading phase, as
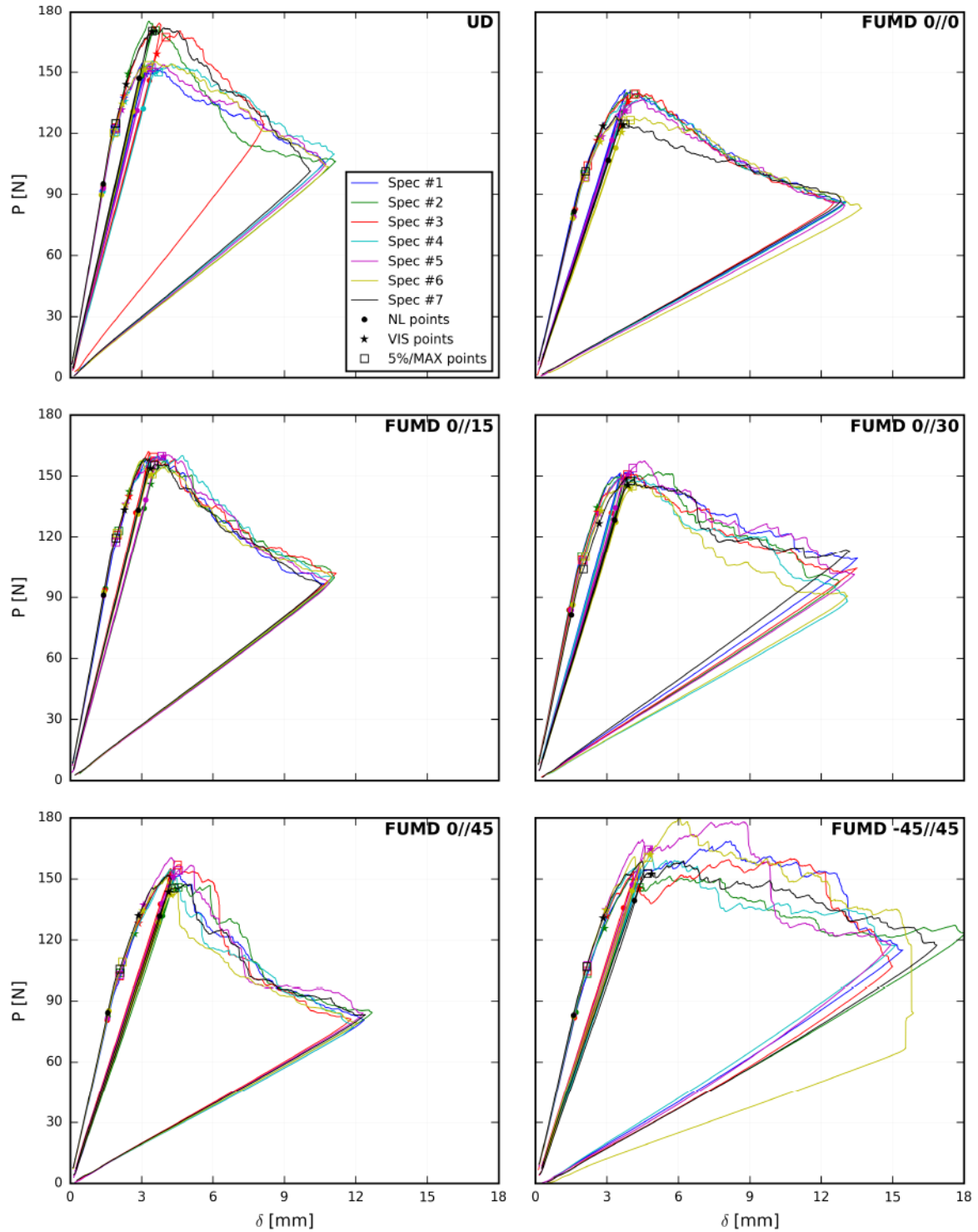
Figure 8.4: Force-displacement experimental curves obtained from all DCB specimens of all types.

explained in Subsection 8.6.2.

During the first loading phase, the force displacement plots of all specimens deviate from linearity quite early. The 5%/MAX and VIS initiation points are reached before the peak load as well. Delamination propagation during this phase occurs with increasing

load for all specimen types. Then, the first unloading and the subsequent re-loading follow a linear force-displacement path.

During the next delamination propagation phase, specimens with sequences UD, FUMD 0//0, FUMD 0//15 and FUMD 0//30 show smooth softening curves, typical of stable mode I propagation. On the other hand, specimen with sequence FUMD 0//45 show a faster decrease of the load at the beginning of the propagation, and then a smooth softening similar to all other specimens.

Specimens with sequence FUMD -45//45 show a force displacement behaviour during delamination propagation different from that of all other specimens: initially the force keeps increasing slightly; then, a sudden little drop is observed and the force starts to decrease slowly but steadily. In order to better explain such singular behaviour, ultrasonic C-scans and fracture surfaces of all FUMD -45//45 specimens were observed.

Fig. 8.5 shows the images obtained from the C-scans of the FUMD -45//45 specimens and of one UD specimen, for comparison. The black vertical dashed line indicates the
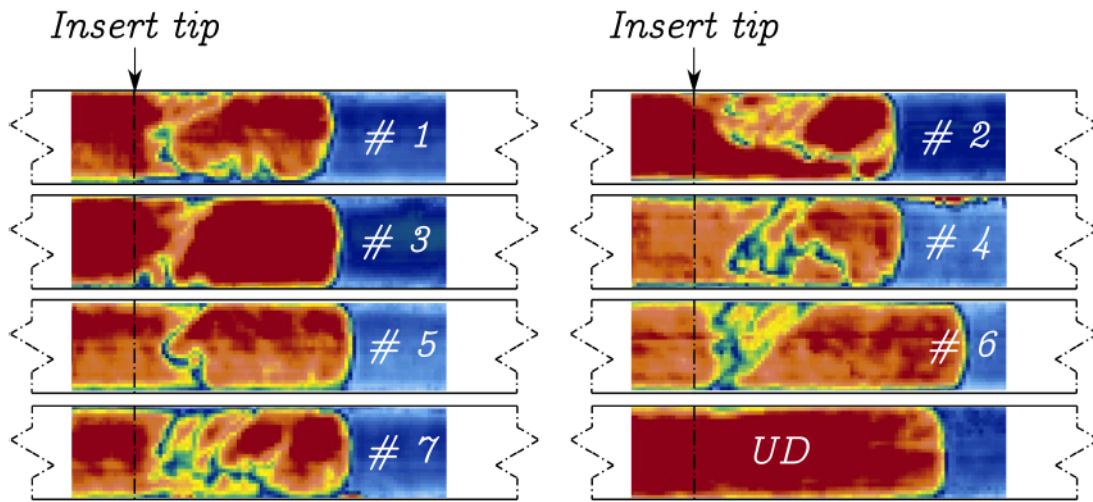

Figure 8.5: C-scans of all FUMD -45//45 specimens and of a UD one.

position of the insert tip. The delamination propagated from the left to the right. The blue regions to the right correspond to the undelaminated portion of the specimens. On the other hand, a continuous red surface, as the one observed for the UD specimen, indicates a discontinuity in the material, and hence, in this case, the delamination plane. In all the C-scans images from FUMD -45//45 specimens some irregular patterns appear and interrupt the delamination plane. While it is not easy to draw conclusions from these images, such patterns might be an indication of some additional damage mechanism or a delamination jump taking place. In order to further investigate the issue, the specimens were opened and fracture surfaces were observed. It was confirmed that in all the FUMD -45//45 specimens the delamination did not stick exclusively to its initial interface. Instead, another delamination interface appeared, toward the bottom of the stacking sequence, which is a 0//-45 interface. This is shown, for the case of specimen number 6, in Fig. 8.6. The other six specimens have an almost identical appearance. Moreover, it is possible to recognise a typical pattern described in other studies [117]: at first, delamination propagates on its initial plane; after few millimetres, on one edge of the specimen, delamination jumps to another interface; such jump then propagates inside the specimen following the direction of the fibre-bundle initially jumped, leaving a typical oblique front that separates the two different delamination planes, see Fig. 8.6.
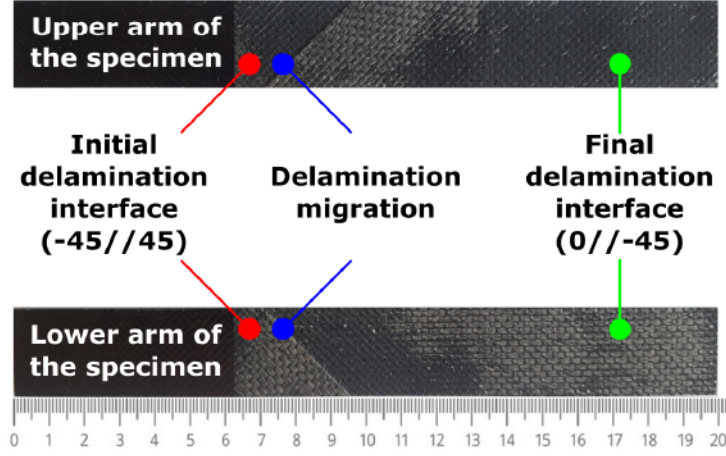
Figure 8.6: Fracture surfaces of specimen FUMD -45//45 number 6, confirming the occurrence of delamination jump.

Since delamination jump affected all FUMD -45//45 specimens, they have not been considered for further analyses. Further analyses are required, and will be performed, to establish if at least the initiation values of G_{Ic} could be considered valid.

On the other hand, both the C-scan images and the observation of the fracture surfaces confirmed that a smooth propagation in the desired delamination plane was obtained with the UD specimens and all other FUMD specimens, as will be shown in the following.

8.7.2 Initiation values of G_{Ic}

Initiation values of G_{Ic} have been obtained for both loading phases. For the first loading phase, the delamination length used for the computation was that of the insert film, a_0. For the second loading phase, the delamination length relevant to each specimen, a_0^{pc}, was that given by the sum of the insert length and the amount of propagation obtained during the first loading phase, and it was determined by visual analysis of the pictures.

Fig. 8.7 reports the G_{Ic} values obtained for all the initiation points considered (NL, VIS and 5%/MAX) and for both loading phases.

Concerning the results obtained from the insert film, the NL point and the 5%/MAX point gave values of G_{Ic} independent from the specimen type, and thus from the delamination interface. However, as explained in subsection 8.6.2, these results may be an artefact of the delamination propagating in the resin pocket existing at the insert film tip. This is particularly relevant for the present case, since the insert film adopted has a thickness of 25 μm, which exceeds the upper limit of 13 μm recommended in [49]. On the other hand, the VIS point values of G_{Ic} show a slight increase with increasing mismatch angle of the plies embedding the delamination plane. This different behaviour might be explained by the fact that VIS points are the last to occur. While NL initiation is likely associated with delamination starting to propagate at the centre of the specimens [72], when propagation is detected visually from the specimen side delamination is likely to have assumed a curved shape and to have propagated more in the central region of the specimens. Consequently, the effects of the resin pocket may be relevant only in a region very close to the specimens edges, and the G_{Ic} obtained might be globally more representative of the actual material behaviour.

The previous hypothesis seems to be corroborated by the results obtained for the delamination advancing from the mode I precrack. In this case, indeed, G_{Ic} values obtained
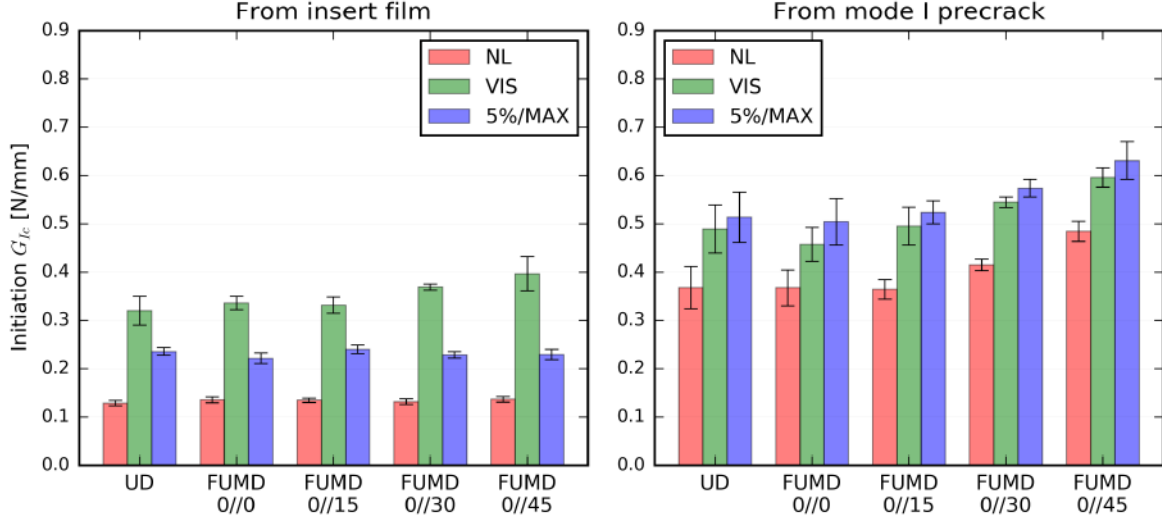
Figure 8.7: Initiation values of G_{Ic}.

with all initiation points show a consistent increasing trend with increasing mismatch angle of the plies embedding the delamination plane. In particular, if FUMD 0//0 and FUMD 0//45 specimens are compared, the G_{Ic} values found are significantly different; since these two specimen types have identical global stiffness, the difference is likely to be mainly dependent on the different orientations of plies embedding the delamination plane. Additionally, it is interesting to observe how the G_{Ic} values obtained from UD and FUMD 0//0 specimens are very similar. These two specimen types share the same delamination interface, but have very different global stiffness properties. Consequently, interlaminar fracture toughness is found to be not dependent on global stiffness, as opposed to what found in other studies. Moreover, this allows to reinforce the hypothesis that the trend observed is not related to the global properties of the specimens, but rather it is caused by ply orientations.

8.7.3   R-curves

Fig. 8.8 shows the average R-curves, obtained as explained in Section 8.6.4, for all types of specimens, along with the relative standard deviations.

The first important observation concerns sequences UD and FUMD 0//0: the resistance curves obtained with these types of specimens have a behaviour which is almost identical. The two curves start from close values of G_{Ic}. The following increase in G_{Ic} is characterised by a similar slope and eventually, for propagation length greater than 30 mm, both curves seem to stabilize at the same level. The scatter band is narrow for both sequences, but particularly for FUMD 0//0. These results confirm that global stiffness of the specimens and stacking sequence do not have an impact on the interlaminar fracture toughness, as long as the delamination interface is the same.

In general, the behaviour of FUMD 0//15 specimens is similar to that of UD and FUMD 0//0 ones, showing an initial increase in G_{Ic} values and an almost stable value for longer propagation length. Some differences are observed in the actual values of G_{Ic}, with respect to sequences UD and FUMD 0//0: they are slightly higher in the first increasing portion of the curve, and slightly lower in the stable portion.
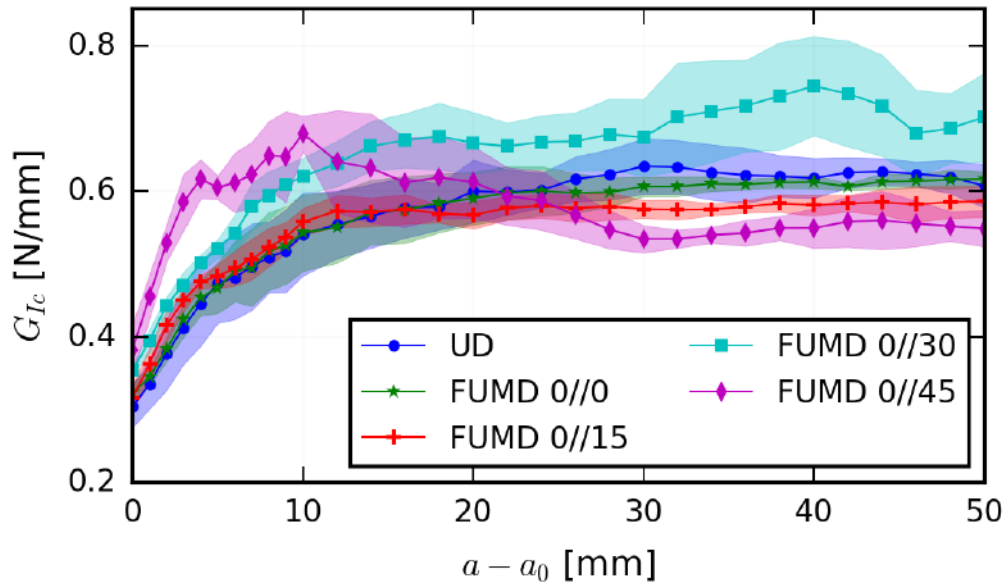
Figure 8.8: R-curves: average curve for all types of specimens and relative standard deviation.

The resistance curve of sequence FUMD 0//30 presents an initial increase steeper than that of sequences UD, FUMD 0//0 and FUMD 0//15. In addition it reaches higher values than those of the other sequences. Hence, it seems that there is an effect of the different delamination interface. For propagation length greater than 20 mm the curve does not seem to grow significantly, but shows some more oscillations with respect to the others. The scatter of the resistance curve of sequence FUMD 0//30 is wider than those of the other sequences.

Eventually, the resistance curve of sequence FUMD 0//45 shows the steepest initial increase. For delamination propagation length up to about 10 mm G_{Ic} value increases and stays higher than that of all other sequences. Then, however, G_{Ic} decreases and stabilizes, for propagation lengths greater than 30 mm, to a value which is lower than those of all other sequences.

8.7.4 Fracture behaviour

In order to explain the trends observed in the R-curves of Fig. 8.8, the fracture behaviour of the different specimens has been investigated.

Transverse yarns debonding

An important remark is that in no specimen tested did fibre-bridging occur, as confirmed by the digital pictures taken during the tests, see e.g. Fig. 8.2.

However, transverse yarn debonding was observed. This mechanism was explained by Alif *et al.* [179, 180] and later observed also by Ozdil and Carlsson [96, 97, 98]. It may occur during interlaminar fracture toughness testing of woven composites. In specimens made with such materials, transverse yarns (with respect to the longitudinal direction of the specimen) are at some point interrupted by the edges of the specimen. Depending on

the position of the interlaced longitudinal yarn, the final portion of the transverse yarn (close to the edge) may be constrained to a different degree. If it is not, transverse yarn debonding may happen: when delamination reaches the transverse yarn it may promote debonding of its unconstrained final portion. Hence, such yarn segment shortly bridges the delamination surfaces [97], before being separated from one of them. In this process
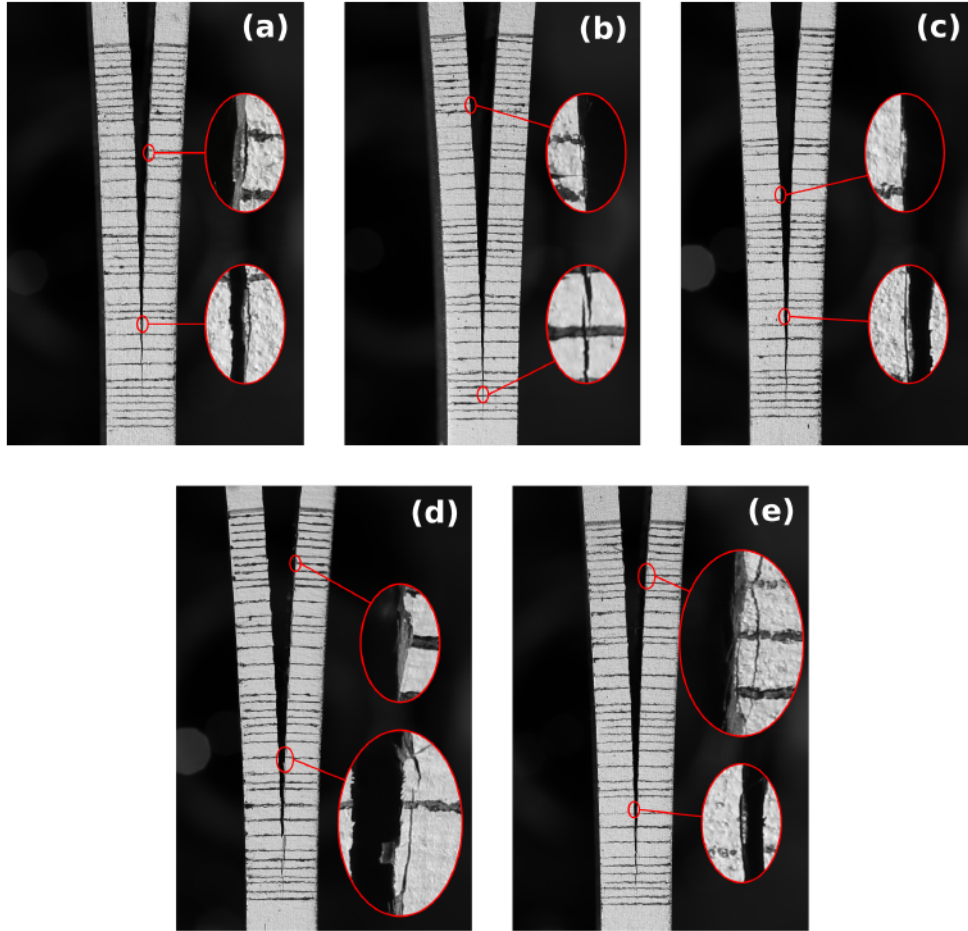

Figure 8.9: Evidence of transverse yarns debonding: UD (a), FUMD 0//0 (b), FUMD 0//15 (c), FUMD 0//30 (d) and FUMD 0//45 (e) specimens.

a certain amount of additional energy is dissipated, which may have an effect on the interlaminar fracture toughness observed [179].

In this study, transverse yarns debonding was observed in all types of specimens, Fig. 8.9. In UD and FUMD 0//0 specimens, the phenomenon was marginal, while it became increasingly important for FUMD 0//15, FUMD 0//30 and FUMD 0//45 specimens. A similar observation was reported in [96], where it was found that for angle-ply specimens fracture toughness increased with ply angle due to the increasing amount of transverse yarn debonding. This also agrees well with the considerations reported in [180]: the importance of transverse yarn debonding is highly dependent on the degree of constraint imposed to transverse yarns close to the edges of the specimens. When UD and FUMD 0//0 specimens are considered, transverse yarns intersecting the specimens edges are only the weft yarns of the material, which make up only 10% of the total fibre weight, while the warp yarns form the remaining 90% fibre weight. In this situation, transverse yarns are highly constrained. When other FUMD sequences are considered, the presence of a non-0°-oriented (*off-axis*) ply embedding the delamination plane implies that also warp

yarns intersect the specimens edges. Furthermore, the greater the orientation angle, the higher the number of warp yarns intersecting the edges. Consequently, a more significant transverse yarns debonding is to be expected, also considering the fact that weft yarns may offer only a limited constraint, due to their low percent weight.

Hence, the transverse yarns debonding may partly explain the differences in the behaviour of the types of specimens, and in particular the different rate of the initial increase of G_{Ic} observed in the resistance curves. However, since the material used is a plain weave composite, this mechanism is restrained to an extremely narrow region close to the edges of the specimens [180].

On the other hand, the decrease in the resistance curve of FUMD 0//45 specimens and the different values of G_{Ic} in the final part of the propagation still need an explanation.

Fracture surfaces observation

Examples of fracture surfaces obtained with UD and FUMD specimens are reported in Fig. 8.10.

As expected, fracture surfaces of UD and FUMD 0//0 specimens look almost identical, Figs. 8.10 (a) and (b). Black and white regions (resin and fibres, respectively) may be observed on both surfaces, with complementary patterns (a black region on one surface corresponds to a whiter region on the other one). This is because separation mainly occurred at the fibre-matrix interface, rather than within the interlaminar resin layer, of both upper and lower plies embedding the delamination. This indicates poor fibre-matrix adhesion properties of the material, when compared to the matrix toughness, which often happens in glass/epoxy composites.

When considering sequence FUMD 0//15, fracture surfaces appear extremely consistent among the different specimens, which is in accordance with the reproducible force-displacement curves, Fig. 8.4, and the very low scatter in the resistance curve, Fig. 8.8. The typical aspect for all specimens is that observed in Figs. 8.10 (c) and (d): once again, separation occurs at the fibre matrix-interface; at the very beginning both the upper (15°) and the lower plies are involved, but after few millimetres propagation occurs almost entirely at the fibre-matrix interface of the 0° ply.

This is not the case when observing FUMD 0//30 specimens, for which the typical aspect of the fracture surfaces is that shown in Figs. 8.10 (e) and (f): the separation runs almost entirely in the fibre-matrix interface of the 30° ply. There is only one exception, which is represented by specimen number 6, in which some areas of separations at the fibre-matrix interface of the 0° ply are observed.

In FUMD 0//45 specimens, separation typically occurs at both fibre-matrix interfaces in the first stages of propagation, and then slowly turns most to the 0° ply fibre matrix interface when delamination advances, as observed in Figs. 8.10 (g) and (h). Once again a single specimen, number 6, represents an exception: separation occurred mostly at the 0° ply for the entire propagation. The previous observations may lead to some important conclusions. In the first place, FUMD 0//30 specimens were the only ones showing a separation almost entirely at the fibre-matrix interface of the off-axis (30°) ply, and concurrently those yielding the highest values of propagation G_{Ic}. On the other hand, UD, FUMD 0//0 and FUMD 0//15 specimens yielded lower and similar values of propagation G_{Ic} and had separation occurring at the 0° ply fibre-matrix interface. It seems, then, that separation at the fibre-matrix interface of the off-axis plies would require higher fracture energies. This hypothesis would also explain the behaviour of FUMD 0//45 specimens: in the first stages of propagation an higher energy is required
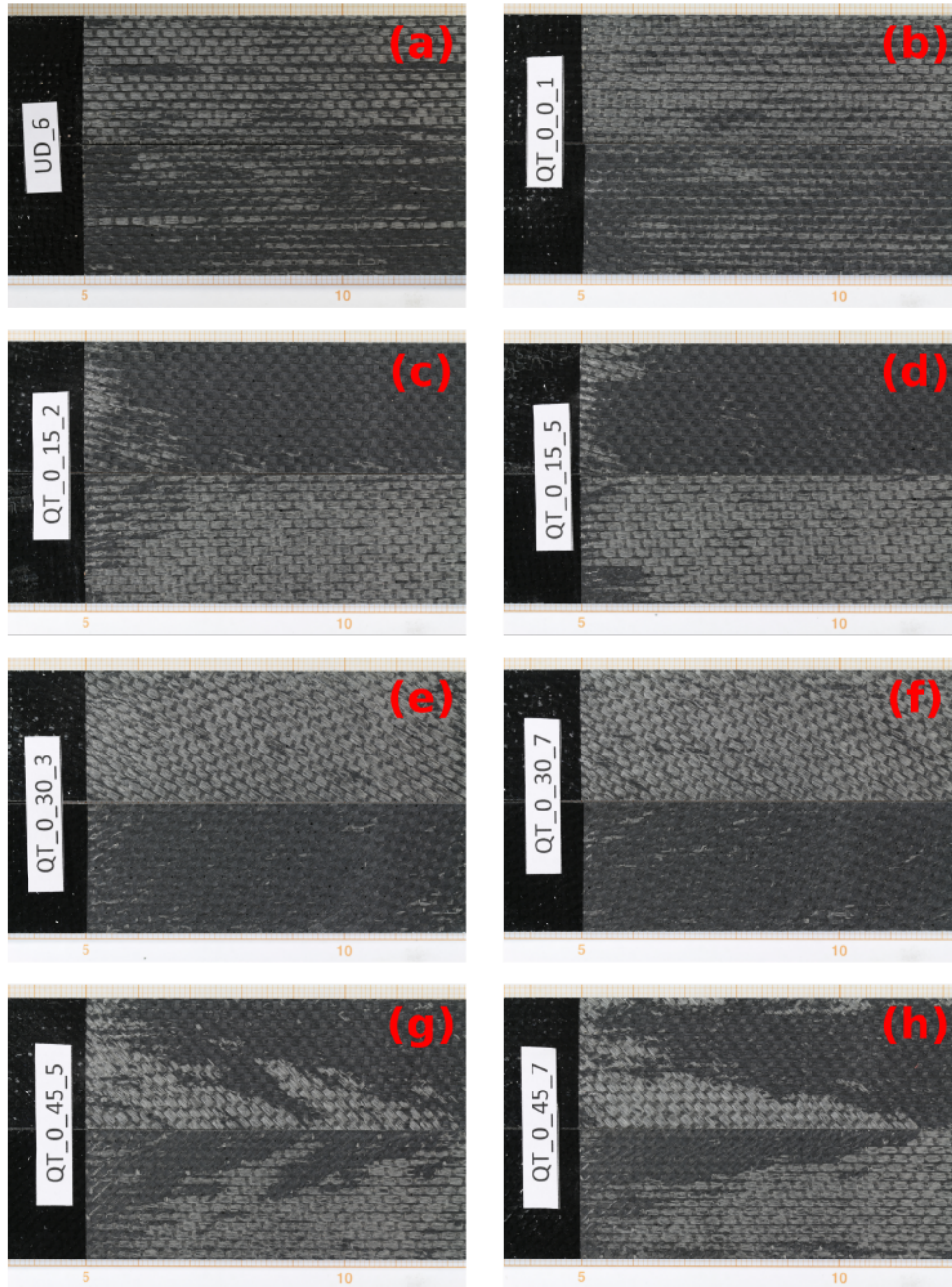
Figure 8.10: Pictures of fracture surfaces of UD and FUMD specimens.

due to the bigger portion of separation occurring at the 45° ply; then energy is reduced because of separation taking place mostly at the 0° ply.

A deeper analysis, comparing fracture surfaces of single specimens to their respective R-curves seems to confirm the previous conclusion. In Fig. 8.11, R-curves of single specimens for sequences FUMD 0//30 (on the left) and FUMD 0//45 (on the right) have been aligned with the pictures of fracture surfaces of two representative specimens.

The fracture surfaces reported on the top of Fig. 8.11 are representative of the typical surfaces observed for the corresponding specimen type.

On the other hand, the fracture surfaces reported at the bottom are those of the outlier specimens (specimen number 6 in both cases): there is a clear correlation in the fact that the R-curves of these specimens are different from those of the others having the same sequence. Moreover, if some relevant point in the resistance curves are observed in the

fracture surfaces (dashed lines), there seems to be a strict correlation between G_{Ic} and the way separation is split among the off-axis and the 0° plies. The difference in fracture energy required between separation at the off-axis plies and the 0° ones could be explained by different mechanism occurring at the micro-scale.
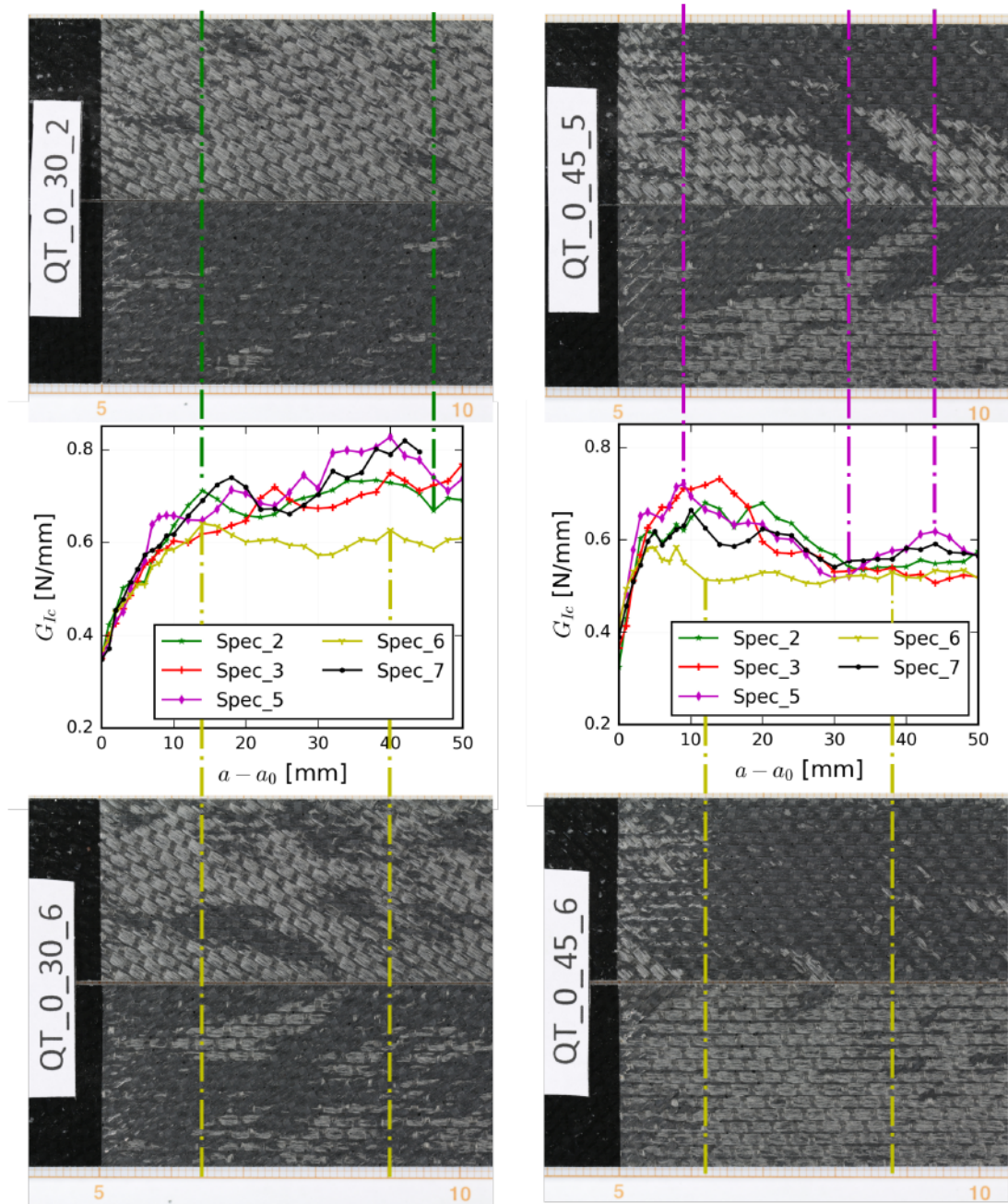

Figure 8.11: Comparison of single specimen resistance curves with respective fracture surfaces.

8.7.5 Specimens arms rotations

Besides the observation of the delamination behaviour of different interfaces, the goal of this experimental study was to collect evidences of the suitability of FUMD specimens for delamination testing.

As explained in Chapter 3, the mechanical behaviour of the specimen has to be such that the ideal kinematic of the delamination test is respected. While this is easily achieved with UD specimens, with MD ones this might not be the case. In a DCB test, for example, in order to truly obtain pure mode I, the specimen must be opened in a symmetric way: its arms should rotate of the same quantity and its midplane should not rotate. If the arms of the specimen are not of equal stiffness, or if couplings exist, their rotations might be different and/or the entire specimen might rotate, thus invalidating the test. According
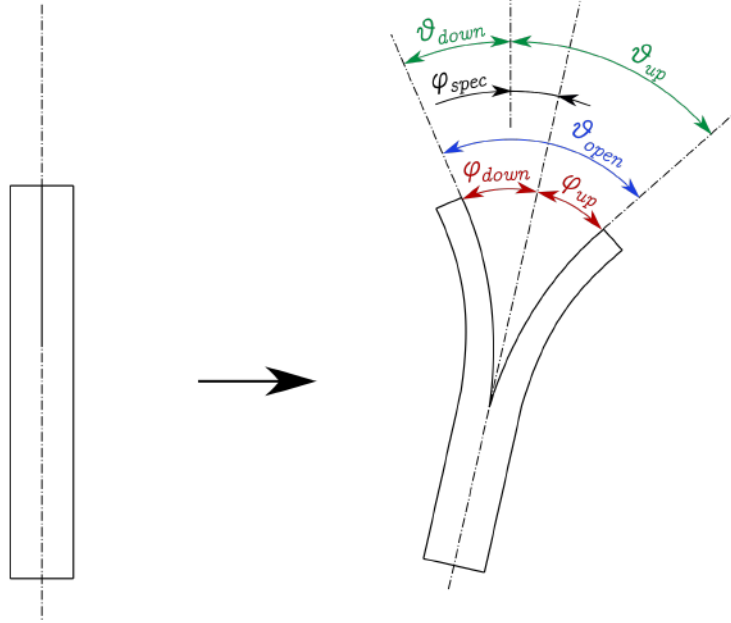

Figure 8.12: Definition of the different rotation angles characterising the DCB specimens during the test.

to Fig. 8.12, different angular quantities may be defined:

- the arm deflections φ_{down} or φ_{up} of the lower and upper arms (according to the bottom-up definition of the stacking sequences in Section 8.3), respectively;

- the overall opening angle of the specimen θ_{open}

- the rotation of the specimen midplane φ_{spec};

- the load points rotations θ_{down} and θ_{up}.

Between these quantities some relationships exist. The opening angle θ_{open} may be obtained both as the sum of the arms deflection angles and the sum of the load point rotations:

$$\theta_{open} = \varphi_{up} + \varphi_{down} = \theta_{up} + \theta_{down}. \tag{8.2}$$

Assuming a positive value of φ_{spec} if the rotation of the specimen is toward its upper arm, the arms deflections are linked to the load points rotations by:

$$\theta_{up} = \varphi_{up} + \varphi_{spec}, \tag{8.3}$$
$$\theta_{down} = \varphi_{down} - \varphi_{spec}. \tag{8.4}$$

If the specimen is symmetric from an elastic point of view, then it is expected that:

$$\varphi_{spec} = 0\,, \tag{8.5}$$

$$\varphi_{up} = \varphi_{down} = \theta_{down} = \theta_{up} = \theta\,, \tag{8.6}$$

$$\theta_{open} = 2\theta\,. \tag{8.7}$$

In this study, both UD and FUMD specimens are theoretically expected to verify in first approximation the relationships in Eqs. (8.5)-(8.7). Hence, the load points rotations θ_{down} and θ_{up}, were measured by means of inclinometers throughout the whole test and for all specimens. To evaluate the behaviour of FUMD delamination specimens and to compare it to that of UD ones, the quantity $\Delta\bar{\theta}$ was defined as follows:

$$\Delta\bar{\theta} = \frac{\theta_{up} - \theta_{down}}{\theta_{up} + \theta_{down}} * 100\,. \tag{8.8}$$

This quantity represents the difference of the load point rotations as a percentage of the total opening angle of the specimen. While ideally $\Delta\bar{\theta}$ should be zero, it is expected, even for UD specimens, that small deviations occur, due to experimental uncertainties (small thickness variations of the arms, specimens placement at the beginning of the test, etc.). Four representative points in the load displacement curves have been chosen to evaluate $\Delta\bar{\theta}$:

1. Half of Maximum Load Point (HMLP);

2. Maximum Load Point (MLP);

3. Reduced Stiffness Point (RSP): the point, during delamination propagation, at which the specimen stiffness is reduced by 50%;
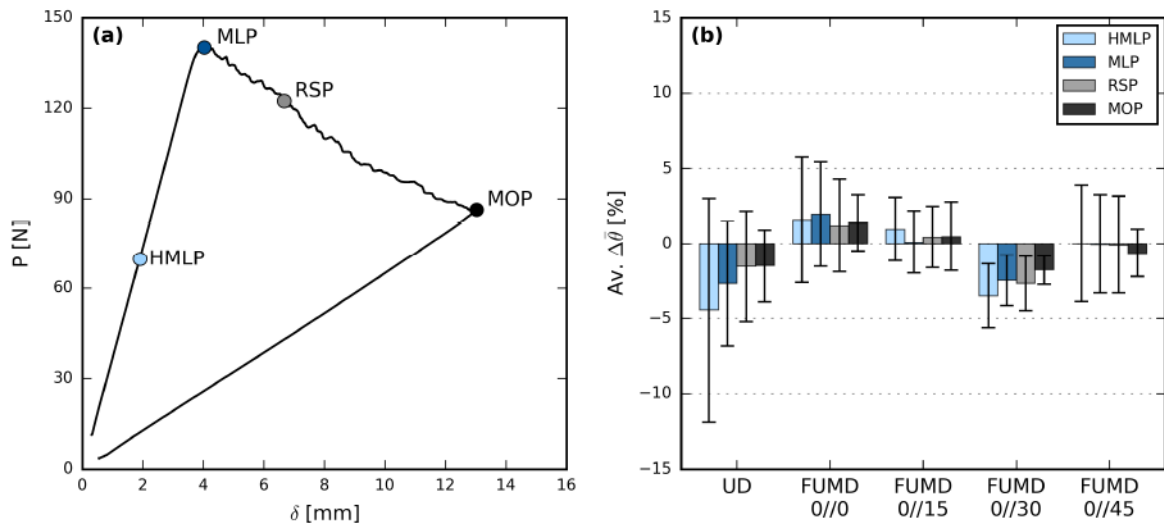
4. Maximum Opening Point (MOP).

Figure 8.13: Illustration of experimental points used to evaluate $\Delta\bar{\theta}$ (a) and mean values and standard deviation obtained for each set of specimens (b).

For illustration purposes, such points are shown in Fig. 8.13 (a), on the force-displacement curve of one of the specimens. The average values of $\Delta\bar{\theta}$ for all sets of specimens have been computed and are shown in Fig. 8.13, along with their standard deviation.

A first general observation is that average values of $\Delta\bar{\theta}$ are very small for all specimen types, and never exceed 5% of the total specimen opening angles.

Considering UD specimens, they show non-null average values of $\Delta\bar{\theta}$. However, the scatter interval defined by the standard deviation is wider than the average value and thus contain the zero. This means that, in general, there was no one arm (upper or lower) that consistently rotated more than the other one. Especially considering the symmetry of UD specimens, the small deviations observed are likely to be due to random variability of manufacturing and test conditions.

Most importantly, average values obtained with FUMD specimens are comparable to, or even lower than, those of UD specimens. Additionally, the standard deviation once again oscillates around zero, confirming the generally symmetric behaviour of the specimens. FUMD 0//30 specimens represent an exception in that their $\Delta\bar{\theta}$ values tend toward the negative side (greater rotation of the lower arm) and their standard deviation do not cross the zero. However, such values remain extremely small and even included within the scatter band of UD specimens.

While further studies using more advanced techniques (such as Digital Image Correlation) could give a more detailed and complete picture, these observations seem to corroborate the suitability of FUMD sequences for delamination testing of MD specimens.

8.7.6 Delamination front analysis via ultrasonic C-scans

When performing delamination tests, one of the most important feature of the standard UD specimen is its capability to give a propagation front as straight and symmetrical as possible. A symmetric and straight delamination front is the consequence of a correct mechanical behaviour of the specimen throughout the test. While this is extremely important in order to perform good tests and correctly reduce data, it also becomes very difficult to be obtained when using MD specimens. It was shown in Chapter 7, by finite elements analysis, that FUMD stacking sequences are the ones that approach the most closely the correct ERR modal partition obtainable with standard UD specimens. The goal of this study was therefore to verify if also delamination fronts obtained with FUMD specimens are satisfactorily similar to those of UD specimens, since such similarity is a first element of experimental validation of the proposed concept.

Therefore, after the tests, ultrasonic C-scans of the specimens were performed in order to observe the delamination fronts. Fig. 8.14 reports representative C-scans for all specimen types. At a first glance, the fronts obtained with FUMD sequences appear quite symmetric and with a mild curvature, comparable with those from UD specimens. In order to compare them in a more rigorous and quantitative way, C-scan images have been post-processed up to the attainment of a one-pixel-thick delamination front. Firstly, predominantly blue pixels were enhanced and predominantly red ones were attenuated. Then artefacts and defects in the images were cleaned away. Eventually, the saturation channel of the image (as this was the technique providing the best results) was used to obtain a binary image, from which pixels corresponding to the delamination front were found. The steps of the procedure are illustrated in Fig. 8.15, for one of the FUMD 0//30 specimens.
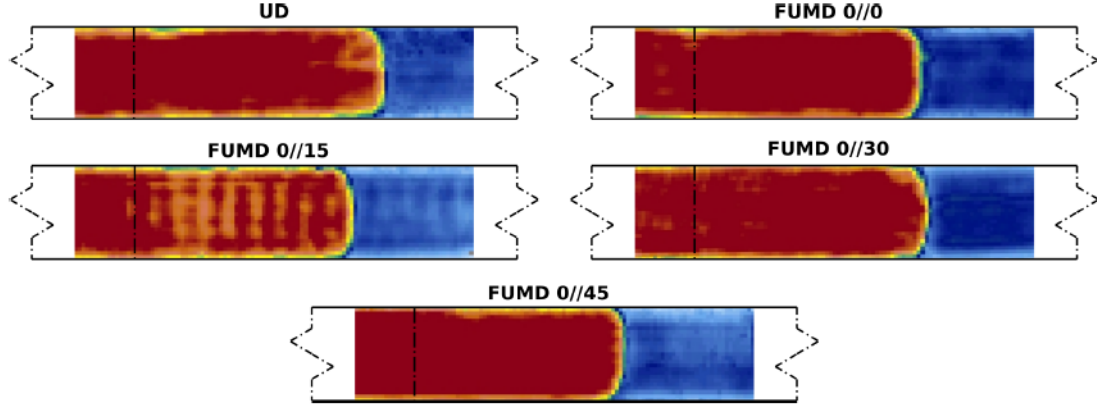
Figure 8.14: Representative C-scans for all sequences adopted. In this view, delamination propagated from the left to the right. The dashed line superposed to the C-scan images is the location of the insert tip.
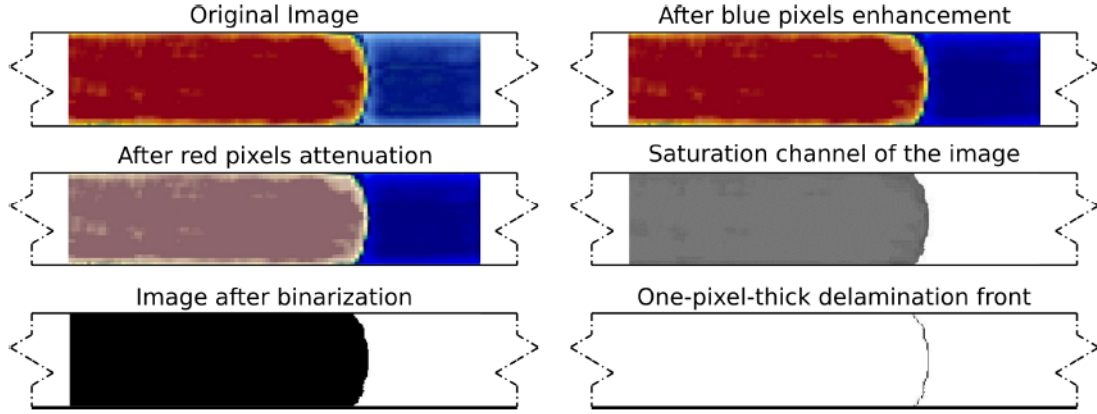

Figure 8.15: Example of C-scan images processing steps, from the original image to the one-pixel-thick delamination front.

To quantitatively evaluate the curvature and the asymmetry of the delamination front, two quantities were defined. The first one, β, is defined as:

$$\beta = \frac{|x^{max} - x^{av}|}{b} , \tag{8.9}$$

and gives an estimation of the curvature of the delamination front. In Eq (8.9), $|x^{max} - x^{av}|$ is the distance between the point of farthest propagation and the average line of the delamination front (note that this quantity does not depend on the origin chosen to measure x), and b is the specimen width. Parameter β would be 0 only for a perfectly straight delamination front, while it would be 1 if the tip of the delamination front lies one specimen width ahead of the average line of the front itself. The second parameter, γ, is defined as follows:

$$\gamma = \frac{\sum\limits_{y} |x^{(y)} - x^{(-y)}|}{b * n_y} , \tag{8.10}$$

and quantifies the asymmetry of the delamination front. In Eq. (8.10), $|x^{(y)} - x^{(-y)}|$ is the difference in propagation length between two specular points(with respect to the specimen longitudinal symmetry plane) of the delamination front; such quantity is summed for all couples of corresponding pixels and then normalized by the number of couples (n_y) and

the specimen width. Hence, γ represents an average measure of propagation asymmetry of specular front pixels relative to the specimen width. This parameter would be equal to 0 only if the delamination front is perfectly symmetric, while it would be 1 if, on average, each couple of corresponding front pixels has a difference in propagation length equal to the specimen width. Both β and γ have been evaluated for all specimens. The average and standard deviation of the results over each set of specimens are reported in Fig. 8.16.
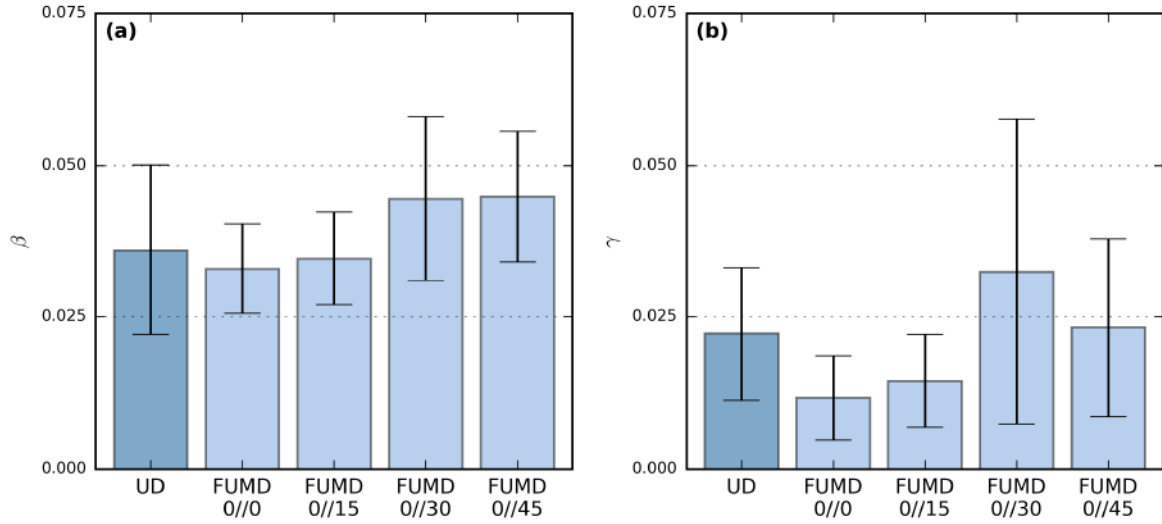

Figure 8.16: Mean values and standard deviation for the parameters β (a), quantifying delamination front curvature and γ (b), quantifying delamination front asymmetry

Values of β found, Fig. 8.16 (a), are extremely small, confirming that fairly straight fronts have been obtained. It seems that a weak correlation between delamination front curvature and interface plies mismatch angle may exist. However, all mean values obtained with FUMD sequences falls within the experimental scatter band of the UD one. This confirms that curvature of delamination fronts obtained with FUMD specimens is comparable to that obtained with UD ones.

On the other hand, it appears that no correlation exists between delamination front asymmetry and the interface plies mismatch angle, Fig. 8.16 (b), which means that FUMD specimens are able to avoid this undesired effect. While FUMD 0//30 specimens are those showing the greatest asymmetry and the widest scatter, UD specimens are not those yielding the lowest values of γ. Such results may indicate that the small asymmetry measured is not directly related to the stacking sequences, but rather it is due to some variability introduced by the manufacturing or by the test setup.

To sum up, these results confirm the good behaviour of FUMD specimens in term of delamination front shape.

8.8 Concluding remarks

In this chapter, the experimental study performed to assess the suitability of FUMD specimens for delamination testing was presented. Five different types of FUMD specimens, having different delamination interfaces, were designed. A glass/epoxy UD-fabric

material was used to reduce the likelihood of delamination jump occurring. The specimens were tested under pure mode I delamination, according to standard procedures. For comparison purposes, also standard UD specimens of the same material were tested.

Four out of five FUMD specimen types did not experience any delamination jump, and the propagation was smooth in the initial delamination plane, as confirmed by C-scan images and fracture surfaces observation. This confirms previous observations that UD-fabric materials may reduce the likelihood of delamination migration.

The behaviour of the material system in terms of mode I interlaminar fracture toughness G_{Ic} was investigated, both for initiation and propagation. The NL and 5%/MAX initiation values of G_{Ic} obtained for delamination from the insert were found to be independent of the delamination interface. This was however attributed to the effect of the insert film, which was thicker than what recommended in standards. The VIS initiation values of G_{Ic} from the insert showed an increasing trend with increasing mismatch angle of the plies embedding the delamination plane. This trend was found again, more evidently, for NL, VIS and 5%/MAX initiation values of G_{Ic} obtained from the mode I precrack. No effect of the global stiffness (and stacking sequence) of the specimens were observed, provided that the delamination interface is the same. No fibre-bridging was observed. The R-curves of the specimens seem to be influenced by two aspects. Firstly, transverse yarns debonding occurred at the edges of the specimens; the entity of this phenomenon changed with the orientations of plies embedding the delamination plane. Secondly, the delamination in this case consisted in the separation at the fibre-matrix interface, and not in a cohesive failure of the resin interlayer. The ply orientation seems to have an effect on the resulting propagation values of G_{Ic}.

Eventually, the tests performed allowed to obtain some preliminary, but promising, indications of the appropriate mechanical behaviour of FUMD specimens. Rotations of the arms of the specimens at different opening and load conditions during the tests were evaluated. Results from FUMD specimens were extremely good when compared to those from UD ones. This confirmed that no undesired rotations, caused by mechanical couplings or by the releasing of thermal residual stresses, happened. Also, the shape of the delamination fronts at the end of the tests was observed by means of ultrasonic C-scans. The resulting images were processed in order to quantitatively evaluate curvature and symmetry. Once again, results obtained with FUMD specimens were comparatively good with respect to UD ones. This again strengthen the idea that FUMD specimens may be a viable solutions to obtain optimal delamination testing conditions for MD laminates and to evaluate their interlaminar fracture toughness.

Summary, conclusions and perspectives

Summary and conclusions

Elastic couplings and undesired thermal effects cause important difficulties in interlaminar fracture toughness testing of MD laminates. In this study, a solution to these problems is proposed. Thanks to this novel class of stacking sequences, it is possible to obtain MD delamination specimens that can be used to test any desired delamination interface, while concurrently having a thermoelastic behaviour that replicates that of UD specimens: they are completely free of elastic couplings and do not develop thermally-induced shearing deformations and curvatures. The process that led to the attainment of FUMD layups and the preliminary studies performed to assess their performances are summarized in the following, accompanied by relevant conclusions.

Adoption and attainment of QT solutions

In order to exploit QT solutions for the design of FUMD layups an algorithm for the creation of a complete database of QT solutions was conceived and implemented.

Despite the fact that QT solutions have demonstrated a great potential in laminate design problems, only few suggestions on how to implement an algorithm for their search were available in the literature [68, 168]. The algorithm conception and implementation presented in this study, while not being the only one possible, should be of help to all those who are willing to obtain a complete database of QT solutions.

By employing the algorithm developed in this study, two important results were obtained. Firstly, for some given numbers of plies and of orientations groups of the sequences, a higher number of QT solutions were found than in previous studies [62, 68, 168], which is arguably good news. Secondly, while finding QT solutions becomes more difficult as the total number of plies increases, in this study it was possible to find longer sequences than in the past.

Superposition rules for QT solutions

After the creation of a rich database of QT solutions, superposition rules were derived, within the framework of CLPT, as analytical closed form solutions.

While it was observed that, in general, the superposition of two QT sequences does not yield a new QT one [168], the rules derived in this study give the conditions (in terms of total number of plies and number of plies per orientation groups) that an arbitrary number of initial QT solutions need to satisfy in order for their superposition to be a QT solution as well.

While the primary goal for the development of the superposition rules was the design of FUMD layups, they have been derived to obtain all possible types of quasi-triviality starting from the superposition of QT solutions of any type. Consequently, thanks to their generality, they may find application in any laminate design problems (especially to design thick laminates). Moreover, when only few sequences have to be superposed, the rules reduce to very simple expressions. From a practical point of view, they allow to design stacking sequences with a tight control over the properties of some sub-sequences to be superposed, but also over the properties of the resulting sequence. In addition, they allow to generate QT solutions of any desired length, thus overcoming the limitations due to computational costs that arise when performing an algorithmic search.

FUMD layups design

Thanks to the adoption of QT solutions and of their superposition rules, FUMD layups have been designed. These layups allow to obtain MD delamination specimens completely free from elastic couplings and that can avoid undesired thermal effects. Moreover, the plies embedding the delamination plane may have any desired orientation.

Recently, QT solutions had been used by different authors in order to design MD delamination specimens [53, 158, 159, 160, 161]. However, in these studies, classic laminate design techniques (e.g. symmetry of the whole laminate, use of the Werren and Norris rule, etc.) were adopted, so that only a limited number of sequences and/or orientations could be used, and only some types of interfaces could be obtained.

Instead, the design process proposed in this study gives a more general framework, wherein more QT solutions and orientations may be chosen with a greater freedom. As a matter of fact, all the cited approaches can be shown to be particular cases of the strategy derived here.

Hence, FUMD layups combine for the first time optimal thermoelastic properties and generality in terms of delamination interface. For this reason, they may represent ideal candidates for a standardisation of interlaminar fracture testing of MD laminates.

FUMD layups numerical assessment

In order to assess the effectiveness of FUMD layups, one FUMD sequence was designed to be compared to other ones taken from relevant literature. All sequences were selected to have a typical 0°//45° delamination interface and a similar number of plies.

It was demonstrated that the FUMD layup was the only one yielding a thermoelastic behaviour qualitatively similar to that of the UD one. By means of FE simulations of a mode I loading condition with DCB specimen, ERR distributions and modal partitions were assessed using VCCT; the FUMD layup was the one leading to the smallest parasite modal contribution. These results gave a first confirmation of how FUMD stacks could possibly be the best choice for delamination testing of MD laminates.

It is noteworthy that a revised VCCT was required to obtain a physically consistent ERR modal partition for mixed mode condition.

Experimental activity

Eventually, an experimental campaign using FUMD delamination specimens was performed. Five different FUMD layups were designed to fabricate DCB specimens having

different delamination interfaces. A glass/epoxy UD-fabric material was used to reduce the likelihood of delamination jump occurring. The specimens were tested under pure mode I, according to standard procedures. For comparison purposes, also standard UD specimens of the same material were tested. Thanks to this study, two main tasks were accomplished.

In the first place, some preliminary experimental evidences that could confirm the good mechanical behaviour of FUMD delamination specimens were collected. In particular, rotations of the arms of the specimens at different opening and load conditions during the tests were evaluated. Results from FUMD specimens were extremely good when compared to those from UD ones. This confirmed that no undesired rotations, caused by mechanical couplings or by the releasing of thermal residual stresses, happened. Then, the shape of the delamination fronts at the end of the tests was observed by means of ultrasonic C-scans. The resulting images were processed in order to quantitatively evaluate curvature and symmetry. Once again, results obtained with FUMD specimens were comparatively good with respect to UD ones.

Secondly, the study performed allowed to investigate, in the optimal conditions given by the use of FUMD specimens, different aspects of interlaminar fracture in MD interfaces, at least for the material considered.

The initiation values of G_{Ic} obtained from the mode I precrack showed an increasing trend as the mismatch angle of the plies embedding the delamination plane grows. On the other hand, sequences with the same delamination interface (namely UD specimens and FUMD specimens having 0°//0° delamination interface), but different global stiffness yielded almost undistinguishable values of G_{Ic}. This leads to the conclusion that, for a fixed interface (and of course in the same conditions of elastic uncoupling and absence of thermal effects), the layup and the global stiffness of the specimen have a negligible effect on interlaminar fracture toughness.

While no fibre-bridging was observed during the tests, the R-curves obtained were influenced by two aspects:

- transverse yarns debonding occurring at the edges of the specimens. The importance of this phenomenon increased with growing mismatch angle of the plies at the delamination interface. The occurrence and the development of this phenomenon likely led to the different initial rise in fracture toughness for different specimen types;

- the fracture mechanism at the interface. Delamination in this study consisted mainly in a separation at the fibre-matrix interface, and not in a cohesive failure of the resin interlayer. Ply orientations at the interface seem to have an effect on how and where (upper ply, lower ply or both) this happens. This, in turn, seems to influence the resulting propagation values of G_{Ic}.

To conclude, the experimental study has shown how useful FUMD layups may be in designing optimal delamination specimen to characterise interlaminar fracture. In addition, it has been confirmed that, after removing the bias of elastic couplings and thermal effects, ply orientations at the delamination interface may have an effect on interlaminar fracture toughness. The capability to quantify such effects is of strategic importance for structural design.

Perspectives

The results obtained in this study open many possibilities for further research activities, in different directions.

QT solutions

Despite the fact that QT solutions were only a tool for the scope of this study, a consistent portion of the work dealt with them. Of course, the effort made in this regards proved to be worth, and additionally it opened on some important developments that may be pursued.

Firstly, while the algorithm developed in this study already represented a significant step forward with respect to the previous state of the art, further improvements regarding both its conceptual organisation and the coding implementation are possible. Such adjustment would lead to obtain even better results, in terms of the length of QT solutions that may be reached. This would be useful for those laminate design problems in which high number of plies are required. A rather important field of application could be in the design of thin-ply laminates.

On the other hand, longer QT solutions may be obtained also exploiting the superposition rules, without any upper limit on the total number of plies. However this raises some very interesting questions: how many QT solutions, out of all those existing, may be found by superposition? Do those solutions represent a specific subset with some specific properties? Do the remaining ones have some specific properties of their own?

Interlaminar fracture testing

Some of the most interesting perspectives opened by this study concern interlaminar fracture testing of MD laminates. An ambitious long term goal would be to thoroughly assess the possibility of extending the scope of standard interlaminar fracture tests to FUMD layups, in order to allow the characterisation of non-standard delamination interfaces. Of course, much work is needed to achieve such a goal.

Future activities should focus on two main aspects: the solution of problems that still remain open and the application of FUMD layups to investigate different aspects of interlaminar fracture in MD laminates. These two activities are in fact strictly interrelated. The single most important remaining issue is that of additional damage mechanisms occurring during tests. On the other hand, FUMD layups have solved the problems of elastic couplings and undesired thermal effects in MD delamination specimens. Hence, they offer for the first time the possibility to investigate the appearance of additional damage mechanisms, as well as other aspects of interest in interlaminar fracture of MD laminates, isolating this issue from those of elastic couplings and thermal effects. Furthermore, they offer a variety of stacking sequences, plies orientations and delamination interfaces.

Aspects to be investigated exploiting FUMD layups may be synthesized as follows:

- **Loading mode.** In the present work, only mode I delamination was considered. An obvious step to be taken is to adopt FUMD layups to perform studies also for

mode II and mixed mode I/II conditions. This may be done using standard test methods, such as ENF and MMB tests, or other ones. In particular, the concept of FUMD layups may be extended, with appropriate modifications, to test methods making use of specimens with asymmetric arms, such as the Asymmetric Double Cantilever Beam (ADCB) test;

- **Delamination interface.** FUMD layups offer the possibility to obtain specimens having any desired orientation of plies embedding the delamination plane. In this study only few interfaces were considered. On the other hand, future studies should involve more interface types ($0//\theta$, $\theta//\theta$, $\theta//-\theta$, $\theta_1//\theta_2$) and orientations. Both the effect of the type of interface and of the orientations adopted be investigated;

- **Stacking sequence.** When evaluating interlaminar fracture toughness of MD interfaces, the orientation of the plies embedding delamination is expected to be the primary responsible for the results observed. However, it is important to find out if secondary effects exist. In this context, stacking sequence might play a role. Two aspects have been mentioned in the literature that require further attention: first, the effect of the global stiffness of the specimen; second, the effect of sub-adjacent plies (i.e. plies that are close to those embedding the delamination plane). It is to be understood if they have an impact on the behaviour of the specimen (appearance of additional damage) and on the results in terms of interlaminar fracture toughness. FUMD layups, thanks to the wide design space that they offer, seem the ideal tool to investigate these issues;

- **Material.** In this study, for the experimental activity performed, a UD-fabric material was used. However, the concept of FUMD layups, thanks to its generality, may be applied to other types of composites. Furthermore, there is an interest in doing so, since different materials are expected to show different behaviours and different issues. In woven fabrics, especially balanced ones, delamination migration is less likely to occur, but the complex micro-structure of the interlaminar layer brings complex delamination behaviours that need investigation. On the other hand, UD tape materials may be more susceptible to delamination jump, but research on this aspect is still ongoing.

From a methodological point of view, both numerical and experimental activities may be foreseen, possibly making use of a multi-scale approach.

On the numerical side, one first effort should be devoted to develop models able to reproduce the behaviour observed in the experimental study conducted in this work. Besides, another important step would be to make use of existing models with predictive capabilities with respect to the appearance of damage, both at the micro and the meso scale, to analyse the widest possible pool of FUMD sequences. Thus, candidate layups, that are less likely to give rise to damage other than delamination, may be identified and used to plan further experimental activities.

Such experiments should deal with the different aspects mentioned before. Results from them should highlight the most important variables in play and their role with respect to the the appearance of additional damage mechanisms. They should be used to create a dialogue between experiments and models, and to provide a feedback to correct and refine the actual predictive capabilities of the models adopted.

The ultimate goal of this process is to fully understand how and when damage mechanisms develop in MD specimens, so that they can be accurately modelled. If this objective

is met, it would become possible to predict under which circumstances (delamination interface, stacking sequence, material, specimen geometry, ect.) it is possible to avoid them and thus to obtain optimal conditions to consistently characterise the toughness of MD interfaces.

Bibliography

[1] A. B. Strong, *Fundamentals of composites manufacturing: materials, methods and applications*. Society of Manufacturing Engineers, 2008.

[2] S. S. Pendhari, T. Kant, and Y. M. Desai, "Application of polymer composites in civil construction: A general review," *Composite Structures*, vol. 84, no. 2, pp. 114 – 124, 2008.

[3] J. Graham-Jones and J. Summerscales, *Marine applications of advanced fibre-reinforced composites*. Woodhead Publishing, 2015.

[4] P. Irving and C. Soutis, *Polymer Composites in the Aerospace Industry*. Woodhead Publishing series in composites science and engineering, Elsevier Science, 2014.

[5] R. B. Deo, J. H. Starnes Jr, and R. C. Holzwarth, "Low-cost composite materials and structures for aircraft applications," Conference Paper 20030097981, NASA Langley Research Center, Hampton, VA, United States, March 2003.

[6] C. Soutis, "Fibre reinforced composites in aircraft construction," *Progress in Aerospace Sciences*, vol. 41, no. 2, pp. 143 – 151, 2005.

[7] S. Dutton, D. Kelly, and A. Baker, *Composite materials for aircraft structures*. American Institute of Aeronautics and Astronautics, 2004.

[8] E. J. Barbero, *Introduction to Composite Materials Design*. CRC press, 2017.

[9] M. Hyer and H. Lee, "The use of curvilinear fiber format to improve buckling resistance of composite plates with central circular holes," *Composite Structures*, vol. 18, no. 3, pp. 239 – 261, 1991.

[10] Z. Gürdal, B. Tatting, and C. Wu, "Variable stiffness composite panels: Effects of stiffness variation on the in-plane and buckling response," *Composites Part A: Applied Science and Manufacturing*, vol. 39, no. 5, pp. 911 – 922, 2008.

[11] S. Nagendra, S. Kodiyalam, J. Davis, and V. Parthasarathy, "Optimization of tow fiber paths for composite design," in *36th Structures, Structural Dynamics and Materials Conference*, 1995.

[12] M. A. Nik, K. Fayazbakhsh, D. Pasini, and L. Lessard, "Surrogate-based multi-objective optimization of a composite laminate with curvilinear fibers," *Composite Structures*, vol. 94, no. 8, pp. 2306 – 2313.

[13] M. A. Nik, K. Fayazbakhsh, D. Pasini, and L. Lessard, "Optimization of variable stiffness composites with embedded defects induced by automated fiber placement," *Composite Structures*, vol. 107, pp. 160–166, 2014.

[14] M. Montemurro and A. Catapano, "On the effective integration of manufacturability constraints within the multi-scale methodology for designing variable angle-tow laminates," *Composite Structures*, vol. 161, pp. 145 – 159, 2017.

[15] M. Montemurro and A. Catapano, "A general b-spline surfaces theoretical framework for optimisation of variable angle-tow laminates," *Composite Structures*, vol. 209, pp. 561 – 578, 2019.

[16] A. Catapano, M. Montemurro, J.-A. Balcou, and E. Panettieri, "Rapid prototyping of variable angle-tow composites," *Aerotecnica Missili & Spazio*, Aug 2019.

[17] M. Chiachio, J. Chiachio, and G. Rus, "Reliability in composites – a selective review and survey of current development," *Composites Part B: Engineering*, vol. 43, no. 3, pp. 902 – 913, 2012.

[18] T. Jollivet, C. Peyrac, and F. Lefebvre, "Damage of composite materials," *Procedia Engineering*, vol. 66, pp. 746 – 758, 2013. Fatigue Design 2013, International Conference Proceedings.

[19] M. Naebe, M. M. Abolhasani, H. Khayyam, A. Amini, and B. Fox, "Crack damage in polymers and composites: A review," *Polymer Reviews*, vol. 56, no. 1, pp. 31–69, 2016.

[20] R. Talreja, "Physical modelling of failure in composites," *Philosophical Transactions of the Royal Society A: Mathematical, Physical and Engineering Sciences*, vol. 374, no. 2071, 2016.

[21] A. De Luca and F. Caputo, "A review on analytical failure criteria for composite materials," *AIMS Materials Science*, vol. 4, no. 5, pp. 1165–1185, 2017.

[22] E. Correa, F. París, and V. Mantič, "Fiber–matrix debonding in composite materials: Transverse loading," in *Modeling Damage, Fatigue and Failure of Composite Materials* (R. Talreja and J. Varna, eds.), Woodhead Publishing Series in Composites Science and Engineering, pp. 97 – 116, Woodhead Publishing, 2016.

[23] E. Graciani, V. Mantič, F. París, and J. Varna, "Fiber–matrix debonding in composite materials: Axial loading," in *Modeling Damage, Fatigue and Failure of Composite Materials* (R. Talreja and J. Varna, eds.), Woodhead Publishing Series in Composites Science and Engineering, pp. 117 – 141, Woodhead Publishing, 2016.

[24] K. Gamstedt and S. I. S. Andersen, "Fatigue degradation and failure of rotating composite structures-materials characterisation and underlying mechanisms," Risoe-R 1261(EN), Risø National Laboratory, Roskilde, Denmark, 2001.

[25] S. Abrate, "Matrix cracking in laminated composites: A review," *Composites Engineering*, vol. 1, no. 6, pp. 337 – 353, 1991.

[26] M. Lafarie-Frenot, C. Hénaff-Gardin, and D. Gamby, "Matrix cracking induced by cyclic ply stresses in composite laminates," *Composites Science and Technology*, vol. 61, no. 15, pp. 2327 – 2336, 2001.

[27] O. Castro, P. A. Carraro, L. Maragoni, and M. Quaresimin, "Fatigue damage evolution in unidirectional glass/epoxy composites under a cyclic load," *Polymer Testing*, vol. 74, pp. 216 – 224, 2019.

[28] C. Nageswaran, C. R. Bird, and R. Takahashi, "Phased array scanning of artificial and impact damage in carbon fibre reinforced plastic (CFRP)," *Insight-Non-Destructive Testing and Condition Monitoring*, vol. 48, no. 3, pp. 155–159, 2006.

[29] X. Fan, Q. Sun, and M. Kikuchi, "Review of damage tolerant analysis of laminated composites," *Journal of Solid Mechanics*, vol. 2, 2010.

[30] G. Newaz, "Damage tolerance analysis for advanced composites," *Wiley Encyclopedia of Composites*, pp. 1–9, 2011.

[31] T. D. Dang and S. R. Hallett, "A numerical study on impact and compression after impact behaviour of variable angle tow laminates," *Composite Structures*, vol. 96, pp. 194 – 206, 2013.

[32] C. S. Lopes, C. González, O. Falcó, F. Naya, J. LLorca, and B. Tijs, "Multiscale virtual testing: the roadmap to efficient design of composites for damage resistance and tolerance," *CEAS Aeronautical Journal*, vol. 7, pp. 607–619, Dec 2016.

[33] S. Sridharan, *Delamination behaviour of composites*. Elsevier, 2008.

[34] E. Greenhalgh, M. Hiley, and C. Meeks, "Delamination-dominated failures in polymer composites," in *Failure Analysis and Fractography of Polymer Composites* (E. S. Greenhalgh, ed.), Woodhead Publishing Series in Composites Science and Engineering, pp. 164 – 237, Woodhead Publishing, 2009.

[35] M. R. Wisnom, "The role of delamination in failure of fibre-reinforced composites," *Philosophical Transactions of the Royal Society A: Mathematical, Physical and Engineering Sciences*, vol. 370, no. 1965, pp. 1850–1870, 2012.

[36] L. A. Carlsson, D. F. Adams, and R. B. Pipes, "Characterization of delamination failure," in *Experimental characterization of advanced composite materials*, pp. 249 – 271, CRC Press, 2014.

[37] F. van der Meer, "A level set model for delamination in composite materials," in *Numerical Modelling of Failure in Advanced Composite Materials* (P. P. Camanho and S. R. Hallett, eds.), Woodhead Publishing Series in Composites Science and Engineering, pp. 93 – 107, Woodhead Publishing, 2015.

[38] A. Tabiei and W. Zhang, "Composite Laminate Delamination Simulation and Experiment: A Review of Recent Development," *Applied Mechanics Reviews*, vol. 70, no. 3, 2018.

[39] R. Shrivastava and K. K. Singh, "Interlaminar fracture toughness characterization of laminated composites: a review," *Polymer Reviews*, pp. 1–52, 2019.

[40] S. Hallett and P. Harper, "Modelling delamination with cohesive interface elements," in *Numerical modelling of failure in advanced composite materials*, pp. 55–72, Elsevier, 2015.

[41] S. Abrate, *Impact on Composite Structures*. Cambridge University Press, 1998.

[42] J. E. Grady, *Fracture toughness testing of polymer matrix composites*, vol. 3199. National Aeronautics and Space Administration, Office of Management, 1992.

[43] T. K. O'Brien, "Interlaminar fracture toughness: the long and winding road to standardization," *Composites Part B: Engineering*, vol. 29, no. 1, pp. 57 – 62, 1998.

[44] I. S. Raju and T. K. O'Brien, "Fracture mechanics concepts, stress fields, strain energy release rates, delamination initiation and growth criteria," in *Delamination Behaviour of Composites* (S. Sridharan, ed.), Woodhead Publishing Series in Composites Science and Engineering, pp. 3 – 27, Woodhead Publishing, 2008.

[45] T. Anderson, "Fracture testing of nonmetals," in *Fracture Mechanics: Fundamentals and Applications*, Woodhead Publishing Series in Composites Science and Engineering, pp. 369 – 399, CRC Press, 2017.

[46] G. R. Irwin, *Fracture*, pp. 551–590. Berlin, Heidelberg: Springer Berlin Heidelberg, 1958.

[47] G. R. Irwin, "Onset of fast crack propagation in high strength steel and aluminum alloys," Technical Report NRL-4763; PB-121224, Naval Research Lab, Washington D.C., May 1956.

[48] A. Brunner, B. Blackman, and P. Davies, "A status report on delamination resistance testing of polymer–matrix composites," *Engineering Fracture Mechanics*, vol. 75, no. 9, pp. 2779 – 2794, 2008.

[49] "ASTM D5528-13, Standard Test Method for Mode I Interlaminar Fracture Toughness of Unidirectional Fiber-Reinforced Polymer Matrix Composites," Standard, ASTM International, West Conshohocken, PA, 2013.

[50] "ASTM D7905/D7905M-14, Standard Test Method for Determination of the Mode II Interlaminar Fracture Toughness of Unidirectional Fiber-Reinforced Polymer Matrix Composites," Standard, ASTM International, West Conshohocken, PA, 2014.

[51] "ASTM D6671 / D6671M-19, Standard Test Method for Mixed Mode I-Mode II Interlaminar Fracture Toughness of Unidirectional Fiber Reinforced Polymer Matrix Composites," Standard, ASTM International, West Conshohocken, PA, 2019.

[52] P. Prombut, L. Michel, F. Lachaud, and J. Barrau, "Delamination of multidirectional composite laminates at $0/\theta$ ply interfaces," *Engineering Fracture Mechanics*, vol. 73, no. 16, pp. 2427 – 2442, 2006.

[53] X. Gong, A. Hurez, and G. Verchery, "On the determination of delamination toughness by using multidirectional DCB specimens," *Polymer Testing*, vol. 29, no. 6, pp. 658 – 666, 2010.

[54] J. Andersons and M. König, "Dependence of fracture toughness of composite laminates on interface ply orientations and delamination growth direction," *Composites Science and Technology*, vol. 64, no. 13-14, pp. 2139–2152, 2004.

[55] M. D. Moura, "Interaction of matrix cracking and delamination," in *Delamination Behaviour of Composites* (S. Sridharan, ed.), Woodhead Publishing Series in Composites Science and Engineering, pp. 327 – 343, Woodhead Publishing, 2008.

[56] Y. Gong, B. Zhang, and S. R. Hallett, "Delamination migration in multidirectional composite laminates under mode I quasi-static and fatigue loading," *Composite Structures*, vol. 189, pp. 160 – 176, 2018.

[57] S. Samborski, "Numerical analysis of the DCB test configuration applicability to mechanically coupled Fiber Reinforced Laminated Composite beams," *Composite Structures*, vol. 152, no. Supplement C, pp. 477 – 487, 2016.

[58] S. Samborski, "Analysis of the end-notched flexure test configuration applicability for mechanically coupled fiber reinforced composite laminates," *Composite Structures*, vol. 163, pp. 342 – 349, 2017.

[59] J. Rzeczkowski, S. Samborski, and P. S. Valvo, "Effect of stiffness matrices terms on delamination front shape in laminates with elastic couplings," *Composite Structures*, p. 111547, 2019.

[60] J. D. Gracia, A. Boyano, A. Arrese, and F. Mujika, "Analysis of the DCB test of angle-ply laminates including residual stresses," *Theoretical and Applied Fracture Mechanics*, vol. 94, pp. 197 – 204, 2018.

[61] J. Reddy, *Mechanics of Laminated Composite Plates and Shells: Theory and Analysis, Second Edition*. CRC Press, 2003.

[62] P. Vannucci, *Anisotropic Elasticity*. Springer, Singapore, 2018.

[63] W. Voigt, *Lehrbuch der kristallphysik (mit ausschluss der kristalloptik)*. Leipzig, Berlin, B.G. Teubner, 1910.

[64] R. Schlebusch, "On Voigt and Kelvin matrix notations of second-order tensors," *Proceedings in Applied Mathematics and Mechanics*, vol. 19, no. 1, 2019.

[65] M. M. Mehrabadi and S. C. Cowin, "Eigentensors of linear anisotropic elastic materials," *The Quarterly Journal of Mechanics and Applied Mathematics*, vol. 44, no. 2, p. 331, 1991.

[66] F. Werren, C. Norris, *et al.*, "Mechanical properties of a laminate designed to be isotropic," Technical Report 1841, Forest Products Laboratory, Madison, Wisconsin, 1965.

[67] G. Caprino and I. C. Visconti, "A note on specially orthotropic laminates," *Journal of Composite Materials*, vol. 16, no. 5, pp. 395–399, 1982.

[68] P. Vannucci and G. Verchery, "A special class of uncoupled and quasi-homogeneous laminates," *Composites Science and Technology*, vol. 61, no. 10, pp. 1465 – 1473, 2001.

[69] E. Valot and P. Vannucci, "Some exact solutions for fully orthotropic laminates," *Composite Structures*, vol. 69, no. 2, pp. 157 – 166, 2005.

[70] P. Vannucci and G. Verchery, "A new method for generating fully isotropic laminates," *Composite Structures*, vol. 58, no. 1, pp. 75 – 82, 2002.

[71] E. S. Greenhalgh and M. J. Hiley, "Fractography of polymer composites : Current status and future issues," 2007.

[72] P. Davies, B. R. K. Blackman, and A. J. Brunner, "Standard test methods for delamination resistance of composite materials: Current status," *Applied Composite Materials*, vol. 5, pp. 345–364, Nov 1998.

[73] J. Hutchinson and Z. Suo, "Mixed mode cracking in layered materials," vol. 29 of *Advances in Applied Mechanics*, pp. 63 – 191, Elsevier, 1991.

[74] J. R. Reeder, "A bilinear failure criterion for mixed-mode delamination," in *Eleventh Volume: Composite Materials—Testing and Design*, ASTM International, 1993.

[75] M. Benzeggagh and M. Kenane, "Measurement of mixed-mode delamination fracture toughness of unidirectional glass/epoxy composites with mixed-mode bending apparatus," *Composites Science and Technology*, vol. 56, no. 4, pp. 439 – 449, 1996.

[76] T. K. O'Brien and R. H. Martin, "Round robin testing for mode I interlaminar fracture toughness of composite materials," *Journal of Composites, Technology and Research*, vol. 15, no. 4, pp. 269–281, 1993.

[77] P. Davies, H. Kausch, J. Williams, A. Kinloch, M. Charalambides, A. Pavan, D. Moore, R. Prediger, I. Robinson, N. Burgoyne, K. Friedrich, H. Wittich, C. Rebelo, A. T. Marques, F. Ramsteiner, B. Melve, M. Fischer, N. Roux, D. Martin, P. Czarnocki, D. Neville, I. Verpoest, B. Goffaux, R. Lee, K. Walls, N. Trigwell, I. Partridge, J. Jaussaud, S. Andersen, Y. Giraud, G. Hale, and G. McGrath, "Round-robin interlaminar fracture testing of carbon-fibre-reinforced epoxy and peek composites," *Composites Science and Technology*, vol. 43, no. 2, pp. 129 – 136, 1992.

[78] K. Tanaka, K. Kageyama, and M. Hojo, "Prestandardization study on mode II interlaminar fracture toughness test for CFRP in Japan," *Composites*, vol. 26, no. 4, pp. 257 – 267, 1995.

[79] M. Hojo, K. Kageyama, and K. Tanaka, "Prestandardization study on mode I interlaminar fracture toughness test for CFRP in Japan," *Composites*, vol. 26, no. 4, pp. 243–255, 1995.

[80] A. Brunner, "Experimental aspects of mode I and mode II fracture toughness testing of fibre-reinforced polymer-matrix composites," *Computer Methods in Applied Mechanics and Engineering*, vol. 185, no. 2, pp. 161 – 172, 2000.

[81] B. Blackman, A. Brunner, and J. Williams, "Mode II fracture testing of composites: a new look at an old problem," *Engineering Fracture Mechanics*, vol. 73, no. 16, pp. 2443 – 2455, 2006.

[82] S. Lee, "An Edge Crack Torsion Method for Mode III Delamination Fracture Testing," *Journal of Composites Technology & Research*, vol. 15, no. 3, pp. 193–201, 1993.

[83] M. W. Czabaj, B. D. Davidson, and J. G. Ratcliffe, "A modified edge crack torsion test for measurement of mode III fracture toughness of laminated tape composites," *NASA technical report*, 2016.

[84] C. Audd, B. D. Davidson, J. G. Ratcliffe, and M. W. Czabaj, "Reexamination of the edge crack torsion test for determining the mode III delamination toughness of laminated composites," *Engineering Fracture Mechanics*, vol. 215, pp. 138 – 150, 2019.

[85] T. Kalbermatten, R. Jäggi, P. Flüeler, H. Kausch, and P. Davies, "Microfocus radiography studies during mode I interlaminar fracture tests on composites," *Journal of Materials Science Letters*, vol. 11, no. 9, pp. 543–546, 1992.

[86] S. Hashemi, A. J. Kinloch, and J. G. Williams, "Corrections needed in double-cantilever beam tests for assessing the interlaminar failure of fibre-composites," *Journal of Materials Science Letters*, vol. 8, no. 2, pp. 125–129, 1989.

[87] J. P. Berry, "Determination of fracture surface energies by the cleavage technique," *Journal of Applied Physics*, vol. 34, no. 1, pp. 62–68, 1963.

[88] J. M. Whitney, C. E. Browning, and W. Hoogsteden, "A DCB test for characterizing mode I delamination of composite materials," *Journal of Reinforced Plastics and Chemicals*, vol. 1, pp. 3–14, 1982.

[89] D. Wilkins, J. Eisenmann, R. Camin, W. Margolis, and R. Benson, "Characterizing delamination growth in graphite-epoxy," in *Damage in Composite Materials: Basic Mechanisms, Accumulation, Tolerance, and Characterization*, ASTM International, 1982.

[90] F. X. de Charentenay, J. M. Harry, Y. J. Prel, and M. L. Benzeggagh, "Characterizing the effect of delamination defect by mode I delamination test," in *Effects of defects in Composite Materials*, ASTM International, 1984.

[91] W. Johnson and P. Mangalgiri, "Investigation of fiber bridging in double cantilever beam specimens," *Journal of Composites, Technology and Research*, vol. 9, no. 1, pp. 10–13, 1987.

[92] T. K. O'Brien, "Composite interlaminar shear fracture toughness, G_{IIc}: Shear measurement or sheer myth?," in *Composite Materials: Fatigue and Fracture: 7th Volume*, ASTM International, 1998.

[93] B. D. Davidson, "Standardization of the end-notched flexure test for mode II interlaminar fracture toughness determination of unidirectional laminated composites," *Journal of Testing and Evaluation*, vol. 43, no. 6, pp. 1540–1553, 2015.

[94] A. R. Shahani, R. Abolfathitabar, and H. Shooshtar, "On the validity of LEFM methods to investigate the fracture behavior of angle-ply laminates," *Composites Part B: Engineering*, vol. 160, pp. 249 – 253, 2019.

[95] M. Charalambides and J. Williams, "Mode I delamination of angle-ply epoxy/glass-fibre laminates exhibiting permanent deformation during fracture," *Composites Science and Technology*, vol. 50, no. 2, pp. 187 – 196, 1994.

[96] F. Ozdil, L. Carlsson, and P. Davies, "Beam analysis of angle-ply laminate end-notched flexure specimens," *Composites Science and Technology*, vol. 58, no. 12, pp. 1929 – 1938, 1998.

[97] F. Ozdil and L. Carlsson, "Beam analysis of angle-ply laminate DCB specimens," *Composites Science and Technology*, vol. 59, no. 2, pp. 305 – 315, 1999.

[98] F. Ozdil and L. Carlsson, "Beam analysis of angle-ply laminate mixed-mode bending specimens," *Composites Science and Technology*, vol. 59, no. 6, pp. 937 – 945, 1999.

[99] W. Jordan, "Changing the toughness of graphite fiber/resin based composites by changing their internal structure," *Composites Part B: Engineering*, vol. 31, no. 3, pp. 245 – 252, 2000.

[100] M. F. S. F. De Moura, A. B. Pereira, and A. B. De Morais, "Influence of intralaminar cracking on the apparent interlaminar mode I fracture toughness of cross-ply laminates," *Fatigue & Fracture of Engineering Materials & Structures*, vol. 27, no. 9, pp. 759–766, 2004.

[101] A. Brunner and B. Blackman, "Delamination fracture in cross-ply laminates: What can be learned from experiment?," vol. 32 of *European Structural Integrity Society*, pp. 433 – 444, Elsevier, 2003.

[102] H. Chai, "The characterization of mode I delamination failure in non-woven, multidirectional laminates," *Composites*, vol. 15, no. 4, pp. 277 – 290, 1984.

[103] I. Chou, I. Kimpara, K. Kageyama, and I. Ohsawa, "Mode I and mode II fracture toughness measured between differently oriented plies in graphite/epoxy composites," in *Composite Materials: Fatigue and Fracture: Fifth Volume*, ASTM International, 1995.

[104] J. Schön, T. Nyman, A. Blom, and H. Ansell, "A numerical and experimental investigation of delamination behaviour in the DCB specimen," *Composites Science and Technology*, vol. 60, no. 2, pp. 173 – 184, 2000.

[105] A. de Morais, M. de Moura, A. Marques, and P. de Castro, "Mode-I interlaminar fracture of carbon/epoxy cross-ply composites," *Composites Science and Technology*, vol. 62, no. 5, pp. 679 – 686, 2002.

[106] K. Dadej, J. Bieniaś, and B. Surowska, "Interlaminar cracking resistance of nonhomogeneous composite beams," *Composites Theory and Practice*, vol. 17, pp. 144–148, 2017.

[107] A. Pereira and A. de Morais, "Mixed mode I+II interlaminar fracture of glass/epoxy multidirectional laminates – Part 2: Experiments," *Composites Science and Technology*, vol. 66, no. 13, pp. 1896 – 1902, 2006.

[108] R. Olsson, J. Thesken, F. Brandt, N. Jönsson, and S. Nilsson, "Investigations of delamination criticality and the transferability of growth criteria," *Composite Structures*, vol. 36, no. 3, pp. 221 – 247, 1996.

[109] J. Schön, T. Nyman, A. Blom, and H. Ansell, "Numerical and experimental investigation of a composite ENF-specimen," *Engineering Fracture Mechanics*, vol. 65, no. 4, pp. 405 – 433, 2000.

[110] D. Nicholls and J. Gallagher, "Determination of G_{IC} in angle ply composites using a cantilever beam test method," *Journal of Reinforced Plastics and Composites*, vol. 2, no. 1, pp. 2–17, 1983.

[111] P. Robinson and D. Song, "A modified DCB specimen for mode I testing of multidirectional laminates," *Journal of Composite Materials*, vol. 26, no. 11, pp. 1554–1577, 1992.

[112] A. Laksimi, A. A. Benyahia, M. Benzeggagh, and X. Gong, "Initiation and bifurcation mechanisms of cracks in multi-directional laminates," *Composites Science and Technology*, vol. 60, no. 4, pp. 597 – 604, 2000.

[113] J. H. Hwang, C. S. Lee, and W. Hwang, "Effect of crack propagation directions on the interlaminar fracture toughness of carbon/epoxy composite materials," *Applied Composite Materials*, vol. 8, no. 6, pp. 411–433, 2001.

[114] A. Pereira and A. de Morais, "Mode I interlaminar fracture of carbon/epoxy multidirectional laminates," *Composites Science and Technology*, vol. 64, no. 13, pp. 2261 – 2270, 2004.

[115] C. Blondeau, G. Pappas, and J. Botsis, "Influence of ply-angle on fracture in antisymmetric interfaces of CFRP laminates," *Composite Structures*, vol. 216, pp. 464 – 476, 2019.

[116] M. Gilchrist and N. Svensson, "A fractographic analysis of delamination within multidirectional carbon/epoxy laminates," *Composites Science and Technology*, vol. 55, no. 2, pp. 195 – 207, 1995.

[117] J. Tao and C. T. Sun, "Influence of ply orientation on delamination in composite laminates," *Journal of Composite Materials*, vol. 32, no. 21, pp. 1933–1947, 1998.

[118] A. Pereira, A. de Morais, A. Marques, and P. de Castro, "Mode II interlaminar fracture of carbon/epoxy multidirectional laminates," *Composites Science and Technology*, vol. 64, no. 10, pp. 1653 – 1659, 2004.

[119] A. Pereira and A. de Morais, "Mode II interlaminar fracture of glass/epoxy multidirectional laminates," *Composites Part A: Applied Science and Manufacturing*, vol. 35, no. 2, pp. 265 – 272, 2004.

[120] Y. Shi, D. Hull, and J. Price, "Mode II fracture of $+\theta/-\theta$ angled laminate interfaces," *Composites Science and Technology*, vol. 47, no. 2, pp. 173 – 184, 1993.

[121] A. A. Benyahia, A. Laksimi, N. Ouali, and Z. Azari, "Mechanical behavior and optimization of multidirectional laminate specimens under delamination by bending," *Strength of materials*, vol. 38, no. 6, pp. 613–623, 2006.

[122] T. Sebaey, N. Blanco, C. Lopes, and J. Costa, "Numerical investigation to prevent crack jumping in double cantilever beam tests of multidirectional composite laminates," *Composites Science and Technology*, vol. 71, no. 13, pp. 1587–1592, 2011.

[123] S. W. Tsai, *Theory of composites design - Section 8*. Think composites Dayton, OH, 1992.

[124] S. T. Pinho, C. Davila, and P. P. Camanho, "Failure models and criteria for FRP under in-plane or three-dimensional stress states including shear non-linearity," 2005.

[125] T. Sebaey, N. Blanco, J. Costa, and C. Lopes, "Characterization of crack propagation in mode I delamination of multidirectional CFRP laminates," *Composites Science and Technology*, vol. 72, no. 11, pp. 1251 – 1256, 2012.

[126] C. Canturri, E. S. Greenhalgh, and S. T. Pinho, "The relationship between mixed-mode II/III delamination and delamination migration in composite laminates," *Composites Science and Technology*, vol. 105, pp. 102 – 109, 2014.

[127] B. Chen, T. Tay, S. Pinho, and V. Tan, "Modelling delamination migration in angle-ply laminates," *Composites Science and Technology*, vol. 142, pp. 145 – 155, 2017.

[128] L. Zhao, Y. Wang, J. Zhang, Y. Gong, Z. Lu, N. Hu, and J. Xu, "An interface-dependent model of plateau fracture toughness in multidirectional CFRP laminates under mode I loading," *Composites Part B: Engineering*, vol. 131, pp. 196 – 208, 2017.

[129] R. R. Johnson, M. H. Kural, and G. B. Mackey, "Thermal expansion properties of composite materials," NASA Contractor Report 165632, Lockheed Missiles and Space CO INC, Sunnyvale CA, July 1981.

[130] J. Barnes and G. Byerly, "The formation of residual stresses in laminated thermoplastic composites," *Composites Science and Technology*, vol. 51, no. 4, pp. 479 – 494, 1994.

[131] Z. Guo, "Residual stresses characterization of laminated composites curing by FEM and FBG sensor," *Polymers and Polymer Composites*, vol. 19, pp. 91 – 98, 2011.

[132] P. Robinson, S. Foster, and J. Hodgkinson, "The effects of starter film thickness, residual stresses and layup on G_{Ic} of a 0°/0° interface," *Advanced Composites Letters*, vol. 5, no. 6, pp. 159–163, 1996.

[133] H. Miyagawa, C. Sato, and K. Ikegami, "Fracture toughness evaluation for multidirectional CFRP by the raman coating method," *Composites Science and Technology*, vol. 60, no. 16, pp. 2903 – 2915, 2000.

[134] J. A. Nairn, "Fracture Mechanics of Composites With Residual Thermal Stresses," *Journal of Applied Mechanics*, vol. 64, no. 4, pp. 804–810, 1997.

[135] J. A. Nairn, "Energy release rate analysis for adhesive and laminate double cantilever beam specimens emphasizing the effect of residual stresses," *International Journal of Adhesion and Adhesives*, vol. 20, no. 1, pp. 59 – 70, 2000.

[136] J. A. Nairn, "On the calculation of energy release rates for cracked laminates with residual stresses," *International Journal of Fracture*, vol. 139, no. 2, p. 267, 2006.

[137] T. Yokozeki, T. Ogasawara, and T. Aoki, "Correction method for evaluation of interfacial fracture toughness of DCB, ENF and MMB specimens with residual thermal stresses," *Composites Science and Technology*, vol. 68, no. 3-4, pp. 760–767, 2008.

[138] T. Yokozeki, "Energy release rates of bi-material interface crack including residual thermal stresses: Application of crack tip element method," *Engineering Fracture Mechanics*, vol. 77, no. 1, pp. 84 – 93, 2010.

[139] P. Qiao and Q. Liu, "Energy release rate of beam-type fracture specimens with hygrothermal influence," *International Journal of Damage Mechanics*, vol. 25, no. 8, pp. 1214–1234, 2016.

[140] P. Tsokanas and T. Loutas, "Hygrothermal effect on the strain energy release rates and mode mixity of asymmetric delaminations in generally layered beams," *Engineering Fracture Mechanics*, vol. 214, pp. 390 – 409, 2019.

[141] A. B. De Morais, M. F. De Moura, J. P. Gonçalves, and P. P. Camanho, "Analysis of crack propagation in double cantilever beam tests of multidirectional laminates," *Mechanics of Materials*, vol. 35, no. 7, pp. 641–652, 2003.

[142] R. Krueger, "Virtual crack closure technique: History, approach, and applications," *Applied Mechanics Reviews*, vol. 57, no. 2, p. 109, 2004.

[143] G. R. Irwin, *Fracture*, pp. 551–590. Berlin, Heidelberg: Springer Berlin Heidelberg, 1958.

[144] E. F. Rybicki and M. F. Kanninen, "A finite element calculation of stress intensity factors by a modified crack closure integral," *Engineering Fracture Mechanics*, vol. 9, no. 4, pp. 931–938, 1977.

[145] K. N. Shivakumar, P. W. Tan, and J. C. Newman, "A virtual crack-closure technique for calculating stress intensity factors for cracked three dimensional bodies," *International Journal of Fracture*, vol. 36, pp. R43–R50, Mar 1988.

[146] M. L. Williams, "The Stresses Around Faults In Dissimilar Media," *Bulletin of the Seismological Society of America*, vol. 49, no. 2, pp. 199–204, 1959.

[147] I. S. Raju, J. H. Crews, and M. A. Aminpour, "Convergence of strain energy release rate components for Edge-Delaminated composite laminates," *Engineering Fracture Mechanics*, vol. 30, no. 3, pp. 383–396, 1988.

[148] R. Krueger, K. N. Shivakumar, and I. S. Raju, "Fracture mechanics analyses for interface crack problems-a review," in *54th AIAA/ASME/ASCE/AHS/ASC structures, structural dynamics, and materials conference*, p. 1476, 2013.

[149] S. Samborski, "Prediction of delamination front's advancement direction in the CFRP laminates with mechanical couplings subjected to different fracture toughness tests," *Composite Structures*, vol. 202, pp. 643 – 650, 2018. Special issue dedicated to Ian Marshall.

[150] L. Carreras, B. Bak, A. Turon, J. Renart, and E. Lindgaard, "Point-wise evaluation of the growth driving direction for arbitrarily shaped delamination fronts using cohesive elements," *European Journal of Mechanics - A/Solids*, vol. 72, no. Int. J. Numer. Meth. Eng. 50 2001, pp. 464–482, 2018.

[151] B. Davidson and R. Schapery, "Effect of finite width on deflection and energy release rate of an orthotropic double cantilever specimen," *Journal of Composite Materials*, vol. 22, no. 7, pp. 640–656, 1988.

[152] C. Sun and S. Zheng, "Delamination characteristics of double-cantilever beam and end-notched flexure composite specimens," *Composites Science and Technology*, vol. 56, no. 4, pp. 451 – 459, 1996.

[153] B. Davidson, R. Krüger, and M. König, "Effect of stacking sequence on energy release rate distributions in multidirectional DCB and ENF specimens," *Engineering Fracture Mechanics*, vol. 55, no. 4, pp. 557 – 569, 1996.

[154] B. Davidson, "An analytical investigation of delamination front curvature in double cantilever beam specimens," *Journal of Composite Materials*, vol. 24, no. 11, pp. 1124–1137, 1990.

[155] B. D. Davidson, R. Kruger, and M. König, "Three dimensional analysis and resulting design recommendations for unidirectional and multidirectional end-notched flexure tests," *Journal of Composite Materials*, vol. 29, no. 16, pp. 2108–2133, 1995.

[156] J. J. Polaha, B. D. Davidson, R. C. Hudson, and A. Pieracci, "Effects of mode ratio, ply orientation and precracking on the delamination toughness of a laminated composite," *Journal of Reinforced Plastics and Composites*, vol. 15, no. 2, pp. 141–173, 1996.

[157] R. Hudson, B. Davidson, and J. Polaha, "Effect of remote ply orientation on the perceived mode I and mode II toughness of θ/θ and $\theta/-\theta$ interfaces," *Applied Composite Materials*, vol. 5, no. 2, pp. 123–138, 1998.

[158] M. M. Rehan, J. Rousseau, X. Gong, L. Guillaumat, and J. Ali, "Effects of fiber orientation of adjacent plies on the mode I crack propagation in a carbon-epoxy laminates," *Procedia Engineering*, vol. 10, no. Supplement C, pp. 3179 – 3184, 2011. 11th International Conference on the Mechanical Behavior of Materials (ICM11).

[159] M. B. M. Rehan, J. Rousseau, S. Fontaine, and X. Gong, "Experimental study of the influence of ply orientation on DCB mode-I delamination behavior by using multidirectional fully isotropic carbon/epoxy laminates," *Composite Structures*, vol. 161, no. Supplement C, pp. 1 – 7, 2017.

[160] M. Johar, H. A. Israr, K. O. Low, and K. J. Wong, "Numerical simulation methodology for mode II delamination of quasi-isotropic quasi-homogeneous composite laminates," *Journal of Composite Materials*, vol. 51, no. 28, pp. 3955–3968, 2017.

[161] H. Saito, R. Kikuchi, and I. Kimpara, "Evaluation of mode I interlaminar fracture toughness in asymmetric interlayer in CFRP laminates," *Advanced Composite Materials*, vol. 0, no. 0, pp. 1–15, 2019.

[162] P. Vannucci, R. Barsotti, and S. Bennati, "Exact optimal flexural design of laminates," *Composite Structures*, vol. 90, no. 3, pp. 337 – 345, 2009.

[163] A. Jibawy, B. Desmorat, and A. Vincenti, "Structural rigidity optimization of thin laminated shells," *Composite Structures*, vol. 95, pp. 35 – 43, 2013.

[164] M. Montemurro, A. Pagani, G. A. Fiordilino, J. Pailhès, and E. Carrera, "A general multi-scale two-level optimisation strategy for designing composite stiffened panels," *Composite Structures*, vol. 201, pp. 968 – 979, 2018.

[165] M. Montemurro, M. I. Izzi, J. El-Yagoubi, and D. Fanteria, "Least-weight composite plates with unconventional stacking sequences: Design, analysis and experiments," *Journal of Composite Materials*, vol. 53, no. 16, pp. 2209–2227, 2019.

[166] E. Panettieri, M. Montemurro, and A. Catapano, "Blending constraints for composite laminates in polar parameters space," *Composites Part B: Engineering*, vol. 168, pp. 448 – 457, 2019.

[167] G. Verchery, "Les invariants des tenseurs d'ordre 4 du type de l'élasticité," in *Mechanical Behavior of Anisotropic Solids / Comportment Méchanique des Solides Anisotropes* (J.-P. Boehler, ed.), (Dordrecht), pp. 93–104, Springer Netherlands, 1982.

[168] P. Vannucci and G. Verchery, "Stiffness design of laminates using the polar method," *International Journal of Solids and Structures*, vol. 38, no. 50, pp. 9281 – 9294, 2001.

[169] B. D. Davidson, S. J. Gharibian, and L. Yu, "Evaluation of energy release rate-based approaches for predicting delamination growth in laminated composites," *International Journal of Fracture*, vol. 105, no. 4, pp. 343–365, 2000.

[170] B. D. Davidson, R. D. Bialaszewski, and S. S. Sainath, "A non-classical, energy release rate based approach for predicting delamination growth in graphite reinforced laminated polymeric composites," *Composites Science and Technology*, vol. 66, no. 10, pp. 1479–1496, 2006.

[171] L. Yong, L. Shunling, X. Jun, and T. Jie, "Study on the mode I interlaminar fracture toughness of multi-directional laminates," in *Elementary particle theory* (M. L. Scott, ed.), pp. 431–437, Woodhead Publishing Limited.

[172] M. Shokrieh, M. Heidari-Rarani, and S. Rahimi, "Influence of curved delamination front on toughness of multidirectional DCB specimens," *Composite Structures*, vol. 94, no. 4, pp. 1359 – 1365, 2012.

[173] S. Wang and L. Guan, "On fracture mode partition theories," *Computational Materials Science*, vol. 52, no. 1, pp. 240 – 245, 2012. Proceedings of the 20th International Workshop on Computational Mechanics of Materials - IWCMM 20.

[174] P. S. Valvo, "A revised virtual crack closure technique for physically consistent fracture mode partitioning," *International Journal of Fracture*, vol. 173, no. 1, pp. 1–20, 2012.

[175] P. S. Valvo, "A physically consistent virtual crack closure technique for I/II/III mixed-mode fracture problems," *Procedia Materials Science*, vol. 3, pp. 1983 – 1987, 2014. 20th European Conference on Fracture.

[176] Hexcel, "HexPly®M34 product datasheet." https://www.hexcel.com/user_area/content_media/raw/HexPly_M34_eu_DataSheet.pdf, 2015. [Online; accessed 3-January-2020].

[177] D. Fanteria, L. Lazzeri, E. Panettieri, U. Mariani, and M. Rigamonti, "Experimental characterization of the interlaminar fracture toughness of a woven and a unidirectional carbon/epoxy composite," *Composites Science and Technology*, vol. 142, pp. 20 – 29, 2017.

[178] M. Kotaki and H. Hamada, "Effect of interfacial properties and weave structure on mode I interlaminar fracture behaviour of glass satin woven fabric composites," *Composites Part A: Applied Science and Manufacturing*, vol. 28, no. 3, pp. 257 – 266, 1997.

[179] N. Alif, L. A. Carlsson, and J. W. Gillespie, "Mode I, mode II, and mixed mode interlaminar fracture of woven fabric carbon/epoxy," in *Composite Materials: Testing and Design, Thirteenth Volume*, ASTM International, 1997.

[180] N. Alif, L. A. Carlsson, and L. Boogh, "The effect of weave pattern and crack propagation direction on mode I delamination resistance of woven glass and carbon composites," *Composites Part B: Engineering*, vol. 29, no. 5, pp. 603 – 611, 1998.

[181] P. Suppakul and S. Bandyopadhyay, "The effect of weave pattern on the mode I interlaminar fracture energy of E-glass/vinyl ester composites," *Composites Science and Technology*, vol. 62, no. 5, pp. 709 – 717, 2002.

[182] Y. Wang and D. Zhao, "Characterization of interlaminar fracture behaviour of woven fabric reinforced polymeric composites," *Composites*, vol. 26, no. 2, pp. 115 – 124, 1995.

[183] J.-K. Kim and M.-L. Sham, "Impact and delamination failure of woven-fabric composites," *Composites Science and Technology*, vol. 60, no. 5, pp. 745 – 761, 2000.

[184] "ASTM D3039 / D3039M - 17, Standard Test Method for Tensile Properties of Polymer Matrix Composite Materials," Standard, ASTM International, West Conshohocken, PA, 2017.

[185] "ASTM D3518 / D3518M - 18, Standard Test Method for In-Plane Shear Response of Polymer Matrix Composite Materials by Tensile Test of a ± 45 ° Laminate," Standard, ASTM International, West Conshohocken, PA, 2018.

[186] "ASTM D7264 / D7264M - 15, Standard Test Method for Flexural Properties of Polymer Matrix Composite Materials," Standard, ASTM International, West Conshohocken, PA, 2015.

[187] C. Meola, S. Boccardi, G. Carlomagno, N. Boffa, E. Monaco, and F. Ricci, "Nondestructive evaluation of carbon fibre reinforced composites with infrared thermography and ultrasonics," *Composite Structures*, vol. 134, pp. 845 – 853, 2015.

[188] S. Boccardi, N. D. Boffa, G. M. Carlomagno, L. Maio, C. Meola, and F. Ricci, "Infrared thermography and ultrasonics to evaluate composite materials for aeronautical applications," *Journal of Physics: Conference Series*, vol. 658, p. 012007, 2015.

[189] L. Maio, V. Memmolo, S. Boccardi, C. Meola, F. Ricci, N. Boffa, and E. Monaco, "Ultrasonic and IR thermographic detection of a defect in a multilayered composite plate," *Procedia Engineering*, vol. 167, pp. 71–79, 2016.

[190] M. Todo and P.-Y. Jar, "Study of mode-I interlaminar crack growth in DCB specimens of fibre-reinforced composites," *Composites Science and Technology*, vol. 58, no. 1, pp. 105 – 118, 1998.

[191] D. Stevanovic, P.-Y. Jar, S. Kalyanasundaram, and A. Lowe, "On crack-initiation conditions for mode I and mode II delamination testing of composite materials," *Composites Science and Technology*, vol. 60, no. 9, pp. 1879 – 1887, 2000.

Appendix A

Superposition of three QT solutions

A.1 Introduction

In Chapter 5, superposition rules for QT solutions were derived and specialised to the case of superposition of two sequences. The scope of this appendix is to expand by specialising the superposition rules also to the case of the superposition of three sequences.

A.2 Uncoupling of 3 superposed QT uncoupled or quasi-homogeneous solutions

Before presenting the case of the superposition of three initial QT uncoupled solutions, a brief remark valid for the superposition of any number $q \geq 3$ of initial QT uncoupled solutions is explained: suppose there is an orientation, say $\theta_{\bar{l}}$, which exists in only one of the initial QT solutions, e.g. the r-th. Therefore it is:

$$n_{G_{\bar{l}}^{(i)}} = 0, \qquad \forall i \neq r \,. \tag{A.1}$$

It follows from Eq. (5.33):

$$n_{G_{\bar{l}}^{(r)}}\left(\sum_{i=1}^{r} n_i - \sum_{i=r}^{q} n_i\right) = 0 \,. \tag{A.2}$$

Clearly the condition in Eq. (A.2) is satisfied when:

$$\sum_{i=1}^{r} n_i = \sum_{i=r}^{q} n_i \,. \tag{A.3}$$

This means that in the macro-sequence the number of plies below and above the r-th sequence should be equal, that is QT_r initial solution must be exactly at the center of the macro-sequence. If this is not the case, uncoupling is not possible for the macro-sequence.

Considering now the case $q = 3$, Eqs. (5.33) becomes:

$$n_1(-n_{G_{\bar{l}}^{(2)}} - n_{G_{\bar{l}}^{(3)}}) + n_2(n_{G_{\bar{l}}^{(1)}} - n_{G_{\bar{l}}^{(3)}}) + n_3(n_{G_{\bar{l}}^{(1)}} + n_{G_{\bar{l}}^{(2)}}) = 0,$$
$$l = 1, ..., m^* \,. \tag{A.4}$$

From this relationship the following observations can be inferred:

1. if $n_{G_{\bar{l}}^{(1)}} = n_{G_{\bar{l}}^{(3)}} = 0$ for a given orientation $\theta_{\bar{l}}$, we are in the situation described by Eq. (A.1). In this case, as already seen in Eq. (A.2), it is sufficient to have $n_1 = n_3$ to satisfy Eq. (A.4); then $n_{G_{\bar{l}}^{(2)}}$ can be different from zero: an isolated orientation group may exist in the central sequence;

2. more in general, if $n_{G_{\bar{l}}^{(1)}} = n_{G_{\bar{l}}^{(3)}} = n_{G_{\bar{l}}} \neq 0$, then Eq. (A.4) reduces to:

$$(n_3 - n_1)(n_{G_{\bar{l}}^{(2)}} + n_{G_{\bar{l}}}) = 0, \tag{A.5}$$

This means that if an orientation appears with the same number of plies in sequences QT_1 and QT_3, then, in order to obtain a saturated group, the total number of plies of the two sequences must be equal, $n_1 = n_3$. If this is the case, both the total number of plies n_2 and the number of plies for the concerned orientation $n_{G_{\bar{l}}^{(2)}}$ of sequence QT_2 do not appear in the condition to obtain a saturated group;

3. very interestingly, if the total number of plies of the three sequences is the same, $n_1 = n_2 = n_3$, Eq. (A.4) simplifies to $n_{G_{\bar{l}}^{(1)}} = n_{G_{\bar{l}}^{(3)}}$.

As for the superposition of two sequences, the results obtained here may be used also to obtain a QT uncoupled macro-sequence by the superposition of QT quasi-homogeneous solutions.

A.3 Membrane-bending homogeneity of 3 superposed QT membrane-bending homogeneous solutions

In the case of three superposed QT membrane-bending homogeneous solutions, Eq. (5.42) becomes:

$$n_{G_l^{(3)}} \left[6(n_1 + n_2)(n_3 + 1) - (n_1 + n_2)(n_3 + n_{tot} + 3) \right] - 6(n_1 + n_2) \sum_{k \in G_l^{(3)}} k +$$

$$+ n_{G_l^{(2)}} \left[6n_1(n_2 + n_3 + 1) - (n_1 + n_3)(n_2 + n_{tot} + 3) \right] - 6(n_1 - n_3) \sum_{k \in G_l^{(2)}} k + \tag{A.6}$$

$$+ n_{G_l^{(1)}} \left[-(n_2 + n_3)(n_1 + n_{tot} + 3) \right] + 6(n_2 + n_3) \sum_{k \in G_l^{(1)}} k = 0,$$

$$l = 1, ..., m^*.$$

If $n_1 = n_2 = n_3$ and $n_{G_l^{(1)}} = n_{G_l^{(2)}} = n_{G_l^{(3)}}$, Eq. (A.6) becomes:

$$\sum_{k \in G_l^{(1)}} k - \sum_{k \in G_l^{(3)}} k = 0, \quad l = 1, ..., m^*. \tag{A.7}$$

In this particular case, the contribution of sequence QT_2 disappears, and only k indexes of sequences QT_1 and QT_3 must fulfil the previous condition in order to get a QT membrane-bending homogeneous macro-sequence.

A.4 Membrane-bending homogeneity of 3 superposed QT quasi-homogeneous solutions

When $q = 3$ Eq. (5.44) reduces to:

$$
\begin{aligned}
& n_{G_l^{(1)}}[(n_2 + n_3)(-n_1 + n_2 + n_3)] \\
& + n_{G_l^{(2)}}[(n_1 + n_3)(n_1 - n_2 + n_3) - 6n_1n_3] + \\
& + n_{G_l^{(3)}}[(n_1 + n_2)(n_1 + n_2 - n_3)] = 0, \qquad l = 1, ..., m^*.
\end{aligned}
\tag{A.8}
$$

If the particular case of the superposition of three solutions with the same number of plies is considered, $n_1 = n_2 = n_3 = n$ and Eq. (A.8) simplifies to:

$$
n_{G_l^{(1)}} + n_{G_l^{(3)}} = 2n_{G_l^{(2)}}, \qquad l = 1, ..., m^*,
\tag{A.9}
$$

which is a very simple condition: the sum of plies belonging to a given orientation θ_l in sequences QT_1 and QT_3 must be equal to twice the number of plies sharing the same orientation angle within sequence QT_2. Eq. (A.9) imposes that a given orientation group G_l must be present in the central sequence too, otherwise saturation will not be possible. This is due to the trend of c_k coefficients within the stacking sequence.

Appendix B

Glass/epoxy UD-fabric material experimental characterisation

B.1 Introduction

The material system used to fabricate the delamination specimens that were used in this work is a glass/epoxy composite whose commercial reference is HexPly © M34N/32%/430PUD/G-136x5 and that was available in the form of a pre-impregnated (prepreg) roll. The reinforcement in this composite is constituted by a so-called *UD fabric* material: a plain weave fabric in which 90% of fibre weight is constituted by the warp yarns (E-glass EC9 136) and the remaining 10% fibre weight is constituted by the transverse weft yarns (E-glass EC9 68).

In order to obtain the elastic properties of the material an experimental characterisation program was carried out, following standard procedures. The aim of this appendix is to detail the procedures adopted and the results obtained. Moreover, since data on this particular material are not available in the literature, nor in official data-sheets, the results presented here may prove useful also for others.

B.2 Experimental activity

B.2.1 Test matrix

To design an appropriate experimental program for the characterisation of the material adopted, standard test procedures have been reviewed. In particular, using ASTM standard characterisation tests [184, 185, 186] for polymer matrix composites as a guide, the test plan in Table B.1 has been devised. The test methodology and the corresponding ASTM standards are listed in Table B.1, along with the elastic properties that can be found from each test. Also, details on the specimens' layups, their nominal dimensions and the number of specimens per test are reported. The plates from which specimens have been obtained were fabricated following the same process exposed in Chapter 8 and used for the plates from which delamination specimens were obtained.

It is worth remarking the choice of performing flexural tests. When characterising polymer matrix composites, elastic moduli may be different in tension and compression (usually they are lower in compression). Consequently, both tensile and compressive tests are performed. An alternative option is to substitute compressive tests with flexural ones, which have the great advantage of being much simpler and usually give less dispersed

Test type	ASTM standard	Properties obtained	Specimens n°	Specimen layup	Specimen dimensions [mm]
0° Tension	D3039 [184]	$E_{1,t}, \nu_{12}$	7	$[0]_8$	200 * 20
90° Tension	D3039 [184]	$E_{2,t}$	7	$[90]_8$	200 * 25
±45° Shear	D3518 [185]	G_{12}	7	$[\pm45]_{2S}$	200 * 25
0° Bending	D7264 [186]	$E_{1,f}$	8	$[0]_8$	200 * 20
90° Bending	D7264 [186]	$E_{2,f}$	8	$[90]_8$	200 * 20

Table B.1: Material characterisation test matrix.

results. Typically, flexural moduli fall in between tensile and compressive ones. For the purposes of this study, there was an even greater interest in measuring flexural moduli, since they are of interest when interlaminar fracture tests (in which bending is the main loading condition) are concerned.

B.2.2   Experimental setups

Both 0° and 90° tensile tests, as well as ±45 in-plane shear tests, were carried out in the tensile apparatus shown in Fig. B.1. Two Instron wedge grip have been used to
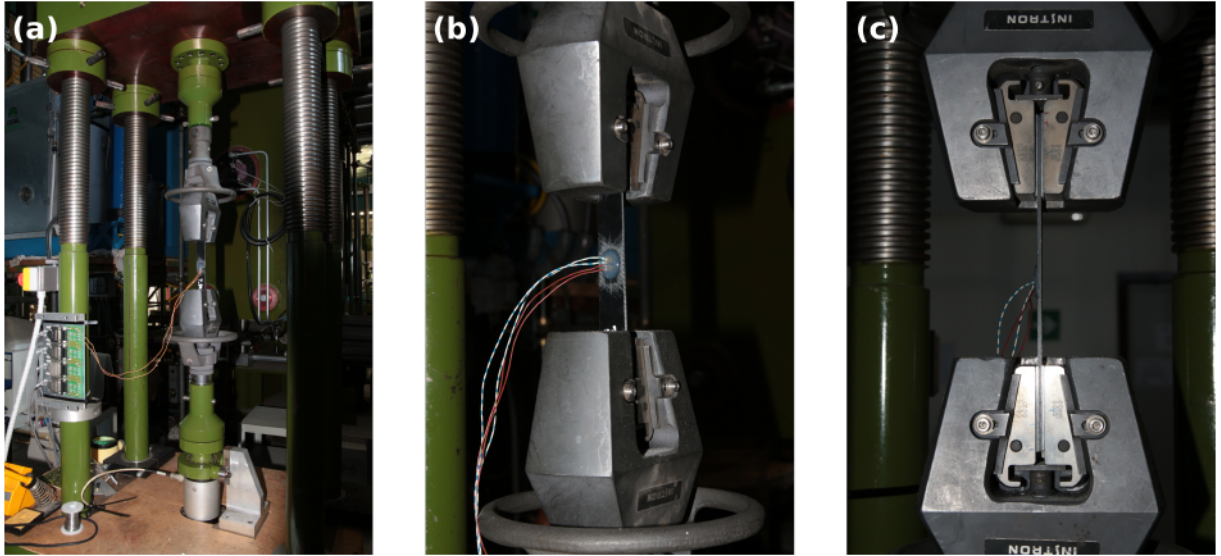

Figure B.1: Tensile testing apparatus used for 0° and 90° tensile tests and ±45 in-plane shear tests. Global view (a) and close-up views from different angles (b-c).

perform the tests. The upper grip is fixed, while the lower one is moved during the tests. Furthermore, the upper wedge grip had the freedom to self-align, which is particularly important for tensile tests, since otherwise deleterious bending stress could be induced and invalidate results. The initial pressure applied by the upper grip was adjusted manually. The force applied by the system is measured by means of a 100 kN load cell. For all tests performed with this machine, the acquisition system was set to register force, displacement and data from strain gauges each 0.1 seconds.

To perform bending tests, the apparatus shown in Fig. B.2 was used. It is equipped
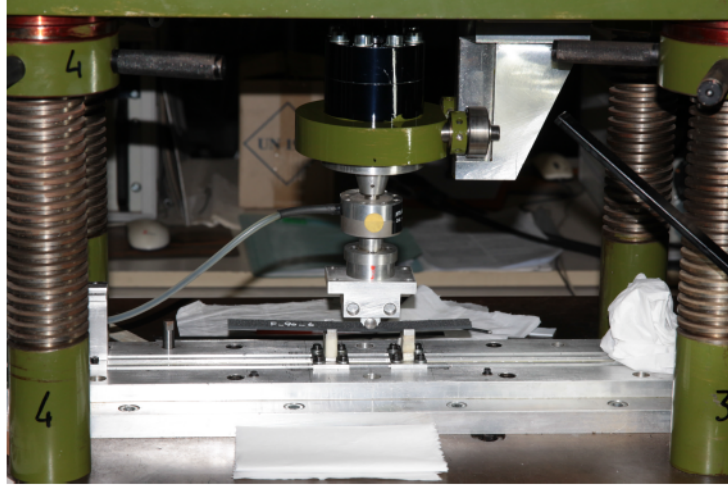
Figure B.2: View of the experimental setup adopted for bending tests on both $[0°]_8$ and $[90°]_8$ specimens.

with supports whose position can be adjusted and with a 2 kN load cell that measure the force applied. During the bending tests the acquisition system was set to record force and cross-head displacement each 0.05 seconds.

B.2.3   0° tensile tests

In order to obtain the Young's modulus of the material in the warp direction, tensile tests on seven specimens with a $[0°]_8$ layup were carried out. The specimens were labelled and their width and thickness were measured at three different sections. Aluminium tabs, 50
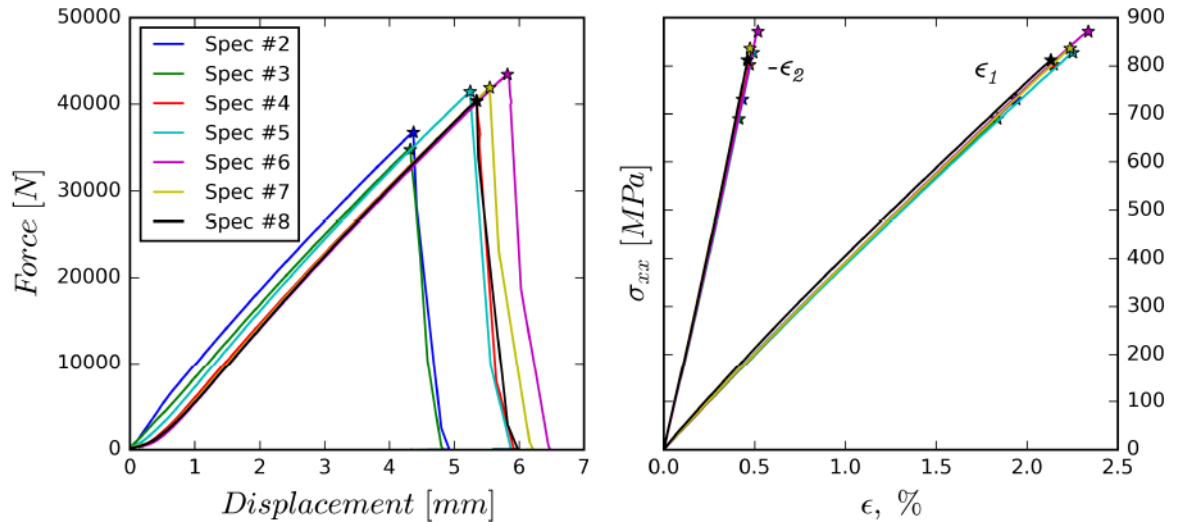

Figure B.3: Force-displacement and stress-strain results of tensile tests on $[0°]_8$ specimens.

millimetres long, were glued to the specimens.

Bidirectional strain gauges were installed with measuring grids to be aligned with specimens' longitudinal and transverse directions. The tests were performed under displacement control with a cross-head speed of 0.5 mm/min. Fig. B.3 shows the results

in terms of force-displacement and stress-strain behaviour obtained from the tests. Both the longitudinal ϵ_1 (warp direction) and the transversal ϵ_2 (weft direction) strains are reported. The longitudinal stress is obtained as the ratio of the applied force F and the cross section area A of each specimen:

$$\sigma_1 = \frac{F}{A} = \frac{F}{t \cdot w}, \tag{B.1}$$

where t and w indicate the specimen thickness and width, respectively. Specimen n. 1 was used for calibration and verification purposes, and was therefore excluded from Fig. B.3 and all subsequent calculations.

Spec. ID	t [mm]	w [mm]	$E_{1,t}$ [GPa]	ν_{12} [-]	X_t [MPa]
2	2.54	19.82	40.5	0.251	729.98
3	2.55	19.80	39.9	0.250	689.73
4	2.54	19.77	40.0	0.245	802.82
5	2.54	19.75	39.9	0.246	827.72
6	2.53	19.75	40.2	0.247	870.81
7	2.54	19.77	40.5	0.241	835.73
8	2.51	19.81	41.9	0.256	811.80
Av.	2.54	19.79	40.5	0.248	795.4
C. V. %	0.42	0.14	1.84	1.74	7.38

Table B.2: Geometric data of all specimens with $[0°]_8$ layup tested and mechanical properties obtained.

Table B.2 reports both geometric data of the specimens and results obtained from experimental tests. The average values and the coefficient of variation (as a percentage) are reported as well. The tensile modulus in the warp direction $E_{1,t}$ was obtained according to the chord method suggested in [184]:

$$E_{1,t} = \frac{\Delta\sigma_1}{\Delta\epsilon_1}, \tag{B.2}$$

where $\Delta\sigma_1$ is the difference in longitudinal stress σ_1 and $\Delta\epsilon_1$ the difference in longitudinal strain ϵ_1 between two points taken at some fixed strain values. In this case, as suggested in [184] the points with 0.1% and 0.3% strain have been used. Poisson's ratio ν_{12} was obtained by the chord method as well:

$$\nu_{12} = \frac{-\Delta\epsilon_2}{\Delta\epsilon_1}, \tag{B.3}$$

using the same strain points as for the tensile modulus. Both $E_{1,t}$ and ν_{12} are very consistent among the specimens, as confirmed by the low coefficients of variation.

All the specimens failed by longitudinal splitting. However, the splits are not confined to the gage section of the specimen and run up to the tabs, see Fig. B.4. Hence, the values of the failure stress X_t are to be taken with caution. Moreover, the initial grip pressure at the beginning of each test was manually adjusted, and the lower values of X_t obtained with specimens 2 and 3 are thought to be related to an excessively high initial
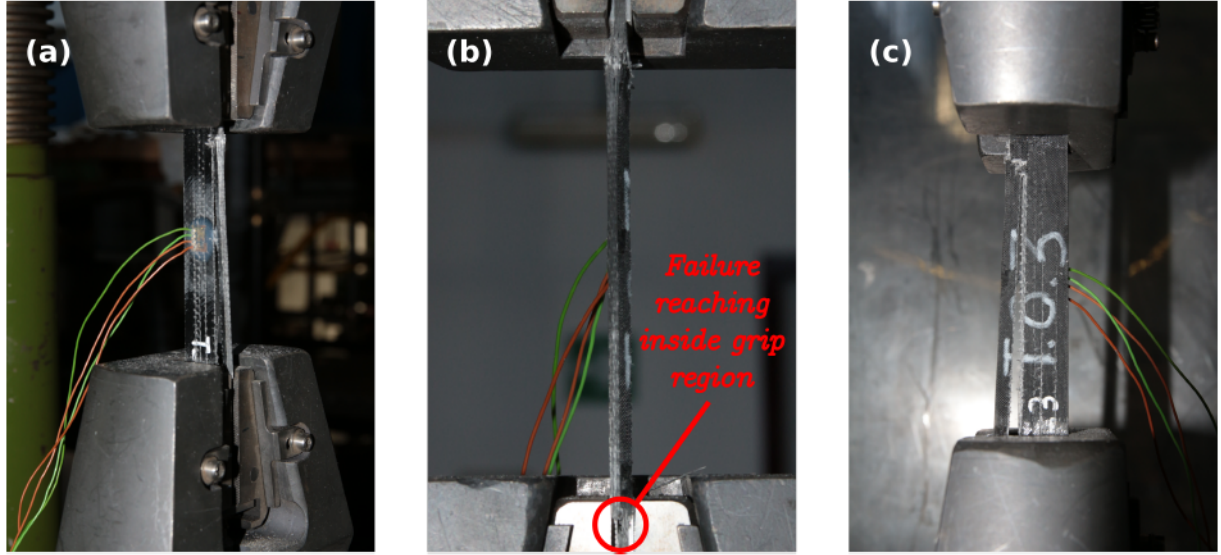
Figure B.4: Failure mode observed in tensile tests of specimens with $[0°]_8$ layup, specimen n. 3: front-side view (a), side view (b), back view (c).

gripping pressure (which was then reduced in all subsequent tests). Since X_t value was not relevant for the purpose of the present work, additional tests to determine it were not performed.

B.2.4 90° tensile tests

In order to obtain the Young's modulus of the material in the weft direction, tensile tests on seven specimens with a $[90°]_8$ layup were carried out. Similarly to the case of $[0°]_8$ specimens, the specimens' width and thickness were measured at three different sections. In this case, 25 millimetres long aluminium tabs were used. Only longitudinal strain gauges were installed on the specimens. The tests were performed under displacement control with a cross-head speed of 0.5 mm/min.

The results in terms of force-displacement and stress-strain behaviour are shown in Fig. B.5. It is worth noting that the subscript 2 has been used to remark that the longitudinal direction being tested in this case is the weft direction of the glass/epoxy composite. Once again, the longitudinal stress is obtained as the ratio of the force and the section area of each specimen:

$$\sigma_2 = \frac{F}{A} = \frac{F}{t \cdot w}. \tag{B.4}$$

Specimens n. 1 and n. 3 were excluded from the results because they failed exactly at their centre section, where a slight mark had been drawn with a gage marker, see Fig B.6.

Table B.3 reports geometric data and results obtained from experimental tests, with their average values and coefficient of variation. $E_{2,t}$ is the tensile chord modulus in the weft direction:

$$E_{2,t} = \frac{\Delta\sigma_2}{\Delta\epsilon_2}. \tag{B.5}$$

In this case, the strains used for the calculation of $E_{2,t}$ were 0.05 and 0.15 %, since some non-linear behaviour in the stress-strain relationship was observed starting around
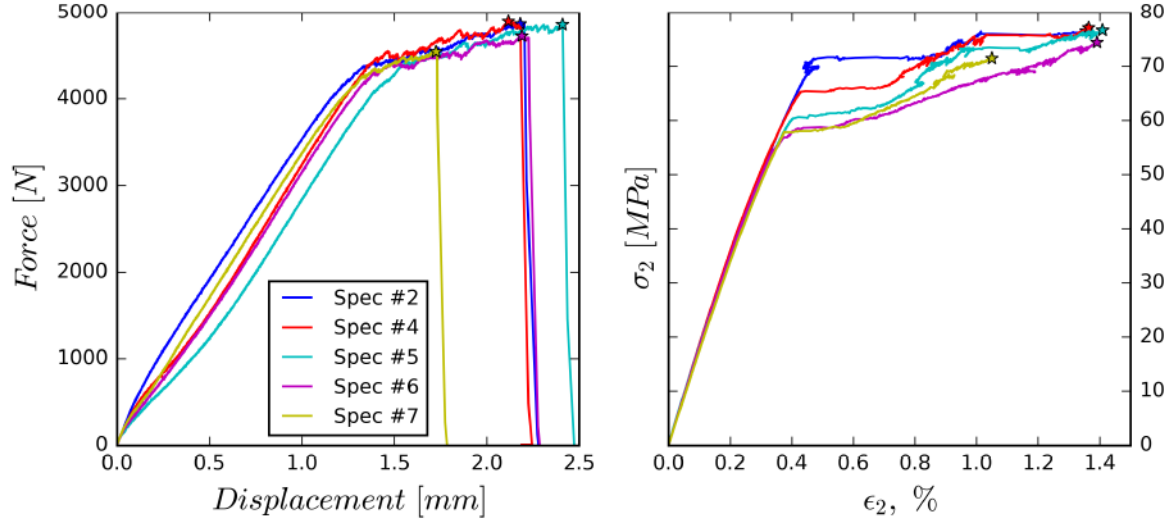
Figure B.5: Force-displacement and stress-strain results of tensile tests on $[90°]_8$ specimens.
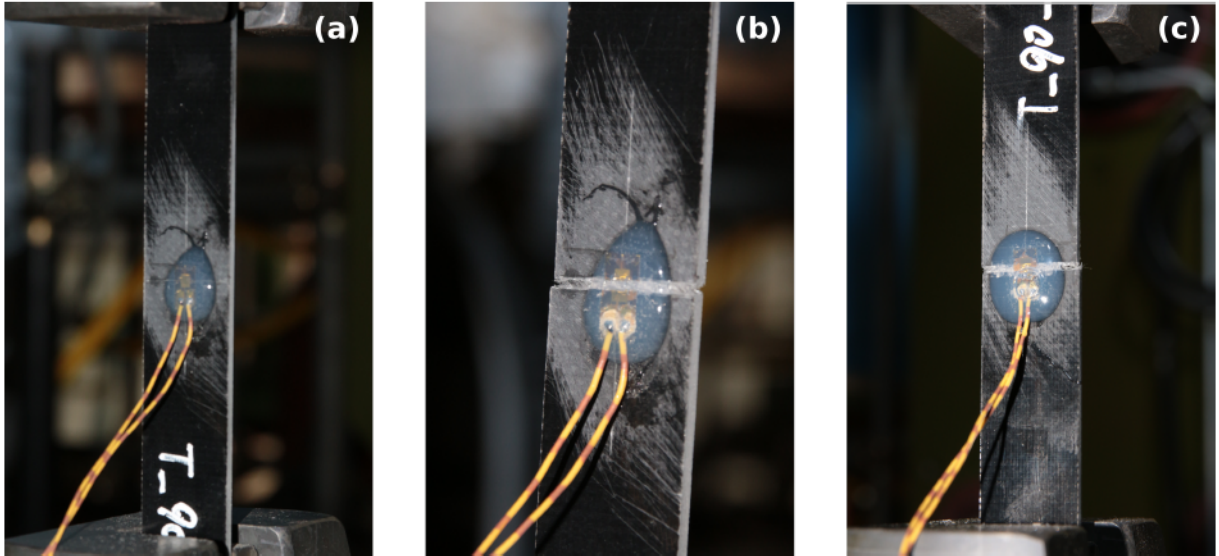

Figure B.6: Invalid failure mode due to a cutter mark acting as a notch. Specimen n. 1 before testing (a) and after failure (b), specimen n. 3 after failure.

$\epsilon_2 = 0.17\%$. Once again, the low value of the coefficient of variation confirms a very good consistency of the measured elastic modulus.

All the specimens reported in Fig B.5 and in Table B.3 failed correctly, Fig B.7. Consequently, the values obtained for the maximum stress S_f may be considered valid. Furthermore, a good consistency is obtained for the failure stress.

B.2.5 ±45° in-plane shear tests

In order to obtain the shear modulus of the material, G_{12}, in plane shear tests [185] on seven specimens with a $[\pm45°]_{2s}$ layup were carried out. The specimens were labelled and their width and thickness were measured at three different sections. 50 millimetres

Spec ID	t [mm]	w [mm]	$E_{2,t}$ [GPa]	S_f [Mpa]
2	2.56	24.86	17.4	76.6
4	2.56	24.82	17.8	77.1
5	2.55	24.81	17.3	76.7
6	2.55	24.90	17.5	74.4
7	2.56	24.81	17.0	71.5
Average	2.56	24.84	17.4	75.3
C. V. %	0.14	0.14	1.61	2.80

Table B.3: Geometric data of all specimens with $[90°]_8$ layup tested and mechanical properties obtained.
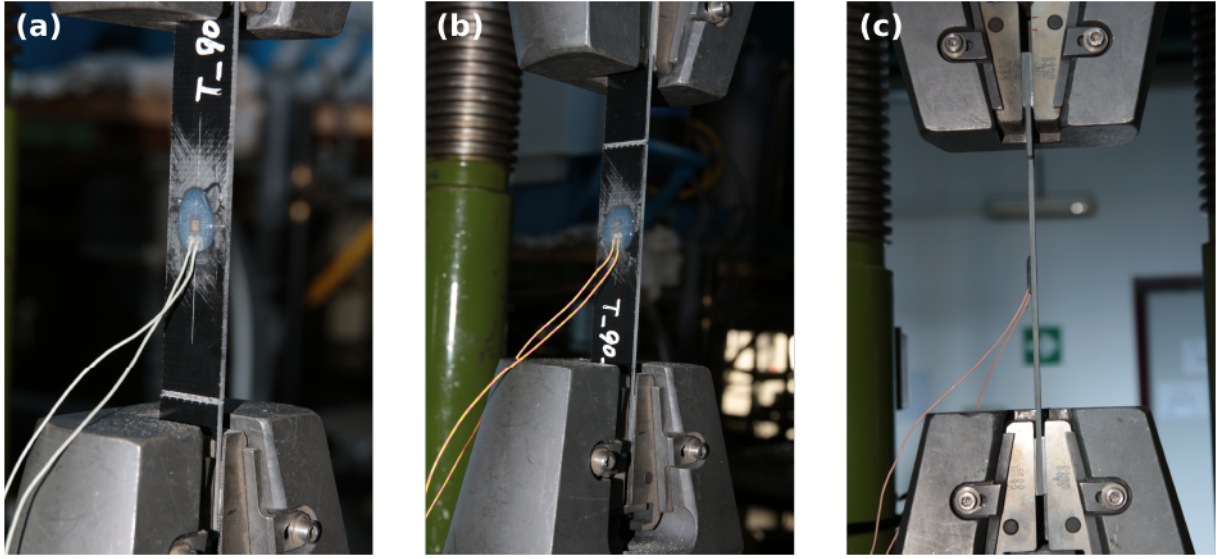

Figure B.7: Failure mode observed in tensile tests on $[90°]_8$ specimens: front-side view of specimen n. 2 (a), front-side view of specimen n. 4 (b) and side view of specimen n. 6 (c).

long aluminium tabs were glued to the specimens. Strain gauges were glued to the specimens in both the longitudinal and transverse directions. The tests were performed under displacement control with a cross-head speed of 0.5 mm/min.

The results in terms of force-displacement and stress-strain behaviour obtained are shown in Fig. B.8. Specimen n. 2 was excluded due to failure exactly at its centre section, in correspondence of the mark drawn to place the strain gauges (much like what happened in $[90°]_8$ specimens n. 1 and 3). On the other hand, results from specimen n. 1 are only partial, since the test was arrested before reaching failure. As a consequence, no failure stress was found for this specimen, but its data were used for modulus computation. Eventually, during test of specimen n. 5 one strain gauges' wire failed. Consequently, strain data are not considered valid for shear modulus computation, but failure stress could be still obtained. According to [185], the in-plane shear stress may be computed as follows:

$$\tau_{12} = \frac{F}{2A} = \frac{F}{2t \cdot w},\tag{B.6}$$

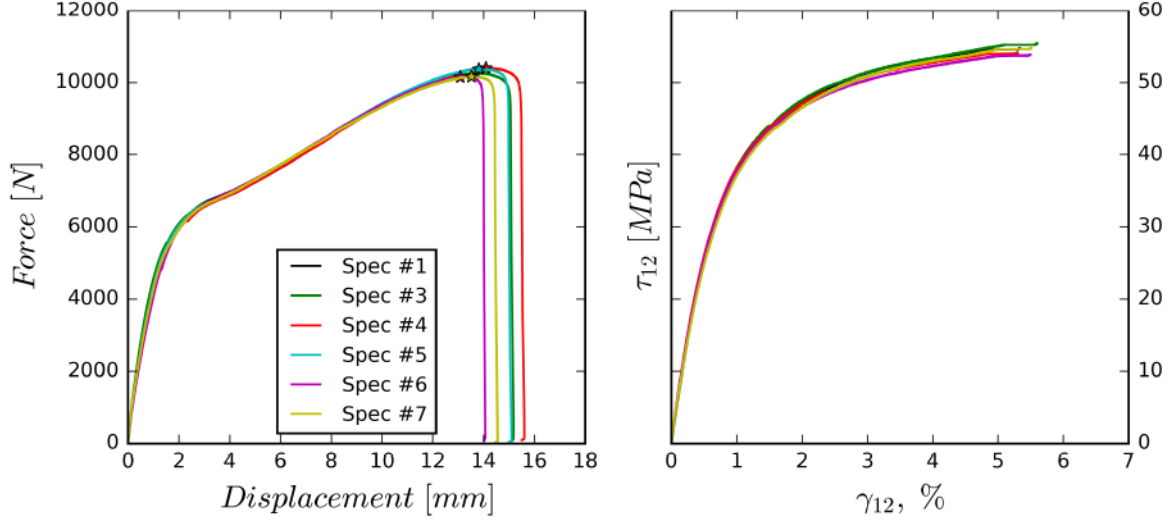with the same notation as before. The shear strain may be obtained from strain gauges'

Figure B.8: Force-displacement and stress-strain results of tensile tests on $[\pm 45°]_{2s}$ specimens.

readings as:

$$\gamma_{12} = \epsilon_1 - \epsilon_2 \,. \tag{B.7}$$

It is worth mentioning that the stress-strain plots in Fig. B.8 are interrupted before specimen failure, due to strain gauges failure. Table B.3 reports geometric data and

Spec ID	t [mm]	w [mm]	G_{12} [GPa]	S_f [Mpa]
1	2.55	24.80	6.01	-
3	2.55	24.83	6.18	81.1
4	2.55	24.87	6.32	82.0
5	2.55	24.91	-	81.6
6	2.55	24.85	6.28	80.1
7	2.54	24.77	6.00	80.8
Average	2.55	24.84	6.16	81.1
C. V. %	0.15	0.18	2.15	0.82

Table B.4: Geometric data of all specimens with $[\pm 45°]_{2s}$ layup tested and mechanical properties obtained.

experimental results, with their average values and coefficient of variation. The shear chord modulus of elasticity is obtained as:

$$G_{12} = \frac{\Delta \tau_{12}}{\Delta \gamma_{12}} \,. \tag{B.8}$$

The strains used for the calculation of G_{12} were 0.05 and 0.15 %, since non-linear behaviour in the stress-strain relationship was observed for higher values. The values of G_{12} obtained show little scatter.

With the exception of specimen n. 2, all other specimens failed in a valid way, Fig. B.9, and the value of maximum shear stress reached is quite consistent among all specimens.
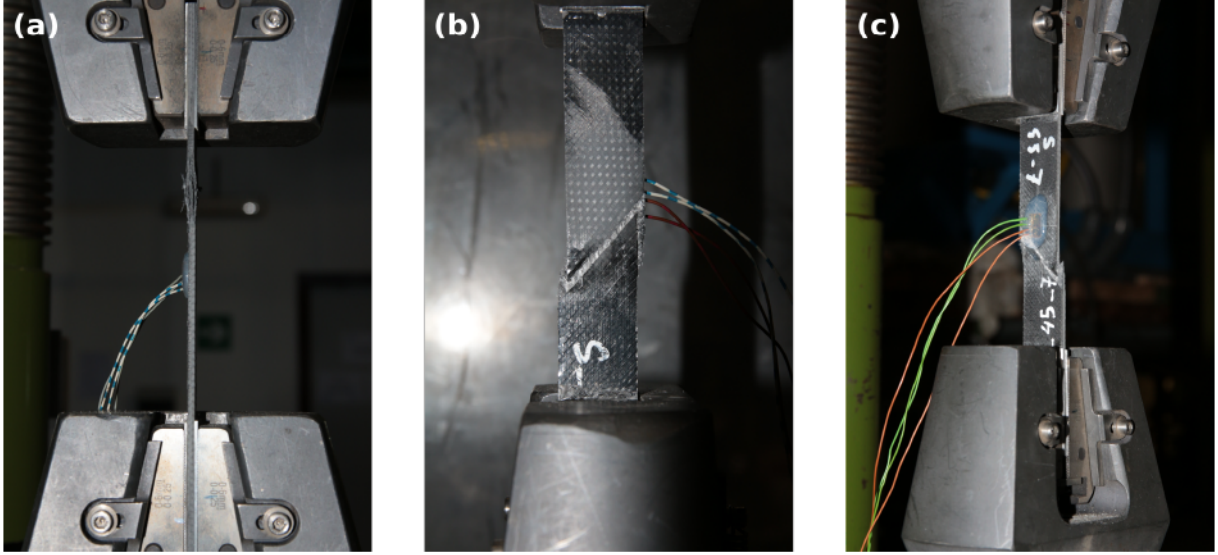
Figure B.9: Failure mode observed in in-plane shear tests on $[\pm 45°]_{2s}$ specimens: side view of specimen n. 3 (a), rear view of specimen n. 5 (b) and front-side view of specimen n. 7 (c).

B.2.6   0° and 90° bending tests

In order to evaluate the flexural elastic properties of the material used, three-point bending tests were performed on both $[0°]_8$ and $[90°]_8$ specimens, Fig B.10. The tests were
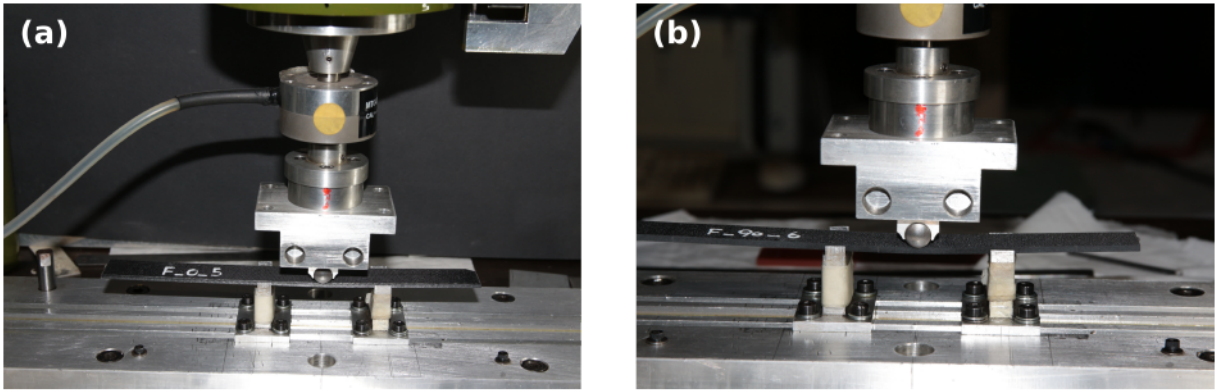

Figure B.10: Pictures of the three-point bending tests: $[0°]_8$ specimen (a) and $[90°]_8$ specimen (8).

performed in displacement control, with a crosshead speed of 0.5 mm/min. No strain gauges were used and the span between the supports adopted was of 64 mm. Moreover the specimens were not brought to failure.

During the three point bending test, the maximum flexural stress in the specimen occurs at the outer surface of the mid-span section, where the specimen is loaded. There such stress is obtained as:

$$\sigma = \frac{3FL}{2wt^2}, \tag{B.9}$$

where F is the applied force, L the support span and w and t the width and thickness of the specimen, respectively. The normal strain in the same point may be obtained as:

$$\sigma = \frac{6\delta t}{L^2}, \tag{B.10}$$

Spec ID	t [mm]	w [mm]	$E_{1,f}$ [GPa]
1	2.48	20.03	38.8
2	2.48	19.71	38.0
3	2.47	20.04	40.0
4	2.54	19.85	37.3
5	2.47	20.06	39.1
6	2.46	20.05	39.3
7	2.48	20.01	40.5
Average	2.48	19.96	39.0
C. V. %	0.98	0.62	2.63

Table B.5: Geometric data of all specimens with $[0°]_8$ layup tested and mechanical properties obtained.

where δ is the cross-head displacement. Similarly to the case of tensile tests, the flexural

Spec ID	t [mm]	w [mm]	$E_{2,f}$ [GPa]
1	2.55	19.91	15.5
2	2.60	19.90	14.8
3	2.56	19.86	15.9
4	2.55	19.82	16.1
5	2.55	19.82	16.4
6	2.55	19.85	16.0
7	2.55	19.82	15.6
8	2.54	19.83	16.2
Average	2.56	19.85	15.8
C. V. %	0.68	0.17	2.95

Table B.6: Geometric data of all specimens with $[90°]_8$ layup tested and mechanical properties obtained.

chord modulus may be obtained as:

$$E_f = \frac{\Delta\sigma}{\Delta\epsilon} . \tag{B.11}$$

In particular the flexural modulus in the warp direction, $E_{1,f}$, is obtained from $[0°]_8$ and that in the weft direction, $E_{2,f}$, is obtained from $[90°]_8$ specimens. The geometric details of all the specimens tested and the values of the elastic modulus found are reported in Tables B.5 and B.6 for $[0]_8$ and $[90]_8$ specimens respectively. The average values of such data and the coefficient of variation are reported as well.

B.3   Summary of results

The main elastic properties of the basic ply material have been determined according to the test matrix presented in Table B.1. The mean values obtained are reported in Table

B.7, along with their relative coefficient of variation. As one can see, very little variation was observed. It is important to remark that, due to the fact that this material is a fabric, the behaviour of the basic ply is orthotropic, and cannot be assumed to be transversely isotropic, as it is often done with UD plies. Interestingly, the flexural longitudinal modulus E_1^f found for the UD delamination specimens using Eq. (3.2) is 44.5 ± 3.0 GPa, a value that is reasonably close to that reported in Table B.7.

	$E_{1,t}$ [GPa]	$E_{1,f}$ [GPa]	$E_{2,t}$ [GPa]	$E_{2,f}$ [GPa]	G_{12} [GPa]	ν_{12} [-]
Average	40.5	39.0	17.4	15.8	6.16	0.248
C. Var. %	1.84	2.63	1.61	2.95	2.15	1.74

Table B.7: Elastic properties of the basic ply of the adopted material obtained by the experimental characterisation campaign.

Appendix C

Activities and outputs

C.1 Trainings and Classes

1. *Scientific integrity in research (MOOC)*, Université de Bordeaux, 15 h;

2. *Scientific calculus with Python 3*, Université de Bordeaux, 19.5 h;

3. *Groupement de Recherche (GdR) week: Composites*, I2M Bordeaux, Talence, 14 h;

4. *French for foreign students 1*, Université de Bordeaux, 40 h;

5. *French for foreign students 2*, Université de Bordeaux, 40 h;

6. *Academic English*, Università di Pisa, 30 h;

7. *Introduction to tensor calculus*, Università di Pisa, 16 h;

8. *Continuum Mechanics*, Università di Pisa, 16 h;

9. *Short Course on Experimental Techniques and Testing of Composite Materials*, Università di Padova, 24 h;

10. *Fatigue and Damage Mechanics of Composite Materials*, Università di Padova, 28 h;

11. *FiBreMoD School*, KU Leuven 10.5 h;

12. *Boost your readings (MOOC)*, Martha Boeglin, 15 h;

Total hours of formation: 268.

C.2 Teaching and supervising activities

1. **Temporary teacher, 10/2017 – 06/2018,**
   Institut Polytechnique de Bordeaux (Bordeaux INP) – ENSEIRB-MATMECA;
   MatMeca (Maths and Mechanics) major, first and second year;
   Travaux Pratiques de mécanique des solides et des fluides (Laboratory course),
   Total of 59 h;

2. **Supervision** 02/2018 – 08/2018, Bordeaux;
   Wenyi Huang's (Polytechnique Orléans) master thesis stage;

3. **Supervision** 06/2019 - 08/2019, Pise;
   Clément Leforestier's (Bordeaux INP) annual stage (4th academic year).

C.3 Journal papers

1. T. Garulli, A. Catapano, D. Fanteria, W. Huang, J. Jumel, E. Martin
   Experimental assessment of of Fully-Uncoupled Multi-Directional specimens for mode I delamination tests, submitted to Composite Science and Technology.

2. T. Garulli, A. Catapano, D. Fanteria, J. Jumel, E. Martin,
   Design and finite element assessment of fully uncoupled multi-directional layups for delamination tests, Journal of Composite Materials, Volume 54(6), 2020, Pages 773–790.

3. T. Garulli, A. Catapano, M. Montemurro, J. Jumel, D. Fanteria,
   Quasi-trivial stacking sequences for the design of thick laminates, Composite Structures, Volume 200, 2018, Pages 614-623.

C.4 Conference papers

1. Monaco E., Boffa N. D., Garulli T., Ricci F., Fanteria D., *Co-infused and secondary bonded composite stiffened panels in compression: numerical and experimental strength assessment combined with NDI and guided waves based SHM*, Proc. SPIE 11381, Health Monitoring of Structural and Biological Systems XIV, 113810C (27 May 2020).

2. Garulli T., Catapano A., Montemurro M., Jumel J., Fanteria D.,
   Quasi-trivial solutions for uncoupled, homogeneous and quasi-homogeneous laminates with high number of plies, ECCM VI, International Center for Numerical Methods in Engineering (CIMNE), GBR (2018): 255-265.

C.5 Conference Participations

1. Monaco E., Boffa N. D., Garulli T., Ricci F., Fanteria D., *Co-infused and secondary bonded composite stiffened panels in compression: numerical and experimental strength assessment combined with NDI and guided waves based SHM*, SPIE Smart Structures Nondestructive Evaluation, 27-30 April 2020 (co-author).

2. Garulli T., Fanteria D., Catapano A., Martin E., *Fully uncoupled multi-directional delamination specimens: a preliminary validation*, FiBreMoD Conference, Leuven, 9-12 December 2019 (speaker).

3. Ricci F., Boffa N. D., Garulli T., Monaco E., Fanteria D., *Coinfused and secondary bonded composite stiffened panels loaded in compression: numerical analyses and experimental tests in linear and post-buckling regimes*, AIDAA 2019, Rome 9-12 September, 2019 (co-author).

4. Garulli T., Catapano A., Fanteria D., Jumel J., *Numerical and experimental validation of the design of multi-directional laminates for pure mode I DCB tests*, JNC 21, Bordeaux, 1 -3 July 2019 (co-author).

5. Garulli T., Catapano A., Fanteria D., Jumel J., *Development and finite elements assessment of stacking sequences for interlaminar fracture toughness testing of angle-ply interfaces*, CompTest 2019, Luleå, 27 - 29 May 2019 (speaker - poster).

6. Garulli T., Catapano A., Fanteria D., Jumel J., *Experimental study of the effects of layers orientation on mode I interlaminar fracture toughness of laminated composites using fully uncoupled multidirectional specimens*, ICCST 12, Sorrento, 8 - 10 May 2019 (speaker).

7. Garulli T., Catapano A., Montemurro M., Jumel J., Fanteria D., *Quasi-trivial solutions for uncoupled, homogeneous and quasi-homogeneous laminates with high number of plies*, ECCM ECFD 2018, Glasgow, 11 - 15 June 2018 (speaker).

C.6 Awards

1. **Idex funding**, Université de Bordeaux.
   Fund for mobility: participation to FiBreMod School and Conference.